

VOLUME 18

NUMBER 1

2025

ISSN 2218-7979
eISSN 2409-370X

International Journal of
Biology
and **Chemistry**



Al-Farabi Kazakh National University

International Journal of Biology and Chemistry is published twice a year by
al-Farabi Kazakh National University, al-Farabi ave., 71, 050040, Almaty, Kazakhstan
website: <http://ijbch.kaznu.kz/>

Any inquiry for subscriptions should be sent to:
Prof. Mukhambetkali Burkitbayev, al-Farabi Kazakh National University
al-Farabi ave., 71, 050040, Almaty, Kazakhstan
e-mail: Mukhambetkali.Burkitbayev@kaznu.edu.kz

EDITORIAL

The most significant achievements in the field of natural sciences are reached in joint collaboration, where important roles are taken by biology and chemistry. Therefore publication of a Journal, displaying results of current studies in the field of biology and chemistry, facilitates highlighting theoretical and practical issues and distribution of scientific discoveries.

One of the basic goals of the Journal is to promote the extensive exchange of information between the scientists from all over the world. We welcome publishing original papers and materials of biological and chemical conferences, held in different countries (by prior agreement, after the process of their subsequent selection).

Creation of International Journal of Biology and Chemistry is of great importance, since scientists worldwide, including other continents, might publish their articles, which will help to widen the geography of future collaboration.

The Journal aims to publish the results of the experimental and theoretical studies in the field of biology, biotechnology, chemistry and chemical technology. Among the emphasized subjects are: modern issues of technologies for organic synthesis; scientific basis of the production of biologically active preparations; modern issues of technologies for processing of raw materials; production of new materials and technologies; study on chemical and physical properties and structure of oil and coal; theoretical and practical issues in processing of hydrocarbons; modern achievements in the field of nanotechnology; results of studies in various branches of biology, chemistry and related technologies.

We hope to receive papers from the leading scientific centers, which are involved in the application of the scientific principles of biological and chemical sciences on practice and fundamental research, related to production of new materials, technologies well ecological issues.

A. Amanzhan^{1,3*}, E.E. Schultz², B.S. Adekenov¹,
O.V. Maslova¹, M.K. Ibraev³, S.M. Adekenov¹

¹Research and Production Center “Phytochemistry”, Karaganda, Kazakhstan

²N.N. Vorozhtsov Novosibirsk Institute of Organic Chemistry of the Siberian Branch of
Russian Academy of Sciences, Novosibirsk, Russia

³Karaganda Buketov University, Karaganda, Kazakhstan

*e-mail: asel.amanzhan@mail.ru

(Received 05 May 2025; received in revised form 05 June 2025; accepted 16 June 2025)

Synthesis of new acetylharmin derivatives and their neurotropic activity

Abstract: Alkaloids containing a β -carboline fragment are of significant interest as potential new physiologically active agents for the treatment of central nervous system disorders. The roots of *Peganum harmala* L. (family *Zygophyllaceae*) are a promising and readily available raw material for the production of active pharmaceutical substances. The β -carboline alkaloid harmine is a promising compound for the development of novel, original neurotropic drugs based on these alkaloids. The article considers the ways of synthesizing new compounds based on the alkaloid harmine and, simultaneously, studies the neurotropic activity of new harmine derivatives containing various substituents at the C-8 position. Harmine was selectively acetylated at the 8-position using acetyl chloride and tin tetrachloride, yielding 8-acetylharmin. This intermediate was then used to synthesize a series of novel harmine derivatives, including 8-{Z}-1-{Z}-(1-(arylidene)hydrazono)ethyl and 8-cinnamoyl analogs. The evaluation of the neurotropic action of samples of C-8 harmine derivatives was carried out on models of experimental stress using the “Open Field” and “Elevated Plus Maze” tests. Several compounds exhibited marked antidepressant activity with sedative effects comparable to those of amitriptyline. It was demonstrated that structural modifications at the C-8 position of harmine contribute to the generation of new pharmacophores capable of crossing the blood-brain barrier and modulating behavioral responses. In particular, the compounds 8-acetylharmin (2) and {(Z)-1-[(Z)-(2-arylidene)hydrazono]ethyl}-harmine (4–5), at a dose of 10 mg/kg, demonstrated behavioral features indicative of reduced anxiety levels in animals. These findings highlight the potential of β -carboline-based harmine derivatives for the development of novel neurotropic agents.

Key words: β -carbolines, harmine, 8-acetylharmin, (Z)-hydrazono-8-acetylharmin, chalcone derivatives of harmine, neurotropic activity.

Introduction

According to epidemiological data, one in four individuals worldwide will face a neurodegenerative disease during their life, and there is a steady increase in the number of these diseases [1]. Neurodegenerative disorders are multifactorial in origin and have been linked to genetic predispositions, disruptions in cellular signaling pathways, programmed neuronal cell death (apoptosis), inflammatory mechanisms, accumulation of misfolded protein aggregates, mitochondrial impairment, oxidative damage, aging processes, sex-specific factors, genetic mutations, ethnic background, environmental influences, and potentially climate-related conditions [2–4].

There is a broad spectrum of neurotropic (neuroprotective) drugs that reduce anxiety and enhance stress resilience. Modern neuroprotectors are compounds with potential effects on different parts of the nervous system in cases of impaired blood supply and myocardial function disorders: AMPA-receptor antagonists (Zonanel, Japan), serotonin agonists (Ripinotan, Piclozotan), membrane modulators (Ceraxon, Spain), and others [5].

Plant alkaloids are widely known as a consistent source of drugs for the treatment of chronic diseases, and possessing properties of polypharmacological modulation, they are potentially useful for the further development of targeted drug agents [6–8]. Harmine (1), an alkaloid belonging to the group

of biologically active compounds, exhibits a wide range of pharmacological properties, including vasodilatory, anti-inflammatory, analgesic, antimicrobial, antioxidant, cholinesterase-inhibiting, antiparkinsonian, antitumor, anti-addictive, and antidepressant activities. These diverse effects have been summarized in several systematic reviews [9–13]. Despite its broad spectrum of established biological activities, the molecular mechanisms underlying harmine's pharmacological actions remain insufficiently elucidated. Recent findings indicate that harmine may exert its pharmacological effects by interacting with a variety of molecular targets, such as monoamine oxidases A and B, benzodiazepine receptors, GABA-A receptors, serotonin receptors of the 5-HT_{2A/C} subtypes, glutamatergic receptors including NMDA and GLT-1, imidazoline receptors (I1 and I2), as well as by modulating the expression and activity of neurotrophic factors [14–20]. Moreover, harmine (1) has been reported to suppress Tau protein phosphorylation through the inhibition of DYRK1A kinase activity, a mechanism that correlates with enhanced memory, spatial learning, and overall cognitive performance in APP/PS1 transgenic mice, as well as in rodent models of scopolamine-induced cognitive deficits [21, 22]. Interestingly, in the late 1920s and early 1930s, harmine hydrochloride was used to treat symptoms of Parkinson's disease such as muscle rigidity, depression, memory deficits, apathy, phobias, fatigue, and attention problems [23]. With respect to its therapeutic potential in the central nervous system (CNS), recent preclinical research has validated the antidepressant properties of harmine (1) [14,18]. More basic and clinical research is needed to elucidate the neurochemical mechanisms underlying these effects.

We have previously studied the pharmacological properties of harmine hydrochloride and established its antidepressant activity [24–27]. The alkaloid harmine (1) is an available metabolite of *Peganum harmala* L., which is widespread in the territory of South Kazakhstan, where its industrial reserves are available [28].

The availability of domestic raw materials for the isolation of the β -carboline alkaloid harmine (1), its high biological activity, and the presence of reaction centers in the molecule make it promising for further targeted chemical modifications. To study the effect of various substituents in the indole fragment of the alkaloid on the pharmacological activity, we carried out a chemical modification with the introduction of various substituents in the C-8 position of the alkaloid harmine (1).

Materials and methods

Reagents and chemicals

All used chemicals (analytical grade) were purchased from E. Merck (Darmstadt, Germany) and Sigma Chemical Co. (Sigma-Aldrich Chemie GmbH, Steinheim, Germany) and were used without further purification. These chemicals are as follows: ethanol ($C_2H_5OH \geq 96\%$), methanol ($CH_3OH \geq 99.8\%$), tin (IV) chloride ($SnCl_4 \geq 98\%$), acetyl chloride (CH_3COCl), methylene chloride (CH_2Cl_2), hydrazine hydrate ($NH_2NH_2 \cdot H_2O$, 50 v/v %), anisaldehyde ($CH_3OC_6H_4CHO \geq 96\%$), 2-fluorobenzaldehyde ($FC_6H_4CHO \geq 97\%$), sodium hydroxide ($NaOH \geq 98\%$), hydrochloric acid ($HCl \geq 36\%$), ethyl acetate ($CH_3COOC_2H_5 \geq 99.5\%$), 2,4-dimethoxybenzaldehyde ($2,4-(CH_3O)_2C_6H_3CHO \geq 97\%$), 2,3,4-trimethoxybenzaldehyde ($(CH_3O)_3C_6H_2CHO \geq 97\%$).

The IR spectrum was recorded on the Avatar 360 ESP device from Thermo Nicolet (Madison, WI, USA) in pellets with KBr.

UV spectra were obtained on a Cary 60 UV-Vis spectrometer in EtOH solutions (10^{-4} mol/L).

HPLC was performed on an Agilent 1100 Series liquid chromatograph (USA) equipped with a QuatPump G1311A pump, a Rheodyne injection valve with a 20 μ l loop, a G1322A column holder, and a G1314A UV detector. For all analyses, a 15 cm \times 0.46 cm Zorbax SB-C18 column with 5 μ m particles (Agilent, Santa Clara, CA, USA) and the following solvents were used: methanol, acetonitrile, and water (analytical reagents with a purity of at least 99.9% obtained from Sigma-Aldrich (Merck-Millipore, St. Louis, MO, USA)).

1H NMR and ^{13}C NMR spectra were recorded by using JEOL JNM-ECZR 500 MHz (1H , 500.16 MHz, ^{13}C , 125.76 MHz). The ^{19}F NMR spectrum of compound 5 was recorded on a JEOL JNM-ECZR 500 MHz spectrometer (282 MHz) in $CDCl_3$.

Silufol TLCP-AI A-UF TLC plates manufactured by Imid (Krasnodar, Russia) were used for thin layer chromatography. The compounds were visualized by developing plates through spraying them with a saturated $KMnO_4$ solution.

Column chromatography was performed on Al_2O_3 (II degrees, Acros, The pore diameter is between 0.035 and 0.070 mm and is 6 nm) using a sum of substances-to-sorbent ratio of 1:20. The purity of the synthesized compounds was controlled by thin-layer chromatography (TLC) and HPLC data.

Plant material

The object of the study was the roots of *Peganum harmala* L., collected in the surroundings of the village of Akshi, Almaty region, Republic of Kazakhstan. Herbarium samples were stored in the herbarium fund of "Research and Production Center "Phytochemistry" (Karaganda, Kazakhstan). Raw materials of the roots of *Peganum harmala* L. were dried by the air-shadow method and ground. The grinding particle size is 2.5 mm.

Air-dried crushed roots of *Peganum harmala* L. after alkalization, were extracted with 96% ethanol on a P-250 percolator (manufactured by Artlife, Tomsk, Russia) for 3 hours with stirring. Liquid extracts were combined and evaporated on a Pilotvap-50 rotary evaporator (Genser Scientific Instruments, Germany).

In this study were investigated various process parameters influencing the yield of extractive substances. The following variables were considered: the ratio of plant material to solvent (X_1), extraction duration per cycle, number of extraction cycles (X_3), extraction temperature (X_2), particle size of the raw material (X_4), and the presence or absence of pre-alkalization (X_5). Based on theoretical principles of equilibrium extraction, the experimental ranges were established as follows: X_1 – from 1:10 to 1:20; X_2 – from 55 to 65 °C; X_3 – from 1 to 3; X_4 – from 2 to 10 mm; X_5 – with or without pre-alkalization. These ranges were determined based on preliminary experimental data. The optimization criterion (Y) was the total yield of extractive compounds.

The quantification of harmine in the extracts was performed using high-performance liquid chromatography (HPLC) on an Agilent 1100 system (Agilent Technologies, USA). This system offers a high level of sensitivity and precision when analyzing complex plant-derived compounds. Chromatographic separation of components was performed using a Zorbax SB-C18 column (geometric parameters: 4.6 × 150 mm) packed with a sorbent with a particle size of 5 µm. The mobile phase, consisting of acetonitrile and 0.1 M aqueous ammonia solution in a volume ratio of 1:1, was eluted at a flow rate of 0.5 mL/min. Analytical signals were recorded at a wavelength of 301 nm. During analysis, the column was maintained at ambient (room) temperature. The injection volume was 20 µL.

Each determination was carried out in triplicate. The resulting set of quantitative data was subjected to statistical analysis. To assess the statistical significance of the observed differences between the study groups, Student's *t*-test was applied; differences

were considered significant at $p \leq 0.05$. Data collection, processing, and graphical representation were carried out using Microsoft Excel.

Synthesis of 8-acetylharmines (2). We cooled the solution of harmine (1) (14.5 mmol) to 0 °C, and then we added acetyl chloride (29 mmol) dropwise under stirring to the cooled solution of harmine. We followed this with the gradual addition of tin (IV) chloride (9.5 mmol). So, we left the reaction mixture for 16 hours at room temperature, giving it a good stir every now and then. Once it was finished, the blend was thinned with 100 µL of methylene chloride, rinsed successively with H₂O (3 × 20 µL), and desiccated over anhydrous magnesium sulfate. So, we took the crude product and purified it using column chromatography on aluminium oxide, and we used chloroform as the eluent. A white microcrystalline powder with a melting point of 152–153 °C was obtained by recrystallizing the purified compound from ethyl acetate. The yield was 2.21 g (85%).

Synthesis of Z-hydrazono-8-acetylharmines (3). A solution of compound 2 (0.5 g, 1.96 mmol) in 25 mL ethanol was treated with excess hydrazine hydrate (2.94 g, 0.06 mol) under stirring. The reaction mixture was heated to 60 °C and stirred for 7–8 h. The resulting precipitate was filtered and recrystallized from ethanol. Yield: 69%, yellow microcrystalline powder, mp 207–209 °C. Molecular formula 8-acetylharmines – C₁₅H₁₆N₄O.

General procedure for the preparation of azines (Z,Z) of configuration (4,5). A methanolic solution of hydrazone (3) (0.37 mmol) was combined with the corresponding aromatic aldehyde (anisaldehyde or 2-fluorobenzaldehyde). The reaction mixture was stirred at 60–65 °C for four hours. Upon completion, the resulting product was purified by recrystallisation from ethanol. Yields of the target compounds ranged from 56% to 82%.

General procedure for the synthesis of 3-(aryl)-1-(1-methyl-7-methoxy-9H-β-carbolin-8-yl)prop-2-en-1-ones (6,7). A solution of 2 mmol of compound (2) and 2.1 mmol of the corresponding aromatic aldehyde (2,4-dimethoxybenzaldehyde, 2,3,4-trimethoxybenzaldehyde) in approximately 15 µL of ethanol was treated with 5 µL of 25% aqueous NaOH at room temperature. The reaction mixture was stirred for 3 hours at a constant temperature of 25 °C. The reaction mixture was subjected to agitation for a period of three hours at a temperature of 25 °C, followed by a subsequent hour of agitation at 60 °C. Then, after it had cooled, we neutralized the mixture with concentrated hydrochloric acid. The resulting solid was then recrystallized using

ethyl acetate. When obtaining chalcones (6, 7), the precipitate formed after neutralization is separated and chromatographed on silica gel using chloroform as the eluent. The part of the substance that we were looking for was separated again from a liquid called ethyl acetate.

Model of neurotropic action

Emotional stress was modelled by placing rats in tight plastic cylinders and immersing them up to their necks in water at 20–22 °C for two hours a day for four days. [29]. The studied substances (1,2,4,5,6) at a dose of 10 mg/kg were administered intragastrically through a tube to the animals for seven days before modeling emotional stress, and then daily, 1 hour before placing the animals in the plastic cylinders. The use of amitriptyline (10 mg/kg, p.o.) as a reference drug was according to the same regimen. All compounds were administered as aqueous solutions. The volume was 1 mL/kg body weight. The reference drug was administered in the same way. Four days after the start of the stress protocol, the behavior of the animals was evaluated using the Open Field Test (OFT) and the Elevated Plus Maze (EPM). These are both widely recognized behavioral assays, as described in the literature [30–36]. Experiments were conducted on 80 adult male outbred white rats weighing 240–380 g, randomly divided into 8 groups (n = 10 per group).

Statistical Analysis

All calculations were carried out using Statistica 8.0. Results were presented as mean±standard error

of the mean (SEM). Differences between groups were evaluated with the nonparametric Mann–Whitney U test [37].

Ethical approvals

The study adhered to the European Convention for the Protection of Animals Used for Experimental and Other Scientific Purposes, as well as institutional and national regulations governing research with new pharmaceuticals. There is a conclusion from the ethical committee of the NJSC “Karaganda Medical University” № 13, Protocol No. 2 dated 05/08/19. Experimental animals were obtained from the animal facility of the Research and Production Center “Phytochemistry” and maintained under standard conditions with ad libitum access to food and water.

Results and discussion

Previously, the extraction of alkaloids from *Peganum harmala* L. for the production of harmine (1) was primarily carried out using maceration. However, this method presents several limitations, the most significant of which is the extended duration of the process. [38–40]. To enhance the efficiency of alkaloid extraction, we designed an experimental matrix incorporating variation of the key extraction parameters (Table 1). The selection of factor ranges for the extraction process was based on preliminary experimental data. The optimization criterion (Y) was defined as the total yield of extractive substances.

Table 1 – Planning matrix and experimental part

№	X ₁	X ₂	X ₃	X ₄	X ₅	Y _{mean} , % (n=3)
1	1:10	65	1	2-3	Treatment with 5% Na ₂ CO ₃ solution	10.25
2	1:15	65	1	7-8		10.6
3	1:20	65	1	7-8		11.0
4	1:20	65	1	2-3		12.0
5	1:10	65	2	7-8		12.9
6	1:20	65	2	7-8	No treatment	9.55
7	1:20	60	2	7-8		7.27
8	1:20	55	3	7-8		7.22

As shown in Table 1, pretreatment of the plant material with a saturated sodium carbonate solution significantly improved the extraction efficiency. This step facilitates the conversion of target alkaloids into their free base forms, thereby enhancing their solubility in the extraction solvent. Even under

otherwise optimized conditions (e.g., solvent-to-material ratio of 3:1), the total yield of extractive substances did not exceed 9.55% in the absence of pretreatment. Furthermore, due to the dense structure of *Peganum harmala* L. roots, the degree of material pulverization was identified as another critical

parameter affecting extraction efficiency. When the raw material was milled to a particle size of 2–3 mm, the overall yield of extractive substances reached 12.9% (in relation to the air-dried plant mass).

Using the experimental data, three mathematical models were developed based on second-order polynomial equations to represent the effects of the chosen variables on extraction efficiency:

$$Y = -11.03 + 0.74X_1 + 0.456X_2 - 133.8X_3 + 0.7375X_4 + 2.995X_5 - 0.255X_1 \cdot X_4 \quad (1)$$

$$Y = -21.6975 + 2.051X_1 + 0.456X_2 - 36.6X_3 + 0.7375X_4 + 3.905X_5 - 12.96X_1 \cdot X_3 - 0.225X_1 \cdot X_4 \quad (2)$$

$$Y = -8.7375 + 0.755X_1 + 0.456X_2 - 166.2X_3 + 2.5025X_4 + 3.905X_5 - 0.225X_1 \cdot X_4 + 32.4X_3 \cdot X_4 \quad (3)$$

The experimental and calculated data were compared based on the calculated models (Table 2).

As can be seen from Table 2, models 2 and 3 show the greatest convergence with the experimental data, compared with model 1 (Figure 1). This improved agreement is attributed to the inclusion of additional interaction terms: $+k \cdot X_1 \cdot X_3$ in Model 2 and $+k \cdot X_3 \cdot X_4$ in Model 3, which enhance the models' predictive accuracy by accounting for synergistic effects between the respective variables.

Table 2 – Comparison of experimental and calculated data on the yield of total extractive substances from *Peganum harmala* L.

№ of experiment	Experimental values, %	Mathematical model 1, %	Mathematical model 2, %	Mathematical model 3, %
1	10.25	10.25	10.25	10.25
2	10.6	10.6	10.6	10.6
3	11.0	10.925	11.0	11.0
4	12.9	12.825	12.9	12.9
5	12.9	15.06	12.9	12.9
6	9.55	9.395	9.55	9.55
7	7.27	7.115	7.27	7.27
8	7.22	7.065	7.22	7.22

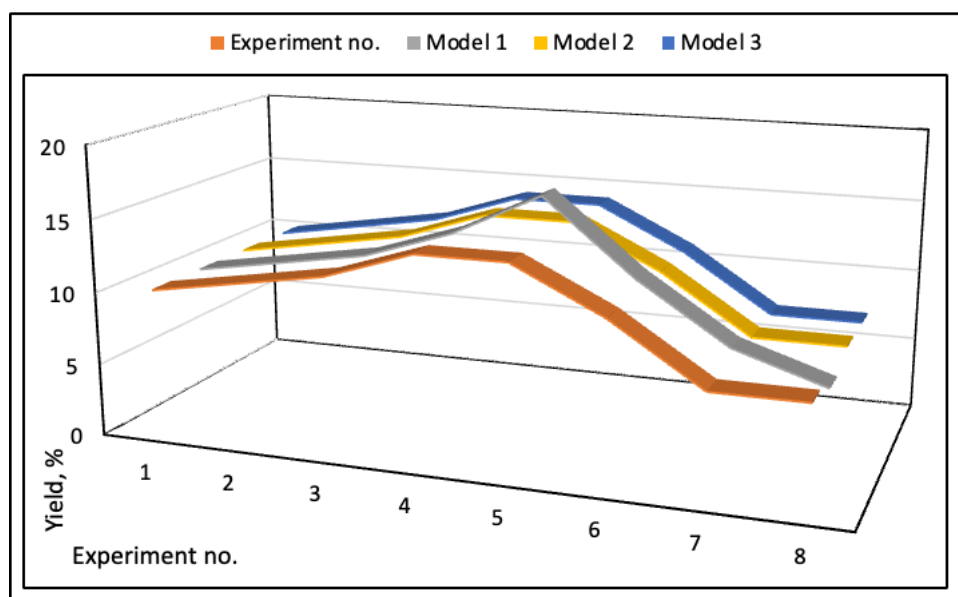


Figure 1 – Comparison of calculated and experimental data

It can therefore be concluded that the optimal extraction mode was represented by the conditions of Experiments № 4 and № 5 (Figure 2).

As can be seen from the data presented in Figure 2, the quantitative extraction of harmine (1) (up to 97% of the content in air-dried raw materials), as

well as the number of extractive substances from the roots of *Peganum harmala* L., is observed with double percolation at a temperature of 65°C for 3 hours; the degree of grinding of the raw material is 2-3 mm, the ratio of raw material to extractant is 1:10 (experiment No. 5).

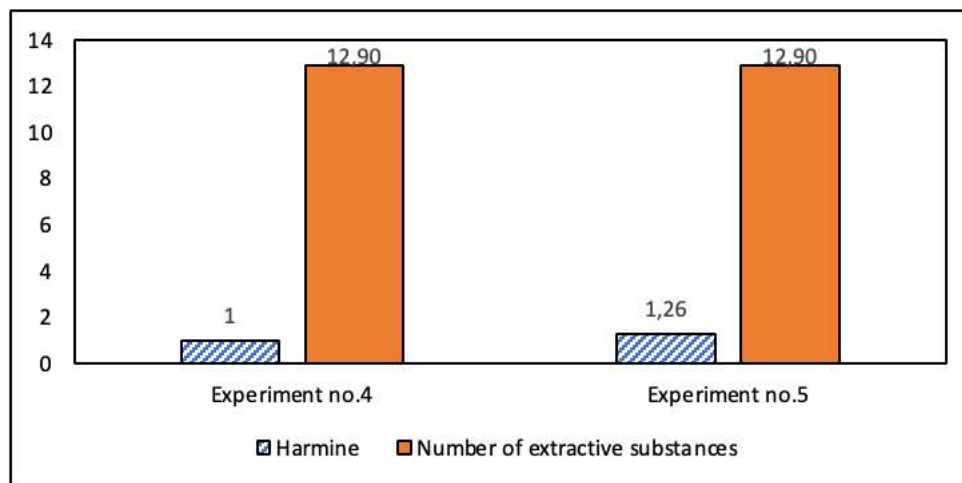


Figure 2 – Relationship between the extraction method and both the yield of harmine (1) and the quantity of extractive substances

Harmine (1) is a widely used renewable material – a substrate for the synthesis of new biologically active compounds [41-42].

β -Carboline alkaloid harmine (1) is easily acylated with acetyl chloride in the presence of SnCl_4 to form 8-acetylharminine (2) (yield 81%), which was used as a starting compound for the synthesis of derivatives (3-7).

We have studied the interaction of 8-acetylharminine (2) with hydrazine hydrate. Hydrazinolysis of 8-acetylharminine (2) in an alcohol medium at a reaction mixture temperature of 60°C proceeds stereoselectively with the formation of (Z)-8-(1-hydrazono)ethylharminine (3) (yield 69%). It has been shown that (Z)-8-(1-hydrazono)ethylharminine (3) readily enters into a condensation reaction with aromatic aldehydes (2-fluorobenzaldehyde and anisaldehyde) with the formation of the corresponding unsymmetrical disubstituted hydrazines (Z,Z) of the (4,5) configuration (yield 56 and 82%, respectively) (Figure 3).

The structure of all compounds was established based on elemental analysis and spectral data (UV, IR, ^1H , ^{13}C , ^{19}F NMR- spectrum).

The ^1H NMR spectrum has shown a singlet signal for the acetyl group protons (CH_3CO) at around 2.42 ppm. The ^{13}C NMR spectrum of compound (2) has shown the signals of the carbon atom of the $\text{C}=\text{O}$ group at δ 200.5 ppm and the methyl group CH_3CO at 20.4 ppm, which are characteristic of the specified substituent.

The characteristic signals of the NH_2 group of (Z)-8-(1-hydrazono)ethylharminine (3) were observed in a weak field in the region of δ 8.03 and 8.05 ppm as a singlet. The signals of the carbon atoms of (Z)-8-(1-hydrazono)ethylharminine (3), belonging to the $\text{CH}_3\text{C}=\text{N}$, $-\text{CH}_3$, $-\text{OCH}_3$ groups, appear in the region of δ 18.51, 21.94, 55.55 as quartets, the carbon atom $\text{C}=\text{N}$ was represented by a singlet at δ 145.95 ppm. The structures of azine derivatives (4, 5) were assigned as (Z,Z)-configured isomers based on analysis of their PMR and ^{13}C -NMR spectra. A notable high-field shift of the benzyldene proton signal in the PMR spectra (δ = 8.43–8.73 ppm) supported the assignment of an asymmetric 2,3-diazine structure in the (Z,Z) configuration. In contrast, the corresponding (Z,E)-isomers typically exhibit this proton signal at δ \approx 9.26 ppm, further corroborating the (Z,Z) configuration of

compounds 4 and 5. The doublet of the carbon atom $\text{CH}=\text{N}$ was located at δ 150.43–157.20 ppm, the singlet of the $-\text{C}=\text{N}$ group in the substituent at the

C-8 atom is shifted downfield relative to the location in the spectrum of hydrazone (3) and was detected at δ 163.59–167.68 ppm.

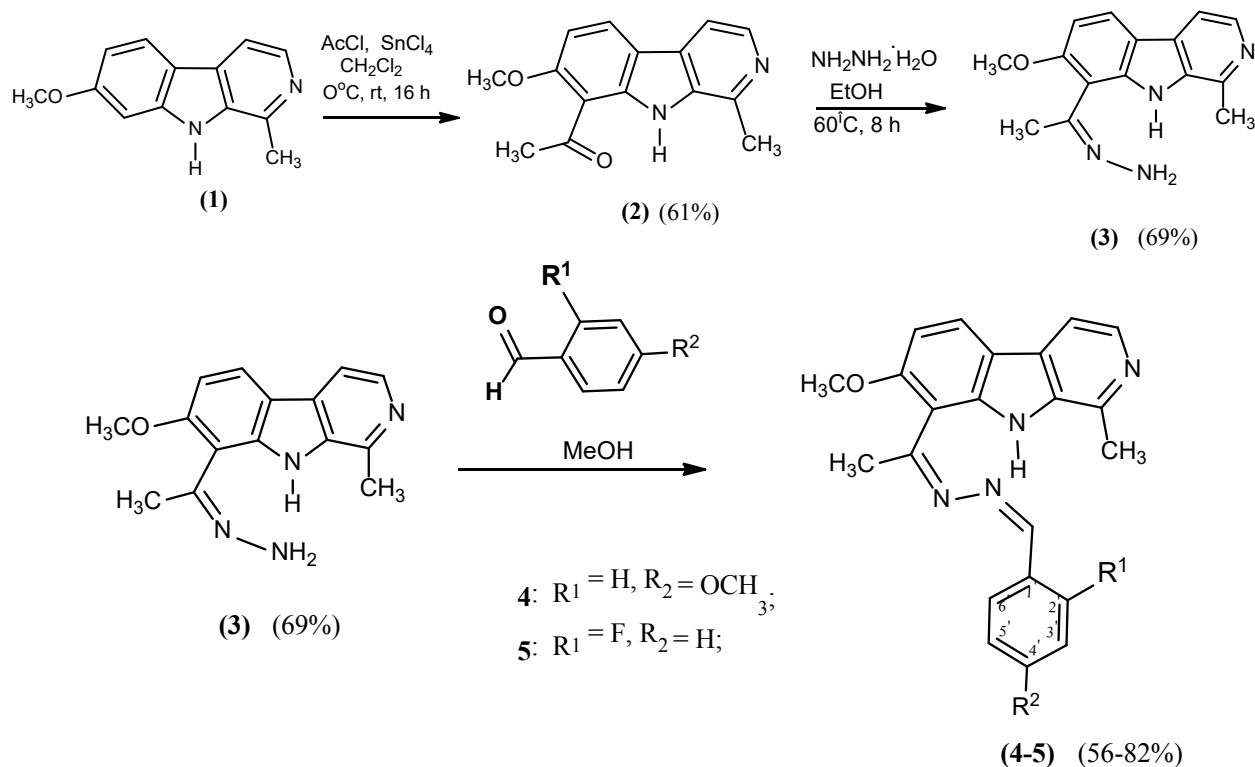


Figure 3 – Chemical modification scheme of (Z)-8-(1-hydrazono) ethylharmine and its (Z,Z)-disubstituted hydrazines

The synthesis of the corresponding chalcones – (E)-arylacryloylharmines or cinnamoyl-substituted harmine derivatives (6-7) – the synthesis (yield 90–95%) was

performed via the Claisen–Schmidt condensation of compound 2 with aromatic aldehydes in ethanol, using an aqueous NaOH solution (Figure 4).

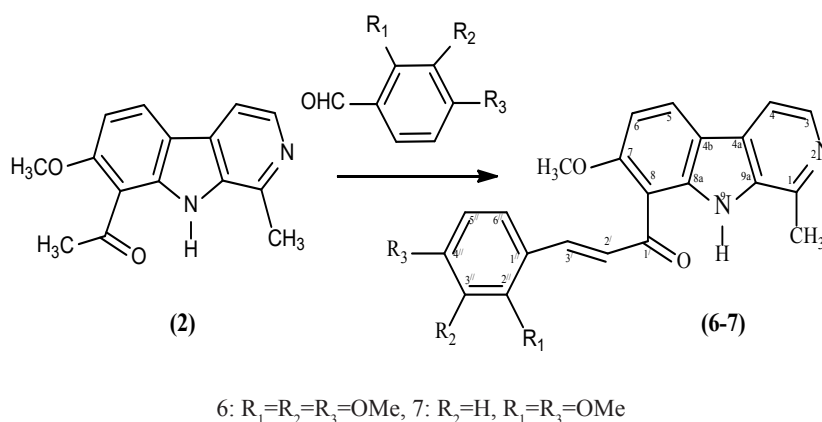


Figure 4 – Synthesis of new 8-arylacryloyl derivatives of harmine

The signals characteristic of the protons of the trans-substituted double bond (CH=CH) were observed as two doublets in the region of 7.42–7.96 and 7.87–8.17 ppm and overlap with the signals of the protons of the aromatic system, the chemical shifts of which are observed in the region of 6.90–8.32 ppm. The values of the spin-spin interaction constants of the protons belonging to the 2', 3' multiple bond in the PMR spectrum ($JH\alpha-H\beta = 15\text{--}16\text{ Hz}$) indicated that the chalcones were formed in the form of geometrically pure trans isomers.

Consequently, in terms of searching for new pharmacologically active compounds based on the β -carboline alkaloid harmine, a synthesis of harmine derivatives containing various substituents at position C-8 was carried out.

The neurotropic activity of newly synthesized harmine derivatives was evaluated *in vivo*. Experimental groups 1–5 received harmine (1), 8-acetylharmine (2), {(Z)-1-[(Z)-(2-arylidene)hydrazono]ethyl}-7-methoxy-1-methyl-9H-pyrido[3,4-b]indoles (4, 5), and (E)-3-aryl-1-(1-

methyl-7-methoxy-9H- β -carbolin-8-yl)prop-2-en-1-one (6), each at a dose of 10 mg/kg. Group 6 served as the comparison group and received the reference drug amitriptyline at 10 mg/kg under the same administration schedule, 7 control group – animals that received the solvent, and Group 8 included intact animals maintained on a standard diet without experimental intervention. All substances, including the reference drug, were administered orally as aqueous solutions.

The animals were kept in standard vivarium conditions, with free access to food and water, and fed a normal diet. In addition, the general condition of the animals was observed, including changes in body weight, motor activity, appetite and response to external stimuli [29–36].

Throughout the experiment, the animals' general condition, behavioral characteristics, motor activity intensity and nature, hair and mucous membrane condition, and food and water consumption were regularly recorded. Table 3 shows the dynamics of the increase in body weight of the animals in all groups.

Table 3 – Variability in rat weight gain during for seven days

Group	Number of animals	Weight, g	
		Before	After
Intact rats	10	262.9 \pm 33.2	275.9 \pm 34.8
Control (No treatment)	10	260.8 \pm 29.7	278.8 \pm 29.7
Comparison group (amitriptyline)	10	252.5 \pm 62.8	265.5 \pm 61.8
(1)	10	303.3 \pm 53.0*	307.3 \pm 49.6*
(2)	10	287.5 \pm 18.6	291.3 \pm 24.3
(4)	10	355.3 \pm 24.2	365.3 \pm 34.2
(5)	10	382.5 \pm 36.5	371.5 \pm 46.1
(6)	10	371.8 \pm 50.6	379.8 \pm 49.6

Note: * indicates statistically significant differences ($p < 0.05$) compared with the control group

No significant deviations in weight gain were observed across the experimental groups, indicating that the tested compounds did not induce adverse systemic effects or metabolic disturbances.

Changes in behavioral responses in the "Open Field" test.

It was found that the animals that received compounds (1-6) had changes in the indices of motor activity (horizontal and vertical movements). At the same time, the motor activity of animals that received harmine (1) significantly decreased in both tests compared to the control group of animals,

the group of intact rats and the group that received amitriptyline. The orientation-exploratory activity of compounds containing arylidenehydrazone substituents (5,6) remained at the level of the amitriptyline group. For 8-acetylharmine (2) and its chalcone (6), a reliable (3-fold) decrease in vertical motor activity was observed while maintaining activity in horizontal movement. In animals receiving amitriptyline and compounds containing an arylidenehydrazone substituent at position C-8 of harmine, the anxiety level in terms of grooming episodes (number of washings) decreased, however,

in terms of the number of acts of bowel movements and urination, the anxiety level indicator was at the level of the control group animals. A reliable change in the anxiety level was observed for animals receiving the chalcone derivative of harmine (6); the number of grooming episodes significantly

increased by an order of magnitude, compared with the group of animals receiving amitriptyline and 4 times compared with the control group), which can serve as an indirect criterion for an increase in anxiety in the group of animals receiving the chalcone derivative of harmine (6) (Table 4).

Table 4 – Effect of the test compounds on rat behavior in the Open Field test

Group	Number of animals	Spectrum of exploratory and research activity		The spectrum of anxiety		
		Number of horizontal movements	Vertical motor activity	Number of grooming episodes	Number of bowel movements	Number of urinations
Intact rats	10	28.3±6.58*	10.7±3.1	1.8±1.6	0.8±0.8	0.6±0.8
Control (no treatment)	10	19.7±4.66*	12.3±3.65*	1.5±1.2	0.3±0.7	0.4±0.5*
Comparison group (amitriptyline)	10	22.6±3.1	14.0±3.0	0.4±0.7*	0.9±1.4	0.5±0.7
(1)	10	8.0±3.2	5.8±2.1	3.8±1.7	2.7±1.4	0.2±0.5
(2)	10	17.0±5.9	4.5±2.5	1.0±0.8	0.3±0.5	0.3±0.5
(4)	10	25.0±11.6*	11.3±3.9	0.3±0.5*	2.0±1.7	1.3±1.3
(5)	10	24.0±6.5*	9.0±3.9	0.0±0.0	0.8±1.5	1.0±1.2
(6)	10	17.8±5.1	4.3±3.3*	5.3±1.3*	2.5±1.6	0.5±0.6

Note: * $p < 0.05$ compared to values in animals of the control group

Assessment of Exploratory Behavior Using the Elevated Plus Maze Test

To further evaluate the exploratory behavior and anxiety-related responses of rats, the elevated plus maze (EPM) test was employed. We recorded how long the rats spent in the open and closed arms, how long they spent on the middle platform, how many times they went into the open and closed arms, how many times they moved their heads up and down, how many times they stretched (rose up on their backs), and how many times they pooped and peed. The results are summarized in Table 5.

As per the statistics displayed, creatures administered harmine (1) demonstrated a considerably elevated quantity of entries into the closed arms ($p > 0.05$) in comparison to the time spent in the open arms. In addition, the number of head dips and the duration of time spent on the central platform were markedly reduced. A statistically significant threefold increase was observed in the time spent in the closed arms, indicating enhanced anxiety-

like behavior in this group. Thus, the introduction of harmine (1) contributed to a significant increase in the anxiety of animals, compared with the animals of the intact group. The introduction of an acetyl, 4-fluorobenzylidenehydrazone substituent (compounds 2, 4) at the C-8 position of harmine significantly reduced the anxiety activity of animals and significantly increased their activity by increasing the time spent in the open arms and on the central platform. It should also be noted that the orientation-exploratory activity of animals receiving 8-substituted harmine derivatives (time spent in the closed and open sleeve and on the central platform, number of defecations and urinations) was at the level of activity of animals receiving amitriptyline. However, the activity of experimental animals was lower than that of intact animals, and significantly depended on the nature of the substituent in the hydrazone and chalcone fragments (comparison of groups receiving compounds 4 and 5 or 6).

Table 5 – Effect of the studied compounds on the behavior of rats in the elevated plus maze test

Group	Time spent in closed sleeve, (sec.)	Time spent in open sleeve, (sec.)	Number of entries into open sleeves (times)	Number of entries into closed sleeves (times)	Number of peeks, (times)	Number of hangings (times)	Number of rearings (times)	Time spent on the central platform, (sec.)	Number of bowel movements	Number of urinations
Intact rats	12,5±19,8*	116,8±23,1*	4,0±2,2	0,8±0,7	3,0±2,4	5,5±1,7	0,3±0,5	50,8±37,8*	0	1,0±0,2
Control (no treatment)	108,7±32,1	21,1±29,1	0,9±0,87*	4,3±1,3	2,0±2,3	4,0±3,5*	0,8±1,75	50,2±27,7	0	0,3±0,48
Comparison group (amitriptyline)	107,3±26,3*	26,7±25,28*	1,2±0,78	3,2±1,4	5,0±2,2	2,9±1,85	0,6±1,3	46,0±19,4*	0,2±0,6	0,1±0,3
(1)	167,0±8,7*	13,0±8,7	1,5±0,6	1,5±0,6	0,3±0,5	1,8±1,7	8,0±3,2	0,5±1,0	0,3±0,5	0,3±0,5
(2)	141,3±40,1	33,5±15,4	1,0±0,8	1,3±0,5	3,0±3,2	4,3±1,5	0	3,5±1,9	0	0,3±0,5
(4)	127,0±5,3*	51,5±18,0	0,9±0,6	1,3±0,5	3,0±1,2	1,5±1,0	0	18,5±8,5	0,5±1,0	0
(5)	135,3±12,8	15,0±2,9	0,3±0,5	2,5±0,6	1,8±2,4	2,0±2,4*	0,3±0,5	10,8±6,9	1,3±1,9	0,3±0,5
(6)	155,0±16,5	9,0±3,7	1,0±0,8	2,5±0,6	2,5±1,3	1,3±1,5	0	6,3±3,3*	0,5±0,6	1,0±1,4

Note: * p<0.05 versus control group; n denotes the number of animals in each group

The anxiolytic activity of the samples in the experimental rat groups was evaluated based on the data presented in Table 5. The anxiety index calculation formula was used to assess the anxiolytic effect. The anxiety index values range from 0 to 1, with an increase in the index indicating increased anxiety-like behavior [27].

An anxiolytic effect was demonstrated in the group of animals that received substances (1), (2), (4), (5) and (6) at a dose of 10 mg/kg, when compared with the control group, under conditions of experimental emotional stress.

In particular, the time spent in the closed arm in group (2) decreased by 12.4%, in group (5) by 17.3%, in group (4) by 12.4% compared to the control group. Administration of the studied compounds, harmine (1) and (2), to rats reduced the number of entries into the closed arms. Introducing compound (2) also increased the number of peeks. The number of hangings increased in group 2. The number of defecations and urinations decreased in group 2.

The average time that the animals spent in the open arms of the apparatus in group 5 was 51.5 ± 18.0 seconds, in group 2 was 33.5 ± 15.4 seconds. The number of entries into the open arms in group 5 was slightly higher than in the control group. Administering the studied compounds (4), (5) and (6) to the animals reduced entries into the closed arms by 41.9%, 69.8% and 41.9% respectively. Group (5) spent an average of 18.5 ± 8.5 seconds on the central platform. For the other groups using the studied compounds, the indicators were lower.

Conclusions

This study implemented an integrated approach encompassing extraction optimization, synthetic development, and pharmacological evaluation to design and investigate novel neurotropic agents derived from the β -carboline alkaloid harmine. A second-order polynomial model effectively optimized the extraction conditions from *Peganum harmala* L. roots, with the best yield (up to 97%) achieved using double percolation at 65 °C for 3 hours, a 1:10 solvent-to-material ratio, and a particle size of 2–3 mm.

The β -carboline alkaloid harmine served as a versatile scaffold for the synthesis of novel C-8-substituted derivatives, including 8-acetylharminine, (Z)-hydrazono analogs, and cinnamoyl derivatives, with high yields and structural clarity confirmed through spectroscopic.

In vivo pharmacological testing revealed that compounds 2, 4, 5 and 6 exhibited significant anxiolytic and antidepressant activity at a dose of 10 mg/kg. In the Open Field Test, these compounds reduced anxiety-related behaviors, such as vertical activity, grooming, defecation and urination, while encouraging horizontal exploration. In the Elevated Plus Maze, compounds 2 and 4 notably increased the time spent in the open arms and on the central platform, which are markers of anxiolytic efficacy comparable to the reference antidepressant amitriptyline.

Of the compounds tested, 8-[(Z)-1-[(Z)-(2-arylidene)hydrazono]ethyl]harminine (compound 4) exhibited the most pronounced anxiolytic properties and was well tolerated. These findings emphasize the important role that C-8 substitution plays in modulating the neuropharmacological activity of harmine, and demonstrate the potential of β -carboline derivatives in the development of multi-target CNS therapeutics.

Consequently, *Peganum harmala* L. should be regarded not only as a renewable source of the biologically active compound harmine, but also as a valuable foundation for designing new neurotropic agents to treat anxiety and depressive disorders.

Acknowledgments

The work is funded by the Science Committee of the Ministry of Science and Higher Education of the Republic of Kazakhstan within the framework of the project No. AP23489904 “Phytosome development – an effective form of targeted transport of original medical compounds in the human body”.

Conflict of interest

The authors declare that they have no conflicts of interest.

References

1. Ayeni E.A., Aldossary A.M., Ayejoto D.A., Gbadegehin L.A., Alshehri A.A., Alfassam H.A., Afewerky H.K., Almughem F.A., Bello S.M., Tawfik E.A. (2022) Neurodegenerative Diseases: Implications of Environmental and Climatic Influences on Neurotransmitters and Neuronal Hormones Activities. *Int. J. Environ. Res. Public Health*, vol. 19(19), pp. 12495-12518. <https://doi.org/10.3390/ijerph191912495>
2. Ball N., Teo W.P., Chandra S., Chapman J. (2019) Parkinson's Disease and the Environment. *Front. Neurol.* vol. 10, pp. 218-225. <https://doi.org/10.3389/fneur.2019.00218>
3. Feigin V.L., Nichols E., Alam T., Bannick M.S., Beghi E., Blake N., Culpepper W.J., Dorsey E.R., Elbaz A., Ellenbogen R.G. et al. (2019) Global, regional, and national burden of neurological disorders, 1990–2016: A systematic analysis for the Global Burden of Disease Study 2016. *Lancet Neurol.*, vol.18, pp. 459–480. [https://doi.org/10.1016/S1474-4422\(18\)30499-X](https://doi.org/10.1016/S1474-4422(18)30499-X)
4. Piscopo P., Bellenghi M., Manzini V., Crestini A., Pontecorvi G., Corbo M., Ortona E., Carè A., Confaloni A. (2021) A Sex Perspective in Neurodegenerative Diseases: MicroRNAs as Possible Peripheral Biomarkers. *Int. J. Mol. Sci.* vol. 22, pp. 4423-4437. <https://doi.org/10.3390/ijms22094423>
5. Durães F., Pinto M., Sousa E. (2018) Old Drugs as New Treatments for Neurodegenerative Diseases. *Pharmaceuticals*, vol. 11(2), pp. 44-65. <https://doi.org/10.3390/ph11020044>
6. Azimova S.S., Yunusov M.S. (2013). Natural compounds. Alkaloids. New York: Springer- Reference. 821 p. ISBN-10:1461405599, ISBN-13:978-1461405597
7. Chaachouay N., Zidane L. (2024) Plant-Derived Natural Products: A Source for Drug Discovery and Development. *Drugs Drug Candidates*, vol. 3, pp. 184–207. <https://doi.org/10.3390/ddc3010011>
8. Bhambhani S., Kondhare K.R., Giri A.P. (2021) Diversity in Chemical Structures and Biological Properties of Plant Alkaloids. *Molecules*, vol. 26(11), pp. 3374-3402. <https://doi.org/10.3390/molecules26113374>
9. Javed M., Rasul A., Hussain G., Jabeen F., Rasool B., Shafiq N., Riaz A., Kaukab G., Ali M. (2018) Harmine and its derivatives: Biological activities and therapeutic potential in human diseases. *Bangladesh J. Pharmacol.*, vol. 13, p. 203-213. <https://doi.org/10.3329/bjpv.v13i3.34990>
10. Li Sh., Zhang Q., Wang Y., Lin B., Li Dahong, Hua H., Hu X. (2024) β -Carboline alkaloids from the roots of *Peganum harmala* L. *Chinese Journal of Natural Medicines*, vol. 22(2), pp. 171-177. [https://doi.org/10.1016/S1875-5364\(24\)60583-2](https://doi.org/10.1016/S1875-5364(24)60583-2)
11. Li S., Cheng X., Wang C. (2017) A review on traditional uses, phytochemistry, pharmacology, pharmacokinetics and toxicology of the genus *Peganum*. *J. Ethnopharmacol.*, vol. 203, pp. 127-162. <https://doi.org/10.1016/j.jep.2017.03.049>
12. Doskaliyev A., Seidakhmetova R.B., Tutai D.S., Galdaeva K., Surov V.K., Adekenov S.M. (2021) Alkaloids of *Peganum harmala* L. and their pharmacological activity. *Open Access Macedonian Journal of Medicinal Science*, vol. 9A, pp. 765-775. <https://doi.org/10.3889/oamjms.2021.6654>
13. Patel K., Gadewar M., Tripathi R., Prasad S.K., Patel D.K. (2012). A review on medicinal importance, pharmacological activity and bioanalytical aspects of beta-carboline alkaloid “harmine.” *Asian Pacific Journal of Tropical Biomedicine*, vol. 2(8), pp. 660–664. [https://doi.org/10.1016/S2221-1691\(12\)60116-6](https://doi.org/10.1016/S2221-1691(12)60116-6)
14. Dos Santos R. G., Osório F. L., Crippa J. A., and Hallak J. E. (2016). Antidepressive and anxiolytic effects of ayahuasca: A systematic literature review of animal and human studies. *Revista Brasileira de Psiquiatria*, vol. 38 (1), pp. 65–72. <https://doi.org/10.1590/1516-4446-2015-1701>.
15. Nunes A. A., Dos Santos R G., Osório F. L., Sanches R. F., Crippa J. A., and Hallak J. E. (2016). Effects of ayahuasca and its alkaloids on drug dependence: A systematic literature review of quantitative studies in animals and humans. *Journal of Psychoactive Drugs*, vol. 48(3), pp. 195–205. <https://doi.org/10.1080/02791072.2016.1188225>.
16. Glennon R.A., Dukat M., Grella B., Hong S., Costantino L., Teitler M., Smith C., Egan C., Davis K., Mattson M.V. (2000) Binding of β -carbolines and related agents at serotonin (5-HT₂ and 5-HT_{1A}), dopamine (D₂) and benzodiazepine receptors. *Drug and Alcohol Dependence*, vol. 60(2), pp. 121–132. [https://doi.org/10.1016/S0376-8716\(99\)00148-9](https://doi.org/10.1016/S0376-8716(99)00148-9).
17. Li Y., Sattler R., Yang E.J., Nunes A., Ayukawa Y., Akhtar S., Ji G., Zhang P.W., Rothstein J.D. (2011). Harmine, a natural beta-carboline alkaloid, upregulates astroglial glutamate transporter expression. *Neuropharmacology*, vol. 60(7–8), pp. 1168–1175. <https://doi.org/10.1016/j.neuropharm.2010.10.016>.
18. Fortunato J.J., Réus G.Z., Kirsch T.R., Stringari R.B., Fries G.R., Kapczinski F., Hallak J. E., Zuardi A.W., Crippa J.A., and Quevedo J. (2010). Effects of β -carboline harmine on behavioral and physiological parameters observed in the chronic mild stress model: Further evidence of antidepressant properties. *Brain Research Bulletin*, vol. 81(4–5), pp. 491–496. <https://doi.org/10.1016/j.brainresbull.2009.09.008>.
19. Sun P., Zhang S., Li Y., Wang L. (2014). Harmine mediated neuroprotection via evaluation of glutamate transporter 1 in a rat model of global cerebral ischemia. *Neuroscience Letters*, vol. 583, pp. 32–36. [doi:10.1016/j.neulet.2014.09.023](https://doi.org/10.1016/j.neulet.2014.09.023).
20. Göckler N., Jofre G., Papadopoulos C., Soppa U., Tejedor F. J., Becker W. (2009). Harmine specifically inhibits protein kinase DYRK1A and interferes with neurite formation. *FEBS Journal*, vol. 276 (21), pp. 6324–6337. <https://doi.org/10.1111/j.1742-4658.2009.07346.x>.
21. He D., Wu H., Wei Y., Liu W., Huang F., Shi H., Zhang B., Wu X., Wang C. (2015) Effects of harmine, an acetylcholinesterase inhibitor, on spatial learning and memory of APP/PS1 transgenic mice and scopolamine-induced memory impairment mice. *Eur. J. Pharmacol.* vol. 768, pp. 96-107. <https://doi.org/10.1016/j.ejphar.2015.10.037>
22. Li S.P., Wang Y.W., Qi S.L., Zhang Y.P., Deng G., Ding W.Z., Ma C., Lin Q.Y., Guan H.D., Liu W. (2018) Analogous β -carboline alkaloids harmaline and harmine ameliorate scopolamine-induced cognition dysfunction by attenuating acetylcholinesterase activity, oxidative stress, and inflammation in mice. *Front. Pharmacol.* vol. 9, pp. 346-361. <https://doi.org/10.3389/fphar.2018.00346>

23. Costa O.A., and Faria L.A. (1936). A planta que faz sonhar: O yagê [The plant that induces dreams: The yage]. *Revista da Flora Medicinal*, vol. 2, pp. 575–624.
24. Adekenov S.M., Salimov R.M., Abaimov D.A., Sariev A.K., Kovalev G.I. (2020). Psychopharmacological properties of harmine hydrochloride in the experiment. *Experimental and clinical pharmacology*, vol. 83, no. 3, pp. 3–6. <https://doi.org/10.30906/0869-2092-2020-83-3-3-6>
25. Nurmaganbetov Zh.S., Arystan L.I., Turmukhambetov A.Zh., et al. (2014) Antidepressant effect of harmine hydrochloride. *Pharmacy and pharmacology*, vol. 2, no. 6-7, pp. 96–98. [https://doi.org/10.19163/2307-9266-2014-2-6\(7\)-96-98](https://doi.org/10.19163/2307-9266-2014-2-6(7)-96-98)
26. Epifantseva E.V., Romanova M.A., Seidakhmetova R.B., Adekenov S.M. (2020) Effect of harmine hydrochloride on behavioral responses of rats with a model of stress-induced disorder. *Medicine and Ecology*, No. 1(94), pp. 77–88. UDC: 616.89, 615.214
27. Seidakhmetova R.B., Rakhimov K.D., Tutay D.S., Mukhanova T.T., Zholbarys A.A., Amanzhan A., Adekenov S.M. (2021) Neurotropic activity of plant alkaloids. *Bulletin of KazNU (experimental biology series)*, No. 3(88), pp. 142–153. <https://doi.org/10.26577/eb.2021.v88.i3.14>
28. Adekenov S. M., Baitulin I. O., Egeubaeva R. A., Saparbaeva N. A. (2010) The current state of natural thickets of common harmala in the territory of Southern Kazakhstan. *Izv. NAN Rep. Kazakhstan (Ser. Biol. Med.)*, No. 5, pp. 55–61.
29. Willner P. (2017) Reliability of the chronic mild stress model of depression: a user survey. *Neurobiol. Stress*, vol. 6, pp. 68–77. <https://doi.org/10.1016/j.ynstr.2016.08.001>
30. Romanenko E.B., Levitskaya N.G., Kamensky A.A. (2007) Study of the nootropic activity of Betamecine. *Experimental and Clinical Pharmacology*, vol. 70, no. 4, pp. 7 – 10.
31. Voronina T.A., Seredenin S.B. (2000) Guidelines for the study of tranquilizing (anxiolytic) action of pharmacological substances. Guide to experimental (preclinical) study of new pharmacological substances. Moscow: Remedium, pp. 126–136.
32. Koplik E.V., Salieva R.M., Gorbunova A.V. (1995) Open field test as a prognostic criterion for resistance to emotional stress in Wistar rats. *J. of higher nervous activity*, vol. 45, no. 4, pp. 775–781.
33. Walf A. A., Frye C. A. (2007). The use of the elevated plus maze as an assay of anxiety-related behavior in rodents. *Nature Protocols*, vol. 2(2), pp. 322–328. <https://doi.org/10.1038/nprot.2007.44>
34. Seibenhener M. L., Wooten M. C. (2015). Use of the Open Field Maze to measure locomotor and anxiety-like behavior in mice. *Journal of Visualized Experiments*, vol. 96, e52434. <https://doi.org/10.3791/52434>
35. Bystrova M.N., Demidova M.A., Galchinskaya I.L., Zholobov I.S. (2012) Research of influence of various medicinal forms of soothing gathering on behaviour of mice in the test «Raised crosswise labyrinth». *Modern Problems of Science and Education*, no. 2, pp. 25–28. UDC: 615.214.22:615.322
36. Khabriev R.U. (2005) Guide to experimental (preclinical) study of new pharmacological substances / edited by Corresponding Member of the Russian Academy of Medical Sciences, Professor R.U. Khabriev. 2nd ed., revised and enlarged. Moscow: OJSC “Izdatelstvo” Medicine “, 832 p. ISBN 5-225-04219-8 (in translation)
37. Nachar N. (2008) The Mann-Whitney U: A Test for Assessing Whether Two Independent Samples Come from the Same Distribution. *Tutorials in Quantitative Methods for Psychology*, vol. 4(1), pp. 13–20.
38. Vachnadze V., Suladze T., Vachnadze N., Kintsurashvili L., Novikova J. (2015) Alkaloids of *Peganum harmala* L. and their biological activity. *Georgian medical news*, N 6, pp. 79–81.
39. Shang X., Pan H., Miao X., Wang D., Wang X., Wang Y., Zhang J. (2017) Method for extracting *Peganum harmala* L. alkaloid under microwave assistance. Patent 104628731B (CN).
40. Khan F.A., Maalik A., Iqbal Z., Malik I. (2013) Recent pharmacological developments in β -carboline alkaloid harmaline. *Eur. J. Pharmacol.*, vol. 721(1-3), pp. 391–394. <https://doi.org/10.1016/j.ejphar.2013.05.003>
41. Liu W., Liu X., Tian L., Gao Y., Liu W., Chen H., Jiang X., Xu Z., Ding H., Zhao Q. (2021) Design, synthesis and biological evaluation of harmine derivatives as potent GSK-3 β /DYRK1A dual inhibitors for the treatment of Alzheimer's disease. *European Journal of Medicinal Chemistry*, vol. 222, pp. 113554–113572. <https://doi.org/10.1016/j.ejmech.2021.113554>.
42. Kumar K., Wang P., Wilson J., Zlatanovic V., Berrouet C., Khamrui S., Secor C., Swartz E.A., Lazarus M., Sanchez R., Stewart A.F., Garcia-Ocana A., DeVita R.J. (2020) Synthesis and biological validation of a harmine-based, central nervous system (CNS)-avoidant, selective, human β -cell regenerative dual-specificity tyrosine phosphorylation-regulated kinase A (DYRK1A) inhibitor. *J. Med. Chem.*, vol. 63(6), pp. 2986–3003. <https://doi.org/10.1021/acs.jmedchem.9b01379>.

Information about authors

Asel Amanzhan – PhD, JSC Scientific and Production Center “Phytochemistry” (Karaganda, Kazakhstan, e-mail: asel.amanzhan@mail.ru)

Elvira Schultz – Doctor of Chemical Sciences, Professor, N.N. Vorozhtsov Novosibirsk Institute of Organic Chemistry of SB RAS (Novosibirsk, Russia, e-mail: schultz@nioch.nsc.ru)

Bekbolat Adekenov – JSC Scientific and Production Center “Phytochemistry” (Karaganda, Kazakhstan, e-mail: adekenovbekbolat@gmail.com)

Olga Maslova – JSC Scientific and Production Center “Phytochemistry” (Karaganda, Kazakhstan, e-mail: m.olga.84@mail.ru)

Marat Ibrayev – Doctor of Chemical Sciences, Professor, Karaganda Buketov University (Karaganda, Kazakhstan, e-mail: makibr@mail.ru)

Sergazy Adekenov – Doctor of Chemical Sciences, Professor, JSC Scientific and Production Center “Phytochemistry” (Karaganda, Kazakhstan, e-mail: arglabin@phyto.kz)

O.G. Cherednichenko , A.L. Pilyugina , D.E. Azizbekova ,
A.S. Amirgaliyeva , K.B. Bespalova* 

Institute of Genetics and Physiology, Almaty, Kazakhstan

*e-mail: kira.b.bespalova@gmail.com

(Received 10 July 2024; received in revised form 30 May 2025; accepted 12 June 2025)

Genomic stability and adaptation in Kazakh Tobet dogs: a cytogenetic analysis

Abstract: There is an urgent need to preserve the ancient and culturally significant Kazakh dog breed Tobet, which is threatened with extinction. The evaluation of genomic instability and adaptive potential of Tobet dogs in comparison with outbred dogs as a model of genetic diversity and adaptability seems to be an interesting study and could shed light on the necessary efforts to improve the Tobet breed. In this context, the aim of this study was to analyze the cytological and cytogenetic (micronucleus test) parameters of peripheral blood cells of Tobet dogs and outbred dogs. The analysis revealed no significant differences in micronucleus frequency between Tobet and outbred dogs, indicating robust genomic stability. However, the observed cytological abnormalities, such as poikilocytosis, suggest potential health issues in the Tobet breed and highlight the need for continued health monitoring. This research underlines the importance of combining traditional breeding methods with modern genetic analyses to ensure the survival of the breed.

Key words: Tobet, purebred dog, outbred dog, genomic instability, adaptive potential, cytogenetic analysis.

Introduction

The Kazakh national dog breed Tobet is an ancient national, cultural and historical heritage of our country. For centuries, Tobet dogs guarded thousands of nomadic cattle, protected livestock from wolves, hunted foxes together with their owners and were even used as labourers. This breed got its name since Tobet dogs choose the highest point to have a better view of the protected area (“tobe” – a hill). Unfortunately, this unique breed has almost disappeared today. The reasons for this are the reduction in grazing areas and the decline in sheep farming, the use of other breeds as priority dogs and the use of the Tobet for dog fighting, spontaneous breeding and finally the lack of a scientific basis for breeding work. The current situation requires urgent action to preserve the Tobet breed [1].

Genetic and other modern methods have revolutionized breeding practice and provide tools for improving breed characteristics. For example, the evaluation of genomic instability and adaptive potential may be a tool that can provide valuable information to breeders. Genomic instability manifests itself as damage to genetic structures, including chromosomes (chromosomal aberrations),

under the influence of stress factors. This analysis makes it possible to favor animals with a more stable genome in breeding. This leads to more predictable and stable results in breeding recovery and selection. The purpose of evaluating the adaptive potential is to determine the genetic traits that ensure the adaptability of the population to environmental conditions. When the values of the factor exceed the optimal limits, the genetic structures of the cells are activated. Such a process is the basis for the organism’s ability to make functional changes in response to environmental influences. The evaluation of adaptive potential enables breeders to select and breed animals that are better adapted to current and future conditions [2, 3].

It should be noted that the breed often has a higher genetic homogeneity due to selective breeding practices, which can predispose it to hereditary diseases and lower adaptability. In contrast, outbred dogs generally benefit from a broader genetic pool, which can lead to greater genetic stability and resilience to certain genetic disorders. It has already been shown that, unlike purebred dogs whose genotype is controlled by strict standards, the genome of outbred dogs is the result of random crossbreeding, leading to a higher degree of genetic diversity and adaptation [4–6]. In addition, while

outbred dogs are more likely to carry deleterious mutations, these mutations are usually in a harmless heterozygous state, presumably because two carriers of the same mutation are less likely to produce offspring. In contrast, purebred dogs are more likely to be genetically affected by one of these disorders due to homozygosity for the mutation [7]. In addition, the breed often descends from a limited number of founder animals, leading to potential founder effects and a higher risk of inherited diseases as the gene pool is more limited [8]. It has been shown that analyzing dogs of a specific breed in comparison to outbred dogs can be an interesting and valuable approach for a more comprehensive evaluation of the breed [9]. Against this background and in the absence of studies on genetic instability in dogs [9–14], the evaluation of genomic instability and adaptive potential of dogs of one breed compared to outbred dogs as a model for genetic diversity and adaptability seems to be an interesting study.

In this context, the aim of this study was to analyze cytological and cytogenetic parameters of peripheral blood cells of Tobet dogs and outbred dogs. The micronucleus test was chosen for these studies because of its informative value, simplicity, and accessibility. Another advantage of the micronucleus test is its independence from karyotype. As is well known, the karyotype of dogs contains a large number ($2n=78$) of small, poorly distinguishable chromosomes [15]. Its low invasiveness and the possibility of conducting ante-mortem screening to determine the dynamics of changes in this indicator over time are also important [16].

Materials and methods

The main object of the study was Tobet dogs. The collection of biomaterials from Tobet dogs was carried out during expeditions, exhibitions, and special events. Testing for compliance with the breed characteristics of the Kazakh Tobet breed was carried out by cynologists from “KANSONAR”, who met the qualification requirements and were experts in Kazakh national breeds and in the group such as the Central Asian Shepherd Dog (CAS), to which the Tobet belongs. The main document for conducting the test and establishing the breed standard that guided the experts was the breed standard for the Kazakh Tobet, which was approved by the Order of the Ministry of ecology and natural resources of the Republic of Kazakhstan dated 30 March 2023 No. 101 “On the Approval of Standards for Kazakh Dog Breeds”.

As a control group for the study also included free-breeding, or outbred dogs, which represent the model for genetic diversity and have a high potential for adaptation. The biomaterial from outbred dogs was collected from Tailed Paradise PF, one of the largest animal shelters in Almaty, where more than 500 dogs live.

Peripheral blood to prepare a blood smear on a glass was collected from the leg vein of Tobet and mixed breed dogs by an experienced veterinarian of the research group using a vacuum tube. All sterility criteria were met.

The collection of the biomaterial was accompanied by the photography of the dogs and the questioning of their owners. The questionnaire included information about the owner, age, sex, origin, place of residence of the dog, its description, and measurements. As studies on unrelated animals are necessary to capture the maximum range of genetic diversity, detailed pedigree information was requested for all dogs. For those dogs for which pedigree information was not available, non-relatedness and/or relatedness was confirmed by owners and handlers. The data from the questionnaire was processed and entered an electronic database. In addition to the questionnaire, the owner's informed consent to carry out a genetic study on their dog was also completed.

The study was approved by the bioethics committee of the RSE at REM Institute of Molecular Biology and Biochemistry named after M.A. Aitkhozhin CS MSHE RK (Protocol No. 1, August 18, 2023). The study is based on the “Bioethical rules for conducting research on humans and animals” and is in accordance with the legislation of the Republic of Kazakhstan and the European Convention on Bioethics. In the study, no experiments are conducted on the animals themselves, i.e., dogs; only biomaterials collected from dogs are used. The collection of all types of biomaterials mentioned in the study is a minimally invasive procedure that causes no harm to the dog.

Peripheral blood was used to prepare and analyze cytogenetic smear preparations. The smears were prepared according to the generally recognized method.

The cytogenetic analysis was carried out on 88 dogs of the Tobet breed, 72 of which are kept in the Almaty region and 16 in Ust-Kamenogorsk, as well as on 36 mixed-breed dogs kept in a kennel in the Almaty region. The sex and age composition of the Tobet dogs is shown in Table 1. The mixed-breed dogs were mainly represented in the third age category.

Table 1 – Age and gender composition of dogs of the Tobet breed

Age group	total	female	male
0-9m	10	3	7
10-15m	24	14	10
16m-8y	48	23	25
9y and older	6	3	3
Total	88	43	45

The preparations were processed under laboratory conditions using a camera. The peripheral blood smears were fixed in 96% ethyl alcohol for 30 minutes, dried and stained with 4% Romanowsky-Giemsa solution for 20 minutes [17].

The frequency of micronuclei and cytological disorders was examined in normochromic erythrocytes of peripheral blood using a AxioLab A.1 microscope (Zeiss, Germany) under oil immersion and a magnification of 10x100. During the cytogenetic examination, all changes in the structure of the erythrocytes that deviated from the normal morphology characteristic of this species were recorded. Up to 10,000 erythrocytes were analysed from each dog. The most characteristic abnormalities of the erythrocytes in the peripheral blood were documented photographically.

Reticulocyte analysis was performed to assess the extent of erythropoiesis [17]. Two reticulocyte stains were used: In the first, 50 µl of brilliant cresyl blue solution was mixed with 50 µl of blood, incubated for 25-30 minutes at 37°C or 1.5 hours at room temperature (18-25)°C and smears were prepared. With this staining, the erythrocytes are greenish-grey, the granular-filamentous substance (reticulum) is blue. In the second variant, similarly prepared smears were stained with May-Grunwald fixative. In this staining variant, the erythrocytes are pink-red, the granular-filamentous substance is light blue. The number of reticulocytes per 1000 erythrocytes was counted and expressed as a percentage.

For the statistical calculations, the arithmetic mean and its deviation ($M \pm SE$) were calculated as a percentage per 100 cells. The significance of the differences between the means was determined using Student's t-test. The threshold for statistical significance was set at $p \leq 0.05$. Statistical data analysis was performed using Microsoft Excel (Microsoft Corporation, Redmond, Washington, DC, USA).

Results and discussion

One of the indicators of the health, stability of the genome and adaptability of populations is cytogenetic homeostasis. It can be characterised by a micronucleus test and the analysis of other cytological disorders of the blood cells.

The red blood cells of mammals represent the final stage of erythropoiesis and are the product of several blast cell divisions. After the last mitosis, the main nucleus is expelled, and the daughter cells enter the stage of anucleated polychromatophilic (immature) and then normochromic (mature) erythrocytes. After the main nucleus has been expelled, the micronuclei, which are a consequence of the occurrence of chromosomal abnormalities in erythroblast cells, remain in the cytoplasm and are visible under the microscope as round or oval, differently sized, densely coloured bodies with a clear outline [18].

In addition, under the influence of unfavorable factors or diseases, other disorders can occur in the red blood cells, among which regenerative and degenerative changes can be distinguished [18]. The former are characterized by reversible changes, such as echinocytes in the early stages, immature forms of red blood cells or nucleated red blood cells. In degenerative (ageing) red blood cells, the elasticity of the cell membrane decreases over time, leading to irreversible changes such as anisocytosis (change in size), anisochromia (change in color), the appearance of various inclusions and poikilocytosis (change in shape) of the red blood cells.

The main advantage of analyzing such cytological and cytogenetic disorders lies in the simplicity and availability of blood. Their application in the context of endangered species and breeds provides an effective tool for monitoring the health of the population and understanding the impact of various factors on its genetic structure, which can be useful in the development and implementation of conservation and recovery strategies.

In this study, the cytological and cytogenetic (micronuclear assay) parameters of peripheral blood cells from Tobet dogs were analyzed. The study included mixed or outbred dogs as a control group. The results of the cytogenetic analysis of the erythrocytes and cytological abnormalities of these dogs are shown in Table 2.

Table 2 – Results of the analysis of cytological and cytogenetic parameters of peripheral blood cells from Tobet dogs and outbred dogs

Sample	Micronuclei, ‰	Cytological abnormalities %
Tobet		
Age group		
0-9m	0.30	0.98
10-15m	0.31	0.81
16m-8y	0.20	1.57
9y and older	0.20	1.65
Gender		
Female	0.24	1.47
Male	0.26	1.54
Total	0.25±0.01	1.50±0.01*
Outbred (control)		
Female	0.21	1,2
Male	0.32	0,9
Total	0.26±0.03	1,05±0,01

Note: * $p \leq 0,01$

It was shown that the frequency of micronuclei in the erythrocytes of the peripheral blood of Tobets dogs was not statistically significantly different from the results obtained when analysing outbred dogs. This result is in contrast to the available literature data, which showed a significant increase in the frequency of micronuclei, nuclear buds and total number of nuclear abnormalities in purebred dogs compared to mongrels [19]. Our results could indicate either a low level of inbreeding in Tobets or a low “pedigree” of these dogs. In addition, the sensitivity of the methods used may make its own adjustments. We have analysed micronuclei in erythrocytes from peripheral blood and Santovito (2024) from cheek epithelial cells. This publication also reports that endogenous factors such as sex and age do not significantly contribute to the increase in genomic damage observed in purebred dogs. In our study, Tobets of age groups 1 and 2 had a higher frequency of micronuclei (0.3‰) than adult animals, and in about 30% of cases the micronuclei were quite large. In Tobets, the differences in the incidence of micronuclei by sex are insignificant, with a slight increase in males. In bred dogs, however, these differences are statistically significant.

In an individual analysis, 10% of the Tobets and 5% of the outbred dogs had a high number of micronuclei in the erythrocytes, which was 3-6 times higher than the average. It is possible that 10% of the Tobets had a high level of inbreeding.

The degree of cytogenetic abnormalities in the body (genetic instability) is not only an indicator of genetic status and health, but also an important indicator for environmental monitoring. Since we studied Tobets from two regions of Kazakhstan, an analysis of the frequency of micronuclei in the studied animals was carried out depending on their place of residence. In Tobets living in Ust-Kamenogorsk, the frequency of erythrocytes with micronuclei (0.25‰) is statistically significantly ($p \leq 0.01$) higher than the indicators in dogs from the Almaty region. It is known that Ust-Kamenogorsk is one of the most industrially polluted cities in Kazakhstan [20].

Cytological abnormalities are usually an indication of the health status of the animal. The presence of an increased level of cytological abnormalities in the erythrocytes of the examined animals indicates the development of degenerative processes in the body caused by various reasons – physiological, medical, environmental [16]. According to the type and extent of cytological abnormalities in the anuclear erythrocytes, two groups of erythrocytes are distinguished: regenerative and degenerative. Regenerative forms are erythrocytes that have undergone reversible changes to the cell membrane. These include – the early stage of echinocytosis as well as immature forms of erythrocytes or nucleated erythrocytes (basophilic, polychromatophilic and oxyphilic erythrocytes, erythrocytes with basophilic granularity and reticulocytes of varying degrees of maturity). There are many classifications of degenerative changes in erythrocytes. These pathological disorders of red blood cells are associated with changes in size (anisocytosis), red blood cell shape (poikilocytosis), changes in normal colour (anisochromia), inclusions in the red blood cells (Jolly-Howell bodies, Pappenheim bodies, Cabot rings, Heinz bodies, basophilic granularity of the cytoplasm, etc.) [16]

Compared to outbred dogs, Tobet has a higher level of various cytological abnormalities, in particular red blood cells of irregular size, especially small (microcytes) or large (macrocytes). In some cases, poikilocytosis was observed. These were mainly echinocytes (tooth-shaped cells), acanthocytes (red blood cells with different sized protrusions) and dacryocytes (tear-like cells) (Fig. 1).

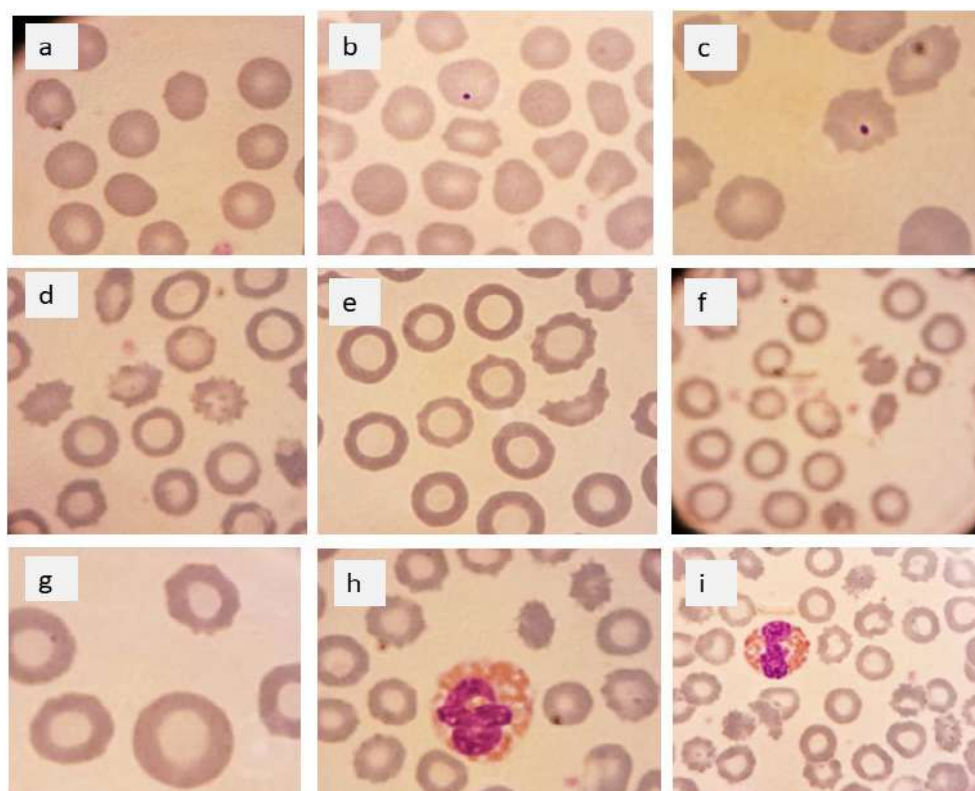


Figure 1 – Preparations of the peripheral blood of Tobet dogs (a) normal red blood cells; (b,c) micronuclei in erythrocytes; d-f – poikilocytosis of erythrocytes with hypochromia; (g) macrocyte; (h,i) toxic granularity of neutrophils, magnification 16 x 100

Given the high percentage of poikilocytosis in some Tobet dogs (10-30%) compared to 3-10% in outbred dogs, it can be assumed that these animals suffer from health problems. It is known from the literature that poikilocytosis, which is characterised by the presence of abnormally shaped red blood cells, may indicate underlying health problems in dogs, including chronic kidney disease, ventricular outflow tract obstruction, severe babesia infestation and congenital heart defects [21-24]. In addition, hypochromia, a low haemoglobin level due to iron deficiency and intoxication, has been reported in some Tobet's dogs. A toxic granularity of neutrophils resembling azurophilic granules has also been observed (Figure 1). Their formation occurs inside the cell due to physicochemical changes in the protein structure of the cytoplasm under the influence of intoxication products, which is observed in infectious or inflammatory processes.

In some dogs of the Tobet breed, the formation of “coins columns” occurs – this is the gluing of red blood cells into chains resembling the shape of coin columns (Figure 2). This usually occurs when the acid-base balance of the blood changes

towards increased acidity (from 7.43 to 7.33) and can be associated with chronic liver inflammation [16]. This phenomenon is related to the aggregation of red blood cells, which has a negative effect on blood microcirculation. Normally, the blood of dogs contains a single number of “coins columns”.



Figure 2 – Preparations of the peripheral blood of Tobet dogs – the formation of “coin columns”, 10x100

Another important indicator of health is the degree of erythropoiesis, which can be assessed by the level of reticulocytes in the blood (Fig. 3-4). In dogs, the reference values are 0.5 – 1.2% [25]. On average, the level of erythropoiesis is at the lower limit of the norm in both Tobets and outbred dogs. There are practically no differences between the sexes. As can be seen from the data presented, the

reticulocyte value is only included in the reference values for young dogs, which is of course explained by the higher erythropoiesis in young animals. With increasing age, this indicator decreases significantly and is below the normal limit, which most likely indicates the presence of physiological and veterinary problems. This, in turn, reduces dogs' adaptive potential and their working qualities [2, 3, 26, 27].

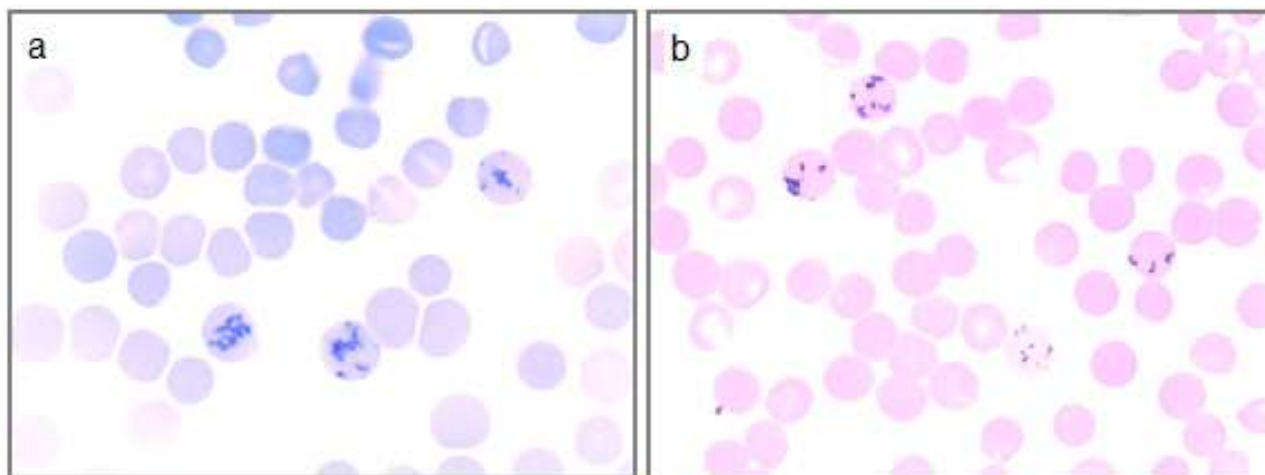


Figure 3 – Reticulocytes in the peripheral blood of dogs (a) first staining method (BCS only); (b) second staining method (BCS+May-Grunwald), 10x100

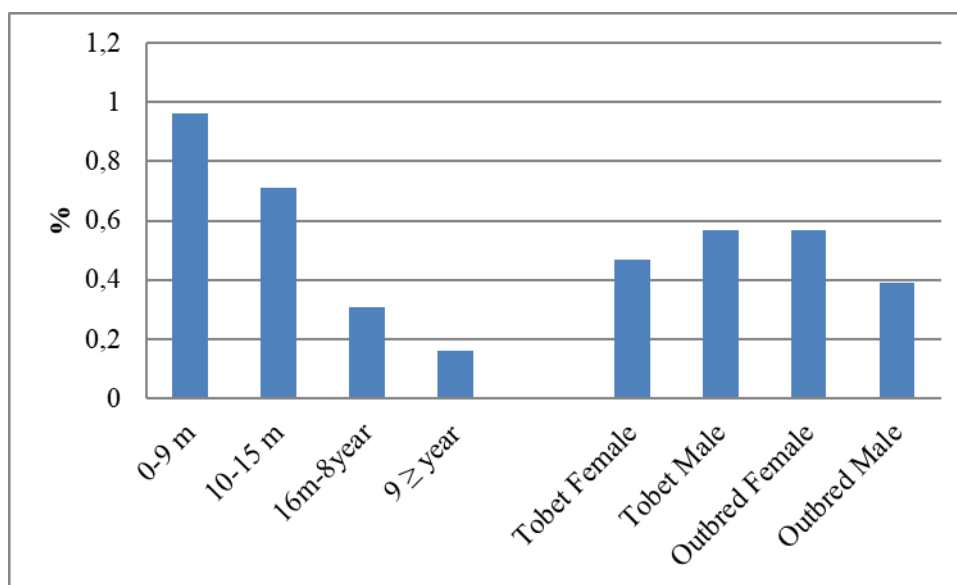


Figure 4 – Reticulocyte content in the blood of the Reticulocyte content in the blood of Tobet dogs and outbred dogs

Thus, preliminary cytological analysis has revealed health problems in some Tobet dogs that may not yet have clinical manifestations. The owners of these dogs have been informed of the need for additional biochemical testing to determine the causes of these problems. The micronucleus test did not reveal any differences in the stability of the genetic apparatus in Tobet dogs and outbred dogs. Unlike Santovito (2024) [19], however, a more thorough study is continuing by analysing the cytogenetic parameters in relation to the age and sex of the animals tested.

Conclusion

The study, which compared the cytological and cytogenetic parameters of Tobet dogs with those of outbred dogs, showed no significant differences in the frequency of micronuclei, indicating comparable genomic stability in both groups. At this stage of the study, it can be assumed that the genetic integrity of Tobet dogs remains intact despite the challenges facing the breed, such as the decline in grazing areas, the decline in traditional breeding methods and the lack of scientific breeding programmes.

However, the discovery of cytological abnormalities, including poikilocytosis – a condition characterized by the presence of abnormally shaped

red blood cells – points to potential health problems in the breed. These abnormalities need to be further investigated to understand their impact on the health and viability of the Tobet breed. Overall, the results of the study argue in favor of integrating traditional and modern breeding approaches to improve the breed's resilience and adaptability. This integrated strategy could be crucial for the survival of the Tobet breed.

Acknowledgments

We would like to thank the dog breeders and owners who provided us with samples and information about this unique breed. Our special thanks to the veterinarians and members of “Kansonar” who helped with sampling and provided expert guidance.

This work was supported by the Committee of Science of the Ministry of Science and Higher Education of Republic of Kazakhstan (BR21881977, Agreement No.417-PTF-23-25 dated November, 15, 2023).

Conflict of interest

All authors are aware of the article's content and declare no conflict of interest.

References

1. Perfil'yeva A.V., Bespalova K.B., Begmanova M.O., Kuzovleva Y.B. (2024) Assessment of the genetic diversity of the Kazakh national dog breed Tobet in the southern region of Kazakhstan. 3i: Intellect, Idea, Innovation, no. 1, pp. 58–67. <https://doi.org/10.52269/22266070>
2. Rocha J.L., Godinho R., Brito J.C., Rasmus N. (2021) Life in deserts: The genetic basis of mammalian desert adaptation. *Trends Ecol. Evol.*, vol. 36, no. 7, pp. 637–650. <https://doi.org/10.1016/j.tree.2021.03.007>
3. Ilardo M., Rasmus N. (2018) Human adaptation to extreme environmental conditions. *Curr. Opin. Genet. Dev.*, no. 53, pp. 77–82. <https://doi.org/10.1016/j.gde.2018.07.003>
4. Bellumori T.P., Famula T.R., Bannasch D.L., Belanger J.M., Oberbauer A.M. (2013) Prevalence of inherited disorders among mixed-breed and purebred dogs: 27,254 cases (1995–2010). *J. Am. Vet. Med. Assoc.*, vol. 242, no. 11, pp. 1549–1555. <https://doi.org/10.2460/javma.242.11.1549>
5. Shannon L.M., Boyko R.H., Castelhana M., Corey E., Hayward J.J., McLean C., et al. (2015) Genetic structure in village dogs reveals a Central Asian domestication origin. *Proc. Natl. Acad. Sci. USA*, vol. 112, no. 44, pp. 13639–13644. <https://doi.org/10.1073/pnas.1516215112>
6. Bui X., Pham T., Tran H., Phung T., Ngo Q., Dinh T.D., et al. (2021) Evaluation of genetic diversity and origin of Song Ma village dogs in Vietnam. *Biomed. Biotechnol. Res. J.*, vol. 5, no. 4.
7. Donner J., Anderson H., Davison S., Hughes A.M., Bouirmane J., Lindqvist J., et al. (2018) Frequency and distribution of 152 genetic disease variants in over 100,000 mixed breed and purebred dogs. *PLoS Genet.*, vol. 14, no. 4, e1007361. <https://doi.org/10.1371/journal.pgen.1007361>
8. Leroy G. (2011) Genetic diversity, inbreeding and breeding practices in dogs: Results from pedigree analyses. *Vet. J.*, vol. 189, no. 2, pp. 177–182. <https://doi.org/10.1016/j.tvjl.2011.06.016>
9. Whippet: preliminary findings – BetterBred.com [Internet]. [cited 2023 Dec 1]. Available from: <https://www.betterbred.com/2020/06/02/whippet-preliminary-findings/>
10. Sargan D.R., Milne B.S., Aguirre Hernandez J., O'Brien P.C.M., Ferguson-Smith M.A., Hoather T., et al. (2005) Chromosome rearrangements in canine fibrosarcomas. *J. Hered.*, vol. 96, no. 7, pp. 766–773. <https://doi.org/10.1093/jhered/esi122>

11. Thomas R., Smith K.C., Ostrander E.A., Galibert F., Breen M. (2003) Chromosome aberrations in canine multicentric lymphomas detected with comparative genomic hybridisation and a panel of single locus probes. *Br. J. Cancer*, vol. 89, no. 8, pp. 1530–1537. <https://doi.org/10.1038/sj.bjc.6601275>
12. Szczerebal I., Nizanski W., Dzimira S., Nowacka-Woszek J., Stachecka J., Biezynski J., et al. (2021) Chromosome abnormalities in dogs with disorders of sex development (DSD). *Anim. Reprod. Sci.*, vol. 230, 106771. <https://doi.org/10.1016/j.anireprosci.2021.106771>
13. Morais C.S.D., Affonso P.R.A.M., Bitencourt J.A., Wenceslau A.A. (2017) Cytogenetic aspects of a canine breast carcinosarcoma – a case report. *Genet. Mol. Res.*, vol. 16, no. 2. <https://doi.org/10.4238/gmr16029433>
14. Dickinson P.J., York D., Higgins R.J., Le Couteur R.A., Joshi N., Bannasch D. (2016) Chromosomal aberrations in canine gliomas define candidate genes and common pathways in dogs and humans. *J. Neuropathol. Exp. Neurol.*, vol. 75, no. 7, pp. 700–710. <https://doi.org/10.1093/jnen/nlw042>
15. Reimann-Berg N., Bullerdiek J., Escobar H., Nolte I. (2012) Chromosome analyses in dogs. *Tierärztl. Prax. Ausg. K Kleintiere Heimtiere*, vol. 40, pp. 191–196.
16. Amirov D.R., Tamimdarov B.F., Shageeva A.R. (2020) *Klinicheskaya gematologiya zhivotnykh: Uchebnoe posobie*. Kazan': Centr informacionnykh tekhnologij KGAVM, 134 p.
17. Merkulova I.P. (2012) *Patofiziologiya krovenosnoj sistemy: uchebnik i metodicheskoe posobie*. Minsk: Sakharov Moscow State Economic University, 120 p.
18. Moroz V.V., Golubev A.M., Afanasyev A.V., Kuzovlev A.N., Sergunova V.A., Gudkova O.E., et al. (2012) Stroenie i funkciya eritrocita v norme i pri kriticheskikh sostoyaniyakh. *General Resuscitation [Internet]*, vol. 8, no. 1, pp.52. <https://www.reanimatology.com/rmt/article/view/246>
19. Santovito A., Saracco M., Scarfo M., Nota A., Bertolino S. (2023) Purebred dogs show higher levels of genomic damage compared to mixed breed dogs. *Mamm. Genome*, vol. 35, no. 1, pp. 90–98. <https://doi.org/10.1007/s00335-023-10020-5>
20. Cherednichenko O.G., Iskandarova K.A., Ismailov S.B. (2010) Cytogenetic assessment of the impact of environmental genotoxins on residents of the village of Kora in the Mangistau region and the city of Ust-Kamenogorsk. In: Akhmatullina N.B., ed. *From Virus Genetics to Human Genetics*, pp. 184–191.
21. Passavin P., Chetboul V., Poissonnier C., Saponaro V., Trehieu-Sechi E., Alvarado M.P., et al. (2021) Red blood cell abnormalities occur in dogs with congenital ventricular outflow tract obstruction. *Am. J. Vet. Res.*, vol. 83, no. 3, pp. 198–204. <https://pubmed.ncbi.nlm.nih.gov/34936577/>
22. Zygnier W., Gójska O., Rapacka G., Jaros D., Wedrychowicz H. (2007) Hematological changes during the course of canine babesiosis caused by large *Babesia* in domestic dogs in Warsaw (Poland). *Vet. Parasitol.*, vol. 145, no. 1–2, pp. 146–151. <https://pubmed.ncbi.nlm.nih.gov/17157987/>
23. Lippi I., Perondi F., Lubas G., Gori E., Pierini A., D'Addetta A., et al. (2021) Erythrogram patterns in dogs with chronic kidney disease. *Vet. Sci.*, vol. 8, no. 7. <https://pubmed.ncbi.nlm.nih.gov/34209294/>
24. Rodionov V.D. (2018) The effect of chronic inflammatory processes in liver tissue on the microrheological characteristics of erythrocytes. *Contemp. Issues Sci. Educ.*, vol. 1. <https://science-education.ru/ru/article/view?id=27372>
25. Complete blood count and biochemical blood analysis. Available from: <http://www.provet-clinic.ru/2011-05-02-17-42-12/obshchij-i-biokhimicheskij-analiz-krovi>
26. Udroi I., Sgura A. (2017) Cytogenetic tests for animal production: state of the art and perspectives. *Anim. Genet.*, vol. 48, pp. 505–515. <https://doi.org/10.1111/age.12581>
27. Pirnajmedin F., Majidi M.M., Jaškūnė K. (2024) Adaptive strategies to drought stress in grasses of the Poaceae family under climate change: Physiological, genetic and molecular perspectives – a review. *Plant Physiol. Biochem.*, vol. 213, 108814. <https://doi.org/10.1016/j.plaphy.2024.108814>

Information about authors

Oksana Cherednichenko – PhD, Head of the Genetic Monitoring Laboratory, Institute of Genetics and Physiology (Almaty, Kazakhstan, e-mail: cherogen70@mail.ru)

Anastassiya Pilyugina – Master of Science, senior researcher at the Genetic Monitoring Laboratory, Institute of Genetics and Physiology (Almaty, Kazakhstan, e-mail: labgenmon@mail.ru)

Dinara Azizbekova – Master of Science, junior researcher at the Genetic Monitoring Laboratory, Institute of Genetics and Physiology (Almaty, Kazakhstan, e-mail: azizbekovad@gmail.com)

Almira Amirgaliyeva – senior researcher at the Laboratory of Molecular Genetics, Institute of Genetics and Physiology (Almaty, Kazakhstan, e-mail: almira-71@mail.ru)

Kira Beshpalova – Master of Science, researcher at Laboratory of Molecular Genetics, Institute of Genetics and Physiology (Almaty, Kazakhstan, e-mail: kira.b.beshpalova@gmail.com)

A.B. Hejran^{1*}, V.K. Yadav², P. Niazi³¹Helmand University, Helmand, Afghanistan²Marwadi University Research Center, Marwadi University, Gujarat, India³Kandahar University, Kandahar, Afghanistan*e-mail: abdulbari.hejran94@gmail.com

(Received 02 December 2024; received in revised form 25 June 2025; accepted 27 June 2025)

Prevalence and impact of Hepatitis B Virus (HBV) in Lashkar Gah City, Afghanistan: a case study

Abstract. Hepatitis B Virus (HBV) remains a critical public health issue in Lashkar Gah City, Afghanistan, necessitating a focused investigation into its prevalence, clinical implications, and management, this case study research aimed to evaluate HBV prevalence across different demographic groups and regions, assess the incidence of chronic infections, and analyze diagnostic and treatment strategies. The study also identified gaps in public health approaches and proposed targeted interventions. 100 diagnosed patients were investigated, data were collected from two key hospitals Bost University Private Hospital and Helmand Provincial Infectious Disease Treatment Hospital and three laboratories. A structured 24-question multiple-choice survey was completed by 100 healthcare specialists, including psychologists, neurologists, and medical doctors. Analysis using IBM SPSS Statistics software revealed a significant male predominance in HBV cases (99%) and higher prevalence in densely populated areas (96%) and warmer climates (92%). In 72% cases, it was chronic, 63% patients had on slight symptoms and 87% cases have long lived with the condition. Nausea, vomiting, and jaundice were the common clinical symptoms reported in 94% of the cases. These results indicate that enhanced diagnostic measures, prevention practices, and population health awareness programs are most required, and the case study also brings significant contributions to the epidemiological role of HBV in Lashkar Gah City and proposes practical recommendations to be addressed by medical workers and decision-makers to advance the management of the disease and lighten the health-related burden on the population.

Key words: Hepatitis B Virus (HBV), Prevalence, Epidemiology, Chronic HBV, Lashkar Gah, Afghanistan.

Introduction

Hepatitis B virus (HBV) is a DNA virus with a lipid coat introduced by the *Hepadnaviridae* family. A particular antigen, at first called the “Australia antigen,” was first found in the serum of an Indigenous Australian to identify the virus. Later, it was proven that this antigen is connected to HBV in those with hepatitis and visualized by electron microscope in 1970. It encompasses a diminutive (3.2 kb) covalently closed circular DNA (cccDNA) within its genome. This cccDNA is transcribed into four distinct transcripts (3.5 kb, 2.4 kb, 2.1 kb, and 0.7 kb), which encode polymerase, HBcAg, HBeAg, HBsAg (L, M, S surface proteins), and HBx, each playing a pivotal role in the HBV lifecycle and hepatocellular damage [1-3]. Prasidhrathsint and Stapleton (2019) highlight that viral hepatitis is a global affliction driven by five principal viruses: Hepatitis A, B, C, D, and E. It causes inflammation of the liver and has a possibility

of developing to a chronic infection leading to cirrhosis and hepatocellular carcinoma (HCC) [4, 5].

Recent studies throughout Afghanistan have illuminated significant demographic disparities in the prevalence of HBV. A retrospective analysis carried out in Kabul between March and September 2023 demonstrated that 63.6% of 217 HBsAg-positive participants exhibited chronic infection, with an almost equal gender distribution (50.7% male, 49.3% female) and a pronounced concentration among individuals over 45 years old (44.2%) [6]. In Herat, a hospital-based case-control investigation identified male gender and younger age as statistically significant risk factors ($p < 0.05$), with male patients experiencing notably lower quality-of-life scores [7]. A mass screening initiative in Jalalabad encompassing more than 17,000 individuals revealed an HBV prevalence of 1.93%, with the highest incidence observed among those aged 31-40 and a male predominance [8]. Pediatric seroprevalence

assessments from Kabul and Mazar-e-Sharif recorded an HBsAg positivity rate of 3.6% among children, markedly elevated in those older than six years, with prevalence increasing from 0.65% in the 1-10 age group to 8% in the 11-20 cohort [9].

Serological markers are an important role in determining the infected patients, assessing the phases of the infection as well as monitoring the progress of antiviral therapies [5]. And Abbott ARCHITECT/Alinity HBsAg assay results in the improvement of recognizing prior acute, late acute and occult Hepatitis B infections by 36.4%, 10.9%. And extends detection duration beyond that of existing assays [10]. This prototype HBsAg assay is anticipated to hold significant diagnostic value [11-13]. And a longitudinal analysis spanning 15 years on HBV genomes conducted in Guangxi, China, revealed that mutations may revert to their original wild type during natural infection. This finding suggests that healthcare professionals should be circumspect when forecasting long-term outcomes based on these mutations alone [14]. A study evaluates the prevalence of HIV, HCV, and HBV among pregnant women in Anyigba, Nigeria, revealing a notably high prevalence of HIV relative to the lower prevalence of HCV and HBV [15-17]. An investigation into the efficacy and potential adverse effects of administering hepatitis B immunoglobulin (HBIG) to pregnant women during their third trimester revealed that HBIG significantly diminished the transmission of HBsAg and HBV-DNA from mother to child [18]. And a study disseminated by the Cochrane Hepato-Biliary Group assessed the efficacy of tenofovir-based antiviral combination therapies in mitigating the transmission of HBV from mother to child among HIV-positive pregnant women co-infected with HBV [19, 20]. And HBV represents a severe hepatic pathology that can be transmitted via horizontal transmission or from mother to infant [21]. And Chronic HBV infection disrupts hepatic metabolic pathways, leading to reduced levels of cholesterol and triglycerides, and a diminished incidence of hepatic steatosis. The contributing factors to hepatic steatosis include elevated ALT levels, increased BMI, male sex, and old age [22, 23]. And HBV affects approximately 350-500 million people globally, often leading to HCC [24-26].

Furthermore, a computational spatial whole-cell model has been developed to investigate the HBV infection cycle in hepatocyte cells. This model forecasts infection dynamics, explores virus-host and drug interactions, and is adaptable for examining other viral pathogens [27]. A phase III clinical trial

conducted in Thailand is evaluating the efficacy and safety of administering maternal tenofovir disoproxil fumarate (TDF) to prevent mother-to-child transmission of HBV, monitoring 328 mother-infant dyads up to six months of age [28, 29]. A cross-sectional analysis revealed a moderate prevalence of Hepatitis B and C virus infections among pregnant women at Felege Hiwot Referral Hospital in Ethiopia [30], a case-control study in Indonesia identified that genetic polymorphisms in HLA-DP and the presence of isolated anti-HBc are critical predictors of occult hepatitis B infection (OBI) among blood donors [31-34]. And the HBV poses a significant global health challenge, inflicting liver disease and impacting over 257 million individuals worldwide. Although an efficacious vaccine exists, contemporary treatments face difficulties due to enduring viral reservoirs, substantial viral load, and compromised immune responses [35]. HBV represents a significant global health threat, being a leading contributor to mortality due to its association with cirrhosis and HCC. The rise in chronic HBV infections can be attributed to various factors, including viral genotypes and co-infection with other blood-borne pathogens [36].

Consequently, current diagnostic techniques encompass both serological and molecular methodologies. The identification of novel biomarkers, such as HBcrAg and HBV RNA, is imperative for the proficient management of infections. HBV is classified into 10 genotypes and 30 subtypes, with genotyping being advised for pegylated interferon therapy to enhance treatment outcomes [37]. HBV reactivation (HBVr) represents a significant challenge within the framework of immunosuppressive drug treatment, where virological and host factors interact in a rather complex way. Sakamoto et al. (2020) conducted a comprehensive study that analyzed serum samples from both HBVr and acute hepatitis B (AHB) patients, revealing a significantly higher prevalence of genotype B among those with HBVr. The research highlighted an increased frequency of mutations throughout the HBV genome, particularly in the envelope region, in HBVr patients compared to their AHB counterparts. The study also observed a notable prevalence of the S3N amino acid substitution in the envelope protein and mutations at G1896A and G1899A in the precore region among HBVr patients. By employing ultradeep sequencing, the research study isolated some of the most key virological factors related to HBVr, thus providing useful information on the methodologies of the development of HBVr and probable system through which the disease may be managed and

controlled more easily [38-40]. The purpose of the research will be to address the knowledge gap on the prevalence of HBV and practices associated with the diagnosis of HBV in the City of Lashkar Gah. In addition, the study intends to build evidence-based plans for treating, preventing and controlling HBV. The useful understanding gained is expected to guide and reinforce the setup and execution of major public health plans, ensuring better healthcare outcomes in Lashkar Gah City and contributing to broader efforts to combat HBV at the local and global levels.

Materials and methods

Research Design

This study employed both descriptive and explanatory research design from May 1, 2024, until August 25, 2024. A descriptive study was used to overview the clinical and laboratory diagnosis of HBV in Lashkar Gah City. The investigation was carried out in Lashkar Gah City using data from two major hospitals (Bost University Private Hospital and Helmand Provincial Infectious Disease Treatment Hospital) and three laboratories (Lamar, Kainat, and Rana Medical Laboratories). A multidisciplinary team of 100 specialists, including psychologists, neurologists, and medical doctors, collaborated on the study. IBM SPSS Statistics (Version 25) software facilitated data analysis.

Sampling Technique

Purposive sampling for HBV in this study involved selecting specialists in HBV diagnosis and treatment in Lashkar Gah City. The sample was gathered at appropriate intervals, focusing on individuals with at least two years of experience in diagnosing or treating HBV patients. Only those who expressed interest in the study and consented to share their information were included. Participants who lacked prior experience with HBV or had not worked in the field within the last two years were excluded. As a result, the research was conducted exclusively with professionals who possessed the most up-to-date knowledge and expertise in the field.

Data Screening

The HBV study containing the data screening procedure was exhaustive and suitable in supporting the accuracy and reliability of the subsequent statistical analysis. This consisted of checking the distribution of the data to ascertain that the parametric tests would have met assumptions. It also involved determining and rectifying any statistical mistakes or

aberrant values which is very important in preserving the integrity of the findings, as outliers can distort the results. This process made it clear that there was complete response on questions on the questionnaire, and any missing data issues that might cause bias or investigational results to lose some power. These procedures were critical in maximizing the accuracy and reliability of the data before carrying out the statistical analysis.

Sampling Technique and Size

The sample size for this investigation was calculated using Yamane's formula (1967), and an anticipated error rate of 0.10. Given the specific population of healthcare professionals in the selected hospitals and laboratories, the sample size was calculated as follows:

$$n = \frac{N}{1 + N(e)^2}$$

Where:

n is the sample size,

N is the population size,

e is the precision and reliability level.

Applying this formula to the study:

$$n = \frac{100}{1 + 100(0.10)^2} = \frac{100}{1 + 1} = \frac{100}{2} = 50$$

With a population size of 100 and a 10% margin of error.

Data Source and Data Acquisition Procedure

The method of gathering primary data presented was a structured questionnaire that was given to medical professionals, psychologists, neurologists and other healthcare practitioners of various hospitals and laboratories that were selected. The questionnaire consisted of 24 multiple-choice questions focused on the clinical and laboratory diagnosis of HBV. Participants were given sufficient time during their work hours to complete the questionnaire and submit their responses. SPSS software was used to analyze the data and generate results. Because healthcare professionals worked with HBV patients regularly, they were able to support thorough and combined use of both clinical and laboratory tests for diagnostics.

Research Variables

Dependent Variable

Prevalence of HBV infection: This variable refers to the incidence rate of HBV infection among

various demographic groups in Lashkar Gah City. The prevalence of HBV is influenced by factors such as socioeconomic status, healthcare access, and population density, all of which are linked to the spread of infectious diseases [41, 42].

Independent Variables

Age group: The prevalence of HBV is strongly correlated with specific age groups, with certain groups being more vulnerable to infection. Younger individuals, particularly those with compromised immune systems, are at higher risk.

Gender: Research indicates a gender disparity in HBV prevalence, with men often being more vulnerable to chronic HBV infections due to biological and social factors [43]. In countries like Afghanistan, cultural practices, healthcare-seeking behavior, and occupational exposures contribute to differing HBV infection rates between genders [44].

Geographical Conditions: Environmental factors such as climate and altitude can impact the transmission and prevalence of HBV. Warmer climates, like Lashkar Gah's hot and arid conditions, can facilitate the transmission of blood-borne diseases, particularly due to factors like population migration and limited healthcare services [45]. This climatic influence may contribute to increased HBV transmission and incidence in the region.

Clinical Symptoms: In adults, the disease caused by acute hepatitis B starts with such non-specific symptoms as anorexia, nausea, emesis, abdominal discomfort, darkened urine, pale stools, and jaundice; and, in severe cases, it can progress into hepatic encephalopathy, ascites, gastrointestinal hemorrhage (due to esophageal varices), coagulopathy, or opportunistic infections [46]. Understanding the clinical symptoms specific to Lashkar Gah could help improve diagnostic and therapeutic strategies.

Diagnostic assays: As observed in our survey, ELISA and RT-PCR were the primary modalities utilized in the diagnosis of HBV in hospitals and diagnostic laboratories all over Lashkar Gah City. The availability of these assays exemplifies their accessibility and diagnostic effectiveness in the

area as part of a regular pattern. ELISA serves as a potential primary screening system to the hepatitis B surface antigens and RT-PCR serves to give a superior sensitivity when it comes to identification of HBV DNA thus making the system capable of classifying the least accurate cases of a chronic disease. These methodologies are also reliable in detection of cases and making therapy interventions, regardless of underdeveloped laboratory infrastructure [47].

Epidemiological Data Analysis

The data collected from the questionnaire were analyzed using IBM SPSS Statistics (Version 25). The primary goal of the analysis was to explore how different variables influenced the incidence and progression of HBV within the studied population. The results provided insights into the most affected age groups, gender distribution, and the effectiveness of laboratory diagnostic tests and treatment protocols for HBV in Lashkar Gah City. Analyzing the data this way gave new insights about the causes of HBV in the region which were valuable when formulating new healthcare policies.

Clinical and Laboratory Diagnosis of HBV in Lashkar Gah City

Diagnostic tests for HBV infection: The primary laboratory tests for diagnosing HBV infection in Lashkar Gah City include the HBsAg test and the CBC. The HBsAg test is overwhelmingly preferred, accounting for 97% of diagnostic cases. The CBC is used much less frequently, only in 3% of the cases. This indicates a strong reliance on HBsAg testing as this population's standard diagnostic method for HBV.

Common diagnostic test for HBV infection: The HBsAg test is consistently identified as the most commonly employed diagnostic test for HBV infection, with a usage rate of 95%. Blood glucose tests are seldom used, with a rate of 5%. This further confirms the critical role of the HBsAg test in the laboratory diagnosis of HBV, underscoring its reliability and importance in detecting the virus Table 1, 2.

Table 1 – HBV clinical and laboratory diagnosis in Lashkar Gah (2022-2023)

Laboratory	Time Period	Test Name	Total Tests	Positive/ Negative Tests	Company/ Method	Sensitivity	Specificity	Accuracy
LEMAR	2022.01.01 – 2022.12.31	PCR HBV (Quantitative) Real Time	92	Positive (+)	One Step HBsAG Rapid Test (01FK10,01FK11) Method of STANDARD DIAGNOSTICS (SD), INC. Republic of Korea	~97%	~98%	~97.5%
LEMAR	2022.01.01 – 2022.12.31	HBS-Ag (ICI)	1164	Positive (+)	One Step HBsAG Rapid Test (01FK10,01FK11) Method of STANDARD DIAGNOSTICS (SD), INC. Republic of Korea	~97%	~98%	~97.5%
LEMAR	2022.01.01 – 2022.12.31	Hepatitis B surface antigen (ELISA)	2	Positive (+)	One Step HBsAg Rapid Test (01FK10,01FK11) Method of STANDARD DIAGNOSTICS (SD), INC. Republic of Korea	~97%	~98%	~97.5%
LEMAR	2023.01.01 – 2023.12.29	PCR HBV (Quantitative) Real Time	96	Positive (+)	One Step HBsAG Rapid Test (01FK10,01FK11) Method of Standard Diagnostics (SD), INC. Republic of Korea	~97%	~98%	~97.5%
LEMAR	2023.01.01 -2023.12.29	HBV-Ag (ICI)	901	Positive (+)	One Step HBsAg Rapid Test (01FK10,01FK11) Method of STANDARD DIAGNOSTICS (SD), INC. Republic of Korea	~97%	~98%	~97.5%
RANA	2023.01.01 – 2023.12.29	HBV-Ag (ICI)	474	Positive (+)	One Step Hepatitis B Surface Antigen Test Cassette (Serum/ plasma) (ICT ^{*1}) and RDT ^{*2} Methods of Healgen Scientific Limited Liability Company [B20183-04] USA	~98%	~99%	~98.5%
KAINAT	2023.01.01 -2023.11.09	HEPATITIS B SURFACE AG	274	Positive (+)	One Step Hepatitis B Surface Antigen Test Cassette (Serum/ plasma)(ICT) and RDT Methods of Healgen Scientific Limited Liability Company [B20183-04] USA	~98%	~99%	~98.5%

Cumulative Data insight:

1. Total Tests Conducted: LEMAR (2022): 1258 tests (92 + 1164 + 2), LEMAR (2023): 997 tests (96 + 901), RANA (2023): 474 tests, and KAINAT (2023): 274 tests.

2. Overall Total Tests: 3003 tests across all laboratories.

3. Average Tests per Lab: Average Tests per Year (LEMAR): $(1258 + 997)/2 \approx 1127.5$ tests per year and Overall Average Tests per Lab: $3003/3 \approx 1001$ tests per lab.

4. Percentage of Tests Conducted: LEMAR (2022): $(1258/3003) * 100 \approx 41.9\%$, LEMAR (2023): $(997/3003) * 100 \approx 33.2\%$, RANA (2023): $(474/3003) * 100 \approx 15.8\%$ and KAINAT (2023): $(274/3003) * 100 \approx 9.1\%$.

Summary:

- LEMAR Laboratory: Conducted a total of 2255 tests over the two years, indicating a high testing capacity.

- RANA and KAINAT Laboratories: Conducted fewer tests but contributed significantly to the overall testing efforts.

Testing Methods and Performance:

- LEMAR Laboratory: Uses One Step HBsAG Rapid Test with high sensitivity (~97%), specificity (~98%), and accuracy (~97.5%).

- RANA and KAINAT Laboratories: Use One Step Hepatitis B Surface Antigen Test Cassette with higher sensitivity (~98%), specificity (~99%), and accuracy (~98.5%).

^{*1}Immunochromatographic Test

^{*2}Rapid Diagnostic Test

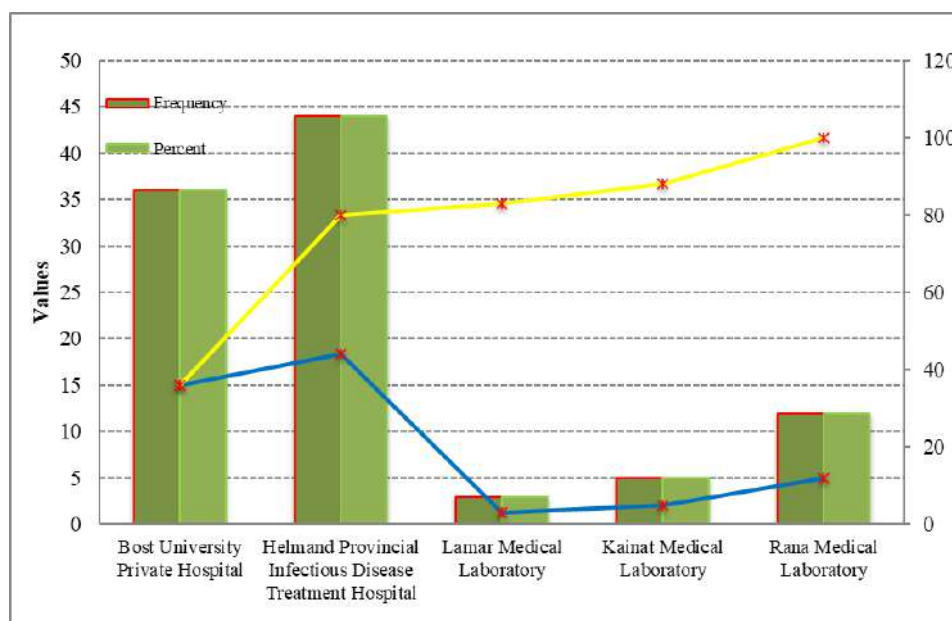
Table 2 – Overview of molecular findings from HBV DNA Quantification via Real-Time PCR in Lashkar Gah City

Parameter	Details
PCR HBV (Quantitative) Real Time	
HBV DNA	Detected
Viral Load	6,904,273 IU/mL
Detection Limit	Up to 120 Copies/mL or 20 IU/mL
Method	CFX 96-Bioered RT-PCR
Amplification and Detection	Conducted simultaneously using Mini Opticon-Bioered RT-PCR and kits from Roboscreen
Controls Applied	Positive, Negative, and Internal Controls
Interpretation	HBV DNA was extracted from patient plasma and amplified using Real-Time PCR.
Comments	Amplification and detection were performed simultaneously using advanced real-time thermo-optical analyzer.
	A quick, sensitive, specific, and reproducible method was established for detecting and quantifying HBV DNA.
	The procedure can analyze the viral load in plasma and serum samples in a range of 26.124 IU/mL to 4 10 IU/mL
	The methodology will be accurate and reliable in terms of diagnostic and clinical management of HBV in Lashkar Gah City

Results and discussion

The HBV infection in Lashkar Gah City has been shown to have a substantial rate of prevalence and clinical effect among various demographical groups of patients and across healthcare facilities. A total of 100 diagnosed patients, 44% of whom were found in Helmand Provincial Infectious Disease Treatment

Hospital and 36% at Bost University private hospital, were investigated in this research; the rest were in three private labs: RANA Medical (12%), Kainat Medical (5%), and Lamar Medical (3%). Information was gathered through a multiple-choice questions. Structured item survey and analyzed using the SPSS program to control diagnosis, symptoms and the treatment practice (Figure 1).

**Figure 1** – Statistical overview of hospital and laboratory patient data

However, the incidence of HBV infection in Lashkar Gah varies considerably depending on the demographics of the population and the geographic location of the area. About 56% of people under the age of 5 are infected with the virus, making them the age group with the highest frequency of the disease among all age groups. The incidence of this condition declines with age, with 41% of instances occurring in those older than 16 years old. When it comes to the distribution of gender, the data reveals a striking contrast, as the majority of people who are infected with HBV are males (99%), while only 1% of people are females. A higher percentage of the infection is found in high-density areas (96%) compared to low-density areas (4%) when it comes to the distribution of the infection among regions. There is also a

significance for geographical conditions, with the spread of HBV being substantially higher in hot regions (92%) compared to cold areas (8%). The prevalence of chronic HBV infection in the region is 63%, which represents a significant burden for communities there. Seventy-two per cent of people who have chronic HBV infection are impacted at a level of 24 per cent, while sixteen per cent are affected at a level of 75 per cent. There is an 87% duration rate, which indicates that the majority of chronic HBV infections continue to exist for several years. An overview of these observations can be seen in (Figure 2). In this case, the figure 1 indicates that the highest frequency of HBV infection occurs in children under 5 years old (56%), which is a critical finding for the case study.

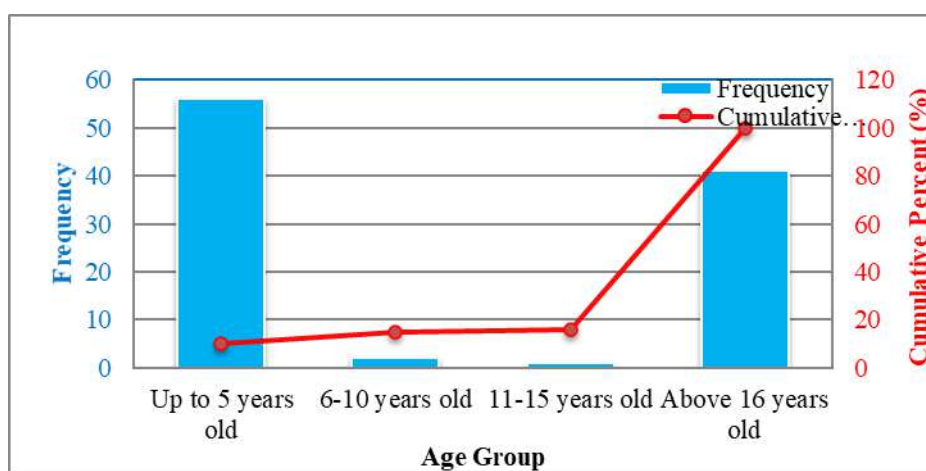


Figure 2 – Breakdown of HBV Infection by Age among those surveyed (Lashkar Gah City n=100)

After analyzing the conducted survey and the epidemiological context, the following data were obtained in accordance with research standards, the epidemiological breadth of HBV infection illuminates its evolution and repercussions. HBV infection incubates for weeks in 60% of cases and months in 34%. After the acute phase, 78% of people develop chronic hepatitis B, with 15% developing HCC and 7% cirrhosis. Nausea, vomiting, and jaundice are the main symptoms of HBV infection in 94% of patients. Joint discomfort and weariness are rare symptoms recorded in 2% of patients. Most people (63%), especially youngsters (62%), have few clinical symptoms. In 95% of cases, the HBsAg test is utilised to diagnose the disease, whereas the CBC is used in 3%. Disease burden varies by age

and gender. Chronic infection prevalence is 63%, and previous infections are 45%. Perinatal infections are 48%, and early childhood infections are 44%, indicating high transmission rates. Only 10% of adolescents and adults have high-level infections. Treatment and management strategies focus on medicine, which 46% of respondents found useful. Many (50%) advocate combining treatments for disease management. The structured item was included in the survey to classify the level of prevalence based on perceived endemicity in order to measure the distribution of HBV infection within Lashkar Gah. It used this three-tier system, which is high, medium, and low, to identify the local differences in the infection burden of different population groups and healthcare access points. This stratification

reflects in the resultant data which provide a more specific epidemiological profile that reflects the local contextual dynamics. Figure 3 shows the prevalence level of HBV in Lashkar Gah City: 58% of cases are classified as high prevalence, 20% as medium, and

22% as low. Figure 4 shows the overall prevalence of HBV infection, where chronic infections are the most common at 63%, adolescent/adult infections at 54%, perinatal infections at 48%, past infections at 45%, and early childhood infections at 44% (Figure 5).

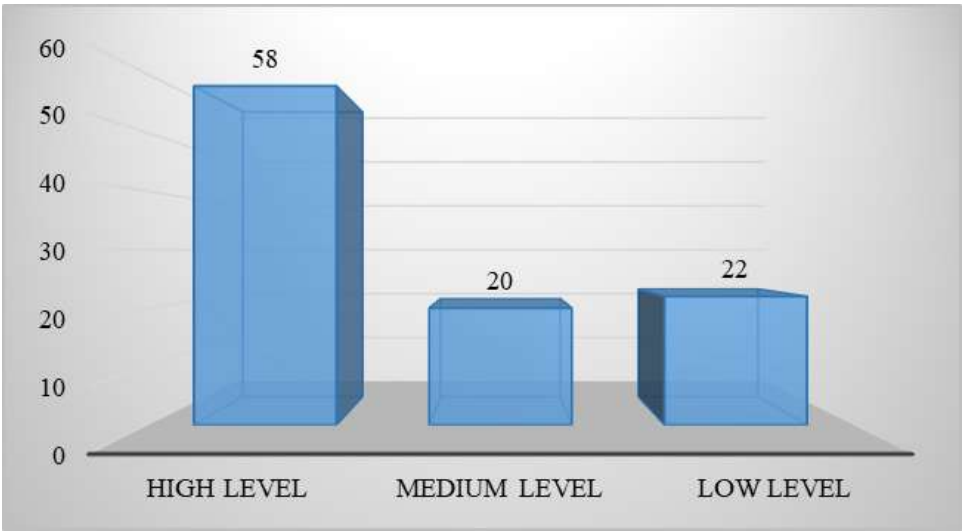


Figure 3 – Prevalence level of HBV in the Lashkar Gah City distributed into high, medium, and low

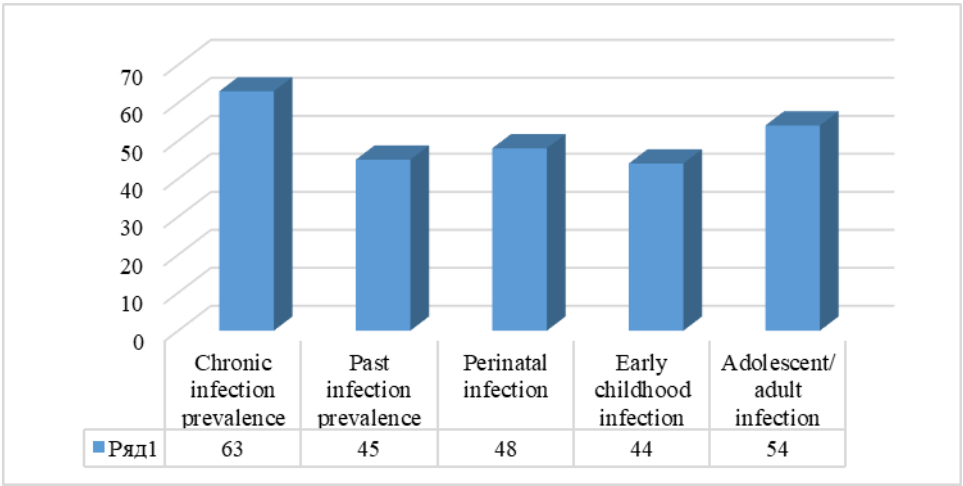


Figure 4 – HBV infection type distribution based on characteristics of endemic samples in the Lashkar Gah City

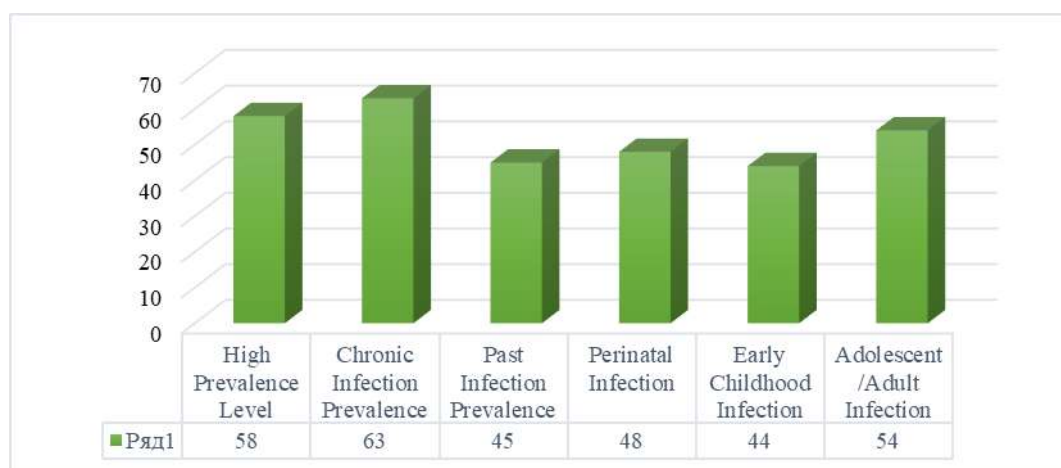


Figure 5 – Overall distribution of various HBV infection types as identified in the study in the Lashkar Gah City

Demographic and Epidemiological Profile of the Population in Lashkar Gah City

It is male predominant in the etiology of the disease with 99% and 1% again in males and females, respectively, implying that there might be underlying socio-cultural, behavioural and biological causes. HBV is mostly localized in high density regions as 96% of cases are encountered, whereas only 4% is in low density regions. This implies that the large number of people can support transmission due to optimal contact between people and maybe inferior health maintenance.

The disease burden of chronic HBV is high with 72 percent severity of those affected being in level 25 percent and 12 percent at level 50 percent and 16 percent at level 75 percent. This makes it vital to have proper managing and treatment approaches. Moreover,

the chronicity of HBV deserves special consideration because 87 percent of cases are chronic, indicating the necessity of permanent medical follow-up. It has an incubation period that varies with 60 percent on several weeks, 34 percent several months and 6 percent longer periods, which leaves a variable factor on the actual time symptoms appear and are determined. It was found that HBV infection in Lashkar Gah City is most prevalent among very young children and older adolescents/adults, exhibits a striking male predominance, is concentrated in densely populated and hot regions, and poses a significant chronic burden on the affected population, table 3 organizes the data from the study into clearly defined categories, highlighting the key findings related to age, gender, geography, chronicity, and the incubation period of HBV infection in Lashkar Gah City.

Table 3 – HBV infection in Lashkar Gah city by different categories

Category	Subgroup/Description	Percentage (%)
Age Group Prevalence	Children under 5 years old	56%
	6-10 years old	2%
	11-15 years old	1%
	Individuals over 16 years old	41%
Gender Distribution	Male	99%
	Female	1%
Geographical Distribution	High-density areas	96%
	Low-density areas	4%
Regional Conditions	Hot regions	92%
	Cold regions	8%

Continuation of the table

Category	Subgroup/Description	Percentage (%)
Chronic HBV Infection Severity	Severity level 25%	72%
	Severity level 50%	12%
	Severity level 75%	16
Duration of Chronic HBV Infection	Long-term (87% duration)	87%
Incubation Period	Several weeks	60%
	Several months	34%
	Extended period	6%

Clinical Manifestations and Symptoms of the Population in Lashkar Gah City

HBV infection in Lashkar Gah City causes nausea, vomiting, and jaundice in 94% of patients. Only 2% of people complain of joint discomfort and tiredness, while 4% claim shortness of breath and chest pain, these symptoms suggest that this population's first HBV symptoms are gastrointestinal and hepatic problems. HBV infection causes minor clinical signs in 63% of cases. Based on survey data from Lashkar Gah City, 63% of HBV-infected individuals reported minimal or absent clinical manifestations. Moreover, 24% indicated symptomatic presentation in roughly 10% of cases, whereas 11% noted moderate symptom occurrence in approximately half of instances. Only 2% reported consistently experiencing clinical symptoms. These findings imply that a considerable proportion of HBV cases may be asymptomatic or exhibit mild symptomatology, potentially impeding prompt detection and timely clinical diagnosis. About 62% of HBV-infected children had few clinical signs. 25% of children have symptoms 10% of the time, and 12% have symptoms 50%. Only 1% of children always have symptoms. The generally low symptoms in the infected population suggest that children, like adults, have a subclinical or mild version of the disease. HBsAg test is of fact a very effective and a popular method of detecting HBV infection as it forms a majority of about 97% of diagnostic procedures employed in the laboratory. These serologic markers are HBsAg that is the initial to occur in acute infection and whose presence is absolute expert regarding active HBV infection hence; it is sensitive and specific when utilized in screening. By contrast, the CBC, sometimes used on average (3%) to supplement general clinical evaluation, has no HBV-specific application or value as a diagnostic measure. Therefore, HBsAg testing use was greatly prevailing in our study which is within international

clinical practices and guarantees the diagnosing quality of HBV candidates. In Lashkar Gah City, HBsAg testing is the main HBV diagnostic method. HBsAg is the most prevalent HBV test, utilised in 95% of cases. Few blood glucose tests are performed 5%. Blood glucose is also used in HBV patients to test liver-related metabolic disbalance and check comorbidity conditions like diabetes to properly evaluate the condition and manage it successfully in the clinical setting. This highlights the relevance of HBsAg testing in this region's HBV clinical diagnosis. Up to 65% of children have HBV for years. Up to 15% of children have the infection for months, while 15% have distinct phases. Up to 5% had the infection for weeks. This suggests that children's infections last a long time and require long-term medical care. With 60% of persons having HBV over different periods, infection duration varies. Around 26% have had the infection for years, and 10% for months. Only 4% had the infection for weeks. This variance in adult infection duration shows that HBV is persistent and requires individualised care. HBV infection in Lashkar Gah City mostly causes nausea, vomiting, and jaundice, with few other symptoms. Both children and adults have subclinical or mild illness presentations, making early detection difficult. The HBsAg test is the primary diagnostic tool used in the region treatment protocols (Figure 6).

Case Studies

In Lashkar Gah City, the impact of HBV is deeply felt, not only on a public health level but also through the personal struggles of affected individuals and their families. Anecdotal data combined with case studies can have a significant contribution to the understanding of the lived experiences of the people affected by HBV, both demonstrating the social and healthcare needs of this population.

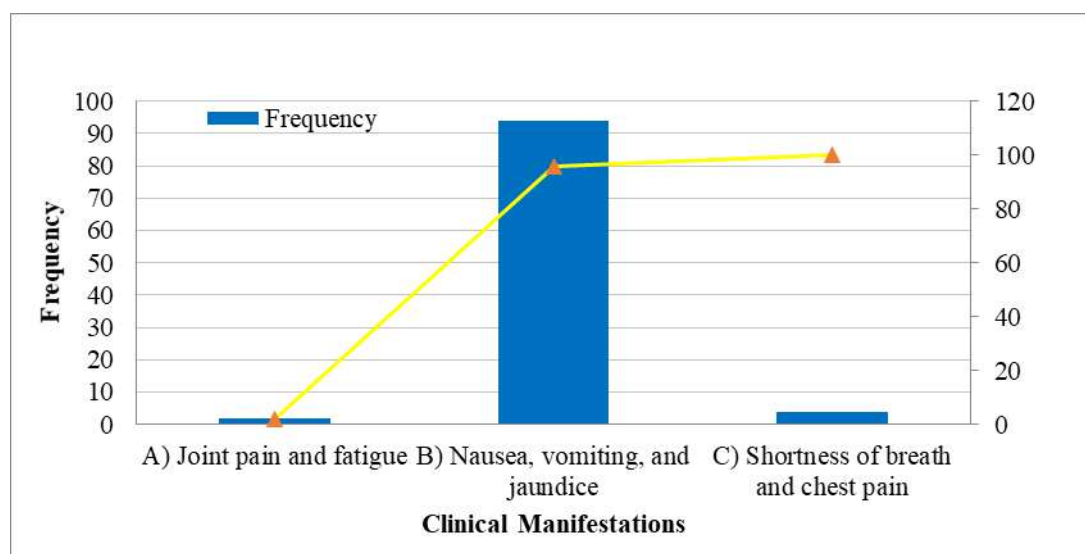


Figure 6 – The initial and acute clinical manifestations of HBV infection are the early indicators of the body's response to the virus.

1. Case Study – A Narrative of a Chronic HBV patient

Ezatullah, a 38-year-old male patient arrived in Lashkar Gah with more than 5-year-old C-HBV. The symptoms identified that led to his diagnosis of the virus included fatigue, jaundice, and nausea. His experience started with inability to get medical attention easily because there were not many resources in the area. Ezatullah spent some months attending the local clinics before being finally referred to the Helmand Provincial Infectious Disease Therapy Hospital. His treatment alternatives were also limited because of limited supply of antiviral medications at the hospital and absence of special care. The situation in the case of Ezatullah presents the problem of living with chronic HBV in a resourceous poor environment and the significance of access to prompt medical care.

The disease is also a major source of social stigma in the case of Ezatullah, as it is not only a health challenge. The result was the social isolation of his family as most people in their neighborhood thought that HBV was very contagious and therefore people with it were believed to have poor personal hygiene. Ezatullah experienced a number of difficulties obtaining employment because of the wrong image about his condition. When people are socially stigmatized about the HBV, they tend to avoid any treatment knowing that they will be looked down and discriminated by other members of the society. The case of Ezatullah reflects on the importance of improved education on public health

to struggle against these misperceptions and decrease the stigmatism of HBV.

2. Case Study The Story of a Chronic HBV Patient, effect on the life of a Child

Amina, a 4-year-old girl, was detected with HBV in a screening process in her local health care facility in Lashkar Gah. Her mother did not know about the virus until she was surprised to find that her daughter had developed HBV since they did not get proper vaccination because of the lack of resources. The diagnosis was especially grim because Amina had a chronic infection that would need management over the long-term and such kind of provision was not easily available in the city. She had a mild jaundice and tiredness and her parents were concerned about her.

The situation of Amina stresses the role of vaccination in the prevention of HBV spread especially in susceptible populations such as children. The inability of her mother to get proper treatment to Amina emphasizes the lack of a better healthcare infrastructure in Lashkar Gah where specialized healthcare facilities and antiviral drugs are not easily accessible. In addition, family members of Amina were emotionally traumatized since they had an uncomfortable future without knowing how to control her condition in the long run. The case demonstrates the important role of early diagnosis of the disease and long-term care of children infected with HBV, which can overcome adverse health effects.

Anecdotal Evidence: The Problems of Healthcare Providers

The problem is that healthcare professionals in Lashkar Gah have little resources at their disposal and the healthcare infrastructure is not sufficient to help them find solutions to diagnosing HBV and treating it properly, as Dr. Ali, a general practitioner at Bost University Private Hospital, demonstrated. Dr. Ali describes the cases when patients came to the hospital with already developed stages of HBV infection only to realise that they did not have access to the tools of diagnosis or the curing antiviral drugs. In other patients, chronic liver diseases or cirrhosis were already evident before they availed themselves to the doctor, which was currently caused by a long-term un-diagnosed HBV infection, yet no therapy had been previously saved.

According to Dr. Ali, health professionals tend to be in a rut of attempting to treat a large number of patients without sufficient resources to do so. To make matters worse, there is little supply of vaccines, particularly among the at-risk groups such as pregnant women. In addition, the fact that there is no sustained professional education in HBV governance, not including a coordinated approach to mobilizing communities toward the development of the public health scenario, complicates the task of managing it effectively.

A Deeper Insight on Societal Influence Awareness using the Public Healthers Perspective.

Most urban settlements in the Lashkar Gah have a huge difference of awareness on HBV transmission and prevention. According to anecdotal evidence, most individuals are ignorant of the fact that the infection may either be contracted through injection sharing, unprotected intercourse, or mother to baby contraction during birth. Farida, one of the community leaders, expressed her frustrations on misconceived knowledge by many families in her community on the fact that HBV is transmitted through casual contact such as hugging and sharing food. This myth makes people fail to take proper preventative measures which in many cases could lead to the prevention of the disease e.g. by vaccination or measures that are less dangerous during medical procedures.

Farida has made a personal initiative to make the community in which she lives more aware of the issue of HBV through such activities as informal programs and provision of educative literature. It shows her initiatives are necessary since grass-root movements can be used to counter the disinformation

and promote installing protective habits, particularly in low-resource regions.

The real-life stories of Ezatullah, Amina, professional healthcare providers, local leaders of the area of Lashkar Gah, clearly show how HBV severely affects a person and communities. Through these case studies, it is clear that much more needs to be done in relation to the development of public health facilities to improve access to vaccines and treatment and the advent of sensitization programs to address the stigma and early diagnosis. Addressing these issues will not only alleviate the burden on healthcare systems but also improve the quality of life for those affected by HBV in Lashkar Gah.

On the other hand, integrated pharmacological and holistic modalities, endorsed by 50% and 46% of respondents respectively in Lashkar Gah City, highlight the significance of amalgamating antiviral treatment with preventive interventions such as immunization and public health awareness in the comprehensive control of HBV infection.

Previous studies indicate that the incidence of HBV in Afghanistan is higher in areas with limited healthcare access, poor sanitation, and socioeconomic challenges [42]. A population-based investigation conducted in the United States revealed that adults with chronic hepatitis B infection exhibited a 1.9-fold elevation in all-cause mortality risk and a 13.3-fold augmentation in liver-related mortality risk relative to uninfected counterparts [48, 49].

According to Abera et al. (2014) revealed that liver hepatitis resulting from co-infection with Hepatitis B and C is the leading cause of morbidity and mortality in HIV-infected children, with 19.5% testing positive for HBsAg or anti-HCV antibodies, thus highlighting the need for routine screening [50, 51]. Karabaev et al. (2017) observed that post-Soviet Kyrgyzstan has experienced a rise in blood-borne infections, with 78% of donors being male and 22% female. The study documented a decline in the prevalence of HBsAg, anti-HCV, and anti-T. Pallidum from 2012 to 2015, while HIV prevalence increased [52]. Ahmadi Gharaei et al. (2021) highlight considerable global and regional disparities in the co-occurrence of hepatitis B and C among HIV-positive incarcerated individuals, with prevalence rates varying from 12% for HBV-HIV co-infection to 62% for HCV-HIV co-infection. The research advocates for enhanced screening and therapeutic interventions, specifically directed at high-risk cohorts. It underscores the efficacy of community-based needle and syringe exchange programs, which averted 25,000 HIV infections in Australia [53]. Chu et al.

(2023) investigated the genotype-specific influence of HLA variants on HBsAg seroclearance in chronic hepatitis B patients, finding that the Rs1710 G allele was linked to seroclearance in both genotype B and C infections, while the Rs2770 G allele was associated exclusively with genotype B infections [54-56].

A study in Uganda found that hepatitis B and C viruses cause liver damage in HIV-positive individuals, with higher rates among women, the prevalence of HBV is 10% in Uganda, while HCV is not documented. The chronicity of these infections depends on age, sex, and immune-competence. Proper diagnosis is crucial for better management, as HIV prevalence in Uganda is 6% among adults aged 15-49 years and 10% in children under five [57].

Research conducted at the University of Nigeria Teaching Hospital revealed that co-infection with hepatitis B and C viruses occurs more frequently than with hepatitis C alone, with instances of triple viral infection also observed. Vigilant screening for these infections is essential for early detection and comprehensive management of HIV patients, especially in Africa, which remains the most severely affected region [58, 59]. A research investigation in Western Saudi Arabia identified an 8.5% prevalence of coinfections among patients with HIV, HBV, and HCV. However, 20 out of every 1,000 cases had undiagnosed coinfections due to insufficient screening protocols. Such coinfections elevate morbidity and mortality rates, with liver disease resulting from HCV or HBV coinfection being the predominant cause of non-AIDS-related fatalities [59].

Additionally, a 34-year-old Caucasian female presented with severe acute hepatitis, coagulopathy, and ascites attributed to a coinfection of HBV and Epstein-Barr virus (EBV) [60]. This case represents the first documented instance of HBV and EBV coinfection in the medical literature. The concomitant infection of HBV and EBV can precipitate severe acute hepatitis with potential for HBV chronicity. The World Health Organization estimates that 400 million individuals globally are carriers of HBV, and coinfections with other viruses tend to exacerbate clinical severity and progression. The optimal treatment strategy for HBV coinfections remains uncertain, with current guidelines emphasizing the identification and treatment of the predominant virus [60, 61].

A study conducted at Adnan Menderes University Medical Faculty in Turkey revealed that hepatitis B infections frequently present with unconventional serological profiles within the liver.

The research identified that a significant number of cases exhibited these atypical serological patterns, and a correlation was found between these profiles in hepatitis B patients [62]. And a study conducted in southern China revealed that 47.4% of anti-HBc-positive blood donors exhibited anti-HBc, indicative of previous HBV exposure [63]. The prevalence of anti-HBc positivity correlated positively with age, with 777 donors also testing positive for anti-HBs. The occurrence of occult hepatitis B infection (OBI) among anti-HBc-positive donors was 2.86%. This study indicates that a minor subset of donors harbors HBV DNA despite HBsAg and NAT screening, underscoring the necessity for more sensitive NAT testing methods [63, 64].

The investigation scrutinized the prevalence of Hepatitis B and C Virus infections among expectant mothers at Borumeda General Hospital in Northeast Ethiopia. Involving 124 participants, the study employed a structured questionnaire to evaluate various factors and sociodemographic attributes. The overall seroprevalence of HBV or HCV infections was determined to be 11.3%. The findings indicate that the prevalence of HBV and HCV infections among pregnant women is notably high, categorizing it within the high endemic bracket of the WHO classification scheme. Consequently, the study advocates for ongoing screening, the provision of hepatitis B vaccinations for women, and the implementation of health education initiatives to enhance awareness regarding these infections [65]. And Plasma levels of HBV DNA and quantitative measurements of HBsAg serve as indicators of infection risk. The advent of the HBV vaccine has significantly diminished the incidence of acute hepatitis B (AHB), with the United States reporting its lowest rates since 1990. High numbers of CHB are common in Southeast Asia, China, sub-Saharan Africa and among Indigenous communities [66]. The number of persons living with CHB worldwide was estimated at 400 million individuals of whom 1.25 million in the United States alone. Serious consequences that are related to the disease are cirrhosis, hepatocellular carcinoma, and liver failure. Although antiviral therapies have been authorized, a limited number of patients are treated [67]. Effective management involves evaluating cirrhosis progression, assessing alcohol consumption and metabolic risk factors, and considering the patient's family medical history [67-69]. Hepatitis B and C viruses present a formidable global health issue, particularly in low- and middle-income nations. Inadequate diagnosis impedes progress towards the 2030 eradication goals. Swift

and precise diagnostic methods are crucial for effective detection and healthcare provision. There is a pressing need for advanced biomarkers and rapid diagnostic technologies [70]. And HBV replicates its genome within the nucleus, utilizing distinctive nuclear import pathways to traverse the cytoplasm and nuclear envelope. Lipofection and paclitaxel treatments demonstrate that capsid translocation is crucial for capsid arrival and genome release [71].

In summation, Stasi, Silvestri, and Voller (2017) note that HBV infection rates are notably elevated in sub-Saharan Africa and East Asia, particularly in correctional facilities. The substantial prevalence in West and Central Africa underscores the imperative for blood screening and vaccination initiatives targeting high-risk demographics [72]. Zheng et al. (2023) elucidate that HBV utilizes the tumor susceptibility gene 101 (TSG101) to facilitate its egress through multiple multivesicular bodies (MVBs). TSG101 recognizes ubiquitinated HBc, thereby enabling the sorting and export of HBV capsids [73]. A study conducted in the Netherlands proposes that implementing universal anti-HBc screening along with HBV nucleic acid amplification testing could potentially eliminate the need for HBV antigen testing, thereby identifying potentially infectious donors with recent infections or occult hepatitis B infection (OBI) [74]. And For instance, research conducted in Nigeria revealed that 17% of blood donors were confirmed to have OBI, with genotype E being predominant. The study advocates for pre-testing blood donors for OBI and/or anti-HBc prior to transfusion to reduce the risk of HBV transmission [75]. At the same time, whether we consider a study conducted in Santiago, Chile, analyzed Hepatitis B and C virus infection rates among individuals living with HIV. The majority of HIV cases were transmitted through sexual contact, with 25.7% of participants having progressed to AIDS and 90.4% receiving antiretroviral therapy (ART). The HBV coinfection rate was comparatively lower than that observed in non-industrialized areas; however, a minimal proportion of patients had received vaccination. The presence of HBV coinfection exacerbates morbidity and mortality in people living with HIV (PLWH) [76]. And the World Health Organization has set a goal to eliminate viral hepatitis worldwide by 2030, emphasizing the importance of understanding the regional prevalence and epidemiology of HBV and HDV coinfection. Advances are being made in developing rapid diagnostic tools for the screening and management of patients with HBV/HDV coinfection. These emerging tools are designed to be

more straightforward, accessible, and economical, particularly benefiting low- and middle-income countries. The implementation of such tools could significantly enhance screening efforts, patient monitoring, and the determination of treatment eligibility [77, 78]. And a study conducted in British Columbia revealed that 14.4% of individuals with diagnoses of HBV, HCV, or HIV had co-infections with one or more of these viruses [79]. Among the population, injection drug use was most common among those identified as Not a Visible Minority (22.1%), whereas severe material and social deprivation was notably higher among visible ethnic minorities. The World Health Organization and the United Nations Programme on HIV/AIDS have set a goal to eradicate these epidemics by the year 2030 [79, 80]. And the Global Burden of Disease Study 2019 provided estimates on the worldwide prevalence of HBV, associated mortality, and disability-adjusted life-years (DALYs) attributable to HBV. The study reported a global prevalence of chronic HBV infection at 4.1% for 2019, marking a 31.3% reduction from 1990. HBV-related illnesses accounted for 550,000 deaths globally in 2019. The findings emphasize the need for accelerated efforts to meet the 2030 elimination targets, advocating for the strategic enhancement and expansion of HBV interventions to achieve eradication. The WHO Global Health Sector Strategy on Viral Hepatitis aims to eliminate viral hepatitis as a significant public health threat [81]. And covalently closed circular DNA (cccDNA) serves as a crucial parameter for evaluating antiviral efficacy in CHB. Nonetheless, measuring cccDNA is invasive and necessitates serum biological markers. Recent investigations have shifted focus to viral indicators, host factors, and emerging detection technologies [82]. According to the EASL 2017 Clinical Practice Guidelines, chronic HBV infection is categorized into five distinct phases, with HBV RNA and HBcrAg emerging as innovative markers for both diagnosis and therapeutic monitoring. Proficiency in these markers can enhance predictions of disease progression and evaluate treatment effectiveness in CHB. However, a standardized assay or commercial kit for precise quantification of HBV cccDNA remains unavailable [82, 83]. And the Advisory Committee on Immunization Practices (ACIP) and the Centers for Disease Control and Prevention (CDC) have published a comprehensive report on strategies for the prevention of HBV infection in the United States [84]. This report advocates for the screening of pregnant women for hepatitis B surface antigen, the administration of the Hepatitis B vaccine and

hepatitis B immune globulin, and the immunization of children and adolescents up to 19 years of age. Additionally, it outlines CDC recommendations for postexposure prophylaxis and synthesizes the

American Association for the Study of Liver Diseases (AASLD) guidelines on maternal antiviral therapy to mitigate perinatal HBV transmission (Table 4) [84-95].

Table 4 – Comparison of main Transmission Drivers of HBV and critical preventive strategies in Lashkar Gah and other epidemic high-risk areas in the world.

Risk Factor	Details	Key Insights
Lashkar Gah city		
Unsafe Medical Practices	44% of patients in Lashkar Gah visit the Helmand Provincial Infectious Disease Therapy Hospital, highlighting concentration of HBV management facilities.	Proper equipment and accessibility are essential for effective prevention and treatment.
Lack of Vaccination	Vaccination efforts are insufficient, particularly among high-risk groups like pregnant women, children, and adolescents.	Vaccination is critical to achieving WHO's 2030 hepatitis elimination goals.
Cultural Practices	Socioeconomic and cultural factors, including injection drug use, lack of healthcare access, and stigma, contribute to HBV prevalence.	Public health education is needed to address cultural and behavioral barriers.
Coinfections (HBV with HCV, HIV, etc.)	Coinfections increase morbidity and mortality, with undiagnosed cases often resulting from poor screening practices.	Improved diagnostics and regular screening are necessary to manage co-infections effectively
High-risk regions globally		
Blood-borne Transmission	Blood donors in Nigeria show a 17% prevalence of occult hepatitis B infection (OBI), highlighting risks from unscreened blood.	Universal blood screening and nucleic acid amplification testing are crucial to reduce transmission.
Socioeconomic and High-Risk Groups	14.4% of HBV, HCV, and HIV patients in British Columbia had co-infections; injection drug use and socioeconomic factors are major contributors	Customized efforts are needed for individuals belonging to at-risk populations and especially those in regions where resources are scarce.
Transmission through sexual contact	In Chile's capital, HIV is often caught through sexual contact and having both HIV and the HBV often makes the effects of HIV worse on people living with it.	Preventive immunization programs combined with targeted educational outreach addressing sexual transmission pathways are indispensable for diminishing infection rates.
Perinatal Transmission	Screening of pregnant women and immunization of newborns are insufficient, leading to increased risk of vertical HBV transmission.	Postexposure prophylaxis and maternal antiviral therapy can significantly reduce perinatal transmission
Global Burden	HBV-related illnesses caused 550,000 deaths globally in 2019 despite a 31.3% decrease in chronic HBV prevalence since 1990	Meeting the 2030 elimination targets requires expanded interventions and improved healthcare systems.
Advances in Diagnosis	Emerging biomarkers (HBV RNA, HBcrAg) and diagnostic techniques offer potential for better disease management but lack standardization	Investment in advanced diagnostics is needed to enhance HBV monitoring and treatment outcomes.

Challenges and Recommendations for the management of HBV infection in Lashkar Gah City

By addressing these challenges and recommendations through targeted interventions,

resource allocation, and international collaboration, Lashkar Gah city can improve its ability to manage and prevent HBV, reduce disease burden, and improve public health outcomes, (Table 5).

Table 5 – Barriers and difficulties in controlling HBV in Lashkar Gah City

Challenge/Barrier	Description	Impact on HBV Control
Inadequate Vaccination Coverage	The study identifies gaps in vaccination efforts, especially among high-risk groups such as children under five. Despite global vaccination recommendations, coverage remains insufficient in Lashkar Gah.	Insufficient vaccination coverage leads to higher infection rates, particularly in younger populations, exacerbating long-term health consequences.
Poor Public Health Awareness	Limited public knowledge and awareness of HBV transmission, prevention, and treatment contribute to ongoing transmission and stigma around the disease.	Poor awareness hinders the adoption of preventive measures like vaccination and timely treatment, prolonging disease burden in the population.
Limited Healthcare Resources	Healthcare infrastructure and resources are limited in Lashkar Gah, affecting the availability of diagnostic tools, treatments, and vaccines.	Limited resources reduce the ability to effectively diagnose and treat HBV, leading to underreporting and undiagnosed cases.
Socio-political Volatility	The issue of political instability and violence in Afghanistan have destabilized healthcare provision and minimized the impact of both the public health initiatives and immunization programs.	Instability makes it difficult to implement coordinated public health strategies, impeding vaccination efforts and necessary health interventions.
Economic Constraints	Economic limitations, both within healthcare systems and at the individual level, impact the affordability and accessibility of HBV-related treatments and preventive services.	Economic barriers prevent widespread access to vaccines, diagnostic tests, and long-term treatment, which is essential to control HBV.
Geographical & Demographic Factors	The study shows higher infection rates in densely populated areas and regions with warmer climates. Certain demographics, such as males and children, are disproportionately affected.	Geographic and demographic factors complicate targeted interventions and resource allocation. Higher prevalence in certain areas demands more focused efforts.
Chronic Nature of HBV	Chronic HBV infection persists in 87% of cases, necessitating long-term treatment and monitoring.	Chronic infections require ongoing healthcare interventions, straining already limited resources and creating a burden on the healthcare system.

Conclusion

This study provides an in-depth analysis of HBV infection in Lashkar Gah City, highlighting significant public health challenges based on laboratory testing, demographic trends, and geographical patterns. Over a span of two years, 3,003 tests were conducted across three private laboratories, with LEMAR contributing approximately 75% of the total testing efforts. The testing methodologies employed demonstrated exceptional reliability, with sensitivities, specificities, and accuracies ranging between 97% and 99%, despite the persistent regional limitations in healthcare resources. Children under five years old were identified as the most affected group, representing 56% of cases, while infection rates showed a notable decline with age, with 41% of cases observed in individuals over 16. HBV infection predominantly affects males (99%), and areas characterized by high population density and hot climates report significantly higher infection

rates (96% and 92%, respectively). Chronic HBV infections, which persist in 87% of cases, necessitate long-term healthcare interventions, as the severity of the condition varies from moderate to severe among patients. Because of the lack of resources, Helmand Bost Provincial Hospital and its laboratories have managed to deal with the huge obstacles and that was primarily possible thanks to the international partners, which have assisted in improving their infrastructure and technology, as well as diagnostic possibilities. The processed to combat HBV in Lashkar Gah would effectively demand a collaborated public health plan involving improved schemes of vaccination, mass community information methods, and entry to diagnostic strategy in disadvantaged areas. Moreover, the enhancement of healthcare systems and research on the approach to prevention and treatment will be important in minimizing the overall burden of diseases and enhancing the health outcome in the population. This multifactor solution is important in terms of long run development of HBV management.

Abbreviations and Acronyms

AHB – Acute Hepatitis B

ALT – Alanine Aminotransferase

BMI – Body Mass Index

BUH – Bost University Hospital

CBC – Complete Blood Count

cccDNA – Covalently Closed Circular DNA

CHB – Chronic Hepatitis B

EBV – Epstein – Barr virus

ENT – Ear, Nose, and Throat

HBcAg – Hepatitis B Core Antigen

HBeAg – Hepatitis B Envelope Antigen

HBIG – Hepatitis B Immunoglobulin

HBsAg – Hepatitis B Surface Antigen

HBV – Hepatitis B Virus

HBVr – Hepatitis B Virus Reactivation

HCC – Hepatocellular Carcinoma

HCV – Hepatitis C Virus

HIV – Human Immunodeficiency Virus

HLA – Human Leukocyte Antigen

MVBs – Multivesicular Bodies

NAT – Nucleic Acid Testing

NGOs – Non-Governmental Organizations

OBI – Occult Hepatitis B Infection

SPSS – Statistical Package for the Social Sciences (IBM SPSS Statistics Version 25)

TDF – Tenofovir Disoproxil Fumarate

TSG101 – Tumor Susceptibility Gene 101

WHO – World Health Organization

Acknowledgements

This research benefited a lot from the great data analysis and SPSS skills provided by the teaching assistant from Helmand University and the team is very grateful for their assistance. Appreciation is also

conveyed to the Helmand Bost Provincial Hospital and all participating laboratories and hospitals, whose support was integral to the successful execution of this study.

Conflict of interest

All authors are aware of the article's content and declare no conflict of interest.

Authors' Contribution

The principal development of the idea of study, data painstaking curation, and formalization of it were primarily developed by Abdul Bari Hejran. He is also the driving force behind the drafting of the initial manuscript as well as high-level supervision during the research procedure. Virendra Kumar Yadav also performed the important task of funding, SPSS software settings and maintenance and verification of the data in a stringent manner. His professionalism greatly contributed to the worth of the manuscript in its review and editing. Parwiz Niazi managed to do a lot of volunteering work by conducting the investigation, formulating the methodological framework, and contributing to resources and software tools necessary. He was prominent in validation, visualization, and intense review and editing of the manuscript.

Data availability statement

The data generated and analyzed during the current study are available from the corresponding author on reasonable request.

References

1. Tsukuda S., & Watashi K. (2020) Hepatitis B virus biology and life cycle. *Antiviral research*, vol. 182, p. 104925. <https://doi.org/10.1016/j.antiviral.2020.104925>
2. Ahn J. C., Ahn J. (2018). Hepatitis B: Standard and novel treatment options. *Clin. Liver Dis.*, vol. 12, no. 1, pp. 19–23. <https://doi.org/10.1002/cld.719>
3. Xu T., Huang Z., Deng Y., Wang S., Su B., Wei W., Wang D., Jiang J., Li A., Zhang G., Yang H., Claret F. X., & Hu W. (2015) Clinical implications of hepatitis B viral infection in Epstein-Barr virus-associated nasopharyngeal carcinoma. *Journal of clinical virology: the official publication of the Pan American Society for Clinical Virology*, vol. 64, pp. 64–71. <https://doi.org/10.1016/j.jcv.2014.11.024>
4. Prasidhthathsint, K., & Stapleton, J. T. (2019). Laboratory Diagnosis and Monitoring of Viral Hepatitis. *Gastroenterology Clinics of North America*, vol. 48, no. 2, pp. 259–279. <https://doi.org/10.1016/j.gtc.2019.02.007>
5. Song J. E., & Kim D. Y. (2016) Diagnosis of hepatitis B. *Annals of translational medicine*, vol. 4, no. 18, p. 338. <https://doi.org/10.21037/atm.2016.09.11>
6. Rahmati, S., Barakzai, Q. A., Rahmani, B., & Faizi, M. (2024). Prevalence of Hepatitis B among patients at Infectious Disease Hospital in Kabul, Afghanistan. *Journal of Preventive Medicine and Hygiene*, 65(1), 101–107. <https://doi.org/10.5455/jpmh.2024.xxxxxx>

7. Shayan, N. A., Rahimi, A., Stranges, S., & Thind, A. (2024). Factors affecting quality of life in hepatitis B patients in Herat, Afghanistan: A case-control study. *Journal of viral hepatitis*, 31(9), 511–523. <https://doi.org/10.1111/jvh.13961>
8. Inamullah Kamawi, Muhammad Ilyas, Umme Habiba, Falak Niaz, & Maqsood Ali. (2024). Hep B UNVEILING THE HEPATITIS B AND HEPATITIS C LANDSCAPE IN JALALABAD: INSIGHTS FROM NUCLEIC ACID AMPLIFICATION TESTING. *Journal of Population Therapeutics and Clinical Pharmacology*, 31(8), 993–999. <https://doi.org/10.53555/jptcp.v31i8.7405>
9. Tanju, I. A., Levent, F., Sezer, R. G., & Cekmez, F. (2014). Hepatitis B, hepatitis C and human immunodeficiency virus seropositivity among children in kabul, afghanistan: a cross-sectional study. *Hepatitis monthly*, 14(3), e16154. <https://doi.org/10.5812/hepatmon.16154>
10. Kuhns, M. C., McNamara, A. L., Holzmayer, V., & Cloherty, G. A. (2019). Molecular and serological characterization of hepatitis B vaccine breakthrough infections in serial samples from two plasma donors. *Virology Journal*, vol. 16, no. 1, pp. 43. <https://doi.org/10.1186/s12985-019-1154-4>
11. Kuhns, M. C., Holzmayer, V., McNamara, A. L., Sickinger, E., Schultess, J., & Cloherty, G. A. (2019). Improved detection of early acute, late acute, and occult Hepatitis B infections by an increased sensitivity HBsAg assay. *Journal of Clinical Virology*, vol. 118, pp. 41–45. <https://doi.org/10.1016/j.jcv.2019.08.001>
12. Lou, S., Taylor, R., Pearce, S., Kuhns, M., & Leary, T. (2018). An ultra-sensitive Abbott ARCHITECT® assay for the detection of hepatitis B virus surface antigen (HBsAg). *Journal of Clinical Virology*, vol. 105, pp. 18–25. <https://doi.org/10.1016/j.jcv.2018.05.009>
13. Kao C. C., Nie Y., Ren S., De Costa N. T. T. S., Pandey R. K., Hong J., Smith D. B., Symons J. A., Beigelman L., & Blatt L. M. (2021) Mechanism of action of hepatitis B virus S antigen transport-inhibiting oligonucleotide polymer, STOPS, molecules. *Mol. Ther. Nucleic Acids*, vol. 27, pp. 335–348. <https://doi.org/10.1016/j.omtn.2021.12.013>
14. Chen Q. Y., Jia H. H., Wang X. Y., Shi Y. L., Zhang L. J., Hu L. P., Wang C., He X., Harrison T. J., Jackson J. B., Wu L., Fang Z. L. (2022). Analysis of entire hepatitis B virus genomes reveals reversion of mutations to wild type in natural infection, a 15-year follow-up study. *Infect. Genet. Evol.*, vol. 97, p. 105184. <https://doi.org/10.1016/j.meegid.2021.105184>
15. Omatola, C. A., Lawal, C., Omosayin, D. O., Okolo, M. O., Adaji, D. M., Mofolorunsho, C. K., & Bello, K. E. (2019). Seroprevalence of HBV, HCV, and HIV and Associated Risk Factors Among Apparently Healthy Pregnant Women in Anyigba, Nigeria. *Viral Immunology*, vol. 32, no. 4, pp. 186–191. <https://doi.org/10.1089/vim.2018.0140>
16. Yazie T. D., & Tebeje M. G. (2019) An updated systematic review and meta-analysis of the prevalence of hepatitis B virus in Ethiopia. *BMC infectious diseases*, vol. 19, pp. 1–13. <https://doi.org/10.1186/s12879-019-4486-1>
17. Zeng Y., Chen P., Xie H., Shen F., & Wei X. (2019) Association between the level of hepatitis B virus DNA and risk of hepatocellular carcinoma: A systematic review and meta-analysis. *International journal of cancer*, vol. 144, no. 9, pp. 2220–2230. <https://doi.org/10.1002/ijc.31885>
18. Eke A. C., Eleje G. U., Eke U. A., Xia Y., & Liu J. (2017) Hepatitis B immunoglobulin during pregnancy for prevention of mother-to-child transmission of hepatitis B virus. *Cochrane Database Syst. Rev.*, vol. 2, no. 2, CD008545. <https://doi.org/10.1002/14651858.CD008545.pub2>
19. Ugwu E. O., Eleje G. U., Ugwu A. O., Nwagha U. I., Ikechebelu J. I., Umeh U. A., & Okafor H. U. (2023) Antivirals for prevention of hepatitis B virus mother-to-child transmission in human immunodeficiency virus positive pregnant women co-infected with hepatitis B virus. *The Cochrane database of systematic reviews*, vol. 6, no. 6, CD013653. <https://doi.org/10.1002/14651858.CD013653.pub2>
20. Wilkins T., Sams R., & Carpenter M. (2019) Hepatitis B: Screening, Prevention, Diagnosis, and Treatment. *American family physician*, vol. 99, no. 5, pp. 314–323. <https://www.aafp.org/afp/2019/0301/p314-s1.html>
21. Chang M. H., Chen D. S. (2015). Prevention of hepatitis B. *Cold Spring Harb. Perspect. Med.*, vol. 5, no. 3, a021493. <https://doi.org/10.1101/cshperspect.a021493>
22. Zhang L., & Wang C. (2020) Evolution of the Hepatitis B Virus Genome and Implications for its Clinical Management. *International journal of molecular sciences*, vol. 21, no. 13, p. 4606. <https://doi.org/10.3390/ijms21134606>
23. Esser K., Cheng X., Wettengel J. M., Lucifora J., Hansen-Palmus L., Austen K., Roca Suarez A. A., Heintz S., Testoni B., Nebioglu F., Pham M. T., Yang S., Zernecke A., Wohlleber D., Ringelhan M., Broxtermann M., Hartmann D., Hüser N., Mergner J., Pichlmair A., et al. (2023) Hepatitis B virus targets lipid transport pathways to infect hepatocytes. *Cell. Mol. Gastroenterol. Hepatol.*, vol. 16, no. 2, pp. 201–221. <https://doi.org/10.1016/j.jcmgh.2023.03.011>
24. Lamontagne, R. J., Bagga, S., & Bouchard, M. J. (2016). Hepatitis B virus molecular biology and pathogenesis. *Hepatology Research*, vol. 2, pp. 163–186. <https://doi.org/10.20517/2394-5079.2016.05>
25. Jiang B., & Hildt E. (2020) Intracellular trafficking of HBV particles. *Cells*, vol. 9, no. 9, p. 2023. <https://doi.org/10.3390/cells9092023>
26. Nguyen, M. H., Wong, G., Gane, E., Kao, J. H., & Dusheiko, G. (2020). Hepatitis B Virus: Advances in Prevention, Diagnosis, and Therapy. *Clinical Microbiology Reviews*, vol. 33, no. 2, e00046–19. <https://doi.org/10.1128/CMR.00046-19>
27. Ghaemi Z., Nafiu O., Tajkhorshid E., Gruebele M., & Hu J. (2023) A computational spatial whole-cell model for hepatitis B viral infection and drug interactions. *Sci. Rep.*, vol. 13, no. 1, p. 21392. <https://doi.org/10.1038/s41598-023-45998-0>
28. Jourdain G., Ngo-Giang-Huong N., Cressey T. R., Hua L., Harrison L., Tierney C., Salvadori N., Decker L., Traisathit P., Sirirungsri W., Khamduang W., Bowonwatanuwong C., Puthanakit T., Siberry G. K., Watts D. H., Murphy T. V., Achalapong J., Hongsiriwon S., Klinbuayaem V., Thongsawat S., et al. (2016) Prevention of mother-to-child transmission of hepatitis B virus: A phase III, placebo-controlled, double-blind, randomized clinical trial to assess the efficacy and safety of a short course of tenofovir disoproxil fumarate in women with hepatitis B virus e-antigen. *BMC Infect. Dis.*, vol. 16, p. 393. <https://doi.org/10.1186/s12879-016-1734-5>

29. Segeral O., Dim B., Durier C., Nhoueng S., Chhim K., Sovann S., Yom S., Vong C., Yin S., Ros B., Ky V., Pech S., Nem B., Hout K., Guillebaud J., Ear E., Caroupaye-Caroupin L., Rekeciewicz C., Fernandez L., Laurent D., ... Laurence Borand for the ANRS-MIE TA PROHM Study Group (2022) Immunoglobulin-free strategy to prevent HBV mother-to-child transmission in Cambodia (TA-PROHM): a single-arm, multicentre, phase 4 trial. *The Lancet. Infectious diseases*, vol. 22, no. 8, pp. 1181–1190. [https://doi.org/10.1016/S1473-3099\(22\)00206-7](https://doi.org/10.1016/S1473-3099(22)00206-7)
30. Molla, S., Munshea, A., & Nibret, E. (2015). Seroprevalence of hepatitis B surface antigen and anti-HCV antibody and its associated risk factors among pregnant women attending maternity ward of Felege Hiwot Referral Hospital, northwest Ethiopia: a cross-sectional study. *Virology Journal*, vol. 12, pp. 204. <https://doi.org/10.1186/s12985-015-0437-7>
31. Mardian, Y., Yano, Y., Wasityastuti, W., Ratnasari, N., Liang, Y., Putri, W. A., Triyono, T., & Hayashi, Y. (2017). Genetic polymorphisms of HLA-DP and isolated anti-HBc are important subsets of occult hepatitis B infection in Indonesian blood donors: a case-control study. *Virology Journal*, vol. 14, no. 1, pp. 201. <https://doi.org/10.1186/s12985-017-0865-7>
32. Wang L., Zou Z. Q., & Wang K. (2016) Clinical Relevance of HLA Gene Variants in HBV Infection. *Journal of immunology research*, vol. 2016, p. 9069375. <https://doi.org/10.1155/2016/9069375>
33. Akgöllü E., Bilgin R., Akkız H., Ülger Y., Kaya B. Y., Karaoğullarından Ü., Arslan Y. K. (2017). Association between chronic hepatitis B virus infection and HLA-DP gene polymorphisms in the Turkish population. *Virus Res.*, vol. 232, pp. 6–12. <https://doi.org/10.1016/j.virusres.2017.01.017>
34. Chu Y. J., Jeng W. J., Pan M. H., Hu H. H., Luo W. S., Su C. Y., Chiang C. T., Jen C. L., Chen C. J., & Yang H. I. (2022) Serum soluble programmed death-1 levels predict the spontaneous HBeAg seroclearance in chronic hepatitis B. *J. Gastroenterol.*, vol. 57, no. 6, pp. 423–432. <https://doi.org/10.1007/s00535-022-01874-8>
35. Prange, R. (2022). Hepatitis B virus movement through the hepatocyte: An update. *Biology of the Cell*, vol. 114, no. 12, pp. 325–348. <https://doi.org/10.1111/boc.202200060>
36. MacLachlan, J. H., & Cowie, B. C. (2015). Hepatitis B virus epidemiology. *Cold Spring Harbor Perspectives in Medicine*, vol. 5, no. 5, a021410. <https://doi.org/10.1101/cshperspect.a021410>
37. Lee, J. H., & Kim, H. S. (2021). Current laboratory tests for diagnosis of hepatitis B virus infection. *International Journal of Clinical Practice*, vol. 75, no. 12, e14812. <https://doi.org/10.1111/ijcp.14812>
38. Sakamoto K., Umemura T., Ito K., Okumura A., Joshita S., Ota M., Sugiyama M., Mizokami M., Yoneda M., & Tanaka E. (2020) Virological Factors Associated With the Occurrence of Hepatitis B Virus (HBV) Reactivation in Patients With Resolved HBV Infection Analyzed Through Ultradeep Sequencing. *The Journal of infectious diseases*, vol. 221, no. 3, pp. 400–407. <https://doi.org/10.1093/infdis/jiz478>
39. Hayashi K., Ishigami M., Ishizu Y., Kuzuya T., Honda T., Tachi Y., Ishikawa T., Katano Y., Yoshioka K., Toyoda H., Kumada T., Goto H., & Hirooka Y. (2016) Clinical characteristics and molecular analysis of hepatitis B virus reactivation in hepatitis B surface antigen-negative patients during or after immunosuppressive or cytotoxic chemotherapy. *J. Gastroenterol.*, vol. 51, no. 11, pp. 1081–1089. <https://doi.org/10.1007/s00535-016-1187-z>
40. Belaiba Z., Ayouni K., Gdoura M., Kammoun Rebai W., Touzi H., Sadraoui A., Triki H. (2022). Whole genome analysis of hepatitis B virus before and during long-term therapy in chronic infected patients: Molecular characterization, impact on treatment and liver disease progression. *Front. Microbiol.*, vol. 13, p. 1020147. <https://doi.org/10.3389/fmicb.2022.1020147>
41. World Health Organization. (2019) Hepatitis B. <https://www.who.int/news-room/fact-sheets/detail/hepatitis-b>
42. Sharma B., Khanal S., & Bhattarai B. (2018) Prevalence and associated factors of Hepatitis B virus infection among urban slum dwellers in Eastern Nepal. *Journal of Infection and Public Health*, vol. 11, no. 6, pp. 867–871. <https://doi.org/10.1016/j.jiph.2018.06.005>
43. Nguyen, V. T., Law, M. G., & Dore, G. J. (2014). Hepatitis B-related hepatocellular carcinoma: Epidemiological characteristics and disease burden. *Journal of Viral Hepatitis*, vol. 16, no. 7, pp. 453–463. <https://doi.org/10.1111/j.1365-2893.2009.01117.x>
44. Azami M., Darvishi Z., Sayehmiri K. (2017). Hepatitis B prevalence and risk factors in Eastern Mediterranean and African countries: A systematic review and meta-analysis. *World J. Gastroenterol.*, vol. 23, no. 40, pp. 7301–7310. <https://doi.org/10.3748/wjg.v23.i40.7301>
45. Alavian S. M., Haghbin H., Lankarani K. B. (2016). Hepatitis B and its environmental factors: A study from the Middle East. *Middle East J. Dig. Dis.*, vol. 8, no. 2, pp. 85–89. <https://doi.org/10.15171/mejdd.2016.16>
46. Tripathi N., Mousa OY. Hepatitis B. [Updated 2023 Jul 9]. In: StatPearls [Internet]. Treasure Island (FL): StatPearls Publishing; 2025 Jan-. Available from: https://www.ncbi.nlm.nih.gov/books/NBK555945/?utm_source=chatgpt.com
47. Li, W. J., Xu, H. X., Wu, D. S., Wu, Y. J., & Xu, W. D. (2017). A novel fully automated system for quantification of Hepatitis B virus DNA using magnetic bead-based method combined with real-time PCR. *Journal of virological methods*, 248, 130–135. <https://doi.org/10.1016/j.jviromet.2017.07.001>
48. Zhou, K., Dodge, J. L., Grab, J., Poltavskiy, E., & Terrault, N. A. (2020). Mortality in adults with chronic hepatitis B infection in the United States: a population-based study. *Alimentary pharmacology & therapeutics*, 52(2), 382–389. <https://doi.org/10.1111/apt.15803>
49. Shim, J. J., Kim, J. W., Oh, C. H., Lee, Y. R., Lee, J. S., Park, S. Y., Kim, B. H., & Oh, I. H. (2018). Serum alanine aminotransferase level and liver-related mortality in patients with chronic hepatitis B: A large national cohort study. *Liver international: official journal of the International Association for the Study of the Liver*, 38(10), 1751–1759. <https://doi.org/10.1111/liv.13705>
50. Abera B., Zenebe Y., Mulu W., Kibret M., Kahsu G. (2014). Seroprevalence of hepatitis B and C viruses and risk factors in HIV infected children at the Felgehiwot referral hospital, Ethiopia. *BMC Res. Notes*, vol. 7, p. 838. <https://doi.org/10.1186/1756-0500-7-838>

51. Atalay A. A., Abebe R. K., Dadhi A. E., Bededa W. K. (2021). Seroprevalence of hepatitis B virus among pregnant women attending Antenatal care in Dilla University Referral Hospital Gedio Zone, Ethiopia: health facility based cross-sectional study. *PLoS One*, vol. 16, no. 3, p. e0249216. <https://doi.org/10.1371/journal.pone.0249216>
52. Karabaev B. B., Beisheeva N. J., Satybaldieva A. B., Ismailova A. D., Pessler F., & Akmatov M. K. (2017) Seroprevalence of hepatitis B, hepatitis C, human immunodeficiency virus, *Treponema pallidum*, and co-infections among blood donors in Kyrgyzstan: A retrospective analysis (2013-2015). *Infect. Dis. Poverty*, vol. 6, no. 1, p. 45. <https://doi.org/10.1186/s41182-017-0107-x>
53. Ahmadi Gharaei H., Fararouei M., Mirzazadeh A., Sharifnia G., Rohani-Rasaf M., Bastam D., Rahimi J., Kouhestani M., Rezaian S., Dianatinasab M. (2021). The global and regional prevalence of hepatitis C and B co-infections among prisoners living with HIV: a systematic review and meta-analysis. *Infect. Dis. Poverty*, vol. 10, no. 1, p. 93. <https://doi.org/10.1186/s40249-021-00876-7>
54. Chu Y. J., Yang H. I., Hu H. H., Liu J., Lin Y. L., Chang C. L., Luo W. S., Jen C. L., & Chen C. J. (2023) HBV genotype-dependent association of HLA variants with the serodecline of HBsAg in chronic hepatitis B patients. *Sci. Rep.*, vol. 13, no. 1, p. 359. <https://doi.org/10.1038/s41598-023-27570-y>
55. Jain S., Su Y. H., Su Y. P., McCloud S., Xue R., Lee T. J., Lin S. C., Lin S. Y., Song W., Steffen J. D., & Hu C. T. (2018) Characterization of the hepatitis B virus DNA detected in urine of chronic hepatitis B patients. *BMC Gastroenterol.*, vol. 18, no. 1, p. 40. <https://doi.org/10.1186/s12876-018-0767-1>
56. Wasityastuti W., Yano Y., Ratnasari N., Triyono T., Triwikatmani C., Indrarti F., Heriyanto D. S., Yamani L. N., Liang Y., Utsumi T., & Hayashi Y. (2016) Protective effects of HLA-DPA1/DPB1 variants against Hepatitis B virus infection in an Indonesian population. *Infection, genetics and evolution: journal of molecular epidemiology and evolutionary genetics in infectious diseases*, vol. 41, pp. 177–184. <https://doi.org/10.1016/j.meegid.2016.03.034>
57. Baseke J., Musenero M., Mayanja-Kizza H. (2015). Prevalence of hepatitis B and C and relationship to liver damage in HIV infected patients attending Joint Clinical Research Centre Clinic (JCRC), Kampala, Uganda. *Afr. Health Sci.*, vol. 15, no. 2, pp. 322–327. <https://doi.org/10.4314/ahs.v15i2.3>
58. Nnakenyi, I. D., Uchechukwu, C., & Nto-Ezimah, U. (2020). Prevalence of hepatitis B and C virus co-infection in HIV positive patients attending a health institution in southeast Nigeria. *African Health Sciences*, vol. 20, no. 2, pp. 579–586. <https://doi.org/10.4314/ahs.v20i2.5>
59. Al-Mughales J. A. (2016). Co-infection assessment in HBV, HCV, and HIV patients in Western Saudi Arabia. *J. Med. Virol.*, vol. 88, no. 9, pp. 1545–1551. <https://doi.org/10.1002/jmv.24503>
60. Rao S. C., Ashraf I., Mir F., Samiullah S., Ibdah J. A., & Tahan V. (2017) Dual Infection with Hepatitis B and Epstein-Barr Virus Presenting with Severe Jaundice, Coagulopathy, and Hepatitis B Virus Chronicity Outcome. *The American journal of case reports*, vol. 18, pp. 170–172. <https://doi.org/10.12659/ajcr.901688>
61. Beran A., Mhanna M., Haghbin H., Sample J. W., Burlen J. (2021). A case of hepatitis B virus reactivation triggered by acute Epstein-Barr virus infection. *Cureus*, vol. 13, no. 10, p. e18676. <https://doi.org/10.7759/cureus.18676>
62. Aydın N., Kırdar S., Uzun N., Eyigör M., Sayan M. (2016). Hepatit B enfeksiyonunda atipik serolojik profiller: HBsAg ve anti-HBs birlikte pozitif olgularda S geni mutasyonlarının araştırılması [Atypical serological profiles in hepatitis B infections: investigation of S gene mutations in cases with concurrently positive for HBsAg and anti-HBs]. *Mikrobiyol. Bult.*, vol. 50, no. 4, pp. 535–543. <https://doi.org/10.5578/mb.32197>
63. Ye X., Li T., Xu X., Du P., Zeng J., Zhu W., Yang B., Li C., & Allain J. P. (2017) Characterisation and follow-up study of occult hepatitis B virus infection in anti-HBc-positive qualified blood donors in southern China. *Blood transfusion = Trasfusione del sangue*, vol. 15, no. 1, pp. 6–12. <https://doi.org/10.2450/2016.0136-16>
64. Hedayati-Moghaddam M. R., Tehranian F., Mosavat A., Miri R., & Ahmadi Ghezeldasht S. (2024) Low prevalence of anti-HBc antibody and lack of HBV DNA among HBsAg-negative blood donors in Iran: A cross-sectional study and review of literature. *Arch. Iran. Med.*, vol. 27, no. 6, pp. 305-312. <https://doi.org/10.34172/aim.28579>
65. Gebretsadik D., Assefa M., Fenta G. M., Daba C., Ali A., & Tekele S. G. (2022) High seroprevalence of hepatitis B and C virus infections among pregnant women attending antenatal clinic in Borumeda General Hospital, Northeast Ethiopia. *Biomed. Res. Int.*, vol. 2022, p. 1395238. <https://doi.org/10.1155/2022/1395238>
66. Burns G. S., Thompson A. J. (2014). Viral hepatitis B: clinical and epidemiological characteristics. *Cold Spring Harb. Perspect. Med.*, vol. 4, no. 12, a024935. <https://doi.org/10.1101/cshperspect.a024935>
67. Rajbhandari, R., & Chung, R. T. (2016). Treatment of Hepatitis B: A Concise Review. *Clinical and Translational Gastroenterology*, vol. 7, no. 9, e190. <https://doi.org/10.1038/ctg.2016.46>
68. Rybicka M., & Bielawski K. P. (2020) Recent Advances in Understanding, Diagnosing, and Treating Hepatitis B Virus Infection. *Microorganisms*, vol. 8, no. 9, pp. 1416. <https://doi.org/10.3390/microorganisms8091416>
69. Guvenir M., & Arian A. (2020) Hepatitis B virus: From diagnosis to treatment. *Pol. J. Microbiol.*, vol. 69, no. 4, pp. 391-399. <https://doi.org/10.33073/pjm-2020-044>
70. Shenge J. A., & Osiowy C. (2021) Rapid diagnostics for hepatitis B and C viruses in low-and middle-income countries. *Frontiers in Virology*, vol. 1, p. 742722. <https://doi.org/10.3389/fviro.2021.742722>
71. Blondot M. L., Bruss V., Kann M. (2016). Intracellular transport and egress of hepatitis B virus. *J. Hepatol.*, vol. 64, no. 1 Suppl, pp. S49–S59. <https://doi.org/10.1016/j.jhep.2016.02.008>
72. Stasi C., Silvestri C., & Voller F. (2017) Emerging Trends in Epidemiology of Hepatitis B Virus Infection. *Journal of clinical and translational hepatology*, vol. 5, no. 3, pp. 272–276. <https://doi.org/10.14218/JCTH.2017.00010>
73. Zheng Y., & Chiu C. W. (2021) Detection and prevention of hepatitis B virus reactivation in patients with hematologic malignancies. *Transfusion and apheresis science: official journal of the World Apheresis Association*, vol. 60, no. 2, p. 102973. <https://doi.org/10.1016/j.transci.2021.102973>




74. Van de Laar T. J., Hogema B. M., Molenaar-de Backer M. W., Marijt-van der Kreek T., & Zaaier H. L. (2021) Blood donor screening in the Netherlands: Universal anti-HBc screening in combination with HBV nucleic acid amplification testing may allow discontinuation of hepatitis B virus antigen testing. *Transfusion*, vol. 61, no. 7, pp. 2116–2124. <https://doi.org/10.1111/trf.16420>
75. Oluyinka, O. O., Tong, H. V., Bui Tien, S., Fagbami, A. H., Adekanle, O., Ojurongbe, O., Bock, C. T., Kremsner, P. G., & Velavan, T. P. (2015). Occult Hepatitis B Virus Infection in Nigerian Blood Donors and Hepatitis B Virus Transmission Risks. *PloS One*, vol. 10, no. 7, e0131912. <https://doi.org/10.1371/journal.pone.0131912>
76. Weitzel T., Rodríguez F., Noriega L. M., Marcotti A., Duran L., Palavecino C., Porte L., Aguilera X., Wolff M., & Cortes C. P. (2020) Hepatitis B and C virus infection among HIV patients within the public and private healthcare systems in Chile: A cross-sectional serosurvey. *PloS one*, vol. 15, no. 1, e0227776. <https://doi.org/10.1371/journal.pone.0227776>
77. Ceesay A., Bouherrou K., Tan B. K., Lemoine M., Ndow G., Testoni B., Chemin I. (2022). Viral diagnosis of hepatitis B and Delta: What we know and what is still required? Specific focus on low- and middle-income countries. *Microorganisms*, vol. 10, no. 11, p. 2096. <https://doi.org/10.3390/microorganisms10112096>
78. Bell T. G., Kramvis A. (2015). Bioinformatics tools for small genomes, such as hepatitis B virus. *Viruses*, vol. 7, no. 2, pp. 781–797. <https://doi.org/10.3390/v7020781>
79. Binka M., Butt Z. A., McKee G., Darvishian M., Cook D., Wong S., Yu A., Alvarez M., Samji H., Wong J., Krajden M., Janjua N. Z. (2021). Differences in risk factors for hepatitis B, hepatitis C, and human immunodeficiency virus infection by ethnicity: A large population-based cohort study in British Columbia, Canada. *Int. J. Infect. Dis.*, vol. 106, pp. 246–253. <https://doi.org/10.1016/j.ijid.2021.03.061>
80. Binka M., Butt Z. A., Wong S., Chong M., Buxton J. A., Chapinal N., Yu A., Alvarez M., Darvishian M., Wong J., McGowan G., Torban M., Gilbert M., Tyndall M., Krajden M., Janjua N. Z. (2018). Differing profiles of people diagnosed with acute and chronic hepatitis B virus infection in British Columbia, Canada. *World J. Gastroenterol.*, vol. 24, no. 11, pp. 1216–1227. <https://doi.org/10.3748/wjg.v24.i11.1216>
81. GBD 2019 Hepatitis B Collaborators (2022) Global, regional, and national burden of hepatitis B, 1990–2019: A systematic analysis for the Global Burden of Disease Study 2019. *Lancet Gastroenterol. Hepatol.*, vol. 7, no. 9, pp. 796–829. [https://doi.org/10.1016/S2468-1253\(22\)00124-8](https://doi.org/10.1016/S2468-1253(22)00124-8)
82. Ou, Q., Guo, J., Zeng, Y., & Chen, H. (2020). Insights for clinical diagnostic indicators of virus and host in chronic hepatitis B infection. *Journal of Viral Hepatitis*, vol. 27, no. 3, pp. 224–232. <https://doi.org/10.1111/jvh.13260>
83. European Association for the Study of the Liver (2017) EASL 2017 Clinical practice guidelines on the management of hepatitis B virus infection. *J. Hepatol.*, vol. 67, no. 2, pp. 370–398. <https://doi.org/10.1016/j.jhep.2017.03.021>
84. Schillie S., Vellozzi C., Reingold A., Harris A., Haber P., Ward J. W., & Nelson N. P. (2018) Prevention of Hepatitis B Virus Infection in the United States: Recommendations of the Advisory Committee on Immunization Practices. *MMWR. Recommendations and reports: Morbidity and mortality weekly report. Recommendations and reports*, vol. 67, no. 1, pp. 1–31. <https://doi.org/10.15585/mmwr.rr6701a1>
85. Connors E. E., Panagiotakopoulos L., Hofmeister M. G., Spradling P. R., Hagan L. M., Harris A. M., Rogers-Brown J. S., Wester C., Nelson N. P., & Contributors (2023) Screening and testing for hepatitis B virus infection: CDC recommendations – United States, 2023. *MMWR. Recomm. Rep.*, vol. 72, no. 1, pp. 1–25. <https://doi.org/10.15585/mmwr.rr7201a1>
86. Kondo Y., Shirai T., Morikawa H., Takayama Y., & Mizushima T. (2018) Long-term outcomes of hepatitis B virus infection in a cohort of Japanese blood donors. *Hepatol. Res.*, vol. 48, no. 7, pp. 533–540. <https://doi.org/10.1111/hepr.13147>
87. Kuhn J. M., Wester C., & Choi A. (2023) Hepatitis B virus epidemiology, diagnostic strategies, and public health approaches to reducing global burden: A comprehensive review. *Int. J. Infect. Dis.*, vol. 126, pp. 80–91. <https://doi.org/10.1016/j.ijid.2023.01.028>
88. Younossi Z. M., & Blach S. (2019) Global epidemiology of Hepatitis B and Hepatitis C: A narrative review. *Hepatology International*, vol. 13, no. 2, pp. 160–168. <https://doi.org/10.1007/s12072-019-10077-6>
89. Zhang Q., Chen Q., Liang J., & Yang L. (2020) Hepatitis B Virus and Hepatitis D Virus Co-Infection: A Review. *Biomolecules*, vol. 10, no. 8, p. 1077. <https://doi.org/10.3390/biom10081077>
90. Zhang W., Liu W., & Zhou Y. (2016) Influence of hepatitis B virus S gene mutations on viral replication and disease progression. *Journal of medical virology*, vol. 88, no. 7, pp. 1147–1157. <https://doi.org/10.1002/jmv.24572>
91. Zhou X., Zhang Y., & Huang Y. (2018) Prevalence of hepatitis B virus infection in China and its relationship with socio-economic status: a national cross-sectional study. *BMJ open*, vol. 8, no. 8, e022784. <https://doi.org/10.1136/bmjopen-2018-022784>
92. Asmatullah, Usmani and Abdul, Qadeer Baseer and Bilal, Ahmad Rahimi and Ajmal, Jahid and Parwiz, Niazi and Abdul, Wahid Monib and Wais, Mohammad Lali (2020) Coronavirus disease 2019 (COVID-19) pandemic: What is the level of knowledge, attitude, and practice in Kandahar, Afghanistan? *African Journal of Microbiology Research*, 14 (9). pp. 465–470. ISSN 1996-0808. <https://doi.org/10.5897/AJMR2020.9369>
93. Niazi, P. (2024). Isolation and Characterization of a (Surfactin-Like Molecule) Produced by *Bacillus subtilis*: Antagonistic Impact on Root-Knot Nematodes. *Scientific Research Communications*, 4(2). <https://doi.org/10.52460/src.2024.010>
94. Ratnaparkhi, M. M., Vyawahare, C. R., & Gandham, N. R. (2025). Hepatitis B virus genotype distribution and mutation patterns: Insights and clinical implications for hepatitis B virus positive patients. *World journal of experimental medicine*, 15(2), 102395. <https://doi.org/10.5493/wjem.v15.i2.102395>
95. Hassan-Kadle, M. A., Osman, M. S., & Ogurtsov, P. P. (2018). Epidemiology of viral hepatitis in Somalia: Systematic review and meta-analysis study. *World journal of gastroenterology*, 24(34), 3927–3957. <https://doi.org/10.3748/wjg.v24.i34.3927>

Information about authors:

Abdul Bari Hejran – Master of Virology, Teaching Assistant at the Department of Biology, Faculty of Education, Helmand University (Helmand, Afghanistan, e-mail: abdulbari.hejran94@gmail.com)

Virendra Kumar Yadav – PhD, Assistant Professor (Research) at Marwadi University Research Center, Department of Microbiology, Faculty of Sciences, Marwadi University (Gujarat, India, e-mail: yadava94@gmail.com)

Parwiz Niazi – PhD, Teaching Assistant at the Department of Biology, Faculty of Education, Kandahar University (Kandahar, Afghanistan, e-mail: parwiz60@gmail.com)

T. Ismagambetova¹ , M. Zholdassova² , D. Arman^{1*} ¹Kazakh-British Technical University, Almaty, Kazakhstan²Brain Institute, Al-Farabi Kazakh National University, Almaty, Kazakhstan

*e-mail: d.arman@kbtu.kz

(Received 25 March 2025; received in revised form 06 May 2025; accepted 02 June 2025)

Source reconstruction of electrical brain activity during attention network task performance

Abstract: Major Depressive Disorder (MDD) significantly affects mood, thought processes, and behavior. Understanding the neurophysiological mechanisms behind depression is essential for developing effective treatments. In this study, we compared source reconstruction of electroencephalography (EEG) data collected during Attention Network Task (ANT) performance from individuals with MDD, healthy controls, and those at risk of developing MDD. Our goal was to analyze the localization of alpha rhythm, particularly in relation to the P300 component. Preliminary findings revealed distinct differences in brain activation patterns among the three groups in key brain areas, particularly the Anterior Cingulate Cortex (ACC) and the Dorsolateral Prefrontal Cortex (DLPFC). Significant group effects in alpha source activity during the P300 interval were observed in response to both congruent and incongruent stimuli. One-way ANOVA results revealed notable differences in alpha activation in the Anterior Prefrontal Cortex (BA10) and ACC (BA24) between MDD and control groups, highlighting potential challenges in higher-order cognitive functions such as decision-making. Increased alpha activation in the Inferior Frontal Gyrus (BA45) in the MDD group suggests possible language processing difficulties. Furthermore, enhanced activation in the medial and dorsolateral prefrontal cortices aligns with their roles in task switching and inhibition. In the incongruent condition, significant differences were more pronounced, particularly in the Right Dorsolateral Prefrontal Cortex (BA9) and Right Anterior Prefrontal Cortex (BA10), which are vital for executive functions. The MDD group exhibited larger alpha source activation in the ACC, indicating reduced brain activation that may impair attention and task management. These preliminary findings are consistent with existing literature on altered alpha source activity in MDD, supporting the notion of cognitive and emotional processing differences in this population. Thus, our study demonstrates distinct differences in alpha source localization during the ANT, revealing significant variations in brain activation patterns related to stimulus congruence, particularly in the ACC and DLPFC across the three participant groups.

Key words: electroencephalography source localization, cognition, Attention Network Task (ANT), P300 component, Major Depressive Disorder (MDD).

Introduction

Major Depressive Disorder (MDD) is a complex mental health condition that greatly impacts mood, thinking, and behavior, as defined in the DSM-5 [1], with about 5% of adults experiencing this disorder worldwide [2,3]. The DSM-5 [1] includes cognitive dysfunction assessments as part of MDD diagnosis. Attentional impairments are prominent in MDD and may relate to impaired neuronal networks for alerting, orienting, and executive control [4]. A meta-analysis by Sinha et al. [5] shows that participants with depression exhibit differences in executive network functioning compared to healthy controls, aligning with previous studies on attention and depression. Executive control, crucial for cognitive functions

such as emotion regulation and concentration, is often impaired in depressive patients [6-8]. Some studies suggest that depressed individuals tend to have a bias toward focusing on negative information [9]. However, Sinha et al. [5] agree with Mineka & Sutton's view [10] that anxiety, not depression, is linked to attentional bias for threatening stimuli. Instead, depressed individuals may struggle to disengage from negative information once attended [11-12], a difficulty related to executive control to a greater extent than to orienting.

The Attention Network Task (ANT) is a valuable tool for studying disorders involving attentional deficits including MDD [13]. The ANT is designed to be emotionally neutral, as such findings regarding executive control deficits do not pertain to emotional

content perceived or remembered. The ANT is used to assess three main attention networks: the Executive Control Network, the Alerting Network, and the Orienting Network. The Executive Control Network is crucial in detecting targets and resolving conflicts, mainly involving the medial frontal and anterior cingulate cortices [14]. The efficiency of the Executive Control Network is measured by looking at response times (RTs) for congruent versus incongruent stimuli, often using a flanker task [15]. The Alerting Network is connected to arousal and involves several brain areas, including the brainstem (especially the locus coeruleus), thalamus, and various frontal and parietal lobe regions [16]. Its efficiency is evaluated by comparing RTs in cued versus uncued situations [17]. The Orienting Network helps select stimuli based on their location or modality, relying on structures such as the pulvinar and superior colliculus [18]. Its efficiency is assessed by examining RT differences between spatial and central cues [19].

Electroencephalography (EEG) source analysis is an effective method for investigating neural sources that influence cognitive processes in depression. EEG studies provide information about the timing and coordination of brain activity during cognitive tasks and show how different regions interact. This approach is complemented by connectivity studies, which explore the functional and structural relationships between brain areas. Together, they enhance our understanding of neural networks and how connectivity disruptions may contribute to cognitive impairments, particularly in conditions such as MDD. Wu et al. [20] conducted a systematic validation study using resting-state EEG signals and highlighted the reliability of resting-state EEG as a biomarker for detecting MDD.

Several studies have examined changes in functional connectivity within and between brain networks in individuals with depression. Specifically, Shim et al. [21] and Miljevic et al. [22] reported disrupted network connectivity, while Knyazev et al. [23] identified the impact of depression on specific brain networks, particularly the connection between task-positive and task-negative networks. EEG measures have also been utilized to explore the neurophysiological features of depression. Lee et al. [24] and Akar et al. [25] have demonstrated associations between changes in EEG power, connectivity measures, nonlinear properties, and depressive symptoms. Whitton et al. [26] examined functional connectivity using EEG in individuals with depression, finding abnormally high-frequency communication among large-scale

functional networks, which provides insights into disturbances in neural communication. The findings indicate that neural activity and connectivity changes could be objective markers for assessing depression severity and treatment outcomes. Depression is significantly influenced by disruptions in functional connectivity and network-level dysregulation, which highlights the importance of investigating how different brain regions communicate and coordinate. Moreover, changes in EEG measures, such as power, connectivity, and nonlinear properties, provide valuable information about the neurophysiological basis of depressive symptoms.

We focused on the P300 component, an event-related potential (ERP) that represents cognitive resource allocation and attentional processes. The P300 is typically observed in the time window of approximately 250 to 500 milliseconds after stimulus presentation and is associated with evaluating stimulus significance and updating working memory [27-29]. Alpha frequency was chosen as a focus of our study due to its distinct psychophysiological significance and its association with behavioral measures, particularly in the context of depression. Previous research has shown that alpha peak frequency correlates with cognitive performance in various tasks, such as visual perception, while alpha peak amplitude often reflects synchronous neural discharging [30-32]. Notably, it was found that both alpha peak amplitude and frequency were related to depressive scores, exhibiting different correlation patterns influenced by factors such as gender [33, 34].

The aim of this study was to explore the specificity in alpha source activity during ANT performance in MDD patients compared to healthy participants and those at risk of MDD. Previous findings indicate individuals with MDD show reduced activation in key brain regions during conflict resolution tasks compared to controls [35]. We expected that alpha source activity in the P300 interval would show differences between groups. Alpha source activity in the P300 interval elicited by congruent and incongruent stimuli was expected to show specific brain areas related to executive control networks. This article presents preliminary results for the executive network to introduce the utility of the source reconstruction method for finding EEG biomarkers of depression.

Methods and materials

Participants. Participants were 90 adults (72 female). The average age for females was 22.62

(SD=7.26) years, and for males – 24.56 (SD=6.28) years. The study was approved by the Ethics Committee of the Faculty of Medicine and Health Care of the Al-Farabi Kazakh National University. After reading the research information purposes and instructions, all subjects signed the consent form. Based on the Inventory Depression Score [36] and an interview with a psychiatrist, participants were assigned to 3 equal groups: a control group, at risk group, and a group with Major Depressive Disorder (MDD).

EEG recording. Neuron-Spectrum-4 system (Neurosoft Ltd, Ivanovo) was used to conduct EEG recordings during Attention Network Task (ANT) performance. The recording was conducted in the following scenarios: 1) participants were instructed to keep their eyes open for 1 minute, 2) participants were instructed to keep their eyes closed for 1 minute, and 3) participants engaged in a computer task for 70 minutes. Ag/AgCl electrodes were positioned on the scalp according to the international 10-20% monopolar system. The electrodes covered the left and right frontal, central, parietal, and occipital regions, specifically F3, F4, F7, F8, C3, C4, P3, P4, O1, O2, FPz, Fz, FCz, Cz, CPz, Pz, and Oz. Two electrodes were employed to record the electrooculogram, capturing vertical and horizontal eye movements. Electrode resistance was monitored throughout the recording, ensuring it remained below 5k Ω . Data were acquired at a sampling rate of 500 Hz, and a bandpass filter ranging from 0.01 to 30 Hz was applied throughout the recording.

Behavioral task. The Attention Network Task (ANT) was implemented using E-Prime 2.0, building on the original design by Fan et al. [37]. This modified version includes 96 trials spread across 9 blocks, totaling 864 trials lasting 70 minutes. Compared to the original 15-minute task, this extension provides a more in-depth look at attentional networks. The adjusted ANT was validated in a behavioral study by Zholdassova et al. [38, 39] to ensure it aligns with the characteristics of the local population.

Task structure. Each trial started with a fixation cross, followed by a cue stimulus, and a central arrow that served as the target. Participants were asked to respond quickly and accurately using the left and right keys, depending on the direction of the arrow. The stimuli were divided into two categories: cue types and flanker types. The cue types included no cue, double cue, central cue, and spatial cue (positioned above or below the fixation). The flanker types consisted of congruent, incongruent, and neutral stimuli.

EEG analysis. Preprocessing. EEG data were analyzed using EEGLAB [40]. The preprocessing steps ensured quality of the EEG data and the extraction of relevant features. Preprocessing included filtering out high and low frequencies, using Independent Component Analysis (ICA) to remove artifacts [41], selecting epochs from –700 to +700 ms around the stimulus presentation, and performing pre-stimulus baseline correction. Artifact-free epochs were chosen for paired executive control stimuli across three categories: 1) incongruent and congruent stimuli, 2) cue and double-cue stimuli, and 3) central and spatial signals.

Source reconstruction. Source reconstruction was done in Statistical Parametric Mapping (SPM) (The MathWorks, Inc.) [42] and involves two main phases: forward modeling and inverse modeling, as shown in Figure 1. To ensure precise localization of the EEG data, we aligned electrode configuration with the head model. The forward problem was addressed by calculating a lead field matrix, which describes how brain activity contributes to the EEG signals registered at the scalp.

The Multiple Sparse Priors (MSP) approach assumes that only a few sources are active at any given time, allowing improved activity localization. The Greedy Search (GS) algorithm was employed to optimize the MSP method [43]. Time-frequency analysis was used to combine temporal and frequency data, which allowed localizing evoked activity within specific time-frequency windows. The P300 component, with an interval between 250 and 500 milliseconds after stimulus presentation, was the focus of the analysis.

The source reconstruction process in SPM consists of several steps (Figure 2): creation of a canonical cortical mesh that serves as a basis for projecting the EEG data; 2) the co-registration step with visualization of several key components, including MRI fiducials (in pink), sensor fiducials (in blue), sensor locations (in green), the canonical cortical mesh (in blue), the inner skull surface (in red), and the scalp surface (in light brown). This step does not require additional parameters when using the canonical mesh. However, MNI coordinates for the fiducial positions must be provided if a non-standard mesh or custom sensor positions are involved [44].

The “EEG-BEM” head model was selected for the forward model. SPM uses a Boundary Element Method (BEM) to visualize the cortical mesh and the brain, skull, and scalp surfaces, marking the electrode positions for clarity [45–46]. In the inversion process, SPM computes the lead field matrix and inverts

the forward model using the MSP algorithm. The progress is displayed in real time in the MATLAB command window. The graphical output includes a Maximum Intensity Projection (MIP) of activity in the source space and a time series of activity for each condition.

The reconstruction process estimates the cortical current sources responsible for the electrical activity detected by EEG, involving building a standard head model, co-registering it with the EEG data, and constructing a forward model to understand how brain sources appear on the EEG sensors. The inversion within a Bayesian framework using MSP was applied,

focusing on a time window of [250 to 500] ms and [8 to 12] Hz, as it provides valuable insights into attentional and cognitive processing. Finally, SPM was used to generate source power images and apply cortical smoothing to enhance the analysis [47-48]. After preprocessing the EEG data and conducting source analysis, statistical analysis was performed, focusing on the P300 component within the alpha frequency range. This analysis examined the relationship and differences between EEG features and experimental conditions. A one-way analysis of variance (ANOVA) was used to assess the main effects and interactions among these factors.

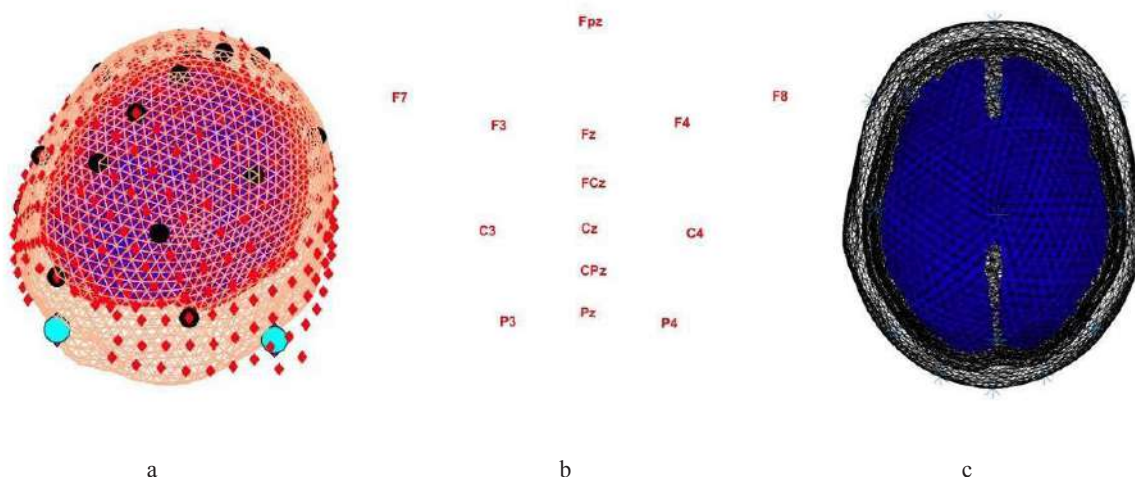


Figure 1 – Source reconstruction in SPM (a) cortical mesh; (b) co-registration of electrodes; (c) “EEG-BEM” head model

Results and discussion

Demographic and clinical data. Table 1 summarizes the demographic data of the participants.

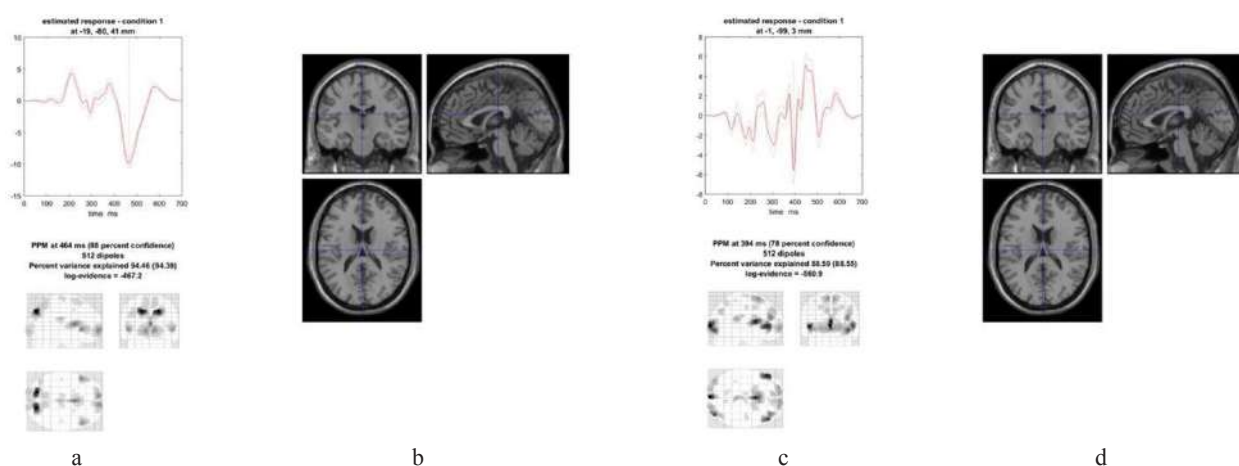
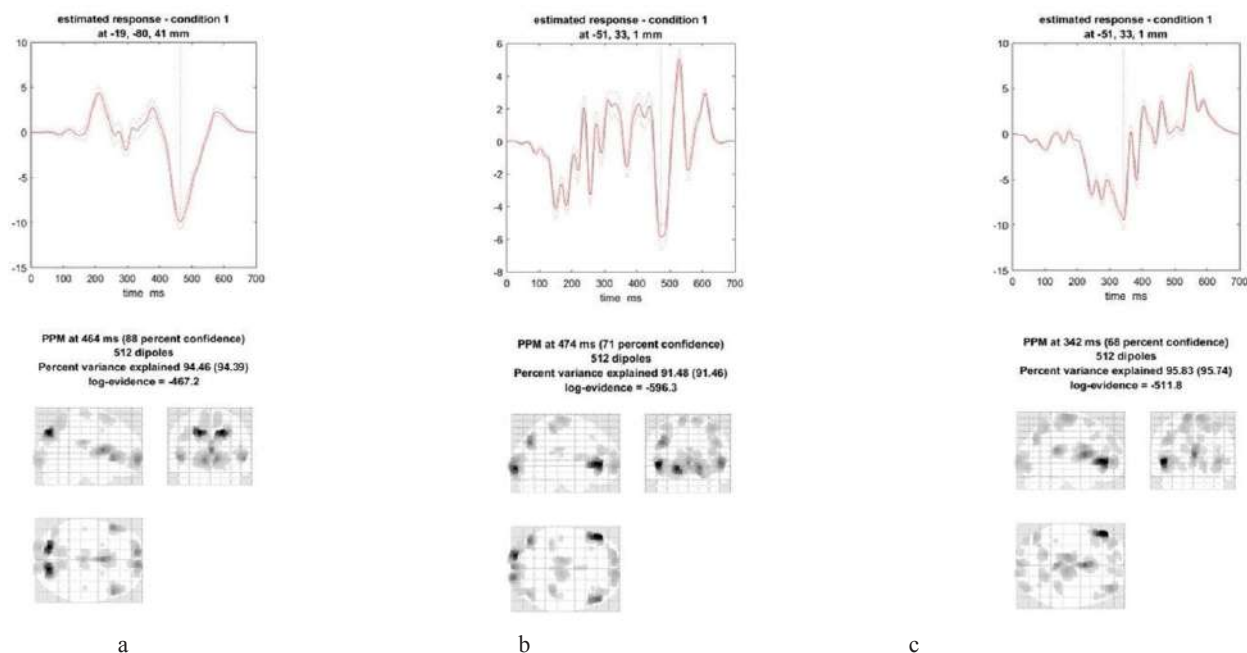
Individual source reconstruction and maximum intensity projection (MIP). In this study, source localization techniques and maximum intensity projection (MIP) were used for each of the 90 participants to explore how their brains responded to two types of stimuli: congruent and incongruent. Figures 2 and 3 show examples of individual source localizations and MIP graphs. The MIP graphs provide a clear visual representation of the maximum activation intensity across the scalp, revealing distinct brain activation patterns for each

stimulus type. The MIP at 300 ms post-stimulus reveals significant activation in each participant group's frontal and parietal regions, which indicates substantial engagement during attentional processing of the stimulus.

Individual source reconstruction and MIP were computed for post-stimulus latency 0-700 ms to visualize spatial distribution. Time series data were extracted from the voxel with the largest magnitude signal within key brain regions identified from the MIP. MIP in subjects from three groups showed different latencies: control group – 464 ms, risk group – 474 ms, MDD group – 342 ms. These individual results will be used in the statistical analysis of group differences in the next steps of our study.

Table 1 – Demographic and clinical data of the participants

Group	Total Participants	Female Participants	Male Participants	Avg. Age (Female), years	SD (Female), years	Avg. Age (Male), years	SD (Male), years
Control	30	24	6	20.71	4.50	23.00	5.45
Risk	30	24	6	23.33	8.27	26.83	7.01
MDD	30	24	6	23.83	7.98	23.83	5.61
Total	90	72	18	-	-	-	-

**Figure 2** – Individual source reconstruction and maximum intensity projection (MIP) for one participant from the Control group for (a,b) congruent stimulus; (c,d) incongruent stimulus**Figure 3** – Individual source reconstruction and maximum intensity projection (MIP) for participants from the (a) Control group; (b) the Risk group; (c) the MDD group

Condition and group effects. A one-way ANOVA analysis for the congruent condition revealed significant differences in the comparison “MDD vs. Healthy” in several brain regions: the Anterior Prefrontal Cortex (BA10), the Anterior Cingulate Cortex (ACC, BA24), and the Inferior Frontal Gyrus (BA45) (Fig. 4, Table 2).

A one-way ANOVA analysis for the incongruent condition revealed significant differences in the comparison “MDD vs. Healthy” in several brain regions: the Anterior Cingulate Cortex (ACC, BA24), the Medial Prefrontal Cortex (mPFC, BA10), and the Right Angular Gyrus (BA39) (Fig. 5, Table 3).

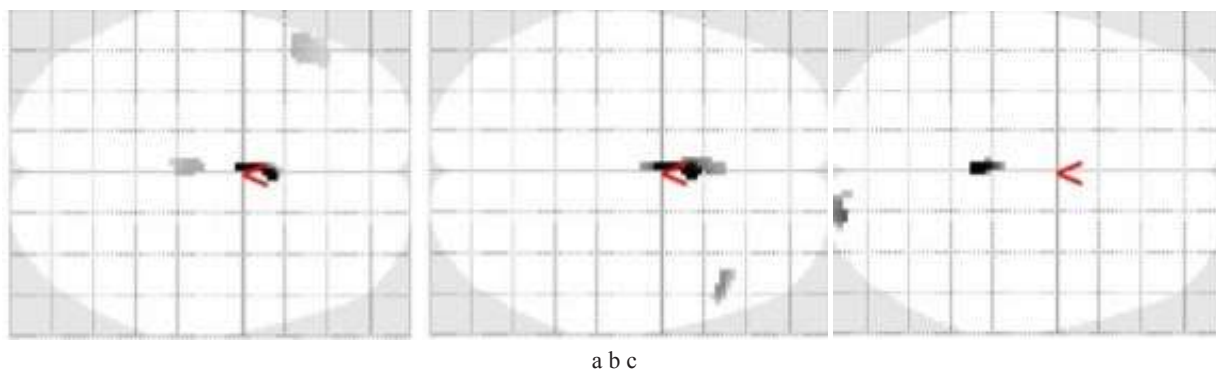


Figure 4 – Brain areas with significant differences (a) MDD vs Healthy; (b) MDD vs Risk; (c) Risk vs Healthy

Table 2 – Brain areas with significant differences: MDD vs Healthy, MDD vs Risk, Risk vs Healthy

No.	Coordinates	Brain area	p-value
MDD vs Healthy			
1	0 2 22	Anterior prefrontal cortex (BA10)	p<0.050
2	4 10 22	Anterior prefrontal cortex (BA10)	
3	0 -24 24	Anterior cingulate cortex (BA24)	
4	-52 20 2	Left Inferior Frontal Gyrus (BA45)	
MDD vs Risk			
1	0 2 20	Medial Prefrontal Cortex (BA9)	p<0.050
2	46 24 4	Dorsolateral Prefrontal Cortex (DLPFC) (Right BA46, BA45)	
Risk vs Healthy			
1	2 -38 20	Anterior Cingulate Cortex (BA24 or BA32)	p<0.050
2	22 94 -16	Right Visual (BA18)	
3	12 -92 -8	Right Visual (BA18)	

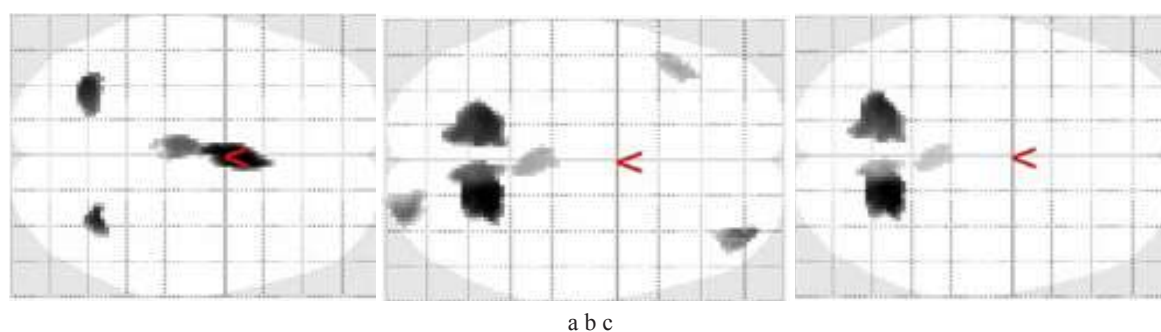


Figure 5 – Brain areas with significant differences (a) MDD vs Healthy; (b) Risk vs MDD; (c) Risk vs Healthy

Table 3 – Brain areas with significant differences: MDD vs Healthy, Risk vs MDD, Risk vs Healthy

No.	Coordinates	Brain area	p-value
MDD vs Healthy			
1	2 4 24	Anterior Cingulate Cortex (ACC) (BA24)	p<0.012
2	-4 -22 26	Anterior Cingulate Cortex (ACC) (BA32)	
3	-4 -34 24	Medial Prefrontal Cortex (mPFC) (BA10)	
4	-32 -66 48	Superior Parietal Lobule and Precuneus (BA7)	
5	32 -62 48	Right Angular Gyrus (BA39)	
Risk vs MDD			
1	20 -56 54	Right Superior Temporal Gyrus (BA22)	p<0.003
2	8 -60 60	Superior Parietal Lobule and Precuneus (BA7)	
3	-16 -58 62	Superior Parietal Lobule and Precuneus (BA7)	
4	-18 -58 62	Superior Parietal Lobule and Precuneus (BA7)	
5	-14 -66 54	Superior Parietal Lobule and Precuneus (BA7)	
6	38 52 0	Right Anterior Prefrontal Cortex (BA10)	
7	40 52 -8	Right Anterior Prefrontal Cortex (BA10)	
8	40 42 6	Right Dorsolateral Prefrontal Cortex (BA46)	
9	26 -92 -16	Right-Visual(BA18)	
10	20 -88 -12	Right-Visual(BA18)	
11	-42 24 36	Left Dorsolateral Prefrontal Cortex (BA9)	
12	4 -40 18	Medial Prefrontal Cortex (mPFC) (BA10)	
13	-2 -34 18	Medial Prefrontal Cortex (mPFC) (BA10)	
Risk vs Healthy			
1	22 -56 52	Superior Parietal Lobule and Precuneus (BA7)	p<0.015
2	20 -66 58	Superior Parietal Lobule and Precuneus (BA7)	
3	8 -60 60	Superior Parietal Lobule and Precuneus (BA7)	
4	-22 -62 52	Superior Parietal Lobule and Precuneus (BA7)	
5	-6 -52 62	Superior Parietal Lobule and Precuneus (BA7)	
6	2 -40 18	Medial Prefrontal Cortex (mPFC) (BA10)	

The aim of this study was to explore the specificity in alpha source activity during Attention Network Task (ANT) performance in Major Depressive Disorder (MDD) patients compared to healthy participants and those at risk of MDD. The study did not address gender differences. Our results revealed significant group effects in alpha source activity in the P300 interval elicited by congruent and incongruent stimuli. The individual MIP graphs illustrate distinct brain activation patterns for each stimulus type, with significant activation in the frontal and parietal regions of all participant groups at 300 ms post-stimulus, indicating substantial engagement during attentional processing.

The one-way ANOVA results for the congruent condition between the MDD and control groups showed significant differences in the alpha source activation in the Anterior Prefrontal Cortex (BA10) and Anterior Cingulate Cortex (BA24), suggesting challenges in higher-order cognitive functions, such as decision-making and attentional switching [4, 49]. Increased alpha source activation in the Inferior Frontal Gyrus (BA45) in the MDD group may be evidence of language processing challenges [50]. Significant activation in the Medial Prefrontal Cortex (BA10) and Dorsolateral Prefrontal Cortex (BA46) in MDD align with research which showed the DLPFC is critical for functions such as task switching, inhibition, and working memory, which are important for resolving conflicts in congruent scenarios [50].

The analysis of one-way ANOVA results for the incongruent condition highlights greater significant differences between MDD and healthy control groups. The Right Dorsolateral Prefrontal Cortex (BA9) and Right Anterior Prefrontal Cortex (BA10) are crucial for executive functions, including cognitive flexibility, decision-making, and attentional control [51-52]. Furthermore, larger alpha source activation of the Anterior Cingulate Cortex (ACC) in the MDD group suggests lower brain activation, which may affect attention and task management in depression. The Medial Prefrontal Cortex (mPFC) is involved in self-referential thinking and decision-making [53], while the Superior Parietal Lobule and Precuneus (BA7) and Right Angular Gyrus (BA39) reflect visual and motor functions [54].

The results of our study are consistent with existing literature indicating altered alpha source activity in patients with MDD. Pizzagalli et al. [55] found that MDD patients exhibit higher alpha activity in certain brain regions compared to healthy controls, reflecting underlying cognitive and emotional processing differences. Additionally, patients with MDD showed distinct EEG patterns, including lower alpha band connectivity and higher gamma band connectivity, indicating altered brain activation in regions such as the ACC during attention-related tasks [56].

Limitations. There are limitations to consider in this study. First, this article focused only on the alpha wave frequency and the P300 component and presented preliminary results. Further analysis will explore other frequency bands and waves in response to other stimuli. Second, a standardized “EEG-BEM” (Boundary Element Model) head model was used for source reconstruction. The model might not capture the participants’ individual differences in brain anatomy. In the next steps, personalized head models will be used.

Conclusion

Our examination of the P300 component at alpha frequency during performance of the Attention Network Task (ANT) showed distinct differences in source localization across three groups: control, individuals with Major Depressive Disorder (MDD), and those at risk of developing MDD. Our findings revealed that brain activation patterns varied significantly when comparing responses to congruent versus incongruent stimuli, particularly in areas such as the Anterior Cingulate Cortex (ACC) and the Dorsolateral Prefrontal Cortex (DLPFC).

Acknowledgments

This research was funded by the Committee of Science of the Ministry of Science and Higher Education of the Republic of Kazakhstan (Grant No. BR27198099).

Conflict of interest

All authors are aware of the article’s content and declare no conflict of interest.

References

1. American Psychiatric Association (2013) Diagnostic and Statistical Manual of Mental Disorders, Fifth Edition Arlington, VA: American Psychiatric Association, 947 p. ISBN 978-0-89042-554-1. <https://doi.org/10.1176/appi.books.9780890425596>.
2. World Health Organization. (n.d.) (from March 31, 2023, accessed March 20, 2025) Depressive disorder (depression). <https://www.who.int/news-room/fact-sheets/detail/depression#:~:text=Globally%2C%20an%20estimated%205%25%20of,mild%2C%20moderate%20and%20severe%20depression.>
3. Olbrich S., Arns, M. (2013) EEG biomarkers in major depressive disorder: discriminative power and prediction of treatment response. *Int. Rev. Psychiatr.*, vol. 25, no. 5, pp. 604–618. <https://doi.org/10.3109/09540261.2013.816269>.
4. Posner M.I., Petersen S.E. (1990) The attention system of the human brain. *Annu. Rev. Neurosci.*, vol. 13, pp. 25–42. <https://doi.org/10.1146/annurev.ne.13.030190.000325>
5. Sinha N., Arora S., Srivastava P., Klein R.M. (2022) What networks of attention are affected by depression? A meta-analysis of studies that used the attention network test. *J. Affect. Disorders Rep.*, vol. 8, pp. 100302. <https://doi.org/10.1016/j.jadr.2021.100302>
6. Perini G., Ramusino M.C., Sinforiani E., et al. (2019) Cognitive impairment in depression: recent advances and novel treatments. *Neuropsych. Dis. Treat.*, vol. 15, pp. 1249–1258. <https://doi.org/10.2147/NDT.S199746>
7. Kustubayeva A., Eliassen J., Matthews G., Nelson E. (2023) fMRI study of implicit emotional face processing in patients with MDD with melancholic subtype. *Front. Hum. Neurosci.*, vol. 17, pp. 1029789. <https://doi.org/10.3389/fnhum.2023.1029789>
8. Kustubayeva A.M., Nelson E.B., Smith M.L., et al. (2022) Functional MRI study of feedback-based reinforcement learning in depression. *Front. Neuroinform.*, vol. 16, pp. 1028121. <https://doi.org/10.3389/fninf.2022.1028121>
9. Beck A. T. (1979) Cognitive therapy and the emotional disorders New York: International Universities Press, 368 p. ISBN: 9780140156898.
10. Mineka, S., Sutton S.K. (1992) Cognitive Biases and the Emotional Disorders. *Psychol. Sci.*, vol. 3, no. 1, pp. 65–69. <https://doi.org/10.1111/j.1467-9280.1992.tb00260.x>
11. Clasen P.C., Wells T.T., Ellis A.J., Beevers C.G. (2013) Attentional biases and the persistence of sad mood in major depressive disorder. *J. Abnorm. Psychol.*, vol. 122, no. 1, p. 74–85. <https://doi.org/10.1037/a0029211>
12. Mathews A., MacLeod C. (2005) Cognitive vulnerability to emotional disorders. *Annu. Rev. Clin. Psychol.*, vol. 1, no. 1, pp. 167–195. <https://doi.org/10.1146/annurev.clinpsy.1.102803.143916>
13. Brunyé T.T., Mahoney C.R., Lieberman H.R., Taylor H.A. (2010) Caffeine modulates attention network function. *Brain Cognition*, vol. 72, pp. 181–188. <https://doi.org/10.1016/j.bandc.2009.07.013>
14. Xuan B., Mackie M.A., Spagna A., et al. (2016) The activation of interactive attentional networks. *NeuroImage*, vol. 129, pp. 308–319. <https://doi.org/10.1016/j.neuroimage.2016.01.017>
15. Togo F., Lange G., Natelson B.H., Quigley K.S. (2015) Attention Network Test: Assessment of cognitive function in chronic fatigue syndrome. *J. Neuropsychol.*, vol. 9, pp. 1–9. <https://doi.org/10.1111/jnp.12030>
16. Matthews G., Zeidner M. (2012) Individual differences in attentional networks: Trait and state correlates of the ANT. *Pers. Indiv. Differ.*, vol. 53, pp. 574–579. <https://doi.org/10.1016/j.paid.2012.04.034>
17. Liu K., Sun G., Li B., et al. (2013) The impact of passive hyperthermia on human attention networks: An fMRI study. *Behav. Brain Res.*, vol. 243, pp. 220–230. <https://doi.org/10.1016/j.bbr.2013.01.013>
18. Moriya J. (2018) Association between social anxiety and visual mental imagery of neutral scenes: The moderating role of effortful control. *Front. Psychol.*, vol. 8, p. 2323. <https://doi.org/10.3389/fpsyg.2017.02323>
19. van Heugten-van der Kloet D., Giesbrecht T., Merckelbach H. (2015) Sleep loss increases dissociation and affects memory for emotional stimuli. *J. Behav. Ther. Exp. Psy.*, vol. 47, pp. 9–17. <https://doi.org/10.1016/j.jbtep.2014.11.002>
20. Wu C.T., Huang H.C., Huang S., et al. (2021) Resting-State EEG Signal for Major Depressive Disorder Detection: A Systematic Validation on a Large and Diverse Dataset. *Biosensors-Basel*, vol. 11, no. 12, p. 499. <https://doi.org/10.3390/bios11120499>.
21. Shim M., Im C.-H., Kim Y.-W., Lee S.-H. (2018) Altered cortical functional network in major depressive disorder: A resting-state electroencephalogram study. *NeuroImage: Clin.*, vol. 19, pp. 1000–1007. <https://doi.org/10.1016/j.nicl.2018.06.012>.
22. Miljevic A., Bailey N.W., Murphy O.W., et al. (2023) Alterations in EEG functional connectivity in individuals with depression: A systematic review. *J. Affect. Disorders*, vol. 328, pp. 287–302. <https://doi.org/10.1016/j.jad.2023.01.126>.
23. Knyazev G.G., Savostyanov A.N., Bocharov A.V., et al. (2016) Task-positive and task-negative networks and their relation to depression: EEG beamformer analysis. *Behav. Brain Res.*, vol. 306, pp. 160–169. <https://doi.org/10.1016/j.bbr.2016.03.033>.
24. Lee P.F., Kan D.P.X., Croarkin P., et al. (2018) Neurophysiological correlates of depressive symptoms in young adults: A quantitative EEG study. *J. Clin. Neurosci.*, vol. 47, pp. 315–322. <https://doi.org/10.1016/j.jocn.2017.09.030>.
25. Akar S.A., Kara S., Agambayev S., Bilgic V. (2015) Nonlinear analysis of EEGs of patients with major depression during different emotional states. *Comput. Biol. Med.*, vol. 67, pp. 49–60. <https://doi.org/10.1016/j.compbimed.2015.09.019>.
26. Whitton A.E., Decy S., Ironside M.L., et al. (2018) Electroencephalography Source Functional Connectivity Reveals Abnormal High-Frequency Communication Among Large-Scale Functional Networks in Depression. *Biol. Psychiatr.: Cogn. Neurosci. Neuroimag.*, vol. 3, no. 1, pp. 50–58. <https://doi.org/10.1016/j.bpsc.2017.07.001>.
27. Zhao Q., Li H., Hu B., (2017). Abstinent heroin addicts tend to take risks: ERP and source localization. *Front. Neurosci.*, vol. 11, 681. <https://doi.org/10.3389/fnins.2017.00681>.
28. Duncan C.C. (1981) The Stroop effect: brain potentials localize the source of interference. *Science*, vol. 214, pp. 938–940. <https://doi.org/10.1126/science.7302571>.
29. Xue S., Wang S., Kong X., Qiu J. (2017) Abnormal neural basis of emotional conflict control in treatment-resistant depression. *Clin. EEG Neurosci.*, vol. 48, pp. 103–110. <https://doi.org/10.1177/1550059416631658>.







30. Klimesch W. (1999) EEG alpha and theta oscillations reflect cognitive and memory performance: A review and analysis. *Brain Res. Rev.*, vol. 29, pp. 169–195. [https://doi.org/10.1016/S0165-0173\(98\)00056-3](https://doi.org/10.1016/S0165-0173(98)00056-3).
31. Katyal S., He S., He B., Engel S.A. (2019) Frequency of alpha oscillation predicts individual differences in perceptual stability during binocular rivalry. *Hum. Brain Mapp.*, vol. 40, pp. 2422–2433. <https://doi.org/10.1002/hbm.24533>.
32. Kamzanova A.T., Kustubayeva A.M., Matthews G. (2014) Use of EEG Workload Indices for Diagnostic Monitoring of Vigilance Decrement. *Hum. Factors*, vol. 56, no. 6, pp. 1136–1149. <https://doi.org/10.1177/0018720814526617>
33. Tement S., Pahor A., Jaušovec N. (2016) EEG alpha frequency correlates of burnout and depression: The role of gender. *Biol. Psychol.*, vol. 114, pp. 1–12. <https://doi.org/10.1016/j.biopsycho.2015.11.005>.
34. Kustubayeva A.M., Kamzanova A.T., Kudaibergenova S., et al. (2020) Major Depression and Brain Asymmetry in a Decision-Making Task with Negative and Positive Feedback. *Symmetry*, vol. 12, p. 2118. <https://doi.org/10.3390/sym12122118>
35. Zhu J., Li J., Li X., et al. (2018) Neural Basis of the Emotional Conflict Processing in Major Depression: ERPs and Source Localization Analysis on the N450 and P300 Components. *Front. Hum. Neurosci.*, vol. 12, 214. <https://doi.org/10.3389/fnhum.2018.00214>.
36. Rush A.J., Giles D.E., Schlesser M.A., et al. (1986) The Inventory for Depressive Symptomatology (IDS): preliminary findings. *Psychiat. Res.*, vol. 18, no. 1, pp. 65–87. [https://doi.org/10.1016/0165-1781\(86\)90060-0](https://doi.org/10.1016/0165-1781(86)90060-0)
37. Fan J., McCandliss B.D., Sommer, T., et al. (2002) Testing the efficiency and independence of attentional networks. *J. Cognitive Neurosci.*, vol. 14, pp. 340–347. <https://doi.org/10.1162/089892902317361886>
38. Zholdassova M., Kustubayeva A., Matthews G. (2021) The ANT Executive Control Index: No Evidence for Temporal Decrement. *Hum. Factors*, vol. 63, no. 2, pp. 254–273. <https://doi.org/10.1177/0018720819880058>.
39. Kustubayeva A., Zholdassova M., Borbassova G., Matthews G. (2022) Temporal changes in ERP amplitudes during sustained performance of the Attention Network Test. *Int. J. psychophysiol.*, vol. 182, pp. 142–158. <https://doi.org/10.1016/j.ijpsycho.2022.10.006>
40. Delorme A., Makeig S. (2004) EEGLAB: an open source toolbox for analysis of single-trial EEG dynamics including independent component analysis. *J. Neurosci. Meth.*, vol. 134, pp. 9–21. <https://doi.org/10.1016/j.jneumeth.2003.10.009>.
41. Jung T.P., Makeig S., Humphries C., et al. (2000) Removing electroencephalographic artifacts by blind source separation. *Psychophysiology*, vol. 37, pp. 163–178. <https://doi.org/10.1111/1469-8986.3720163>.
42. Penny W., Friston K., Ashburner J., et al. (2006) Statistical parametric mapping: The analysis of functional brain images London: Academic Press, 656 p. ISBN 9780123725608
43. Friston K., Harrison L., Daunizeau J., et al. (2008) Multiple sparse priors for the M/EEG inverse problem. *NeuroImage*, vol. 39, no. 3, pp. 1104–1120. <https://doi.org/10.1016/j.neuroimage.2007.09.048>
44. Mattout J., Henson R.N., Friston K.J. (2007) Canonical source reconstruction for MEG. *Comput. Intel. Neurosci.*, vol. 2007, p. 67613. <https://doi.org/10.1155/2007/67613>
45. Geselowitz D. (1967) On bioelectric potentials in an inhomogeneous volume conductor. *Biophys. J.*, vol. 7, pp. 1–11. [https://doi.org/10.1016/S0006-3495\(67\)86571-8](https://doi.org/10.1016/S0006-3495(67)86571-8)
46. Hämäläinen M.S., Sarvas J. (1989) Realistic conductivity geometry model of the human head for interpretation of neuromagnetic data. *IEEE T. Bio-med. Eng.*, vol. 36, no. 2, pp. 165–171. <https://doi.org/10.1109/10.16463>
47. Kim H.C., Ghahramani Z. (2006) Bayesian Gaussian process classification with the EM-EP algorithm. *IEEE T. Pattern Anal.*, vol. 28, no. 12, pp. 1948–1959. <https://doi.org/10.1109/TPAMI.2006.238>
48. Cherkassky V., Friedman J.H., Wechsler H. (1996) From Statistics to Neural Networks: Theory and Pattern Recognition Applications Berlin: Springer Heidelberg, 394 p. ISBN : 9783642791192. <https://doi.org/10.1007/978-3-642-79119-2>.
49. Fan J., McCandliss B. D., Fossella, J., et al. (2005) The activation of attentional networks. *NeuroImage*, vol. 26, no. 2, pp. 471–479. <https://doi.org/10.1016/j.neuroimage.2005.02.004>
50. Hertrich I., Dietrich S., Blum C., Ackermann H. (2021) The Role of the Dorsolateral Prefrontal Cortex for Speech and Language Processing. *Front. Hum. Neurosci.*, vol. 15, p. 645209. <https://doi.org/10.3389/fnhum.2021.645209>
51. Jung J., Lambon Ralph M.A., Jackson R.L. (2022) Subregions of DLPFC display graded yet distinct structural and functional connectivity. *J. Neurosci.*, vol. 42, no. 15, pp. 3241–3252. <https://doi.org/10.1523/JNEUROSCI.1216-21.2022>
52. Friedman N.P., Robbins T.W. (2021) The role of prefrontal cortex in cognitive control and executive function. *Neuropsychopharmacol.*, vol. 47, no. 1, p. 72. <https://doi.org/10.1038/s41386-021-01132-0>
53. Xu P., Chen A., Li Y., et al. (2019) Medial prefrontal cortex in neurological diseases. *Physiol. Genomics*, vol. 51, no. 9, pp. 432–442. <https://doi.org/10.1152/physiolgenomics.00006.2019>
54. Shibata K., Watanabe T., Kawato M., Sasaki Y. (2016) Differential Activation Patterns in the Same Brain Region Led to Opposite Emotional States. *PLoS Biol.*, vol. 14, no. 9, e1002546. <https://doi.org/10.1371/journal.pbio.1002546>
55. Pizzagalli D.A., Nitschke J.B., Oakes T.R., et al. (2002) Brain electrical tomography in depression: The importance of symptom severity, anxiety, and melancholic features. *Biol. Psychiat.*, vol. 52, no. 2, pp. 73–85. [https://doi.org/10.1016/S0006-3223\(02\)01313-6](https://doi.org/10.1016/S0006-3223(02)01313-6)
56. Huang Y., Yi Y., Chen Q., et al. (2023) Analysis of EEG features and study of automatic classification in first-episode and drug-naïve patients with major depressive disorder. *BMC Psychiatry*, vol. 23, p. 832. <https://doi.org/10.1186/s12888-023-05349-9>

Information about the authors:

Tomiris Ismagambetova – Master’s student, Kazakh-British Technical University (Almaty, Kazakhstan, e-mail: ismagambetova@physics.kz)

Manzura Zholdassova – PhD, researcher at the Brain Institute, Al-Farabi Kazakh National University (Almaty, Kazakhstan, e-mail: zholdassova@kaznu.kz)

Diana Arman – Assistant Professor, Kazakh-British Technical University (Almaty, Kazakhstan, e-mail: d.arman@kbtu.kz)

D.E. Karabalayeva¹ , M.S. Kurmanbayeva^{1*} , S.K. Mukhtubayeva^{2,3} ,
M.Zh. Zhumagul^{1,2,3} , A.B. Kusmangazinov¹ , R.K. Anatoliy¹ 

¹Al-Farabi Kazakh National University, Almaty, Kazakhstan

²Astana International University, Astana, Kazakhstan

³Astana Botanical Garden, Astana, Kazakhstan

*e-mail: meruyert.kurmanbayeva@kaznu.edu.kz

(Received 02 May 2025; received in revised form 19 June 2025; accepted 23 June 2025)

Study of *Trollius dschungaricus* Regel (Ranunculaceae Juss.) in the flora of the Saty Gorge

Abstract: The article presents the results of an analysis of herbarium and contemporary data on the distribution of *Trollius dschungaricus* within the Saty Gorge, located in the eastern part of the Kungey Alatau range. The study is primarily based on herbarium specimen collections, supplemented by data from the online platforms GBIF and iNaturalist, as well as materials gathered during field expeditions to natural populations.

A floristic list has been compiled, including 157 species of higher vascular plants belonging to 113 genera and 37 families. The greatest species diversity is concentrated in the following families: Poaceae, Asteraceae, Fabaceae, Lamiaceae, Amaranthaceae, and Rosaceae. Twelve species dominate the plant cover. Out of the total number of species, 152 (95.0%) have forage value, with 18 of them also possessing medicinal properties. Eight species are classified as poisonous. The life forms of the flora are predominantly represented by perennial plants – 136 species, including 100 with prolonged vegetative growth, 18 shrubs, 5 subshrubs and semishrubs each, 2 dwarf subshrubs, as well as 6 tree species.

Perennials play an edificatory role in the plant communities of the surveyed area, whereas annuals (14 species) mainly form modification-type herbaceous layers. Biennial plants are represented by 8 species.

An ecological analysis of the flora indicates a predominance of xerophytic species in the conditions of the mid-mountain belt, as well as the presence of mesophytes and halophytes associated with river valleys and temporary watercourses.

Key words: *Trollius dschungaricus*, Saty Gorge, eastern part of the Kungey Alatau Range, population, floristic composition.

Introduction

The conservation of the gene pool of natural flora is one of the most pressing issues today. The Kungey Alatau Range is a unique and remarkable region of the Northern Tien Shan, located at the junction of three botanical-geographical provinces that differ in their natural characteristics: the Central Tien Shan–Zaalai, the Kashgar–Eastern Tien Shan transitional, and the Jungarian transitional provinces. The study area is of particular interest as a transboundary region with the Republic of Kyrgyzstan, characterized by a high degree of botanical diversity. Due to its borderland physical and geographical position, the formation of its flora has been influenced by several major botanical-geographical centers [1].

The study of *T. dschungaricus* in the Saty Gorge, eastern part of the Kungey Alatau Range, is based on the fact that the species composition has remained in its natural state due to its inaccessibility, and it serves as a reference in floristic terms for the entire Northern Tien Shan. To create a comprehensive conservation picture that can protect and restore endangered species, including *T. dschungaricus* in the studied area, it is necessary to characterize the condition of the populations of this species and determine how they respond to various natural and anthropogenic factors.

The genus *Trollius* L. (family Ranunculaceae Juss.) consists of approximately 40 species, primarily distributed in the extratropical regions of the Northern Hemisphere. In Russia, around 19–20

species are known, with the greatest species diversity observed in Siberia, where 12 species occur [2]. The flora of China includes about 16 species, 8 of which are endemics [3]. Within the flora of Kazakhstan, five species of this genus have been recorded: *T. dschungaricus* Regel, *T. altaicus* C.A. Mey., *T. asiaticus* L., *T. lilacinus* Bunge, and *T. micranthus* (Winkl. et Kom.) Pachom [4–5].

Plants of the genus *Trollius* are characterized by large, brightly colored flowers—primarily orange or yellow—with petals of a narrowed shape and nectaries at the base, as well as trilobed or deeply three-lobed leaves [6]. The range of *T. dschungaricus* covers the eastern mountainous regions of Central Asia and Western China [7].

T. dschungaricus is a perennial herbaceous plant, 15–70 cm tall, with a short rhizome. The stem is erect, slightly raised at the base, usually bearing 1–3 flowers, smooth, with remnants of last year's leaves at the lower part. The basal leaves are long-petioled, palmately five-lobed; their lobes are broad, with 3–5 segments along the edge, having wide, blunt teeth. Stem leaves vary in shape: the lower ones are petiolate, while the upper ones are sessile, with a blade similar to the basal leaves or slightly more deeply divided. The apical leaves gradually decrease in size [8–9].

The peduncle is 2–15 cm long and significantly elongates during fruiting. The flowers are large, up to 6 cm in diameter, with bright golden-yellow sepals, slightly reddish on the outside, ranging from 4 to 15 (sometimes up to 20) in number. The petals-nectaries are about 8 mm long, orange, almost equal in length to the stamens, linear in shape, with a rounded tip, slightly widened and thickened at the end, almost equal in length to the stamens. The nectary pit is located about 1 mm high, with the petal slightly narrowing below it. The stigmas are yellow, and the ovaries are brownish, noticeably wrinkled at the base of the style during blooming. The fruits consist of numerous leaflets up to 10 mm long, gathered in a spherical head; the leaflet tip is straight, slightly bent, about 2 mm long. The seeds are brown-black, shiny, rounded, and slightly angular. Blooming occurs in June [10–11].

T. dschungaricus grows in the coniferous and deciduous forest belt, as well as in alpine meadows, occurring at elevations up to 3800 meters above sea level. The species' range covers the Jungarian, Zailiyskiy and Kungey Alatau, Ketpen, Terskey, Kyrgyz Alatau, and the Western Tien Shan [12].

The climatic conditions characteristic of this species' habitat can be described as sharply

continental. This is reflected in significant annual and daily temperature fluctuations, as well as in the abrupt transition from winter to summer.



Figure 1 – Appearance of *T. dschungaricus* in the flora of the Saty Gorge

In particular, the climate of the Saty Gorge is marked by cold and arid conditions with a short growing season. The hydrothermal coefficient exceeds a value of 1, indicating that precipitation surpasses evaporation [13]. Climatic parameters vary depending on the altitudinal zone: with increasing elevation, air temperature and atmospheric pressure decrease, while humidity, solar radiation, and the amount of precipitation increase. Based on the combination of natural and climatic characteristics, the studied area is classified as a mid-mountain zone. According to long-term observations, the average annual air temperature in the region is +2.0 °C. The warmest month is July, with an average monthly temperature of +14.8 °C, while the coldest is January (–13.7 °C). The annual precipitation amounts to 378 mm, with about 40% (191 mm) falling during the summer period [14]. The growing season lasts less than 170 days. The sum of active temperatures during this period does not exceed 2000 °C, with total precipitation ranging from 150 to 200 mm. The first frosts occur in early September, and the last ones—in the third decade of May. The frost-free period lasts approximately 107 days [9].

The wind regime is characterized by the predominance of southwesterly winds during the summer months and northerly winds in the winter period. The surveyed area is dominated by plant communities typical of the mid-mountain zone,

reflecting the adaptation of *T. dschungaricus* to a cold and relatively dry climate with a short growing season.

The study of the range and ecological-floristic characteristics of rare and narrowly endemic plant species, such as *T. dschungaricus*, represents an important task of modern botany and biodiversity conservation. The eastern part of the Kungey Alatau range, including the Saty Gorge, remains poorly studied in terms of floristic composition and the structure of plant communities, which makes this research especially relevant. The relevance of this work lies in the need to clarify the distribution boundaries of *T. dschungaricus*, assess the condition of its natural populations, and identify the floristic diversity in the area of its occurrence.

The novelty of this study lies in the comprehensive analysis of herbarium materials, modern digital data (GBIF and iNaturalist), as well as results from field expeditions conducted in natural habitats. This approach makes it possible to gain a more complete understanding of the ecological preferences of

the species and its habitat conditions, as well as to expand knowledge of the floristic composition of the studied area.

The aim of this study is to analyze the distribution range of *T. dschungaricus* within the Saty Gorge and to characterize the floristic composition of the associated plant communities. The study also examines the biological and ecological features of the identified species, including their life forms, forage and medicinal value, as well as their adaptation to local environmental conditions.

Materials and methods

Field research was conducted from 2022 to 2024 in natural phytocoenoses of the Saty Gorge, located in the eastern part of the Kungey Alatau Range, within the territory of the Kolsai Lakes National Park (Raiymbek District, Almaty Region). The geographical coordinates of the surveyed site are 43°01'29.6" N, 78°23'20.5" E, with an elevation of 2733 meters above sea level.

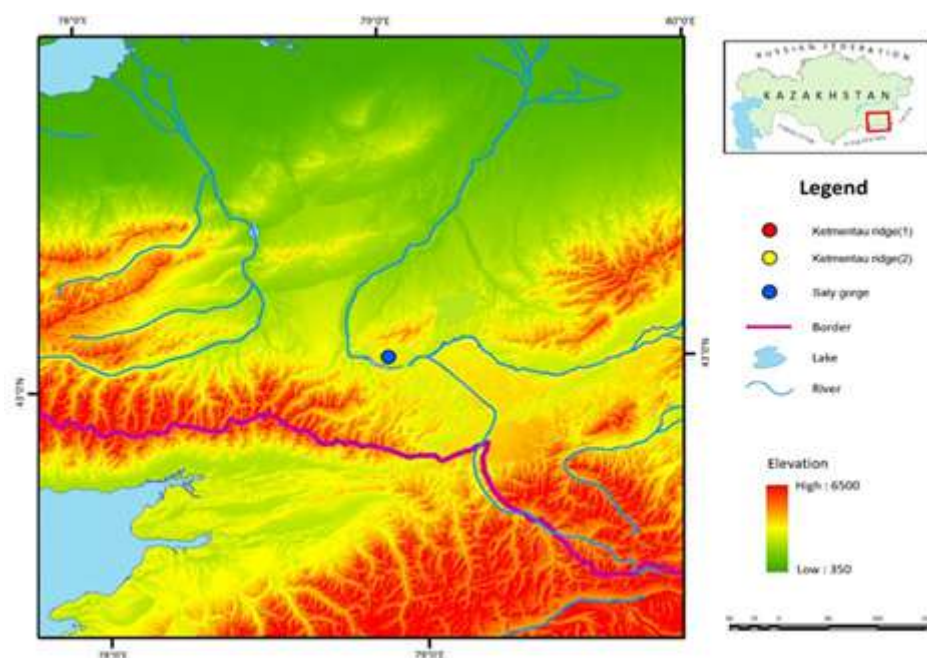


Figure 2 – Study sites of *T. dschungaricus* in the eastern part of the Kungey Alatau Range

The floristic composition of plant communities associated with *T. dschungaricus* was studied within the protected area of the Kolsai Lakes National Park, in the Saty Gorge of the Satinsky rural district (Almaty Region). The study site is bordered as follows: to the north by the lands of the Algabass rural district, to the east by the Karabalyk rural district, to the south by forest fund lands, and to the west and northwest by the lands of the Talgar District.

Classical methods of floristic, ecological-geographical, and geobotanical analysis were used to study the species composition and structure of plant communities. Herbarium material was collected following the standard field geobotanical techniques [15-17]. To clarify the range of *T. dschungaricus*, route reconnaissance methods.

As part of monitoring studies aimed at identifying plant species found in the community, sample plots of various sizes: 5×10 m in rocky areas, 10×20 m in meadow communities, and 50×100 m in forest communities. Species density and the area occupied by the population, followed by quantitative accounting.

During field studies, GPS navigation devices (Garmin, Etrex 2010), habitat maps, and a digital camera for photo documentation (Nikon D3200 18-55 VR II Kit, 2015) were used to reference descriptive points.

For taxonomic research, the following sources were used for plant species identification: Flora of

Kazakhstan [5], Key to the Plants of Central Asia [18], and the compiled works of M.S. Baytenov [19], Flora of Kazakhstan [20]. Publications dedicated to the flora and vegetation of the Kungey Alatau Range [21] were also consulted.

Resources from the Herbarium Fund of the Institute of Botany and Phytointroduction (Almaty, Kazakhstan) (acronym AA) were used for the clarification of herbarium materials. Plant names are given according to the databases Plants of the World Online (POWO) (URL: <https://powo.science.kew.org/>) [7] and the website Plantarium (URL: <https://www.plantarium.ru/>) [22].

Results and discussion

To establish the studied locations of *T. dschungaricus* in the eastern part of the Kungey Alatau Range, an inventory of the Herbarium Funds of Almaty (AA) and Al-Farabi Kazakh National University (AFAKNU) was conducted, along with a review of the GBIF and iNaturalist platforms [21-22]. As a result, key distribution sites of the species in this region were identified (see Figure 3).

A total of 95 specimens of *T. dschungaricus* were studied from the herbarium collection, collected in the floristic region of the Zailiyskiy – Kungey Alatau. Of these, 16 specimens are stored in the Herbarium Fund of Almaty (AA), and 2 in (AFAKNU), with 6 specimens registered in GBIF and 7 in iNaturalist.

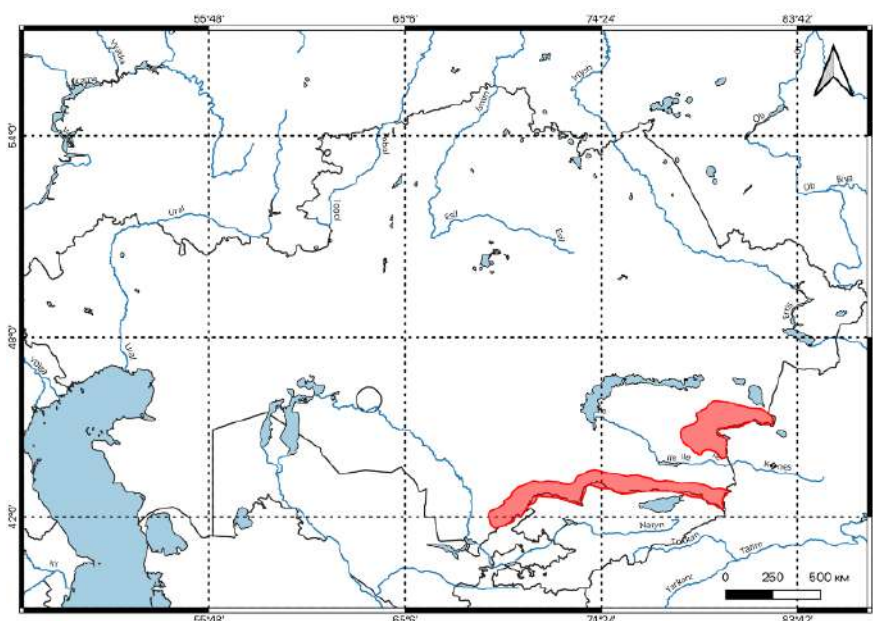


Figure 3 – Distribution map of *T. dschungaricus* in the Kungey Alatau

The herbarium specimens span the period from 1936 to 2023. The earliest specimen was collected by B.A. Bykov and is stored in (AFAKNU) herbarium collection.

In addition, the herbarium collection of the Institute of Botany and Phytointroduction (Almaty, Kazakhstan) was supplemented with *T. dschungaricus* specimens collected on June 16, 2023, by D.Ye. Karabalayeva. The specimens were gathered in the Almaty Region, Raiymbek District, within the territory of the Kolsai Kolderi National Park, near the village of Saty, at an elevation of 1709 m (coordinates: N42°99'47.60", E78°38'98.12").

Based on the inventory of herbarium materials and label data, an expedition route was established through the Saty Gorge, which represents the most typical habitat of *T. dschungaricus* in the eastern part of the Kungey Alatau Range. The floristic list compiled from field survey data includes 160 plant species belonging to 113 genera and 37 families. The highest number of species occurs in the families Poaceae, Asteraceae, Fabaceae, Lamiaceae, Amaranthaceae, and Rosaceae. The floristic composition involving *T. dschungaricus* in the Saty Gorge, Raiymbek District, Almaty Region, is presented in Table 1.

Table – Floristic composition involving *T. dschungaricus* in the Saty Gorge within the eastern part of the Kungey Alatau Range

Names of species	Family	Life forms [25]	Ecological groups
<i>Juniperus turkestanica</i> Kom.	Cupressaceae Gray	Shrub	Xerophyte
<i>J. sabina</i> L.	Cupressaceae Gray	Shrub	Xerophyte
<i>Picea schrenkiana</i> Fisch. & C.A.Mey.	Pinaceae Spreng. ex F.Rudolphi	Tree	Mesophyte
<i>Ephedra intermedia</i> Schrenk & C.A.Mey.	Ephedraceae Dumort.	Subshrub	Xerophyte
<i>E. distachya</i> L.	Ephedraceae Dumort.	Subshrub	Xerophyte
<i>Botriochloa ischaemum</i> (L.) Keng.	Poaceae Barnhart	Perennial	Xerophyte
<i>Lasiagrostis splendens</i> (Trin.) Kunth.	Poaceae Barnhart	Perennial	Xerophyte
<i>Stipa caucasica</i> Schmalh.	Poaceae Barnhart	Perennial	Xerophyte
<i>S. kirghisorum</i> P.A.Smirn.	Poaceae Barnhart	Perennial	Xerophyte
<i>S. capillata</i> L.	Poaceae Barnhart	Perennial	Xerophyte
<i>S. sareptana</i> A.K.Becker	Poaceae Barnhart	Perennial	Xerophyte
<i>Phleum phleoides</i> (L.) H.Karst.	Poaceae Barnhart	Perennial	Mesophyte
<i>Alopecurus pratensis</i> L.	Poaceae Barnhart	Perennial	Mesophyte
<i>A. soongoricus</i> Fisch. & C.A.Mey.	Poaceae Barnhart	Perennial	Xerophyte
<i>Agrostis gigantea</i> Roth.	Poaceae Barnhart	Perennial	Mesophyte
<i>Calamagrostis epigejos</i> (L.) Roth	Poaceae Barnhart	Perennial	Mesophyte
<i>Helictotrichon pubescens</i> (Huds.) Pilg.	Poaceae Barnhart	Rhizomatous perennial	Mesophyte
<i>H. asiaticum</i> (Roshev.) Grossh.	Poaceae Barnhart	Rhizomatous perennial	Mesophyte
<i>Phragmites communis</i> Trin.	Poaceae Barnhart	Rhizomatous perennial	Hydrophyte
<i>Koeleria gracilis</i> Pers.	Poaceae Barnhart	Perennial	Xeromesophyte
<i>Dactylis glomerata</i> L.	Poaceae Barnhart	Perennial	Mesophyte
<i>Poa bulbosa</i> Steud.	Poaceae Barnhart	Perennial	Xeromesophyte
<i>P. stepposa</i> (Krylov) Roshev.	Poaceae Barnhart	Perennial	Xeromesophyte
<i>P. pratensis</i> L.	Poaceae Barnhart	Perennial	Mesophyte
<i>P. angustifolia</i> L.	Poaceae Barnhart	Perennial	Xeromesophyte
<i>P. alpina</i> L.	Poaceae Barnhart	Perennial	Psychrophyte

Continuation of the table

Names of species	Family	Life forms [25]	Ecological groups
<i>Puccinellia distans</i> (Jacq.) Parl.	Poaceae Barnhart	Perennial	Mesoxerophyte
<i>Festuca sulcata</i> Hack.	Poaceae Barnhart	Perennial	Xeromesophyte
<i>F. kryloviana</i> Reverd.	Poaceae Barnhart	Perennial	Xeromesophyte
<i>Bromus inermis</i> Leyss.	Poaceae Barnhart	Perennial	Mesophyte
<i>B. tectorum</i> L.	Poaceae Barnhart	Annual	Xerophyte
<i>Agropyron repens</i> (L.) Beauv.	Poaceae Barnhart	Perennial	Mesophyte
<i>A. pectiniforme</i> Roem. & Schult.	Poaceae Barnhart	Perennial	Xerophyte
<i>Eremopyrum orientale</i> (L.) Jaub. & Spach	Poaceae Barnhart	Annual	Xerophyte
<i>Hordeum bogdanii</i> Wilensky	Poaceae Barnhart	Perennial	Xerophyte
<i>Leymus angustus</i> (Trin.) Pilg.	Poaceae Barnhart	Perennial	Xerophyte
<i>Kobresia capilliformis</i> N.A.Ivanova	Cyperaceae Juss.	Perennial	Hydrophyte
<i>Carex humilis</i> Willd. ex Kunth.	Cyperaceae Juss.	Perennial	Hydrophyte
<i>C. pachystylis</i> J. Gay.	Cyperaceae Juss.	Perennial	Hydrophyte
<i>C. aneurocarpa</i> V. Krecz.	Cyperaceae Juss.	Perennial	Hydrophyte
<i>C. karoï</i> Freyn.	Cyperaceae Juss.	Perennial	Hydrophyte
<i>C. songorica</i> Kar. & Kir.	Cyperaceae Juss.	Perennial	Hydrophyte
<i>Eremurus tianschanicus</i> Pazij & Vved. ex Pavlov	Asphodelaceae Juss.	Perennial	Mesophyte
<i>Allium oreoprasum</i> Schrenk.	Amaryllidaceae J.St.-Hil.	Perennial	Mesophyte
<i>A. fetisowii</i> Regel	Amaryllidaceae J.St.-Hil.	Perennial	Mesophyte
<i>Tulipa kolpakowskiana</i> Regel	Liliaceae Juss.	Perennial	Mesophyte
<i>Iris tenuifolia</i> Pall.	Iridaceae Juss.	Perennial	Xerophyte
<i>I. brevifolia</i> (Iridaceae Juss.	Perennial	Xerophyte
<i>Salix triandra</i> L.	Salicaceae Mirb.	Tree	Hydrophyte
<i>S. caprea</i> L.	Salicaceae Mirb.	Shrub	Hydrophyte
<i>Urtica cannabina</i> L.	Urticaceae Juss.	Perennial	Mesophyte
<i>U. urens</i> L.	Urticaceae Juss.	Annual	Mesophyte
<i>Rumex confertus</i> Willd.	Polygonaceae Juss.	Perennial	Hydrophyte
<i>Atraphaxis virgata</i> ((Regel) Krasn.	Polygonaceae Juss.	Shrub	Xerophyte
<i>A. frutescens</i> (L.) K.Koch	Polygonaceae Juss.	Shrub	Xerophyte
<i>Polygonum aviculare</i> L.	Polygonaceae Juss.	Annual	Hydrophyte
<i>P. patulum</i> M.Bieb.	Polygonaceae Juss.	Annual	Mesophyte
<i>Chenopodium album</i> L.	Amaranthaceae Juss.	Annual	Hydrophyte
<i>Atriplex tatarica</i> L.	Amaranthaceae Juss.	Annual	Halophyte
<i>Eurotia ceratoides</i> (L.) C.A.Mey.	Amaranthaceae Juss.	Shrublet	Halophyte
<i>Kochia prostrata</i> (L.) Schrad.	Amaranthaceae Juss.	Half-shrub	Halophyte
<i>Salsola arbuscula</i> Pall.	Amaranthaceae Juss.	Shrub	Halophyte
<i>Climacoptera brachiata</i> (Pall.) Botsch.	Amaranthaceae Juss.	Annual	Halophyte
<i>Anabasis salsa</i> (Ledeb.) Benth. ex Volkens	Amaranthaceae Juss.	Half-shrub	Halophyte
<i>Nanophyton erinaceum</i> (Pall.) Bunge	Amaranthaceae Juss.	Bushlet	Halophyte
<i>Aconitum leucostomum</i> Vorosch.	Ranunculaceae Juss.	Perennial	Hydrophyte
<i>A. soongaricum</i> (Regel) Stapf	Ranunculaceae Juss.	Perennial	Hydrophyte
<i>Ceratocephala orthoceras</i> DC.	Ranunculaceae Juss.	Annual	Hydrophyte

Continuation of the table

Names of species	Family	Life forms [25]	Ecological groups
<i>Thalictrum collinum</i> Wallr.	Ranunculaceae Juss.	Perennial	Mesophyte
<i>Th. simplex</i> L.	Ranunculaceae Juss.	Perennial	Mesophyte
<i>Papaver croceum</i> Ledeb.	Papaveraceae Juss.	Perennial	Xerophyte
<i>Sedum alberti</i> Regel	Crassulaceae J.St.-Hil.	Perennial	Xerophyte
<i>Descurainia sophia</i> (L.) Webb ex Prantl	Brassicaceae Burnett	Annual	Hydrophyte
<i>Erysimum diffusum</i> Ehrh.	Brassicaceae Burnett	Biennial	Mesophyte
<i>Alyssum desertorum</i> Stapf	Brassicaceae Burnett	Annual	Xerophyte
<i>Spiraea hypericifolia</i> L.	Rosaceae Juss.	Shrub	Mesophyte
<i>Cotoneaster oliganthus</i> Pojark.	Rosaceae Juss.	Shrub	Mesophyte
<i>C. multiflorus</i> Bunge	Rosaceae Juss.	Shrub	Mesophyte
<i>Sorbus tianschanica</i> Rupr.	Rosaceae Juss.	Tree	Mesophyte
<i>Potentilla erecta</i> (L.) Raeusch.	Rosaceae Juss.	Perennial	Mesophyte
<i>P. asiatica</i> (Th. Wolf) Juz.	Rosaceae Juss.	Perennial	Mesophyte
<i>Sanguisorba officinalis</i> L.	Rosaceae Juss.	Perennial	Mesophyte
<i>Rosa platyacantha</i> Schrenk.	Rosaceae Juss.	Shrub	Xerophyte
<i>Cerasus tianschanica</i> Pojark.	Rosaceae Juss.	Shrub	Mesophyte
<i>Orostachys thyrsiflora</i> Fisch.	Crassulaceae J.St.-Hil.	Biennial	Xerophyte
<i>Rosularia platyphylla</i> (Schrenk) A.Berger	Crassulaceae J.St.-Hil.	Perennial	Xerophyte
<i>Medicago falcata</i> L.	Fabaceae Lindl.	Perennial	Mesophyte
<i>Halimodendron halodendron</i> (Pall.) Voss	Fabaceae Lindl.	Shrub	Xerophyte
<i>Trifolium repens</i> L.	Fabaceae Lindl.	Perennial	Mesophyte
<i>T. pratense</i> L.	Fabaceae Lindl.	Perennial	Mesophyte
<i>Caragana aurantiaca</i> Koehne	Fabaceae Lindl.	Shrub	Xerophyte
<i>C. balchaschensis</i> (Kasn. ex Kom.) Pojark.	Fabaceae Lindl.	Shrub	Xeromesophyte
<i>C. pleiophylla</i> (Fabaceae Lindl.	Shrub	Xeromesophyte
<i>Astragalus sulcatus</i> L.	Fabaceae Lindl.	Perennial	Xeromesophyte
<i>Oxytropis merkensis</i> Bunge	Fabaceae Lindl.	Perennial	Xerophyte
<i>Vicia cracca</i> L.	Fabaceae Lindl.	Perennial	Mesophyte
<i>Hedysarum Semenovii</i> Regel et Herd.	Fabaceae Lindl.	Perennial	Mesoxerophyte
<i>Geranium pratense</i> L.	Geraniaceae Juss.	Perennial	Mesophyte
<i>G. collinum</i> Stephan ex Willd.	Geraniaceae Juss.	Perennial	Mesoxerophyte
<i>Peganum harmala</i> L.	Nitrariaceae Lindl.	Perennial	Xerophyte
<i>Nitraria schoberi</i> L.	Nitrariaceae Lindl.	Shrub	Xerophyte
<i>Hypericum perforatum</i> L.	Hypericaceae Juss.	Perennial	Мезофит
<i>Tamarix ramosissima</i> Ledeb.	Tamaricaceae Link.	Shrub	Xerophyte
<i>Helianthemum songaricum</i> Schrenk ex Fisch. & C.A.Mey.	Cistaceae Juss.	Shrub	Xerophyte
<i>Hippophae rhamnoides</i> L.	Elaeagnaceae Juss.	Shrub	Xerophyte
<i>Elaeagnus argentea</i> Pursh	Elaeagnaceae Juss.	Tree	Xerophyte
<i>Scaligeria setacea</i> (Schrenk) Korov.	Apiaceae Lindl.	Perennial	Xerophyte
<i>Daucus carota</i> L.	Apiaceae Lindl.	Biennial	Mesophyte
<i>Goniolimon sewerzowii</i> Herder	Plumbaginaceae Juss.	Perennial	Xerophyte
<i>Limonium michelsonii</i> Lincz.	Plumbaginaceae Juss.	Perennial	Xerophyte

Continuation of the table

Names of species	Family	Life forms [25]	Ecological groups
<i>Gentianella turkestanorum</i> (Gand.) Holub	Gentianaceae Juss.	Perennial	Mesophyte
<i>Convolvulus tragacanthoides</i> Turcz.	Convolvulaceae Juss.	Shrublet	Xerophyte
<i>C. arvensis</i> L.	Convolvulaceae Juss.	Perennial	Hydrophyte
<i>Echium vulgare</i> L.	Boraginaceae Juss.	Biennial	Mesophyte
<i>Scutellaria transiliensis</i> Juz.	Lamiaceae Martinov	Perennial	Xerophyte
<i>Nepeta pannonica</i> L.	Lamiaceae Martinov	Perennial	Mesophyte
<i>Dracocephalum integrifolium</i> Bunge	Lamiaceae Martinov	Perennial	Xerophyte
<i>Eremostachys speciosa</i> Rupr.	Lamiaceae Martinov	Perennial	Xerophyte
<i>Phlomis oreophila</i> Kar.et Kir	Lamiaceae Martinov	Perennial	Xerophyte
<i>Eriophyton oblongatum</i> (Schrenk) Bendiksby	Lamiaceae Martinov	Perennial	Xerophyte
<i>Lagochilus diacanthophyllus</i> Bong. & C.A.Mey.	Lamiaceae Martinov	Perennial	Xerophyte
<i>Salvia deserta</i> Schangin	Lamiaceae Martinov	Perennial	Xerophyte
<i>Ziziphora clinopodioides</i> Lam	Lamiaceae Martinov	Perennial	Xerophyte
<i>Origanum vulgare</i> L.	Lamiaceae Martinov	Perennial	Mesophyte
<i>Thymus marschallianus</i> Willd.	Lamiaceae Martinov	Half-shrub	Xerophyte
<i>Patrinia intermedia</i> (Hornem.) Roem. & Schult.	Caprifoliaceae Juss.	Perennial	Mesophyte
<i>Scabiosa ochroleuca</i> L.	Caprifoliaceae Juss.	Perennial	Mesophyte
<i>Verbascum songoricum</i> Schrenk ex Fisch. & C.A.Mey.	Scrophulariaceae Juss.	Biennial	Xerophyte
<i>Plantago media</i> L.	Plantaginaceae Juss.	Perennial	Mesophyte
<i>Galium verum</i> L.	Rubiaceae Juss.	Perennial	Mesophyte
<i>Lonicera tatarica</i> L.	Caprifoliaceae Juss.	Shrub	Mesophyte
<i>Galatella fastigiiformis</i> Novopokr.	Asteraceae Bercht. & J.Presl	Perennial	Xerophyte
<i>G. punctata</i> (Waldst. & Kit.) Nees	Asteraceae Bercht. & J.Presl	Perennial	Mesophyte
<i>Leontopodium fedtschenkoanum</i> Beauverd	Asteraceae Bercht. & J.Presl	Perennial	Xerophyte
<i>Ambrosia artemisiifolia</i> L.	Asteraceae Bercht. & J.Presl	Annual	Xerophyte
<i>Achillea millefolium</i> L.	Asteraceae Bercht. & J.Presl	Perennial	Mesophyte
<i>Ajania fastigiata</i> (C.Winkl.) Poljakov	Asteraceae Bercht. & J.Presl	Perennial	Mesophyte
<i>Artemisia rutifolia</i> Stephan ex Spreng.	Asteraceae Bercht. & J.Presl	Half-shrub	Xerophyte
<i>A. santolinifolia</i> (Pamp.) Turcz. ex Krasch.	Asteraceae Bercht. & J.Presl	Half-shrub	Xerophyte
<i>A. absinthium</i> L.	Asteraceae Bercht. & J.Presl	Perennial	Xerophyte
<i>A. scoparia</i> Waldst. & Kit.	Asteraceae Bercht. & J.Presl	Annual, Perennial	Xerophyte
<i>A. dracunculus</i> L.	Asteraceae Bercht. & J.Presl	Perennial	Mesophyte
<i>A. scopaeformis</i> Ledeb.	Asteraceae Bercht. & J.Presl	Perennial	Xerophyte
<i>A. transiliensis</i> Poljakov	Asteraceae Bercht. & J.Presl	Half-shrub	Xerophyte
<i>A. tianschanica</i> Krasch. ex Poljakov	Asteraceae Bercht. & J.Presl	Half-shrub	Xerophyte
<i>A. heptapotamica</i> Poljakov	Asteraceae Bercht. & J.Presl	Perennial	Xerophyte
<i>A. sublessingiana</i> (B.Keller) Krasch. ex Poljakov	Asteraceae Bercht. & J.Presl	Perennial	Xerophyte
<i>Arctium tomentosum</i> Mill.	Asteraceae Bercht. & J.Presl	Biennial	Hygrophyte
<i>Alfredia acantholepis</i> Kar. & Kir.	Asteraceae Bercht. & J.Presl	Perennial	Xerophyte
<i>Cirsium vulgare</i> (Savi) Ten.	Asteraceae Bercht. & J.Presl	Biennial	Hygrophyte

Continuation of the table

Names of species	Family	Life forms [25]	Ecological groups
<i>C. esculentum</i> (Siev.) C.A.Mey.	Asteraceae Bercht. & J.Presl	Perennial	Mesophyte
<i>Centaurea iberica</i> Trevir. ex Spreng.	Asteraceae Bercht. & J.Presl	Perennial	Mesophyte
<i>C. squarrosa</i> Willd.	Asteraceae Bercht. & J.Presl	Biennial	Xerophyte
<i>Cichorium intybus</i> L.	Asteraceae Bercht. & J.Presl	Perennial	Mesophyte
<i>Tragopogon dubius</i> Scop.	Asteraceae Bercht. & J.Presl	Biennial	Mesophyte
<i>Taraxacum officinale</i> F.H.Wigg.	Asteraceae Bercht. & J.Presl	Perennial	Mesophyte
<i>Chondrilla ambigua</i> Fisch. ex Kar. & Kir.	Asteraceae Bercht. & J.Presl	Perennial	Mesophyte

The highest number of species in plant communities with *T. dschungaricus* are represented by the following families: Poaceae (20%), Asteraceae (17%), Lamiaceae (7%), Fabaceae (7%), Rosaceae (6%), Ranunculaceae (3%), Amaranthaceae (5%), Cyperaceae (4%), and Polygonaceae (3%) of the total

number of species, as shown in the diagram (Figure 4).

In terms of life forms, herbaceous perennials predominate (65%), followed by shrubs (12%), herbaceous annuals (9%), biennial plants (5%), trees (4%), shrubs and shrublets (3%), and subshrubs (1%) (Figure 5).

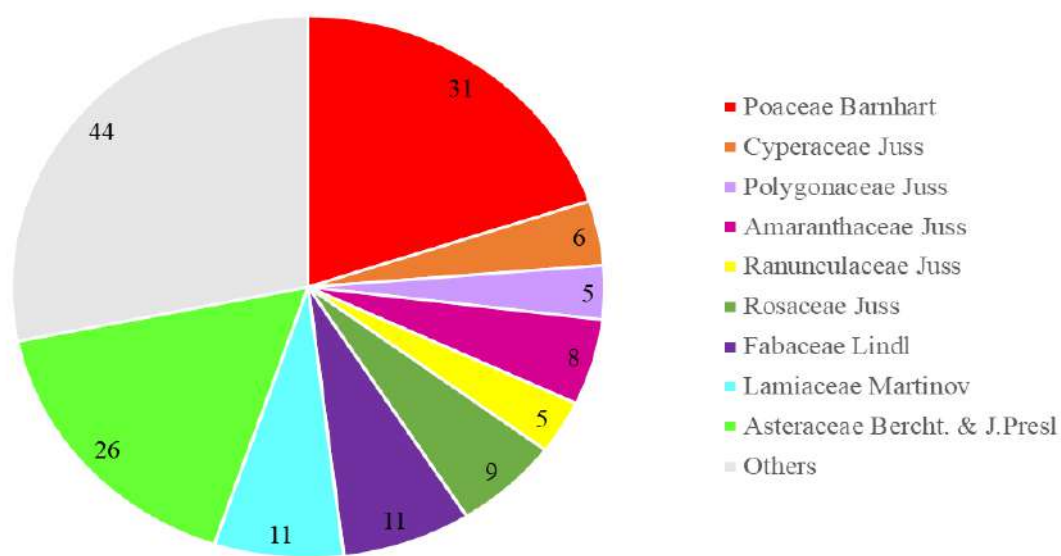


Figure 4 – Spectrum of leading plant families in the territory of Kolsai Lakes National Park

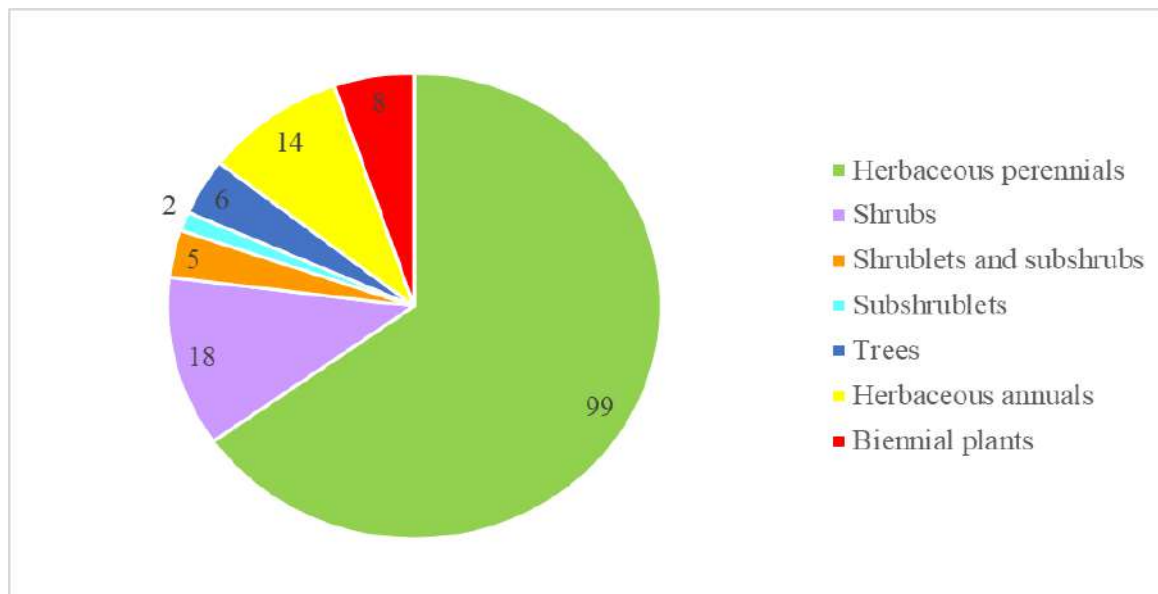


Figure 5 – Life forms according to Serebryakov (1962) [26] in the territory of Kolsai Lakes National Park

The predominant life form in the studied area is perennial plants (137 species), among which are: long-living herbaceous perennials (99 species), shrubs (18 species), subshrubs and semi-shrubs (5 species each), semi-shrubs (2 species), and trees (6 species). Perennials play an edifying role in the studied area, forming the main structure of the vegetation cover. Annuals, represented by 14 species, mainly form modifications of the

grassland. Biennial plants make up 8 species (Figure 5).

As for the composition of life forms depending on temperature, humidity, and substrate structure, it is determined by the predominance of ecological plant groups: xerophytes (40%), mesophytes (35%), mesoxerophytes (2%), hygrophytes (5%), hydrophytes (7%), xeromesophytes (6%), halophytes (4%), and psychophytes (1%) (Figure 6).

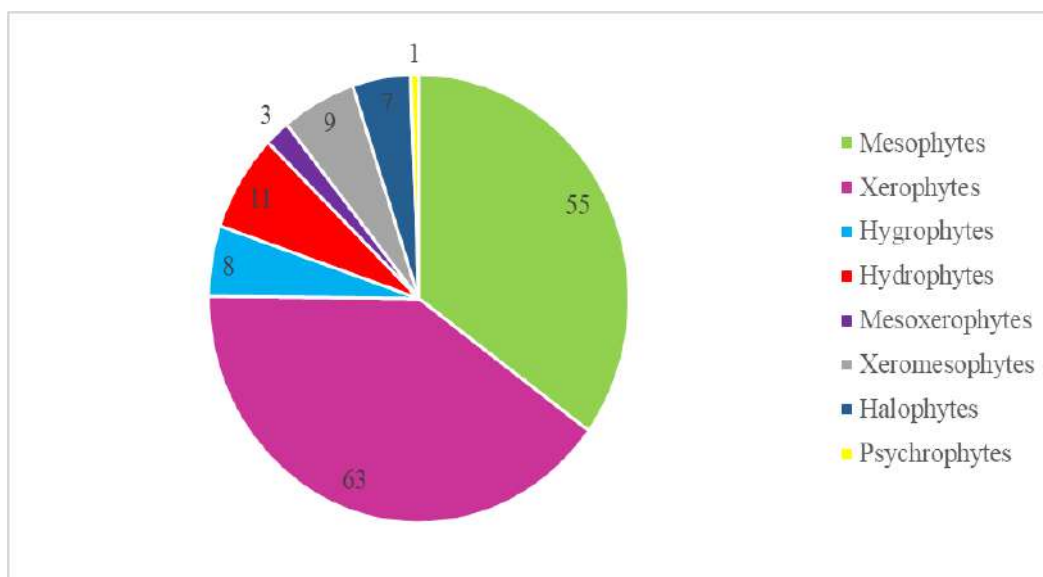


Figure 6 – Ecological plant groups in the territory of Kolsai Lakes National Park

The ecological analysis of the flora of the area showed a wide distribution of xerophytes in the conditions of the mid-mountain zone, as well as the presence of mesophytes and halophytes in river valleys and dry streambeds. The relief plays an important role in the spatial distribution of the vegetation cover. Depending on the habitat conditions and species composition, the natural forage lands are systematized within two main relief forms: the mid-mountain zone and the valleys of mountain rivers.

The predominant vegetation in the surveyed area is that of the mid-mountain zone. The leading types of vegetation in these conditions are relatively homogeneous in terms of background coverage, including steppe communities with species such as *Stipa kirghisorum*, *S. caucasica*, *Festuca valesiaca*, as well as shrub and mixed grassland communities.

On the mountains, hills, and intermountain valleys, sod-forming grasses are widely distributed. The most common species is *Festuca valesiaca* (fine fescue), less frequently *Stipa sareptana* (sarepta feathergrass), and more rarely, the feathergrasses: Kirgiz and Caucasian (*Stipa kirghisorum*, *S. caucasica*).

In the Saty Gorge area, the dominant plant communities are *Festuca*, *Stipa*, and mixed grasslands. In the southern part of the region, on the gently rolling and hilly areas of the terrain, *Festuca* communities prevail, and these are widespread throughout the district. *Stipa* communities mainly occupy flat intermountain valleys, and they are less commonly found on the slopes of the hills.

In depressions, on slopes and peaks, the proportion of *Festuca* and *Stipa* decreases, and mixed grass forms begin to dominate. On the steep slopes of the gorges, shrubs are often encountered.

On the northern slopes of the ridges, there are communities of sod-forming grass-polygonal grassland and grass-mixed grassland types, with exposures of native rocks.

The conducted study made it possible to refine the current distribution range of *T. dschungaricus* and to characterize the ecological features of its habitats in the eastern part of the Kunkey Alatau Range. A multi-level approach that included the analysis of herbarium specimens and field investigations proved effective in identifying natural populations of the species and assessing the accompanying floristic diversity.

The coenofloristic analysis showed that the studied plant communities are characterized by high

species richness and a composition typical of the mid-mountain zone. The predominance of mesophytic species and the dominance of the families *Poaceae*, *Asteraceae*, *Lamiaceae*, *Fabaceae*, and *Rosaceae* indicate a stable adaptation of the vegetation cover to moderately humid conditions. The identified species demonstrate significant ecological plasticity, which enables them to thrive under fluctuating temperature and moisture regimes.

Thus, *T. dschungaricus* is part of stable plant communities and can be considered an ecologically significant component of the region's flora. The obtained data expand our understanding of the biodiversity and vegetation structure of the eastern Kunkey Alatau and can serve as a foundation for future ecological monitoring and environmental planning.

Conclusion

A comprehensive study of the current state of the ornamental and valuable species *T. dschungaricus* in the eastern part of the Kunkey Alatau Range is an important step toward a deeper understanding of its ecology and conservation. Research on this species requires a multi-level approach that includes both the analysis of historical data and field investigations. The initial stage of the work involved the inventory of herbarium materials stored in major herbarium collections, such as those at the Institute of Botany and Phytointroduction (AA) and Al-Farabi Kazakh National University (AFAKNU), as well as data from online platforms like GBIF and iNaturalist. This made it possible to determine the geographic coordinates and locations of the species, which served as the basis for planning field expedition routes and identifying the habitats of *T. dschungaricus* in the study region.

A detailed analysis of the coenoflora of *T. dschungaricus* was conducted in the Saty Gorge. The investigation of the coenoflora revealed a high similarity in species composition between the flora of this gorge and the general flora of the Kunkey Alatau Range, indicating that the studied plant community is typical for this region.

One of the key findings was the predominance of mesophytic species, which in turn influenced the dominance of families such as *Poaceae* (20%), *Asteraceae* (17%), *Lamiaceae* (7%), *Fabaceae* (7%), and *Rosaceae* (6%). This reflects the vegetation's adaptation to the moderately humid conditions characteristic of the area. It also confirms that the

plant species associated with *T. dschungaricus* exhibit high ecological plasticity and can thrive under varying levels of moisture and temperature, making them an important component of the region's ecosystems.

Thus, the research not only revealed the distribution patterns, ecological specificity, and phytocoenotic role of *T. dschungaricus* in the eastern part of the Kungey Alatau Range, but also made a significant contribution to the understanding of the region's floristic diversity and plant community structure.

The obtained results form an important foundation for the development of conservation measures aimed at protecting the declining population of this highly ornamental species. Furthermore, the presented data can be used in long-term ecological monitoring programs of the flora in the eastern Kungey Alatau

and in planning sustainable natural resource use within protected natural areas.

Acknowledgements

The research was carried out within the framework of project No. AP26194223 of the Committee of the Ministry of Science and Higher Education of the Republic of Kazakhstan. Funding: The research was carried out within the framework of project No. AP26194223 of the Committee of the Ministry of Science and Higher Education of the Republic of Kazakhstan.

Conflict of interest

All authors are aware of the article's content and declare no conflict of interest.

References

1. Mukhtubayeva S. K. (2017). Konspekt flori vostochnoi chasti hrebta Kungei Alatau [Prospectus of the flora of the eastern part of the Kungai Alatau Range] *Proc. Int. of Bot and Phytointer.*, vol. 23, no. 11, pp. 272.
2. Luferov A., Erst A., Luferov D., Shmakov A., Wang W. (2018). The genus *Trollius* (Ranunculaceae) in the Russian Far East. *Turczaninowia.*, vol. 21, no. 2, pp. 110–116. <https://doi.org/10.14258/turczaninowia.21.2.12>
3. Li L., Tamura M. (2001). *Trollius* L. In: Flora of China., vol. 6. Ranunculaceae. St Louis: MO: Missouri Botanical Garden. 133–438 p.
4. Kubentayev S. A., Kotukhov Y. A., Gemejiyeva N. G., Mukhtubayeva S. K. (2019). Current state of populations of rare medicinal plants of the Kazakhstan Altai. *Botanical Research of Siberia and Kazakhstan.*, vol. 25, 102–111 p.
5. Flora of Kazakhstan. (1960). Under Ed. NV Pavlov. Almaty: Academy of Sciences of the KazSSR vol 4, no 1, 82–83 p.
6. Serebryanyi M. M. (2019). Towards a taxonomic revision of the genus *Trollius* (Ranunculaceae) in the Asian part of Russia. *I. Trollius chinensis*: taxonomic and geographical reconsiderations. *Higher Plant Systematics News.*, vol 50, 101–114 p.
7. The International Plant Names Index and World Checklist of Vascular Plants 2025. Published on the Internet at <http://www.ipni.org> and <https://powo.science.kew.org/>
8. Doronkin V.M., Polozhij A.V., Kurbatsky V.I., Vydrina S.N., Lukmanova L.Z. (2003) Flora Sibiri [Flora of Siberia] Novosibirsk: Nauka, 104 p. ISBN 5-02-032040-4.
9. Kurmanbayeva M. S., Karabalayeva D. E., Zhumagul M. J., Kusmangazinov A. B. (2025). Assessment of the current state of populations of the species *Trollius dschungaricus* Regel in the flora of the Ketpen Range of the Kungai Alatau. *Eurasian Journal of Ecology.*, vol. 82, no 1. <https://doi.org/10.26577/EJE202582109>
10. Fan W., Luo Y. (2025). Conservation methods for *Trollius* mountain flowers in Xinjiang, China under climate change: Habitat networks construction based on habitat suitability and protected areas optimization response. *Journal of Environmental Management.*, vol.376, 124519 p. <https://doi.org/10.1016/j.jenvman.2025.124519>
11. Mitrenina E. Y., Erst A. S., Skaptsov M. V., Veklich T. N., Chernysheva O. A., Kutsev M. G., Kuznetsov A. A. (2020). Cytogenetic characteristics of some *Trollius* L. species (Ranunculaceae) from Asian Russia. *Ukrainian Journal of Ecology.*, vol.10, no 6, 321–328 p.
12. Abdulina, S. A. (1999). Spisok sosudistih rastenii Kazahstana [List of vascular plants of Kazakhstan] Edited by R. V. Kamelin. Almaty, 187 p.
13. Krupa, E. G., Barinova, S. M., Romanova, S. M., & Malybekov, A. B. (2016). Hydrobiological assessment of the high mountain Kolsay Lakes (Kungey Alatau, Southeastern Kazakhstan) ecosystems in climatic gradient. *British Journal of Environment and Climate Change*, vol 6, no 4, 259–278 p. <http://dx.doi.org/10.9734/BJECC/2016/26496>
14. Zubairov B., Lentschke J., Schröder H. (2019). Dendroclimatology in Kazakhstan. *Dendrochronologia.*, vol. 56, 125602 p. <https://doi.org/10.1016/j.dendro.2019.05.006>
15. Ilin M.M. (1948). Obschie voprosi izucheniya sirevih rastenii, Metodika polevogo issledovaniya sirevih rastenii [General questions of raw plants study, Methodology of field study of raw plants]. M.L. Izd-vo AN SSSR., 7–24 p.
16. Zaugolnova L.B. Denisova L.V. Nikitina S.V. (1993). Podhodi k ochenke sostoyaniya cenopopulyacii rastenii [Approaches to assessing the status of plant populations] Byul. MOIP: Otd. Biol, 100–108 p.
17. Skvorcov A.K. (1977). Gerbarii [Herbarium] Moskva: Nauka, 199 p.

18. Kovalevskaya S.S. (1993). *Opredelitel rastenii Srednei Azii* [A Guide to the Plants of Central Asia] Tashkent: FAN, vol. 10., 692 p. ISBN: 5-648-01604.
19. Baitenov M. S. (1985). *Visokogornaya flora Severnogo Tyan Shanya* [High-altitude flora of the Northern Tien Shan] Alma-Ata: Nauka, 230 p. ISBN 9965-473-87-0
20. Vvedenskii A. I. (1971). *Allium L. Luk*, *Opredelitel rastenii Srednei Azii* [Central Asia Plant Identifier] vol 2, 39-89 p.
21. Yerekeyeva S., Bazarbayeva T., Saykenov B., Makhamedova B., Ocnean M., Balan Ioana M. (2019). Quality of species composition and extent of knowledge of medicinal plants of the ridge Kungei Alatau of the Northern Tien Shan. *Agricultural Management/Lucrari Stiintifice Seria I, Management Agricol*, vol 21, no 2.
22. Plantarium (URL: <https://www.plantarium.ru/>)
23. GBIF Backbone Taxonomy. Checklist dataset <https://doi.org/10.15468/39omei>, accessed via GBIF.org on 2025-03-06.
24. iNaturalist. Retrieved 19 June 2025, from <https://www.inaturalist.org/search?utf8=%E2%9C%93&q=Trollius+L&commit=%D0%9D%D0%B0%D0%B9%D1%82%D0%B8>
25. Raunkiaer C. (1934). *The Life Forms of Plants and Statistical Plant Geography*. Oxford University Press, London.
26. Serebryakov I.G. (1962). *Ekologicheskaya morfologiya rastenii Jiznennie formi pokritosemennih i hvoinih* [Ecological morphology of plants Life forms of covered seeds and conifers] Moskva: Vyshaya shkola, 378 p.

Information about authors

Dina Karabalayeva – Master of Technical and Technological Sciences, PhD-student of the Department of Biodiversity and Bioresources, Al-Farabi Kazakh National University (Almaty, Kazakhstan, e-mail: dina.20.1996@mail.ru)

Meruyert Kurmanbayeva – Doctor of Biological Sciences, Dean of the Faculty of Biology and Biotechnology, Professor of the Department of Biodiversity and Bioresources, Al-Farabi Kazakh National University (Almaty, Kazakhstan, e-mail: kurmanbayevakz@gmail.com)

Saule Mukhtubayeva – Candidate of Biological Sciences, Associate Professor at the Astana International University, Researcher at the Astana Botanical Garden (Astana, Kazakhstan, e-mail: mzhakypzhan@mail.ru)

Moldir Zhumagul – PhD, Acting Associate Professor at the Astana International University, Senior Researcher at the Astana Botanical Garden, Researcher at the Al-Farabi Kazakh National University (Astana, Kazakhstan, e-mail: mzhakypzhan@mail.ru)

Adil Kusmangazinov – PhD, Deputy Dean for Academic and Educational Work of the Faculty of Biology and Biotechnology, Senior Lecturer of the Department of Biodiversity and Bioresources, Al-Farabi Kazakh National University (Almaty, Kazakhstan, e-mail: adil_06.1996@mail.ru)

RaiymbekAnatoliy – PhD-student of the Department of Biodiversity and Bioresources, Al-Farabi Kazakh National University (Almaty, Kazakhstan, e-mail: raymbek_buldurta@mail.ru)

O.Yu. Maslov^{1*}, M.A. Komisarenko¹, S.V. Ponomarenko²,
 S.V. Kolisnyk¹, T.P. Osolodchenko², M.Yu. Golik¹,
 S.I. Polishchuk¹

¹ National University of Pharmacy, Kharkiv, Ukraine

² I. Mechnikov Institute of Microbiology and Immunology, National Academy
 of Medical Sciences of Ukraine, Kharkiv, Ukraine

*e-mail: alexmaslov392@gmail.com

(Received 11 October 2024; received in revised form 23 June 2025; accepted 26 June 2025)

Comparing phytochemical profile, antimicrobial and antioxidant activities of anthocyanin raspberry fruit thick and catechins green tea leaf extracts

Abstract: The aim of the study was investigate and compare phytochemical composition, antimicrobial, and antioxidant potential of raspberry fruit thick and green tea leaf liquid extracts. The quantification of biologically active substances (BAS) was performed using spectrophotometric, titrimetric, and HPLC analysis methods. Antioxidant activity was measured through a potentiometric method, while antimicrobial and antifungal effects were assessed using the well method and determining the minimum inhibition concentration. The total content of phenolic compounds was 0.60 and 10.10%, organic acids – 4.60 and 1.60% for raspberry fruit thick and green tea leaf extract. The total content of catechins in the green tea leaf extract was 10500.0 mg/100 g, where epicatechin-3-O-gallate was dominated (3730.0±74.6 mg/100 g). The total content of anthocyanins in the raspberry fruit thick extract was 109.86 mg/100 g, where cyanidin-3-O-sophoroside was dominated (134.56±2.68 mg/100 g). Both extracts possessed a high antioxidant potential, and effective antimicrobial and anti-fungi effects. The antioxidant, antimicrobial and anti-fungi activity of raspberry fruit extract was higher than green tea leaf extract. In addition, we assumed that anthocyanins had higher antioxidant, antimicrobial and anti-fungi properties than catechins. These findings would promote application of raspberry fruits extract as pharmaceuticals and nutraceuticals.

Key words: raspberry, fruit, green tea, comparing analysis, antimicrobial activity, antioxidant. activity

Introduction

The dangerous of bacterial infections has been evaluated by the international research group. A statistical data has contained about 343 million patient records and pathogen isolates, as result researches have been estimated 13.7 million infection-related deaths at the period of 2019 year. The bacterial infection diseases have been caused 14% of all deaths and 56% of sepsis cases throughout the world in 2019. The mortality level was 100 deaths per 100,000 population. The 55% out 7.7 million deaths have been caused with 3 Gram-negative (-) strains: *Escherichia coli*, *Klebsiella pneumonia*, *Pseudomonas aeruginosa*; and 2 Gram-positive (+): *Staphylococcus aureus* and *Streptococcus pneumonia*. The number one in causing death among infection diseases was *S. aureus*, around 1.1 million patients were died

during 2019. In this year, 225,000 children died due to infection diseases of *S. pneumonia*, whereas among newborn deaths was *K. pneumonia* strain (29,000). According to statistical data, bacterial infection easily surpassed by HIV, cancer, self-harm in a number of deaths during a period of 2019 year [1]. Moreover, a 1.0 billion patients are suffered by fungal infections of the skin, nails, and hair, with over 150 million affected by serious fungal diseases that can be fatal [2]. Therefore, the search and elaboration of new antimicrobial medicines against G(+) and G(-), fungi strains is topical for medicine and pharmacy.

Today, medical plants that are rich source of flavan-3-ols and anthocyanins have a high attention from scientific community [3]. Above all, it relates with fact that some resistance pathogens are more sensitive to natural products, secondly, natural compounds have potent antioxidant effect and

moreover, the side effects are rarely happened after application of natural compounds than after synthetic drugs [4].

Raspberry fruit was chosen as a perspective source of anthocyanins, whereas a green tea leaf is the source of catechins. Raspberries (*Rubus idaeus* L.) are cultivated throughout America, Eastern Europe, Russia, Asian as well as raspberry are closely related to blackberries and other brambles or cranberries. A red and black raspberry is the most widespread throughout the world [5]. *R. idaeus* fruits composition is represented by a variety of flavonoid derivatives, is represented by anthocyanin, quercetin derivatives as well as phenolicarboxylic acids, organic acids, vitamin C [6]. The composition of green tea leaf (*Camellia sinensis* L.) contains: catechins (epigallocatechin-3-O-gallate, epicatechin, (+)-catechin, epigallocatechin), organic acids (oxalic acid), flavonoids (rutin) and hydroxycinnamic acids (caffeic acid) [7].

The recent literature search has showed that in many researches was estimated anti-inflammatory, anti-radical, cytotoxic and antihypertensive activity of aqueous-ethanolic *R. idaeus* extracts due to presents of high content of anthocyanin compounds [8, 9]. *C. sinensis* leaf catechins are not inferior to derivatives of anthocyanins, and there are a lot of scientific researches that have proofed a variety of pharmacological activity: anti-inflammatory, antimicrobial, anti-hyperglycemic, immune-modulation, and anticancer effects [10, 11, 12]. Moreover, in folk medicine *R. idaeus* shoot and *C. sinensis* leaf are traditionally applied to treat fever, skin infections, diabetes, cancers and liver diseases [13, 14]. In our view, the anthocyanins and catechins are perspective for the development of new antimicrobial, anti-fungi and antioxidant pharmaceuticals. But, according available literature sources indexed in Scopus and Web of Science, there are a low number of researches that evaluate and compare antimicrobial and antioxidant activity of anthocyanins and catechins.

Therefore, the aim of investigation was to assess antimicrobial, anti-fungal and antioxidant potential of *R. idaeus* fruit thick and *C. sinensis* leaf liquid extracts and provide phytochemical analysis of obtained extracts.

Materials and methods

Plant material

«» The study focused on *R. idaeus* fruits, which were harvested from areas where they are naturally

grown. The collection took place in 2021 following the fruiting season, near the village of Ternova in the Kharkiv region (50°19'31" N, 36°66'93" E). The study focused on the leaf of *Camellia sinensis* from the Chun Myn variety, which was gathered as raw material in the Anhui province of China during the months of March through May in 2021 (31°03'41" N, 116°33'25" E).

Reagents

« Acetonitrile (purchased from «Allchem», Kharkiv), acetic acid (purchased from «Allchem», Kharkiv), phosphoric acid (purchased from «Allchem», Kharkiv), methanol (purchased from «Allchem», Kharkiv), $K_3[Fe(CN)_6]$ was chemical pure (purchased from «Allchem», Kharkiv), $K_4[Fe(CN)_6]$ was chemical pure (purchased from «Allchem», Kharkiv), cyanidine-3-O-glucoside ($\geq 98.0\%$), cyanidin-3-O-sophoroside ($\geq 98.0\%$), pelargonidin-3-O-sophoroside ($\geq 98.0\%$), cyanidin-3-O-rutinoside ($\geq 98.0\%$), cyaniding-3-rutinoside-5-glucoside ($\geq 98.0\%$), epicatechin ($\geq 98.0\%$), epigallocatechin-3-O-gallate ($\geq 98.0\%$), epigallocatechin ($\geq 98.0\%$), epicatechin-3-O-gallate were purchased in Sigma Aldrich Company, Lublin, Poland.

Equipment

« Potentiometric measurements were performed on a HANNA 2550 pH meter (FRG) with a glass electrode HI11310 (FRG). The quantitative analysis of biologically active compounds was performed on a UV-1000 spectrophotometer (LabAnalyt, China) with matched 1 cm quartz cells

Extraction procedure

«» A 100.0 g (exact mass) of *R. idaeus* fruits was pressed, then it was added of 96% ethanol in a threefold amount to the extraction, after that filtration, then obtained filtrate was concentrated by a vacuum-evaporator at a temperature of 50-60°C until the humidity of the extract is 25%.

The *C. sinensis* extract was obtained by the following way: the raw material was conducted with 60% ethanol at 80° C within 1 hour with a condenser, ratio raw material/solvent – 1/20. The extraction technique was completed twice to provide totally extract all BAS, then the filtrates were joint and evaporated by vacuum rotary to ratio of extract to raw material 1:2.»

Phytochemical analysis

« The total phenolic compounds were quantified using the Folin-Ciocalteu method, with absorbance readings taken at 760 nm [15]. For the quantification of total anthocyanin content, molecular adsorption analysis was utilized, with measurements of

absorbance at 546 nm. The content of total organic acids was established through acid-base titration, using a potentiometric method to determine the end-point [16]. The total catechins were assessed using the vanillin reagent assay, where absorbance was measured at 505 nm [17].

HPLC analysis of *C. sinensis* leaf extract and *R. idaeus* thick fruit extract

For the analysis, a Prominence LC-20 Shimadzu liquid chromatography system with a Thermo Scientific Synchronis aQ C18 column (4.6 × 250) was utilized. All analyses were conducted at a temperature of 40 °C. The mobile phases consisted of a methanol aqueous solution (A) and a 1.0% solution of phosphoric acid (B). The gradient protocol started with 20–42% A over the first 15 minutes, shifted to 42–43% A from 15 to 25 minutes, changed to 43–90% A from 25 to 45 minutes, maintained 90% A from 45 to 55 minutes, decreased to 20% A from 55 to 60 minutes, and then held at 20% A from 60 to 70 minutes. Prior to use, the mobile phases were filtered using 25mm × 0.45 µm Supelco Iso-Disc Filters PTFE 25-4 and degassed. A flow rate of 0.5 mL/min was maintained, and the injection volume of the samples was 5 µL. Detection wavelengths were set at 255, 286, 350 and 530 nm. Chromatographic peaks of analytes were identified by the following similarity indexes, which were calculated between the test substance and the standard according to the formulas:

$$I_T = 1 - |T_{st} - T_u|$$

$$I_{255} = 1 - |h_{255_{st}} - h_{255_{u}}|$$

$$I_{286} = 1 - |h_{286_{st}} - h_{286_{u}}|$$

$$I_{350} = 1 - |h_{350_{st}} - h_{350_{u}}|$$

where, I_T – retention time similarity index, T_{st} – retention time of standard (min), T_u – test substance retention time (min), I_{255} , I_{286} and I_{350} – spectral similarity indices, $h_{255_{st}}$, $h_{286_{st}}$ and $h_{350_{st}}$ – spectral characteristics of the standard, h_{255_u} , h_{286_u} и h_{350_u} – spectral characteristics of the test substance.

The least among the three similarity index values of spectral characteristics dictates the similarity level (IL) between substances and standards based on these traits. A higher IL value increases the probability of more precise identification of the substance. Substances whose similarity index with the catechin standard was at least 0.7, and whose peaks on the chromatogram appeared between the catechin peak

and the earliest flavonoid peak, were classified as catechins [18].

Antioxidant activity

Antioxidant activity of extract was evaluated by potentiometric method [19]. Determination of antioxidant activity was made by following assay: a 2 mmol/L solution of $K_3[Fe(CN)_6]$ was prepared by weighing 0.8232 g into a 25.0 mL volumetric flask, dissolving a compound in a distilled water and filling the flask to volume with the same solvent. A 0.02 mmol/L of $K_4[Fe(CN)_6]$ was prepared by weighing 0.0921 g into a 250.0 mL volumetric flask, dissolving a compound in a distilled water and filling the flask to volume with the same solvent. Then a 5.00 mL aliquot of both prepared solutions was taken and transferred into a 250.0 mL volumetric flask and made up to the mark by 0.067 mol/L phosphate buffer solution. A 50.00 mL of prepared mediator solution was transferred in an electrochemical cell. The initial potential of mediator solution was measured after initial one was established, a 1.00 mL of aliquot of the prepared solutions was added and a final potential was measured. The difference (ΔE) between the initial (E_0) and final (E_1) potentials was found. Antioxidant activity was calculated according to the following equation and expressed as mmol-equiv./m_{dry res.}:

$$AOA = \frac{C_{ox} - \alpha \times C_{red}}{1 + \alpha} \times K_{dil} \times 10^{-3} \times \frac{m_1}{m_2}$$

where, $\alpha = \frac{C_{ox}}{C_{red}} \times 10^{(\Delta E - E_{ethanol})nF/2.3RT}$; C_{ox} – concentration of $K_3[Fe(CN)_6]$, mol/L; C_{red} – concentration of $K_4[Fe(CN)_6]$, mol/L; $E_{ethanol} = 0.0546 \cdot C_{\%} - 0.0091$; $C_{\%}$ – concentration of ethanol; ΔE – change of potential; $F = 96485.33$ C/mol – Faraday constant; $n = 1$ – number of electrons in electrode reaction; $R = 8.314$ J/molK – universal gas constant; $T = 298$ K; K_{dil} – coefficient of dilution, mL.; m_1 – mass of dry residue; m_2 – mass of dry residue in 1.0 mL of extract or prepared solution of standard.

The standardized *C. sinensis* leaf liquid extract, which was obtained by 60% ethanol and solution of epigallocatechin-3-O-gallate were used as the reference standards.

Test organisms

«*S. aureus* ATCC 25923, *E. coli* ATCC 25922, *B. subtilis* ATCC 6538, *C. albicans* ATCC 885/653, *P. vulgaris* NTCS 4636, and *P. aeruginosa* ATCC 27853 were employed following established

guidelines for evaluating the antimicrobial efficacy of pharmaceuticals.

Screening antimicrobial and anti-fungi activity of extracts

The method of diffusion of the drug into agar carried out using the method of “wells”. Preparation of suspensions of microorganisms with a certain concentration of microbial cells (optical density) was carried out using a turbidity standard (0.5 units on the McFarland scale). The Densi-La-Meter device (manufactured by PLIVA-Lachema, Czech Republic; wavelength 540 nm) was used. The suspension was prepared according to the instructions for the device and the information sheet on innovations in the health care system No. 163-2006 “Standardization of the preparation of microbial suspensions”, Kyiv [20]. Synchronization of cultures was carried out using low temperature (4°C) [21]. The microbial load was 107 microbial cells per 1 ml of medium and was set according to the McFarland standard. An 18-24-hour culture of microorganisms was used for the work. Mueller-Hinton agar was used for bacteria, whereas Sabouraud agar was used for *Candida albicans*. As reference standards were gentamycin and fluconazole.

Assay of determination of minimum inhibitory concentration (MIC)

MIC is defined as the smallest concentration of an antibacterial agent that entirely prevents bacterial

growth. The MIC for various extracts was determined through the broth microdilution technique [22].

Statistical analysis

«For all the experiments, two samples were analyzed and all the assays were carried out in 5 times. The results were expressed as mean values with confident interval. The MS EXCEL 7.0 was used to provide statistical analysis.»

Results and discussion

According to obtained results shown in Table 1, the *C. sinensis* leaf extract (10.10±0.25%) had higher content of phenolic compounds, than in *R. idaeus* thick fruit extract (0.60±0.02%).

Table 1 demonstrates that the total content of anthocyanin in *R. idaeus* thick fruit extract was 0.10±0.002%, whereas in *C. sinensis* leaf extract anthocyanin was not presence. The percentage of anthocyanin out of total polyphenols was 17% in *R. idaeus* extract.

The highest amount of organic acids was determined in *R. idaeus* thick fruits extract (4.60±0.50%), whereas in the *C. sinensis* leaf extract it was lower 65% (1.60±0.02%). In *R. idaeus* extract, the total organic acids were in 8.5 times higher than polyphenols, whereas in the *C. sinensis* leaf, the total organic acids were in 6.3 times lower than polyphenols. (Table 1)

Table 1 – Quantitative content of total phenolic compounds, anthocyanin and organic acids

Sample	Total phenolic compounds, %±SD	Total anthocyanin, %±SD	Total catechin, %±SD	Total of organic acids, %±SD
<i>R. idaeus</i> extract	0.60±0.02	0.10±0.002	NP	4.60±0.50
<i>C. sinensis</i> leaf extract	10.10±0.25	NP	10.47±0.25	1.60±0.10

Note: SD – Standard Deviation, n=5;
NP – not present

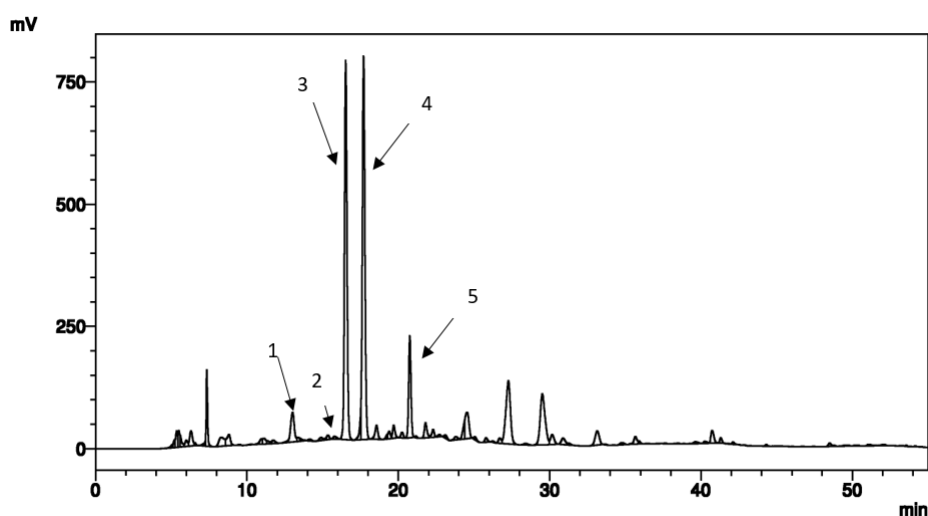
The HPLC method was used to carry out a qualitative and quantitative analysis of catechins and anthocyanins in the obtained extracts of *C. sinensis* leaf and *R. idaeus* fruits extract. According to the results of the study, 5 catechins were identified in *C. sinensis* leaf extract, whereas in *R. idaeus* fruits extract 6 anthocyanins (Fig. 1, 2).

The total content of catechins in the obtained *C. sinensis* leaf extract was 10500.0 mg/100 g. Among catechins, epigallocatechin-3-O-gallate dominates – 3730.0±74.6 mg/100 g (35.52% out of the total catechins), whereas the lowest content was (+)-catechin 210 mg/100 g (2.00% out of the total catechins). (Table 2, Figure 2)

Table 2 – Chemical composition of catechins in *C. sinensis* leaf extract by HPLC-UV analysis

№	Catechins	Retention time, min	Similarity index, I _L	Content of catechins in <i>C. sinensis</i> leaf extract, mg/100 g of extract ±SD	Part out of total catechins, %
1	Epigallocatechin	13.013	0.875	2760.0±55.2	26.29
2	(+)-catechin	13.780	0.996	210.0±4.2	2.00
3	Epicatechin	16.494	0.851	1010.0±20.2	9.62
4	Epigallocatechin-3-O-gallate	17.686	0.990	3730.0±74.6	35.52
5	Epicatechin-3-O-gallate	20.754	0.814	2788.0±55.8	26.57
	Total			10500.0	

Note: SD – Standard Deviation, n=5

**Figure 2** – HPLC fingerprint (255 nm) of the *C. sinensis* leaf extract

As shown in Table 3, cyanidin-3-O-sophorose dominated among all anthocyanins (47.4% out of the total anthocyanins), cyanidin-3-rutinoside-5-glucoside (29.0% out of the total anthocyanins) was in second place, and the lowest content was pelargonidin-3-O-sophorose (0.47% out of the total anthocyanins).

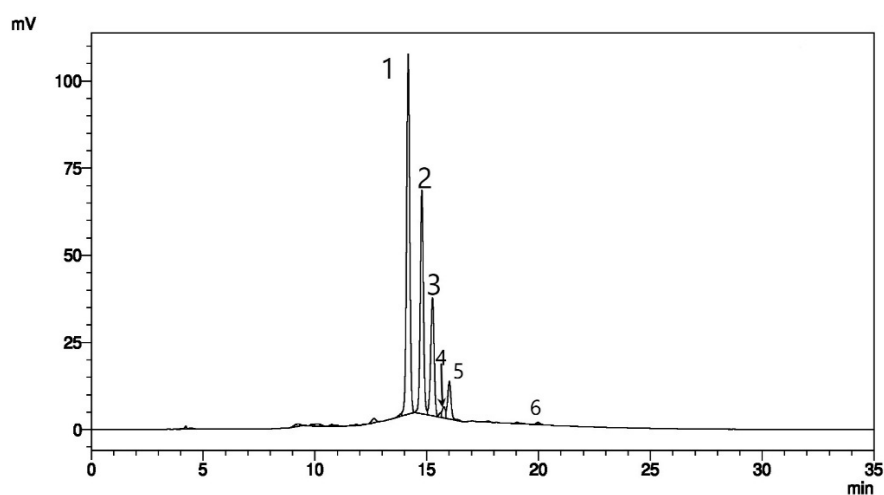
The content of BAS in *R. idaeus* fruit extract was quantified by spectrophotometric, titrimetric and HPLC methods of analysis. The organic acids were present in both extracts, where the highest content of organic acids was determined in *R. idaeus* fruits extract than in *C. sinensis* leaf extract. In our view, it relates with different purpose of organic acids accumulation. The organic acids

are precursor for biosynthesis of sugars in fruits, whereas in leaf, organic acids only play a role in photosynthesis as result there is no purpose of high accumulation organic acids in leaf [23]. Ivanovic *et al.* [24] investigated anthocyanin content of *R. idaeus* fruit 80% metanol extract by HPLC method. According to their results, it was detected following anthocyanins (mg/100 g per extract): cyanidin-3-sophorose (20.4mg /100 g), cyanidin-3-O-rutinoside (3.0 mg/100 g), cyanidin-3-O-glucoside (6.0 mg/100 g), pelargonidin-3-sophorose (2.85 mg/100 g). Comparing with our results, the content of anthocyanins in our research was higher, but cyaniding-3-O-sophorose was dominated in both extracts.

Table 3 – Chemical composition of anthocyanins in *R. idaeus* fruit thick extract by HPLC analysis

№	Anthocyanins	Retention time, min	Content of anthocyanins in extract, mg/100 g of extract \pm SD	Part out of total anthocyanins, %
1	Cyanidin-3-O-sophorose	14.170	52.14 \pm 1.04	47.46
2	Cyanidin-3-rutinoside-5-glucoside	14.780	31.90 \pm 0.64	29.03
3	Cyanidine-3-O-glucoside	15.255	18.15 \pm 0.36	16.52
4	Cyanidin-3-O-rutinoside	16.200	5.59 \pm 0.11	5.08
5	Cyanidin 3-O-xylosyl-rutinoside	16.393	1.61 \pm 0.03	1.46
6	Pelargonidin-3-O-sophorose	19.977	0.47 \pm 0.01	0.45
Total			109.86	

Note: SD – Standard Deviation, n=5

**Figure 3** – HPLC fingerprint (530 nm) of the *R. idaeus* fruit thick extract

A potentiometric method for determining antioxidant activity was used to evaluate the effect of the obtained extracts. Table 4 shows that the level of antioxidant activity of *R. idaeus* fruits extract significantly interferes to the *C. sinensis* leaf extract. The antioxidant activity of *C. sinensis* leaf is higher in 7.7 times of *R. idaeus* extract.

In light of the data obtained, it can be established that the *C. sinensis* leaf extract has the highest level of antioxidant activity. According to the modern classification of antioxidant activity, which was previously developed by us [25], it was found that

all extracts obtained have a high level of antioxidant activity. Moreover, a comparative analysis of the “strength” of antioxidant activity was carried out with the gold standard *C. sinensis* leaf. Further, it was prepared solutions (in terms of the amount of polyphenols expressed as gallic acid) of extracts with 0.03 M concentration of *R. idaeus* thick fruits extract, *C. sinensis* leaf and epigallocatechin-3-O-gallate. As a result of the study, it was found that the level of antioxidant activity of *R. idaeus* extract was higher 56% of *C. sinensis* leaf extract and 49% epigallocatechin-3-O-gallate. (Table 5)

Table 4 – Level of antioxidant activity of *R. idaeus* thick extract, *C. sinensis* leaf extract

Sample	Antioxidant activity, mmol-equiv./m _{dry res.} ±SD	Conditional term of antioxidant level
<i>R. idaeus</i> thick fruits extract	70.95±1.42	High level
<i>C. sinensis</i> leaf extract	548.79±10.98	Very high level
SD – standard deviation, n=3		

Table 5 – Level of antioxidant activity of *R. idaeus* thick extract, *C. sinensis* leaf extract and standard: epigallocatechin-3-O-gallate at concentration 0.03 mol/L

Sample	Concentration, mol/L	Antioxidant activity, mmol-equiv./m _{dry res.} ±SD
<i>R. idaeus</i> thick fruits extract	0.03 ^a	60.81±1.22
<i>C. sinensis</i> leaf extract		27.49±0.54
Epigallocatechin-3-O-gallate		30.78±0.62
Note: SD – standard deviation, n=5; a – molar concentration of raspberry thick extract and green tea leaf extract was calculated as total phenolic compounds expressed as gallic acid		

At first glance, the *C. sinensis* leaf extract had significantly higher antioxidant potential than *R. idaeus* fruit extract. However, comparing extracts at the same molar concentration, it was found that *R. idaeus* fruit extract had 2 times higher the level of antioxidant activity than *C. sinensis* leaf extract. In our view, it relates with the fact that anthocyanins more potent antioxidants than catechins. Lapidot *et al.* [26] determined antioxidant activity of malvidin-3-glucoside, catechin, malvidin and resveratrol by the method of oxidation myoglobin with H₂O₂. It was shown that inhibition efficiency of the antioxidant decreased in following order: malvidin-3-glucoside > catechin > malvidin > resveratrol. In research of Muselik *et al.* [27], it was carried out evaluation the level of antioxidant activity of derivatives of catechins: epicatechin, (+)-catechin, epicatechin, epicatechin-3-O-gallate, galocatechin; and anthocyanins: cyanidin-galactoside, malvidin-3-glucoside and delphinidin-3-glucoside by ferric reducing antioxidant power assay. It was found the level of antioxidant activity decreased in the following order: epicatechin-3-O-gallate > delphinidin-3-glucoside > cyanidin-galactoside > galocatechin > malvidin-3-glucoside > epicatechin > catechin. The antioxidant activity of epicatechin-3-O-gallate had the highest antioxidant power whereas the catechin – the lowest one, where cyanidin-3-galactoside interfere to epicatechin-3-O-gallate, but greater than other derivatives of catehins. The major part of composition of *C. sinensis* leaf is presented by epicatechin-3-O-gallate and low amount – epicatechin and (+)-catechin. However, it

is quite difficult to evaluate the contribution of each compound on total antioxidant power of extract as well as it is unknown whether catechins interact by synergistic way or antagonistic one. Thus, the level of antioxidant activity of extract depends not only on composition of extract, but also, on ration and interaction of compounds.

In this research work, the antimicrobial and antifungal activity of the obtained *R. idaeus* thick fruits and *C. sinensis* leaf extract was investigated against the following strains of *S. aureus*, *B. subtilis*, *E. coli*, *P. vulgaris*, *P. aeruginosa*, as well as a strain of the fungus *C. albicans*. According to the obtained results, extracts obtained from the *R. idaeus* fruit and *C. sinensis* leaf had an effective antimicrobial and antifungal effect.

Among pathogens strains, *R. idaeus* fruits extract was the most inhibits *S. aureus* strains (35.00±0.20 mm), whereas at the second place were *B. subtilis* (33.0±0.2 mm) Gramm-positive strains *P. vulgaris* was the most resistance bacteria to the action of *R. idaeus* fruits extract (21.0±0.2 mm). Comparing results with *C. sinensis* leaf extract, it was determined that *R. idaeus* fruits extract was 17, 21, 30 and 13% better inhibit bacterial strains of *S. aureus*, *B. subtilis*, *E. coli* and fungi *C. albicans* than *C. sinensis* leaf extract, respectively. Comparing obtained results with reference standard gentamycin, it was found that *S. aureus*, *B. subtilis* and *E. coli* were 37, 27 and 46% more sensitive to *R. idaeus* fruits extract than gentamycin. Whereas, *P. vulgaris* and *P. aeruginosa* was 16 and 3% more sensitive to gentamycin.

Anti-fungal investigation against *C. albicans* showed that *R. idaeus* fruits extract 20 and 13% more actively inhibit the growth of fungi than *C. sinensis* leaf and fluconazole, respectively.

The investigated extracts significantly inhibit the bacterial and fungi strains with MIC. In the previously above conducted antimicrobial study, the extract of *R. idaeus* fruits was the most active independently of the tested strains. Table 7 shows,

the *R. idaeus* fruits extract with MIC value of 0.14 μ M was the most active against *S. aureus*, whereas *C. sinensis* leaf extract MIC values was 80% lower. The highest MIC value of *C. sinensis* leaf extract was against fungi pathogens *C. albicans*. The MIC value of *R. idaeus* fruits extract against pathogens *E. coli*, *P. vulgaris* and *B. subtilis* was significantly lower than in the case of *C. sinensis* leaf extract.

Table 6 – Retardation zone (mm) resulting from the screening of antimicrobial activity of *R. idaeus* thick extract, *C. sinensis* leaf extract and standards: gentamycin, fluconazole

Sample	Concentration, mM	Diameter of the growth retardation zone, mm \pm SD					
		Gramm-positive		Gramm-negative			Fungi
		<i>S. aureus</i> ATCC 25923	<i>B. subtilis</i> ATCC 6633	<i>E. coli</i> ATCC 25922	<i>P. vulgaris</i> ATCC 4636	<i>Paeruginosa</i> ATCC 27853	<i>C.albicans</i> ATCC 653/885
<i>R. idaeus</i> thick extract	0.009 ^a	35.0 \pm 0.2	33.0 \pm 0.2	30.0 \pm 0.2	21.0 \pm 0.4	25.0 \pm 0.3	23.0 \pm 0.3
<i>C. sinensis</i> leaf extract	0.009 ^a	29.0 \pm 0.2	26.0 \pm 0.3	21.0 \pm 0.4	24.0 \pm 0.3	28.0 \pm 0.2	21.0 \pm 0.4
Gentamycin	0.003	22.0 \pm 0.2	24.0 \pm 0.3	25.3 \pm 0.3	25.0 \pm 0.3	25.6 \pm 0.3	12.0 \pm 0.6
Fluconazole	0.003	18.0 \pm 0.2	12.0 \pm 0.6	14.3 \pm 0.5	12.3 \pm 0.6	10.0 \pm 0.7	20.0 \pm 0.5

Note: SD – standard deviation, n=5;
a – molar concentration of raspberry thick extract and green tea leaf extract was calculated as total phenolic compounds expressed as gallic acid

Table 7 – Minimal inhibitory concentration of the different *R. idaeus* thick extract, and *C. sinensis* leaf extract against the 6 references pathogens

Sample	MIC, μ M					
	<i>S. aureus</i> ATCC 25923	<i>B. subtilis</i> ATCC 6633	<i>E. coli</i> ATCC 25922	<i>P. vulgaris</i> ATCC 25922	<i>Paeruginosa</i> ATCC 27853	<i>C.albicans</i> ATCC 653/885
<i>R. idaeus</i> thick extract	0.14	0.28	1.13	0.56	0.28	0.56
Green tea leaf extract	0.70	0.70	2.80	2.80	2.80	5.60

The analyzed *R. idaeus* fruit and *C. sinensis* leaf extracts showed high antimicrobial and antifungal activity against the following strains of *S. aureus*, *P. aeruginosa*, *P. vulgaris*, *B. subtilis* and *C. albicans*. According to the obtained data, at first glance it can be considered that the antimicrobial and antifungal activity of *R. idaeus* fruit and *C. sinensis* leaf extracts is significantly inferior to the action of gentamicin and fluconazole, because their concentration of solutions was in 3 times lower than the content of polyphenols in the extract. However, we would like to note that gentamicin has serious toxicity to the

auditory nerve, kidneys and liver, which can lead to serious complications of the disease. Comparing the antifungal effects of fluconazole and *R. idaeus* fruit and *C. sinensis* leaf extracts, it was found that they inhibited the growth of the fungal strain at the same level, while the concentration of fluconazole was also lower, like gentamicin. We can declare that fluconazole is a leader as anti-fungi medicine, but at the same time it weakly inhibits the growth of gram-negative and gram-positive bacteria, but to *R. idaeus* fruit and *C. sinensis* leaf extracts both strains of bacteria and fungus are sensitive. Thus, *R. idaeus*

fruit and *C. sinensis* leaf extracts is a combined pharmaceutical that affects different mechanisms of vital activity of bacteria and fungi, thereby having a wide spectrum of action against different strains of bacteria and fungi, and at the same time not possessing serious toxicity.

The *R. idaeus* fruit is a rich source of anthocyanins, whereas *C. sinensis* leaf of catechins. It is well known that anthocyanins biosynthesis pathway is based on chemical conversion of catechins. Li *et al.* [28] declared that at the beginning of ripening period the content of anthocyanin start increasing, whereas the content of catechins decreasing. However, a question which of this group of flavonoids possess higher antimicrobial and anti-fungi activity is still actually for today. In our research, it was comparing antimicrobial potential of *R. idaeus* fruit and *C. sinensis* leaf extracts. In the antimicrobial and anti-fungi tests, which carried out by method of well, it was shown the *R. idaeus* fruit extract was more active against pathogens *P. aeruginosa*, *E. coli*, *B. subtilis*, *C. albicans* whereas *P. vulgaris* were sensitive to both extracts practically at the same level. Furthermore, it was determined MIC values for both extracts, as result *R. idaeus* fruit extract had better results than *C. sinensis* leaf extract. Therefore, based on mentioned results, it was assumed that antimicrobial and anti-fungi activity of anthocyanins higher than catechins. However, both extracts had a high content of organic acids and its presence should not be neglected. Further in our research, we planned to answer on question whether impact organic acids on antimicrobial potential or not.

Conclusion

It was found that total phenolic compounds were higher in *C. sinensis* leaf extract, whereas total organic acids were in *R. idaeus* fruit thick extract. Both extracts possessed a high antioxidant potential, and effective antimicrobial and anti-fungi effects. Although we assumed that anthocyanins had higher antioxidant, antimicrobial and anti-fungi properties than catechins. In future studies, the hypothesized impact of organic acids on antimicrobial and anti-fungi effects should be verified by isolation of organic acids from both extracts. These findings would promote application of *R. idaeus* fruits extract as pharmaceuticals and nutraceuticals.

Acknowledgments

The research was carried out within the framework of the topic "Development of anhydrous gel based on phenolic compounds for the treatment of purulent wounds caused by antibiotic-resistant *Pseudomonas aeruginosa*" of the list of scientific studies of the Ministry of Health of Ukraine, carried out at the expense of the state budget of Ukraine No. 0124U002080. We are grateful for the provided scientific and material help pharmaceutical company "Zdravopharm", Kharkiv, Ukraine.

Conflict of interest

All authors are aware of the article's content and declare no conflict of interest.

References

1. Ikuta K.S., Swetschinski L. R., Robles A. G. et al. (2022) Global mortality associated with 33 bacterial pathogens in 2019: a systematic analysis for the Global Burden of Disease Study 2019. *Lancet*, vol. 400, pp. 2221-2248. [https://doi.org/10.1016/s0140-6736\(22\)02185-7](https://doi.org/10.1016/s0140-6736(22)02185-7)
2. Denning D. W. (2024) Global incidence and mortality of severe fungal disease. *Lancet Infect Dis*, vol. 24, no. 7, pp. e428-438. [http://doi.org/10.1016/S1473-3099\(23\)00692-8](http://doi.org/10.1016/S1473-3099(23)00692-8)
3. Arsene M.M., Viktorovna P.I., Davares A.K., Parfait K., Andreevna S.L., Mouafo H.T., Rehailia M., Vyacheslavovna Y.N., Pavlovna S.I., Manga I.A., Sergueievna D.M. (2022) Antimicrobial and Antibiotic-Resistance Reversal Activity of Some Medicinal Plants from Cameroon against Selected Resistant and Non-Resistant Uropathogenic Bacteria. *Front Biosci Elite*, vol.14, no. 4, p. 25. <https://doi.org/10.31083/j.fbe1404025>
4. Álvarez-Martínez F. J., Barrajón-Catalán E., Micol V. (2020) Tackling Antibiotic Resistance with Compounds of Natural Origin: A Comprehensive Review. *Biomedicines*, vol. 8, no. 10, p. 405. <https://doi.org/10.3390/biomedicines8100405>
5. Maslov O., Komisarenko M., Kolisnyk S., Tkachenko O., Akhmedov E., Poluain S., Kostina T., Kolisnyk O. (2023) Study of qualitative composition and quantitative content of free organic acids in lingberry leaves. *Fitoterapia*, no. 1, pp. 77-82. <https://doi.org/10.32782/2522-9680-2023-1-77>
6. Kobori R., Yakami S., Kawasaki T., Saito A. (2021) Changes in the Polyphenol Content of Red Raspberry Fruits during Ripening. *Horticulturae*, vol. 7, no. 12, p. 569. <https://doi.org/10.3390/horticulturae7120569>
7. Derymedvid L.V., Horopashna D.O., Kalko K. O., Mishchenko O. Ya., et. al. (2021) Anti-inflammatory properties of raspberry shoot extract. *Pharmacologyonline*, vol. 2, pp. 657-662. <https://doi.org/10.5281/zenodo.10464322>

8. Szymanowska U., Baraniak B., Bogucka-Kocka A. (2018). Antioxidant, Anti-Inflammatory, and Postulated Cytotoxic Activity of Phenolic and Anthocyanin-Rich Fractions from Polana Raspberry (*Rubus idaeus* L.) Fruit and Juice—In Vitro Study. *Molecules*, vol. 23, no. 7, p. 1812. <https://doi.org/10.3390/molecules23071812>
9. Jia H., Liu J., Ufur H., He G., et. al. (2011). The antihypertensive effect of ethyl acetate extract from red raspberry fruit in hypertensive rats. *Pharmacogn Mag*, vol. 7, no. 25, p.19. <https://doi.org/10.4103/0973-1296.75885>
10. Ohishi T., Goto S., Monira P., Isemura M., Nakamura, Y. (2016). Anti-inflammatory Action of Green Tea. *Antiinflamm Antiallergy Agents Med Chem*, vol. 15, no. 2, pp. 74–90. <https://doi.org/10.2174/187152301566616091515443>
11. Zhao T., Li C., Wang S., Song X. (2022) Green Tea (*Camellia sinensis*): A Review of Its Phytochemistry, Pharmacology, and Toxicology. *Molecules*, vol. 27, no. 12, p. 3909. <https://doi.org/10.3390/molecules27123909>.
12. Lin C.C., Lin H.H., Chang H., Chuang L.T., Hsieh C.Y., Lu S.H., Hung C.F., Chang J.F. (2022) Prophylactic Effects of Purple Shoot Green Tea on Cytokine Immunomodulation through Scavenging Free Radicals and NO in LPS-Stimulated Macrophages. *Curr Issues Mol Biol*, vol. 44, no. 9, pp. 3980-4000. <https://doi.org/10.3390/cimb44090273>
13. Krauze-Baranowska M., Głód D., Kula M., Majdan M., Hałas R., Matkowski A., Kozłowska W., Kawiak A. (2014). Chemical composition and biological activity of *Rubus idaeus* shoots – a traditional herbal remedy of Eastern Europe. *BMC Complement Altern Med*, vol.14, no. 1, p. 480. <https://doi.org/10.1186/1472-6882-14-480>
14. Yang C. S., Chen G., Wu, Q. (2014). Recent Scientific Studies of a Traditional Chinese Medicine, Tea, on Prevention of Chronic Diseases. *J Tradit Complement Med*, vol. 4, no. 1, pp. 17–23. <https://doi.org/10.4103/2225-4110.124326>
15. Matić P., Sabljic M., Jakobek L. (2017). Validation of Spectrophotometric Methods for the Determination of Total Polyphenol and Total Flavonoid Content. *JAOAC INT*, vol. 100, no. 6, pp. 1795–1803. <https://doi.org/10.5740/jaoacint.17-0066>
16. Pharmacopeia Europe 8th Edition. (2014) Strasbourg: Council of Europe, 1380 p ISBN 978-928-71-7527-4.
17. He Q., Yao K., Jia D., Fan H., Liao X., Shi B. (2009). Determination of total catechins in tea extracts by HPLC and spectrophotometry. *Nat Pro Res*, vol. 23, no. 1, pp. 93–100. <https://doi.org/10.1080/14786410801886682>
18. Khodakov I. V. (2013) Method for the identification of polyphenols in plant extracts using HPLC. Determination of the composition of soy isoflavones. *Methods Obj Chem Anal*, vol.8, no. 2, pp. 132–142.
19. Maslov O.Y., Kolisnyk S.V., Komissarenko N.A., Kostina T.A. (2021) Development and validation potentiometric method for determination of antioxidant activity of epigallocatechin-3-O-gallate. *Pharmacologyonline*, no. 2, pp. 35-42. <https://doi.org/10.5281/zenodo.7813098>
20. Volyanskiy Y. L., Mironenko L. G., Kalinichenko S. V. (2006) Standardization of the preparation of microbial suspensions [Standartyzatsiia pryhotuvannya mikrobykh suspenzii]. Newsletter of innovations in health care. [Informatsiinyi lyst pro novovvedennia v systemi okhorony zdorovia].
21. Bonnet M., Lagier J. C., Raoult D., Khelaifia S. (2020). Bacterial culture through selective and non-selective conditions: the evolution of culture media in clinical microbiology. *New Micro New Inf*, vol. 34, p. 100622. <https://doi.org/10.1016/j.nmni.2019.100622>
22. Mbarga M.J., Podoprigora I.V., Volina E.G., Ermolaev A.V., Smolyakova L.A. (2021) Evaluation of Changes Induced in the Probiotic *Escherichia coli* M17 Following Recurrent Exposure to Antimicrobials. *J Pharm Res Int*, vol. 1, no. 4, pp.158-167. <https://doi.org/10.9734/jpri/2021/v33i29b31601>
23. Arena M.E., Povilonis I.S., Borroni V., Pérez E., Pellegrino N., Cacciatore C., Radice S. (2023) Changes in Carbohydrates, Organic Acids, and Minerals at Different Development Stages of *Hexachlamys edulis* Fruit, a Wild South American Species with Horticultural Potential. *Horticulturae*, vol. 9, no. 3, p. 314. <https://doi.org/10.3390/horticulturae9030314>
24. Ivanovic M., Pavlovic A., Mitic M., Pecev Marinkovic E., et. al. (2016) Determination of total and individual anthocyanins in raspberries grown in South Serbia. *Zbornik radova*, vol. 21, no. 23, pp. 263-267. <https://doi.org/10.5281/zenodo.15720829>
25. Maslov O.Y., Kolisnyk S.V., Komissarenko M.A., Altukhov A.A., Dynnyk K.V., Stepanenko V.I. (2021) Study and evaluation antioxidant activity of dietary supplements with green tea extract. *Curr Issues Pharm Med*, vol. 14, no. 2, pp. 215-219. <https://doi.org/10.14739/2409-2932.2021.2.233306>
26. Lapidot T., Harel S., Akiri B., Granit R., Kanner J. (1999) pH-Dependent Forms of Red Wine Anthocyanins as Antioxidants†. *J Agric Food Chem*, vol. 47, no. 1, pp. 67-70. <https://doi.org/10.1021/jf980704g>
27. Muselik J., García-Alonso M., Martín-López M., Žemlička M., Rivas-Gonzalo J. (2007) Measurement of Antioxidant Activity of Wine Catechins, Procyanidins, Anthocyanins and Pyranoanthocyanins. *Int J Mol Sci*, vol.8, no. 8, pp. 797-809. <https://doi.org/10.3390/i8080797>
28. Li J., Shi C., Shen D., Han T., Wu W., Lyu L., Li W. (2022) Composition and Antioxidant Activity of Anthocyanins and Non-Anthocyanin Flavonoids in Blackberry from Different Growth Stages. *Foods*, vol. 11, no. 18, p. 2902. <https://doi.org/10.3390/foods11182902>

Information about authors:

Olexander Maslov – PhD, Assistant of the Department of General Chemistry, National University of Pharmacy (Kharkiv, Ukraine, e-mail: alexmaslov392@gmail.com)

Mykola Komissarenko – PhD, Assistant of the Department of Pharmacognosy and Nutriciology, National University of Pharmacy (Kharkiv, Ukraine, e-mail: a0503012358@gmail.com)






Svitlana Ponomarenko – PhD, Leader Researcher of the Laboratory of Biochemistry and Biotechnology, I. Mechnikov Institute of Microbiology and Immunology of the NAMS of Ukraine (Kharkiv, Ukraine, e-mail: syonomarenko@i.ua)

Sergii Kolisnyk – DSc, Professor, Head of the Department of General Chemistry, National University of Pharmacy (Kharkiv, Ukraine, e-mail: s_kolesnik@nuph.edu.ua)

Tetiana Osolodchenko – PhD, Head of the Laboratory of Biochemistry and Biotechnology, I. Mechnikov Institute of Microbiology and Immunology of the NAMS of Ukraine (Kharkiv, Ukraine, e-mail: imi_lbb@ukr.net)

Mykola Golik, – DSc, Professor, Department of General Chemistry, National University of Pharmacy (Kharkiv, Ukraine, e-mail: aptekar4009@gmail.com)

Sofia Polishchuk – M.Sc., Department of General Chemistry, National University of Pharmacy (Kharkiv, Ukraine, e-mail: chemistry29@meta.ua)

M. Narmuratova¹ , S. Orazova^{1*} , A. Serikbayeva² ,
Zh. Narmuratova³ , A. Zhardamalieva¹ 

¹ Al-Farabi Kazakh National University, Almaty, Kazakhstan

² Kazakh National Agrarian Research University, Almaty, Kazakhstan

³ K.I. Satbayev Kazakh National Research Technical University, Almaty, Kazakhstan

*e-mail: saltanat.ozazova@kaznu.edu.kz

(Received 2 June 2025; received in revised form 20 June 2025; accepted 25 June 2025)

Mare's milk as a source of biologically active immunoglobulins: a review of scientific data

Abstract: Mare's milk is a valuable source of biologically active immunoglobulins (Ig), which play a key role in passive immune defense. Unlike cow's milk, it contains a high concentration of IgG, IgA and secretory IgA, which makes it promising for functional nutrition and therapeutic use. Mare's milk immunoglobulins have a high affinity for pathogens, help neutralize viruses, bacteria and toxins, and modulate the immune response of the mucosa. Of particular interest is their association with lactoferrin, which enhances their antimicrobial and anti-inflammatory properties. Modern studies confirm the effectiveness of mare's milk immunoglobulins in the prevention of gastrointestinal infections, allergic reactions and inflammatory diseases. Due to its high digestibility and low allergenicity, it is considered an alternative to cow's milk for infant and dietary nutrition. Promising directions include the creation of "immune-enriched products" based on mare's milk and the use of its immunoglobulins in biomedicine, including the creation of probiotics and drugs for correcting the microbiota. This review summarizes the current knowledge on the structure, functions, and practical applications of mare's milk immunoglobulins, emphasizing their potential in nutrition and clinical practice.

Key words: mare's milk, immunoglobulins, biologically active peptides, whey proteins.

Introduction

Mare's milk has been traditionally consumed in various cultures for its health benefits and nutritional content [1]. Mare's milk is a nutrient-rich substance, containing proteins, fats, carbohydrates, phosphorus, calcium, vitamin C, and many other essential components [2-5]. Although it has a lower fat content than both human and cow's milk, it boasts a higher proportion of unsaturated fatty acids – comparable to human milk – which can help prevent high cholesterol and atherosclerosis [6]. Its protein makeup, mainly whey and casein, falls between human and cow's milk levels. The unique structure and composition of its casein micelles make mare's milk more digestible than cow's milk. Furthermore, its whey protein content is similar to that of human milk and exceeds that of cow's milk [7-10].

Mare's milk is also recognized as a functional food for humans, offering health-supporting properties [8]. It may help manage or prevent conditions like human rotavirus as a means of providing passive

immunity, ulcerative colitis, gastric ulcers, severe IgE-mediated cow's milk allergy [10]. It can also support the immune system during cancer treatments [11]. Both human and mare's milk serve as primary nutritional sources for newborns in their respective species [12].

Proteins in mare's milk release bioactive peptides upon digestion, which contribute to blood pressure regulation, antimicrobial action, and anti-inflammatory effects. Most of the energy in mare's milk comes from lactose (58–70 g/kg), not fat (5–20 g/kg), resulting in lower calorie content compared to cow's milk [8]. Additionally, it acts as a prebiotic, promoting healthy gut flora by encouraging the growth of beneficial bacteria and suppressing harmful ones [13].

Mare's milk is especially valuable for human health due to its content of all nine essential amino acids and a higher level of immunoglobulin A (IgA) than in human or cow's milk. IgA plays a critical role in immune defense by identifying harmful microbes [13]. It also supports skin regeneration and protec-

tion, offering benefits for conditions like eczema, psoriasis, and atopic dermatitis [11].

However, milk composition can vary depending on factors such as the mare's age, lactation stage, season, and breed. Various breeds – including Andalusian, Arabian, Quarter Horse, Thoroughbred, Lusitano, and Shetland – show differences in milk solids, protein, fat, and lactose content [14-20].

Besides the significance of homologous transfer of passive immunity from mother to neonate, there is growing interest in the possibility of heterologous transfer – using immunoglobulins derived from one species to confer passive immunity in another. The concept of influencing the immune status of animals through vaccination against human-related diseases, and subsequently collecting those immunoglobulins from colostrum or milk, has been recognized for some time [20, 21]. This area remains a focus of ongoing research in both animal science and human medicine [21-28].

Composition of Immunoglobulins in Mare's Milk. Mare's milk predominantly contains immunoglobulins IgG, with lesser amounts of IgA and IgM. The concentration of immunoglobulins varies throughout lactation, generally peaking in early lactation and declining thereafter. Typical concentrations reported in studies are approximately 1.0–2.5 g/L for IgG, significantly higher compared to cow's milk, which contains about 0.1–0.5 g/L [23]. Species where offspring are born without antibodies and immunity is transferred through mammary secretions (such as horses, pigs, cows, and goats). The colostrum IgG concentration in many other species is usually greater than 75% of the total antibody content in bovine mammary secretions, but the high IgG concentration in colostrum decreases rapidly with each subsequent milking [29].

Structural Features: The immunoglobulins in mare's milk are mainly of the polymeric form, with IgG being the most abundant, followed by dimeric IgA and pentameric IgM. These immunoglobulins are glycoproteins capable of binding to specific antigens, thereby neutralizing pathogens.

They are divided into different types, including IgM, IgA, IgG, IgE, and IgD [14]. IgG, IgA, and IgM are the most abundant types and are found in breast milk. IgM has relatively low specificity and is not very effective in primary infections. IgA is mainly found in the secretions of the mucous membranes and helps prevent infections of the mucous membranes by causing agglutination of microorganisms. IgG is the most common immunoglobulin in colostrum and bovine milk. There are several subclasses

of IgG, with IgG1 and IgG2 being the main types in the bloodstream.

Monomeric immunoglobulins have a common structural molecule consisting of two identical heavy chains and two identical light chains, with a total molecular weight of about 160 kDa [22,30]. Both heavy and light chains contain constant and variable sections. These chains are connected by disulfide bonds, which give the immunoglobulin a characteristic Y-shaped structure [31]. The class of immunoglobulin depends on the number and location of disulfide bonds. Each molecule has two antigen-binding sites located in the Fab (antigen-binding fragment), which includes variable amino acid domains. The opposite end contains an Fc (constant fragment), which has a constant amino acid sequence within each subclass and determines the specific affiliation of the immunoglobulin. The Fc region is responsible for binding to Fc receptors in different types of cells.

Polymeric immunoglobulins such as IgA and IgM consist of monomeric units linked by a covalent bond to an attached (J) chain [31,32]. As a result, dimeric forms of IgA and pentameric forms of IgM are formed. The J-chain bond also gives them certain characteristics, such as a large number of antigen-binding sites (high valence), which allows these immunoglobulins to bind bacteria effectively; a limited ability to activate the complement system, which helps prevent inflammation; and a strong affinity for the polymer immunoglobulin receptor (pIgR). This receptor facilitates the transport of IgA and IgM through epithelial cells to mucous secretions such as milk [33].

Factors Influencing Content: The immunoglobulin profile is affected by lactation stage, mare's health, diet, and environmental conditions. For example, colostrum, the first milk postpartum, contains the highest immunoglobulin concentrations.

Milk immunoglobulins come from both systemic and local resources. For example, IgG comes from blood serum [23]. Plasma IgG-producing cells are present in breast tissue, but the IgG content in colostrum is lower compared to its amount in blood. Colostrum and milk contain secretory immunoglobulins (sIgA and SIGMA), which are produced by plasma cells located in the mammary gland. Lymphocytes from the GALT system (intestinal-associated lymphoid tissue) migrate to the mammary gland, providing a direct link between the effect of antigens on the immune system of the mother's mucosa and the secretory set of breast immunoglobulins. This means that colostrum and milk from non-immunized cows may contain antibodies specific to pathogens that the

intestines and other mucous membranes of the newborn may encounter. These observations support the idea that cow colostrum can provide passive immune protection against human pathogens.

The immune link between intestinal lymphoid tissue (GALT) and the mammary gland is particularly interesting in relation to breast milk, where the main immunoglobulin is secretory IgA (sIgA), which is one of the key factors underlying the importance of breastfeeding [10].

Transepithelial transport of IgA and IgM through breast epithelial cells occurs through the polymer immunoglobulin receptor (pIgR), which binds dimeric IgA and pentameric IgM in mucosal tissues [39]. The polymeric nature of IgA and IgM is determined by their binding to the J-chain peptide [33]. Only IGA or IgG containing the J-chain have a high affinity for pIgR [40,41].

Isolation of immunoglobulins. In the milk processing, immunoglobulins are also subjected to processing – heating, exposure to acids, high pressure – as a result of which their structure and biological activity change. The methods used for the concentration or isolation of immunoglobulins are classical for the study of proteins and include salt precipitation, column chromatography [45]. Affinity chromatography methods are used to determine IgG, such as lectin-based methods [46], column chromatography of proteins A or G [47, 48], as well as recently developed methods including immobilization of protein A/G on electrospinning membranes [49], metal chelation chromatography [50, 51] and adsorption with using microparticles of polyanhydride are used [52]. Various methods for detecting and quantifying IgG include radial immunodiffusion [53], enzyme immunoassay (ELISA) [54] and newer methods such as enzyme immunoassay using heat [55] and sensors based on surface plasmon resonance [56].

Digestive enzymes action. Immunoglobulins are generally more resistant to digestion in the gastrointestinal tract than other milk proteins; for example, caseins are fermented in the stomach, which prolongs their presence, while whey proteins such as α -lactalbumin are digested quickly and β -lactoglobulin is digested more slowly. Pepsin, the main protease of the stomach, cleaves IgG into the fragment F(ab')₂, which preserves two antigen-binding sites [31,57]. The activity of antibody fragments has been studied for therapeutic use [58]. Pancreatic proteases additionally break down immunoglobulins in the small intestine. The sensitivity of immunoglobulin subclasses to the action of proteolytic enzymes differs. Trypsin cleaves bovine IgG1 to a

greater extent than IgM, while chymotrypsin cleaves IgM to a greater extent than IgG [59]. Bovine IgG1 is more sensitive to pepsin than IgG2, and IgG2 is more vulnerable to trypsin digestion [60]. IgG digestion in the intestine is the slowest among whey proteins, and the newborn receives fewer amino acids [61]. In vitro studies of the intestinal contents of young lambs have shown that IgA is more resistant to digestion than IgG [25].

The cleavage of immunoglobulins proceeds throughout the gastrointestinal tract [62]. In adults who consume bovine serum, about 59% of IgG and IgM are excreted from the jejunum, while only 19% are excreted from the ileum [62]. These indicators are comparable to the rate of digestion of milk proteins in adults, which are approximately 42% absorbed in the jejunum and 93% in the ileum [63], which emphasizes the relative resistance of immunoglobulins to destruction in the gastrointestinal tract. In infants who were fed bovine immunoglobulin products, about 10% of ingested IgG is found in the feces, while in adults less than 4% of ingested IgG is found in the feces [64]. Encapsulation of immunoglobulin preparations can significantly increase IgG excretion in feces, although only low levels are detected in the ileum of adults [65].

The pH of milk fluctuates during the calving period, decreasing to about 6.4, and then rising within a few days to about 6.6–6.9, which is typical for mature milk [66]. Thus, colostrum is slightly more acidic than mature milk. The effect of pH on the stability of immunoglobulins has been studied in a number of papers [67–70]. It was found that bovine IgG remains stable for several hours at a temperature of 37°C between pH 6 and 7, but decreases significantly at pH < 3 or ≥ 10 [67,68]. Acidic or alkaline conditions, especially at higher temperatures, can further destabilize IgG [69,70]. Emulsification can protect IgG from extreme pH values and proteolytic degradation, although homogenization and ultrasound treatment can reduce the residual IgG content due to shear stress [68].

Effects of heat treatment. Immunoglobulins are sensitive to high temperatures. Exposure to a temperature of 75°C can reduce the level of detectable bovine IgG by 40% within five minutes, and at a temperature of 95°C, IgG is completely denatured within 15 seconds [68]. Heating causes conformational changes that impair the antigen binding ability [69,71,72], and the antigen binding region is particularly thermolabile. Although heat treatment reduces the IgG content in colostrum, the rate of this decrease is lower than that of isolated IgG. The addition of

protectors such as sugar or glycerin can improve IgG stability when heated [73].

Many milk processing techniques involve heat treatment of colostrum, milk, or whey. Among the main immunoglobulin types in cow's milk, IgG is the most resistant to heat, while IgM is the most sensitive [74]. Standard pasteurization methods, such as those used in commercial milk and skim milk powder, preserve between 25% and 75% of the IgG found in raw milk. In contrast, milk processed using ultra-high temperature (UHT) techniques contains very little detectable IgG [75]. Despite this, antigen-specific IgG remains relatively stable under regular pasteurization conditions compared to UHT-treated milk or infant formulas made from cow's milk, which undergo more intense heat processing [76].

High-pressure processing is yet another non-thermal approach that can inactivate microbes and certain enzymes, thereby increasing product shelf life [77]. To effectively inactivate bacterial spores, high-pressure treatment must be paired with moderate heat [78]. Depending on the specific conditions, this method can lead to partial or significant loss of IgG activity in colostrum or other IgG-rich fluids [79]. However, when applied to human breast milk, high-pressure processing has shown minimal effects on IgA content [80].

Biological activities of Immunoglobulins. Several risk factors were significantly associated with foal serum IgG and mare colostrum Brix (%) in the Gallacher K. et al work. Foal serum IgG concentration was associated with colostrum Brix %, year of birth and foal birthweight. Mare colostrum IgG concentration was significantly associated with foal serum IgG concentration. The 112 colostrum samples with low Brix (<20%), 56 of these resulted in foals with serum IgG concentrations ≤ 8 g/L (indicating partial or complete FTPI), which suggests that further high-quality colostrum supplementation for these foals needs to happen more promptly in practice. [81]

A review of the literature showed that several constituents in mare's milk may have potential antiviral effects. Proteins of the innate immune system (lysozyme, lactoperoxidase, LF), specific immunoglobulins (IgM, IgG, and secretory IgA), lipid components, cytokines or prostaglandins help in the protection [82]

Supplementation of mare's milk has been shown to aid in the recovery of gut microbiota following intrapartum and postnatal antibiotic therapy by reducing antibiotic resistance gene load and through pre/probiotic and immunomodulatory effects. Antimicrobial and antiviral activity of mare's milk is

associated with a high content of lysozyme, immunoglobulins, lactoperoxidase and lactoferrin [83,84]. Antiviral mechanisms include increased production of macrophages, increased phagocytosis, elevated production of differentiation cluster-positive IgG and IgA immunoglobulins, as well as cytokines. Mare's milk can act as an anti-inflammatory agent, reducing the expression of IL-6, IL-1, TNF- α , and γ -interferon [85,86,87]

M. Jordana Rivero et al. studied the nutritional composition, fatty acid profile, and IgG concentration of the milk produced by Chilean Corralero horse (CCH) mares from breeding farms located in southern Chile. Immunoglobulin G concentration was only affected by dietary factors and pasture composition rather than maternal parity or other known factors [88].

In our study was shown the potential bioactivity, including allergenicity, toxicity, and physicochemical properties, as well as the applicability of 56 peptides from the most active fractions of lactoferrin (LF) isolated from equine milk hydrolysate, it was determined using the Peptide Ranker online database (<http://distilldeep.ucd.ie/PeptideRanker/>). The studied peptides were classified as cationic (13), anionic (23), and neutral (20). The findings revealed that only the cationic and neutral peptides demonstrated significant biological activity (>0.75). Furthermore, peptide bioactivity was positively correlated with phenylalanine content. These research findings can significantly contribute to the MS-based proteomics of equine milk LF and shed light on the composition of its bioactive peptides. Further research is required to comprehensively investigate the biochemical nature and pathways of bioactive peptides responsible for the antimicrobial and antioxidant properties of LF from equine milk [89]. The products of Lactoferrin hydrolysis by trypsin contained polymeric immunoglobulin receptor, which was confirmed at LC-MS/MS analysis.

Conclusion

Mare's milk is a unique natural source of biologically active immunoglobulins with significant therapeutic and prophylactic potential. Due to the high content of IgG, IgA, and sIgA, as well as their connection with other immunoactivity components (such as lactoferrin and lysozyme), it demonstrates pronounced antimicrobial, antiviral, and immunomodulatory properties.

Research confirms that mare's milk immunoglobulins are able to: enhance the protection of mu-

cous membranes (gastrointestinal tract, respiratory tract) due to interaction with Fc receptors; suppress pathogens by neutralizing toxins, agglutinating bacteria and blocking viral adhesion; controlling inflammatory processes, reducing the risk of allergies and autoimmune reactions.

An important advantage of mare's milk is its hypoallergenicity and high digestibility, which makes it a promising alternative to cow's milk, especially in baby and therapeutic nutrition. Prospects for further research are related to the development of immunoenriched products (mixtures, fermented drinks) based on mare's milk, the use of Ig in biomedicine, the creation of drugs for the correction of microbiota, and the prevention of infections. Also, the optimization of immunoglobulin isolation technologies to increase their stability and bioavailability.

Thus, mare's milk is not only a valuable food product, but also a multifunctional biological

system that opens new opportunities for nutrition, preventive, and clinical medicine. Further study of its components will expand the scope of application in personalized nutrition and biotechnology.

Acknowledgments

This research was funded by the Committee of Science of the Ministry of Science and Higher Education of Republic of Kazakhstan (AP19676645 Biotechnology of obtaining biologically active peptides from whey proteins of mare's milk; Agreement No. 277/23-25 dated August 03, 2023).

Conflict of interest

All authors are aware of the article's content and declare no conflict of interest.

References

1. Pietrzak-Fiećko R., Tomczyński R., Smoczyński S.S. (2013) Effect of lactation period on the fatty acid composition in mares' milk from different breeds. *Arch Anim Breed.*, vol. 56, no. 1, pp. 335-43. <https://doi.org/10.7482/0003-9438-56-033>
2. Musaev A., Sadykova S., Anambayeva A., Saizhanova M., Balkanay G., Kolbaev M. (2021) Mare's Milk: Composition, Properties, and Application in Medicine. *Arch Razi Inst.*, vol. 76, no. 4, pp. 1125-1135. <https://doi.org/10.22092/ari.2021.355834.1725>
3. Salamon R.V., Salamon S., Csapó-Kiss Z., Csapó J. (2009) Composition of mare's colostrum and milk I. Fat content, fatty acid composition, and vitamin contents. *Acta Univ. Sapientiae.*, vol. 2, no. 1, pp. 119-31. <http://193.16.218.141/acta-alim/C2-1/alim2-10.pdf>
4. Kenzig A.R., O'Meara K.M., Kremer C.J., Jogan K.S., Jack N.E., Cole K. (2009) Colostral, milk and serum immunoglobulin G concentrations in quarter horse mares and their foals. *J. Equine Vet. Sci.*, vol. 29, pp. 486-487. <https://doi.org/10.1016/j.jevs.2009.04.177>
5. Barreto I., Urbano S.A., Oliveira C.A.A., Macedo C.S., Borba L.H.F., Chags B.M.E., et al. (2020) Chemical composition and lipid profile of mare colostrum and milk of the quarter horse breed. *PLoS One*, vol. 15, e0238921. <https://doi.org/10.1371/journal.pone.0238921>
6. Malacarne M., Martuzzi F., Summer A., Mariani P. (2002) Protein and fat composition of mare's milk: some nutritional remarks with reference to human and cow's milk. *Int Dairy J.*, vol. 12, no. 11, pp. 869-877. [https://doi.org/10.1016/S0958-6946\(02\)00120-6](https://doi.org/10.1016/S0958-6946(02)00120-6)
7. Csapó-Kiss Z., Stefler J., Martin T., Makray S., Csapó J. (1995) Composition of mares' colostrum and milk. Protein content, amino acid composition and contents of macro and micro-elements. *Int Dairy J.*, vol. 5, no. 4, pp. 403-415. [https://doi.org/10.1016/0958-6946\(94\)00014-G](https://doi.org/10.1016/0958-6946(94)00014-G)
8. Pieszka M., Łuszczynski J., Zamachowska M., Augustyn R., Długosz B., Hędrzak M. (2016) Is mare milk an appropriate food for people? – a review. *Ann Anim Sc.*, vol. 16, no. 1, pp. 33-51.
9. Claeys W.L., Verraes C., Cardoen S., De Block J., Huyghebaert A., Raes K., et al. (2014) Consumption of raw or heated milk from different species: An evaluation of the nutritional and potential health benefits. *Food Control*, vol. 42, pp. 188-201. <https://doi.org/10.1016/j.foodcont.2014.01.045>
10. Businco L., Giampietro P.G., Lucenti P., Lucaroni F., Pini C., Di Felice G., et al. (2000) Allergenicity of mare's milk in children with cow's milk allergy. *J Allergy Clin Immunol*, vol. 105, no. 5, pp. 1031-1034. <https://doi.org/10.1067/mai.2000.106035>
11. Nagpal R., Behare P., Rana R., Kumar A., Kumar M., Arora S., et al. (2011) Bioactive peptides derived from milk proteins and their health beneficial potentials: an update. *Food Funct.*, vol. 2, no. 1, pp. 18-27. <https://doi.org/10.1039/c0fo00180a>
12. Sheng Q., Fang X. (2009) Bioactive Components in Mare Milk. In: *Bioactive Components in Milk and Dairy Products*, pp. 195-213. Wiley-Blackwell. <https://doi.org/10.1002/9780813821504.ch11>
13. Foekel C., Schubert R., Kaatz M., Schmidt I., Bauer A., Hipler U.C., et al. (2009) Dietetic effects of oral intervention with mare's milk on the Severity Scoring of Atopic Dermatitis, on faecal microbiota and on immunological parameters in patients with atopic dermatitis. *Int J Food Sci Nutr.*, vol. 60, Suppl 7, pp. 41-52. <https://doi.org/10.3109/09637480903139071>
14. Uniacke-Lowe T., Huppertz T., Fox P.F. (2010) Equine milk proteins: Chemistry, structure and nutritional significance. *Int Dairy J.*, vol. 20, no. 9, pp. 609-629. <https://doi.org/10.1016/j.idairyj.2010.03.003>

15. Pieszka M., Kulisa M., Łuszczynski J., Borowiec F., Jackowski M. (2004) The effect of selected factors on the content of fat, protein and lactose in the milk of Arabian mares. *Zeszyty Naukowe Przegląd Hodowlany*, vol. 72, pp. 235–241.
16. Fuentes F.C., Gonzalo C., Vinuesa M., Sanchez J.M., Hevia M., Quiles A. (1993) Study of the milk composition in mares of the Andalusian and Arabian races during the first four days of lactation. *ITEA Producción Animal*, vol. 89A, pp. 103–111.
17. Barreto Í.M.L.G., Urbano S.A., Oliveira C.A.A., Macêdo C.S., Borba L.H.F., Chags B.M.E., et al. (2020) Chemical composition and lipid profile of mare colostrum and milk of the quarter horse breed. *PLoS One*, vol. 15, no. 9, e0238921. <https://doi.org/10.1371/journal.pone.0238921>
18. Karav S., Salcedo J., Frese S.A., Barile D. (2018) Thoroughbred mare's milk exhibits a unique and diverse free oligosaccharide profile. *FEBS Open Bio*, vol. 8, no. 8, pp. 1219–1229. <https://doi.org/10.1002/2211-5463.12499>
19. Santos A.S., Silvestre A.M. (2008) A study of Lusitano mare lactation curve with Wood's model. *J Dairy Sci.*, vol. 91, no. 2, pp. 760–766. <https://doi.org/10.3168/jds.2007-0347>
20. Schryver H.F., Oftedal O.T., Williams J., Cymbaluk N.F., Antczak D., Hintz H.F. (1986) A comparison of the mineral composition of milk of domestic and captive wild equids (*Equus przewalski*, *E. zebra*, *E. burchelli*, *E. caballus*, *E. assinus*). *Comp Biochem Physiol A Comp Physiol*, vol. 85, no. 2, pp. 233–235. [https://doi.org/10.1016/0300-9629\(86\)90288-3](https://doi.org/10.1016/0300-9629(86)90288-3)
21. Campbell B., Petersen W.E. (1963) Immune milk – A historical survey. *Dairy Sci. Abstr.*, vol. 25, pp. 345–358.
22. Uruakpa F.O., Ismond M.A.H., Akobundu E.N.T. (2002) Colostrum and its benefits: A review. *Nutr. Rev.*, vol. 22, pp. 755–767. [https://doi.org/10.1016/S0271-5317\(02\)00373-1](https://doi.org/10.1016/S0271-5317(02)00373-1)
23. Hurley W.L. (2003) Immunoglobulins of the mammary secretions. In: *Advanced Dairy Chemistry: Proteins*, 3rd ed., vol. 1, part A, Fox P.F., McSweeney P.L.H. (Eds.), Kluwer Academic/Plenum Publishers, New York, NY, USA, pp. 421–447.
24. Van de Perre P. (2003) Transfer of antibody via mother's milk. *Vaccine*, vol. 21, pp. 3374–3376. [https://doi.org/10.1016/S0264-410X\(03\)00336-0](https://doi.org/10.1016/S0264-410X(03)00336-0)
25. Stelwagen K., Carpenter E., Haugh B., Hodgkinson A., Wheeler T.T. (2009) Immune components of bovine colostrum and milk. *J Anim Sci.*, vol. 87, pp. 3–9. <https://doi.org/10.2527/jas.2008-1377>
26. Korhonen H., Marnila P., Gill H.S. (2000) Bovine milk antibodies for health. *Br. J. Nutr.*, vol. 84, Suppl. 1, pp. 135–146. <https://doi.org/10.1017/s0007114500002361>
27. Struff W.G., Sprotte G. (2007) Bovine colostrum as a biologic in clinical medicine; a review. Part I: Biotechnological standards, pharmacodynamic and pharmacokinetic characteristics and principles of treatment. *Int. J. Clin. Pharmacol. Ther.*, vol. 45, pp. 193–202. <https://doi.org/10.5414/cpp45193>
28. Struff W.G., Sprotte G. (2008) Bovine colostrum as a biologic in clinical medicine; a review. Part II: Clinical studies. *Int. J. Clin. Pharmacol. Ther.*, vol. 46, pp. 211–225. <https://doi.org/10.5414/cpp46211>
29. Rouse B.T., Ingram D.G. (1970) The total protein and immunoglobulin profile of equine colostrum and milk. *Immunology*, vol. 19, pp. 901–907.
30. Gapper L.W., Copstake D.E.J., Otter D.E., Indyk H.E. (2007) Analysis of bovine immunoglobulin G in milk, colostrum and dietary supplements: A review. *Anal. Bioanal. Chem.*, vol. 389, pp. 93–109. <https://doi.org/10.1007/s00216-007-1391-z>
31. Mix E., Goertsches R., Zettl U.K. (2006) Immunoglobulins—basic considerations. *J. Neurol.*, vol. 253, Suppl. 5, pp. 9–17. <https://doi.org/10.1007/s00415-006-5002-2>
32. Woof J.M. (2007) The structure of IgA. In: *Mucosal Immune Defense: Immunoglobulin A*, Kaetzel C.S. (Ed.), Springer, New York, NY, USA, Chapter 1, pp. 1–24.
33. Johansen F.E., Braathen R., Brandtzaeg P. (2000) Role of J chain in secretory immunoglobulin formation. *Scand. J. Immunol.*, vol. 52, pp. 240–248. <https://doi.org/10.1046/j.1365-3083.2000.00790.x>
34. Spenser J., Boursier L., Edgeworth J.D. (2007) IgA plasma cell development. In: *Mucosal Immune Defense: Immunoglobulin A*, Kaetzel C.S. (Ed.), Springer, New York, NY, USA, pp. 25–42.
35. Brandtzaeg P. (2010) The mucosal immune system and its integration with the mammary glands. *J. Pediatr.*, vol. 156, Suppl. 2, pp. S8–S15. <https://doi.org/10.1016/j.jpeds.2009.11.014>
36. Hanson L.Å., Silfverdal S.-A., Stromback L., Erling V., Zaman S., Olcen P., Telemo E. (2001) The immunological role of breast feeding. *Pediatr. Allergy Immunol.*, vol. 12, Suppl. 14, pp. S15–S19. <https://doi.org/10.1034/j.1399-3038.2001.121404.x>
37. Brandtzaeg P. (2003) Mucosal immunity: Integration between mother and the breast-fed infant. *Vaccine*, vol. 21, pp. 3382–3388. [https://doi.org/10.1016/s0264-410x\(03\)00338-4](https://doi.org/10.1016/s0264-410x(03)00338-4)
38. Li-Chan E., Kummer A., Losso J.N., Nakai S. (1994) Survey of immunoglobulin G content and antibody specificity in cow's milk from British Columbia. *Food Agric. Immunol.*, vol. 6, pp. 443–451. <https://doi.org/10.1080/09540109409354856>
39. Kaetzel C.S., Bruno M.E.C. (2007) Epithelial transport of IgA by the polymeric immunoglobulin receptor. In: *Mucosal Immune Defense: Immunoglobulin A*, Kaetzel C.S. (Ed.), Springer, New York, NY, USA, pp. 43–89.
40. Johansen F.E., Braathen R., Brandtzaeg P. (2001) The J chain is essential for polymeric Ig receptor-mediated epithelial transport of IgA. *J. Immunol.*, vol. 167, pp. 5185–5192. <https://doi.org/10.4049/jimmunol.167.9.5185>
41. Braathen R., Hohman V.S., Brandtzaeg P., Johansen F.E. (2007) Secretory antibody formation: Conserved binding interactions between J chain and polymeric Ig receptor from humans and amphibians. *J. Immunol.*, vol. 178, pp. 1589–1597. <https://doi.org/10.4049/jimmunol.178.3.1589>
42. Ishikawa H., Kanamori Y., Hamada H., Kiyono H. (2005) Development and function of organized gut-associated lymphoid tissues. In: *Mucosal Immunology*, 3rd ed., Mestecky J., Lamm M., Strober W., Bienenstock J., McGhee J.R., Mayer L. (Eds.), Elsevier Academic Press, Burlington, MA, USA, pp. 385–405.
43. Tai Y.S., Liu B.Y., Wang J.T., Sun A., Kwan H.W., Chiang C.P. (2001) Oral administration of milk from cows immunized with human intestinal bacteria leads to significant improvements of symptoms and signs in patients with oral submucous fibrosis. *J.*

Oral Pathol. Med., vol. 30, pp. 618–625. <https://doi.org/10.1034/j.1600-0714.2001.301007.x>.

44. Kaetzel C.S., Bruno M.E.C. (2007) Epithelial transport of IgA by the polymeric immunoglobulin receptor. In: *Mucosal Immune Defense: Immunoglobulin A*, Kaetzel C.S. (Ed.), Springer, New York, NY, USA, pp. 43–89.
45. Sasaki M., Davis C.L., Larson B.L. (1976) Production and turnover of IgG1 and IgG2 immunoglobulins in the bovine around parturition. *J. Dairy Sci.*, vol. 59, pp. 2046–2055. [https://doi.org/10.3168/jds.S0022-0302\(76\)84486-4](https://doi.org/10.3168/jds.S0022-0302(76)84486-4)
46. Porto A.C.R.C., Oliveira L.L., Ferraz L.C., Ferraz L.E.S., Thomaz S.M.O., Rosa J.C., Roque-Barreira M.C. (2007) Isolation of bovine immunoglobulins resistant to peptic digestion: New perspectives in the prevention of failure in passive immunization of neonatal calves. *J. Dairy Sci.*, vol. 90, pp. 955–962. <https://doi.org/10.3168/jds.2006-248>
47. Zettlitz K.A. (2010) Protein A/G chromatography. In: Kontermann R., Dübel S. (eds) *Antibody Engineering*. Springer-Verlag, Berlin, Germany, vol. 1, pp. 531–535. https://doi.org/10.1007/978-3-642-01144-3_27
48. Darcy E., Leonard P., Fitzgerald J., Danaher M., O'Kennedy R. (2011) Purification of antibodies using affinity chromatography. *Methods Mol. Biol.*, vol. 681, pp. 369–382. https://doi.org/10.1007/978-1-60761-913-0_24
49. Ma Z., Lan Z., Matsuura T., Ramakrishna S. (2009) Electrospun polyethersulfone affinity membrane: Membrane preparation and performance evaluation. *J. Chromatogr. B*, vol. 877, pp. 3686–3694. <https://doi.org/10.1016/j.jchromb.2009.09.030>
50. Kaneko T., Wu B.T., Nakai S. (1985) Selective concentration of bovine immunoglobulins and α -lactalbumin from acid whey using FeCl_3 . *J. Food Sci.*, vol. 50, pp. 1531–1536. <https://doi.org/10.1111/j.1365-2621.1985.tb10552.x>
51. Al-Mashikhi S.A., Nakai S. (1988) Separation of immunoglobulin and transferrin from blood serum and plasma by metal chelate interaction chromatography. *J. Dairy Sci.*, vol. 71, pp. 1756–1763. [https://doi.org/10.3168/jds.S0022-0302\(88\)79747-7](https://doi.org/10.3168/jds.S0022-0302(88)79747-7)
52. Carrillo-Conde B., Garza A., Anderegg J., Narasimhan B. (2010) Protein adsorption on biodegradable polyanhydride microparticles. *J. Biomed. Mater. Res. A*, vol. 95A, pp. 40–48. <https://doi.org/10.1002/jbm.a.32809>
53. Mancini G., Carbonara A.O., Heremans J.F. (1965) Immunochemical quantification of antigens by single radial immunodiffusion. *Immunochemistry*, vol. 2, pp. 235–254. [https://doi.org/10.1016/0019-2791\(65\)90049-8](https://doi.org/10.1016/0019-2791(65)90049-8)
54. Kummer A., Kitts D.D., Li-Chan E., Losso J.N., Skura B.J., Nakai S. (1992) Quantification of bovine IgG in milk using enzyme-linked immunosorbent assay. *Food Agric. Immunol.*, vol. 4, pp. 93–102. <https://doi.org/10.1080/09540109209354881>
55. Ma L., Wang C., Hong Y., Zhang M., Su M. (2010) Thermally addressed immunosorbent assay for multiplexed protein detections using phase change nanoparticles. *Anal. Chem.*, vol. 82, pp. 1186–1190. <https://doi.org/10.1021/ac902572g>
56. Crosson C., Thomas D., Rossi C. (2010) Quantification of immunoglobulin G in bovine and caprine milk using a surface plasmon resonance-based immunosensor. *J. Agric. Food Chem.*, vol. 58, pp. 3259–3264. <https://doi.org/10.1021/jf9038382>
57. Fang W.D., Mukkur T.K.S. (1976) Physicochemical characteristics of proteolytic cleavage fragments of bovine colostrum immunoglobulin G1 (IgG1). *Biochem. J.*, vol. 155, pp. 25–30. <https://doi.org/10.1042/bj1550025>
58. Carter P.J. (2006) Potent antibody therapeutics by design. *Nat. Rev. Immunol.*, vol. 6, pp. 343–357. <https://doi.org/10.1038/nri1837>
59. Brock J.H., Arzabe F.A., Pineiro A., Olivito A.-M. (1977) The effect of trypsin and chymotrypsin on the bactericidal antibody activity of bovine colostrum. *Immunology*, vol. 32, pp. 207–213. <https://www.ncbi.nlm.nih.gov/pmc/articles/PMC1457585/>
60. De Rham O., Isliker H. (1977) Proteolysis of bovine immunoglobulins. *Int. Arch. Allergy Appl. Immunol.*, vol. 55, pp. 61–69. <https://doi.org/10.1159/000231847>
61. Yvon M., Levieux D., Valluv M.-C., Pelissier J.-P., Mirand P.P. (1993) Colostrum protein digestion in newborn lambs. *J. Nutr.*, vol. 123, pp. 586–596. <https://doi.org/10.1093/jn/123.4.586>
62. Roos N., Mahe S., Benamouzig R., Sick H., Rautureau J., Tome D. (1995) 15N-labeled immunoglobulins from bovine colostrum are partially resistant to digestion in human intestine. *J. Nutr.*, vol. 125, pp. 1238–1244. <https://doi.org/10.1093/jn/125.5.1238>
63. Mahe S., Huneau J.-F., Marteau P., Thuille F., Tome D. (1992) Gastroileal nitrogen and electrolyte movements after bovine milk ingestion in humans. *Am. J. Clin. Nutr.*, vol. 56, pp. 410–416. <https://doi.org/10.1093/ajcn/56.3.410>
64. Kelly C.P., Chetham S., Keates S., Bostwick E.F., Roush A.M., Castagliuolo I., LaMont J.T., Pothoulakis C. (1997) Survival of anti-*Clostridium difficile* bovine immunoglobulin concentrate in the human gastrointestinal tract. *Antimicrob. Agents Chemother.*, vol. 41, pp. 236–241. <https://doi.org/10.1128/AAC.41.2.236>
65. Warny M., Fatimi A., Bostwick E.F., Laine D.C., Lebei F., LaMont J.T., Pothoulakis C., Kelly C.P. (1999) Bovine immunoglobulin concentrate-*Clostridium difficile* retains *C. difficile* toxin neutralizing activity after passage through the human stomach and small intestine. *Gut*, vol. 44, pp. 212–217. <https://doi.org/10.1136/gut.44.2.212>
66. Hurley W.L. (1987) Mammary function during the nonlactating period: Enzyme, lactose, protein concentrations, and pH of mammary secretions. *J. Dairy Sci.*, vol. 70, pp. 20–28. [https://doi.org/10.3168/jds.S0022-0302\(87\)79985-0](https://doi.org/10.3168/jds.S0022-0302(87)79985-0)
67. Shimizu M., Nagashima H., Hasimoto K. (1993) Comparative studies in molecular stability of immunoglobulin G from different species. *Comp. Biochem. Physiol. B*, vol. 106, pp. 255–261. [https://doi.org/10.1016/0305-0491\(93\)90163-F](https://doi.org/10.1016/0305-0491(93)90163-F)
68. Chen C.-C., Chang H.-M. (1998) Effect of thermal protectants on the stability of bovine milk immunoglobulin G. *J. Agric. Food Chem.*, vol. 46, pp. 3570–3576. <https://doi.org/10.1021/jf970974n>
69. Dominguez E., Perez M.D., Puyol P., Sanchez L., Calvo M. (2001) Effect of pH on antigen-binding activity of IgG from bovine colostrum upon heating. *J. Dairy Res.*, vol. 68, pp. 511–518. <https://doi.org/10.1017/S002202990100505X>
70. Gao W., Chen L., Xu L.B., Huang X.H. (2010) Specific activity against diarrheagenic bacteria in bovine immune milk and effect of pH on its antigen-binding activity upon heating. *J. Dairy Res.*, vol. 77, pp. 220–224. <https://doi.org/10.1017/S0022029910000137>
71. Calmettes P., Cser L., Rajnavolgy E. (1991) Temperature and pH dependence of immunoglobulin G conformation. *Arch. Biochem. Biophys.*, vol. 291, pp. 277–283. [https://doi.org/10.1016/0003-9861\(91\)90133-W](https://doi.org/10.1016/0003-9861(91)90133-W)
72. Dominguez E., Perez M.D., Calvo M. (1997) Effect of heat treatment on the antigen-binding activity of anti-peroxidase immunoglobulins in bovine colostrum. *J. Dairy Sci.*, vol. 80, pp. 3182–3187. [https://doi.org/10.3168/jds.S0022-0302\(97\)76291-5](https://doi.org/10.3168/jds.S0022-0302(97)76291-5)

73. Chen C.-C., Tu Y.-Y., Chang H.-M. (2000) Thermal stability of bovine milk immunoglobulin G (IgG) and the effect of added thermal protectants on the stability. *J. Food Sci.*, vol. 65, pp. 188–193. <https://doi.org/10.1111/j.1365-2621.2000.tb15973.x>
74. Mainer G., Sanchez L., Ena J.M., Calvo M. (1997) Kinetic and thermodynamic parameters for heat denaturation of bovine milk IgG, IgA and IgM. *J. Food Sci.*, vol. 62, pp. 1034–1038. <https://doi.org/10.1111/j.1365-2621.1997.tb15016.x>
75. Li-Chan E., Kummer A., Loso J.N., Kitts D.D., Nakai S. (1995) Stability of bovine immunoglobulins to thermal treatment and processing. *Food Res. Int.*, vol. 28, pp. 9–16. [https://doi.org/10.1016/0963-9969\(95\)93577-D](https://doi.org/10.1016/0963-9969(95)93577-D)
76. Mainer G., Dominguez E., Randrup M., Sanchez L., Calvo M. (1999) Effect of heat treatment on anti-rotavirus activity of bovine colostrum. *J. Dairy Res.*, vol. 66, pp. 131–137. <https://doi.org/10.1017/S0022029998003322>
77. Balasubramaniam V.M., Ting E.Y., Stewart C.M., Robbins J.A. (2004) Recommended laboratory practices for conducting high-pressure microbial inactivation experiments. *Innov. Food Sci. Emerg. Technol.*, vol. 5, pp. 299–306. <https://doi.org/10.1016/j.ifset.2004.04.001>
78. Balasubramaniam S., Balasubramaniam V.M. (2003) Compression heating influence of pressure transmitting fluids on bacteria inactivation during high pressure processing. *Food Res. Int.*, vol. 36, pp. 661–668. [https://doi.org/10.1016/S0963-9969\(03\)00069-3](https://doi.org/10.1016/S0963-9969(03)00069-3)
79. Trujillo A.J., Castro N., Quevedo J.M., Arguello A., Capote J., Guamis B. (2007) Effect of heat and high-pressure treatments on microbiological quality and immunoglobulin G stability of caprine colostrum. *J. Dairy Sci.*, vol. 90, pp. 833–839. [https://doi.org/10.3168/jds.S0022-0302\(07\)71568-6](https://doi.org/10.3168/jds.S0022-0302(07)71568-6)
80. Permanyer M., Castellote C., Ramirez-Santana C., Audi C., Pérez-Cano F.J., Castell M., Lopez-Sabater M.C., Franch A. (2009) Maintenance of breast milk immunoglobulin A after high-pressure processing. *J. Dairy Sci.*, vol. 93, pp. 877–883. <https://doi.org/10.3168/jds.2009-2424>
81. Gallacher K., Champion K., Denholm K.S. (2025) Mare colostrum quality and relationship with foal serum immunoglobulin G concentrations and average daily weight gains. *Equine Vet. J.*, vol. 57, pp. 904–914. <https://doi.org/10.1111/evj.14471>
82. Sheng Q., Fang X. (2009) Bioactive components in mare milk. In: *Bioactive Components in Milk and Dairy Products*, pp. 195–204. Wiley-Blackwell. ISBN: 9780813803623
83. Suez J., Zmora N., Zilberman-Schapira G., et al. (2018) Post-antibiotic gut mucosal microbiome reconstitution is impaired by probiotics and improved by autologous FMT. *Cell*, vol. 174, pp. 1406–1423.e16. <https://doi.org/10.1016/j.cell.2018.08.047>
84. Pärnänen K., Karkman A., Hultman J., et al. (2018) Maternal gut and breast milk microbiota affect infant gut antibiotic resistance and mobile genetic elements. *Nat. Commun.*, vol. 9, 3891. <https://doi.org/10.1038/s41467-018-06393-w>
85. Miguel M.G., Cardoso P.G., Lago L.D., Schwan R.F. (2010) Diversity of bacteria present in milk kefir grains using culture-dependent and culture-independent methods. *Food Res. Int.*, vol. 43, pp. 1523–1528. <https://doi.org/10.1016/j.foodres.2010.04.030>
86. Adiloğlu A.K., Gönülateş N., İşler M., Şenol A. (2013) The effect of kefir consumption on human immune system: A cytokine study. *Mikrobiyol. Bül.*, vol. 47, pp. 273–281. <https://doi.org/10.5578/mb.4709>
87. Detha A., Sudarwanto M., Latif H., Datta F.U.D., Puji L. (2013) Fractionation and identification of antimicrobial activity of Sumba mare's milk protein against subclinical mastitis bacteria in dairy cattle. *Global Veterinaria*, vol. 11, pp. 674–680. [https://www.idosi.org/gv/gv11\(5\)13/26.pdf](https://www.idosi.org/gv/gv11(5)13/26.pdf)
88. Rivero M.J., Cooke A.S., Gandarillas M., Leon R., Merino V.M., et al. (2024) Nutritional composition, fatty acids profile and immunoglobulin G concentrations of mare milk of the Chilean Corralero horse breed. *PLOS ONE*, vol. 19, e0310693. <https://doi.org/10.1371/journal.pone.0310693>
89. Narmuratova M., Narmuratova Zh., Kanayat Sh., Meldebekova A., Yusof Y.A. (2024) In silico determination of physico-chemical properties of lactoferrin peptides isolated from equine milk. *ES Food & Agroforestry*, vol. 17, 1196. <https://doi.org/10.30919/esfaf1196>

Information about authors

Meiramkul Narmuratova – Candidate of Biological Sciences, Associate Professor of the Department of Biotechnology, Al-Farabi Kazakh National University (Almaty, Kazakhstan, e-mail: meiramkul.narmuratova@kaznu.edu.kz)

Saltanat Orazova – Candidate of Biological Sciences, Senior Lecturer of the Department of Biotechnology, Al-Farabi Kazakh National University (Almaty, Kazakhstan, e-mail: saltanat.orazova@kaznu.edu.kz)

Serikbayeva Asiya – Doctor of Biological Sciences, Professor of the Department of Zooengineering and Biotechnology, Kazakh National Agrarian Research University (Almaty, Kazakhstan, e-mail: serikbayeva@yandex.ru)

Zhanar Narmuratova – PhD, Senior Lecturer of the Department of Chemical and Biochemical Engineering, K.I. Satbayev Kazakh National Research Technical University (Almaty, Kazakhstan, e-mail: janarka.90b@gmail.com)

Anar Zhardamalieva – M.Sc., main specialist of the Department of Biodiversity and Bioresources, Al-Farabi Kazakh National University (Almaty, Kazakhstan, e-mail: zhardamalieva.anar@mail.ru)

A.B. Tolegen^{1,2}, N.V. Romadanova^{1*}, M.M. Aralbayeva¹,
 N.K. Rymkhanova^{1,2}, Y.V. Ulkhatova³, M.M. Asqahanov³,
 N.V. Mikhailenko¹, S.V. Kushnarenko¹

¹Institute of Plant Biology and Biotechnology, Almaty, Kazakhstan

²Al-Farabi Kazakh National University, Almaty, Kazakhstan

³N.I. Vavilov All-Russian Institute of Plant Genetic Resources (VIR), Saint Petersburg, Russia

*e-mail: nataromadanova@gmail.com

(Received 12 May 2024; received in revised form 26 June 2025; accepted 27 June 2025)

Utilizing Plant Preservative Mixture™ to eliminate endophytic bacterial contamination and establish *in vitro* cultures of blackberry varieties

Abstract: Bacterial, fungal, and viral contaminations pose a pervasive challenge to *in vitro* propagation of berry crops, presenting significant economic hurdles for the preservation of plant genetic resources and the commercialization of micropropagation. This study aimed to diagnose endophytic and viral contamination in commercial blackberry cultivars and while developing an *in vitro* method to eliminate bacterial contamination from the Chacanska Bestrna variety. The Plant Preservative Mixture™ (PPM™) was utilized as a broad-spectrum bactericidal agent within the blackberry *in vitro* tissue culture. Contaminated shoots were cultured on Murashige and Skoog medium supplemented with 0.2% v/v PPM™, maintained over a 12-week period through three subcultures, before being transferred to medium devoid of PPM™ for an additional 12 weeks. The results were evaluated after 12 and 32 weeks of culture on medium without PPM™. This study demonstrated that PPM™ is an effective control agent and can be successfully used to manage the growth of endophytic contamination. For the Chacanska Bestrna blackberry variety, 100% aseptic shoots were obtained *in vitro* without any negative effects on the shoot growth. However, the results indicate the opportunity for further testing of PPM™ on other blackberry varieties experiencing bacterial contamination, as it is possible that the contamination in this study was superficial and the selected concentration of the bactericide proved to be successful. To obtain virus-free planting stocks, *in vitro* rooted shoots were transferred to a soil substrate consisting of peat (40%), black soil (50%), and perlite (10%), and then adapted in a greenhouse at 20-23°C. The survival rate of blackberry varieties in greenhouse conditions was 93-99%.

Key words: blackberry; tissue culture; *in vitro* contamination; micropropagation; broad-spectrum biocide.

Introduction

The cultivation of berries stands as one of the most vibrant and flourishing sectors within the realm of agriculture, marked by its dynamic growth and lucrative potential. According to the Food and Agriculture Organization (FAO), the Republic currently produces about 420 thousand tons of fruits and berries, while the population of the country requires more than 2.5 million tons of products according to world standards; about 70% of fruit and berry products are imported [1]. One of the limiting factors in the development of this industry in Kazakhstan is the lack of high-quality planting material. In this regard, the de-

velopment of micropropagation techniques to obtain healthy planting material for berry crops is extremely important.

Blackberry is a valuable berry crop, the fruits of which have high nutritional and healing properties, due to their rich chemical composition. These exquisite berries possess approximately 10% carbohydrates along with a medley of organic acids, pectin, fiber, and a rich array of vitamins including P, B, E, and C, complemented by a diverse spectrum of macro and microelements [2]. The allure of blackberries extends beyond their delightful taste and captivating aroma; they are celebrated for their robust concentrations of anthocyanins and phenols, both of which

exhibit powerful antioxidant and anticancer properties [3]. Furthermore, blackberries lend themselves to the creation of high-quality processed delicacies, such as jams, jellies, marmalade, juices, and extracts, as well as delightful wines and beverages. These fruits are equally adept at swift freezing, perfect for crafting vibrant food colorings that enhance culinary creations. Despite the high value of this berry crop, blackberries are still not as popular among farmers in Kazakhstan as raspberries and strawberries. The main difficulties in cultivating this crop are associated, first of all, with the need to select high-quality, highly productive varieties suitable for the soil and climatic conditions of the country, as well as the use of modern agricultural technologies [4]. In addition, Kazakhstani farmers use blackberry planting stocks purchased from foreign producers because there is no high-quality, pathogen-free material of domestic production available.

Traditionally, varieties of berry crops are propagated by green or woody cuttings, which is often not very effective [5-7]. Micropropagation is currently the only way to produce healthy planting material on an industrial scale, widely used in many countries [8]. The development of blackberry micropropagation technologies is being fruitfully pursued in the USA [9], Russia [10-11], and European Union countries [12-13]. There are no scientific publications on micropropagation of blackberries in Kazakhstan.

When producing planting material, it is very important to monitor its virological status. Blackberry varieties are propagated vegetatively and can accumulate viruses during various development stages. More than 30 different viruses are known to infect native and cultivated blackberries [14-16]. *Raspberry bushy dwarf virus* (RBDV) is the most harmful and widespread pathogen of *Rubus* genus including blackberry [17]. RBDV was discovered worldwide in *Rubus* commercial growing regions, including North and South America, Europe, China, and New Zealand [13-19, 17-23]. The occurrence of RBDV both in cultivated and native raspberry plants was recently reported in Kazakhstan [24]. *Blackberry yellow vein associated virus* (BYVaV) has been described in the USA in blackberries with symptoms of vein clearing, yellow mottling and plant decline [25]. Black raspberry (*Rubus occidentalis*) plantings in Oregon (USA) also declined by *Black raspberry necrosis virus* (BRNV) [26]. *Apple mosaic virus* (ApMV), which is widespread throughout the world, has also been found in symptomless *Rubus* plants in the United States and Germany [16].

One of the indispensable stages of micropropagation is *in vitro* culture initiation. Contamination of field plant material with bacterial and fungal pathogens can significantly reduce the percentage of aseptic shoots. Surface disinfection helps eliminate epiphytic bacterial and fungal contaminations; however, sterilizing agents usually have no effect on endophytic bacteria that inhabit inner tissues and organs [8, 27, 28, 29]. A wide variety of endophytic bacteria have been identified in tissue culture of various plants, including *Curtobacterium*, *Mycobacterium*, *Paenibacillus*, *Pseudomonas*, *Stenotrophomonas* found in *in vitro* shoots of *Rubus ideaus* [25, 30]. Antibiotic treatment has been shown to be effective in eliminating bacterial contamination from micropropagated strawberry plants [31]. A combination of several antibiotics may have advantages over the use of a single antibiotic in preventing the emergence of resistant strains [27, 31, 32]. The use of the broad-spectrum biocide Plant Preservative Mixture™ (PPM™) has shown high efficiency in eliminating endophytic contamination from explants taken in field collections of various plants and propagated *in vitro*: rhododendron and European birch [33], *Acacia* [32], *Malus* [35], and walnut [36].

The purpose of this work was to study the weight of PPM™ on the elimination of endophytic bacteria and the production of blackberry varieties aseptic plants.

Materials and methods

Plant Material. One-year-old shoots of three blackberries varieties were cut for *in vitro* initiation in June 2023 from the field collection of the “Semi-rechye” nursery in Almaty region. Three blackberry varieties were used: Chester, Natchez (USA) and Chacanska Bestrna (Serbia).

***In vitro* Culture Initiation and Micropropagation.** Cuttings approximately 15-20 cm long were washed in soapy water and rinsed in tap water, then apices (1.5-2.5 cm long) were excised from the stem and in a laminar flow hood were surface disinfected with 0.1% mercuric chloride with a few drops of “Tween 20” for 5 or 7 min. Following washing with sterile water, the delicate shoot apices were placed within 25 × 250 mm glass tubes, cradled in Murashige and Skoog medium (MS) [35] enriched with doubled dose of iron chelate, 0.5 mg L⁻¹ 6-benzylaminopurine (BAP), 0.01 mg L⁻¹ indolyl-3-butyric acid (IBA), 30 g L⁻¹ sucrose, 4 g L⁻¹ agar sourced from (PhytoTechnology Laboratories®, Lenexa, KS, USA), 1.25 g L⁻¹ Gelrite™ (PhytoTechnology Laboratories®,

Lenexa, KS, USA). The medium was adjusted to pH 5.7 using 0.1 N NaOH, followed by autoclaving at 121°C for 20 min.

The burgeoning shoot cultures thrived within a growth room-maintained 24°C basking under a 16-hour photoperiod (light intensity of 40 $\mu\text{mol}\cdot\text{m}^{-2}\cdot\text{s}^{-1}$) illuminated by the gentle glow of two types of OP-LE tubular fluorescent lamps: YK21RR 16/G 21 W 6500 K RGB and YK21RL 16/G 21 W 4000 K RGB (Opplé, China).

The number of viable shoots, shoots with bacterial and fungal contamination, and necrosis were evaluated using visual inspection during the first two weeks culturing. Visually clean shoots were indexed for endophytic contamination using 523 detection medium [36]. The bases of the shoots were placed in Petri dishes with 523 medium with 10 $\text{g}\cdot\text{L}^{-1}$ sucrose, 8 $\text{g}\cdot\text{L}^{-1}$ casein hydrolysate (Sigma-Aldrich, St. Louis, MO, USA), 4 $\text{g}\cdot\text{L}^{-1}$ yeast extract, 6 $\text{g}\cdot\text{L}^{-1}$ GelriteTM, 2 $\text{g}\cdot\text{L}^{-1}$ KH_2PO_4 , 0.15 $\text{g}\cdot\text{L}^{-1}$ $\text{MgSO}_4\cdot 7\text{H}_2\text{O}$, pH 6.9.

Contaminated shoots 2-3 cm in size with 3-5 leaves, after testing on the 523 medium with identified endophytic bacterial contamination were divided into 2 parts: 1) cultivated on MS medium mentioned earlier for three passages during 4 weeks each – Control; 2) cultured on MS medium with 0.2% (volume/volume,) for three passages during 4 weeks each (Experiment 1 (E1)). After this all shoots were transferred to MS medium without PPMTM for three subcultures during 4 weeks each (Experiment 2 (E2)). After each cultivation, indexing for endophytes was carried out using 523 medium. After experiment E2, *in vitro* shoots were further propagated under the conditions described above, after 8 cultivations of 4 weeks each (32 weeks), *in vitro* shoots were again tested on 523 medium (Experiment 3 (E3)).

Virus detection. *In vitro* shoots were evaluated for five viruses: *Raspberry bushy dwarf virus* (RBDV), *Strawberry necrotic shock virus* (SNSV), *Apple mosaic virus* (ApMV), *Black raspberry necrosis virus* (BRNV), and *Blackberry yellow vein associated virus* (BYVaV) by multiplex reverse transcription polymerase chain reaction (RT-PCR). Sequences of oligonucleotides used for virus detection are presented in Table 1.

Total RNA was extracted from *in vitro* blackberry leaves using the CTAB method [39, 40, 41]. The quality of the exported RNA was evaluated in Tris-acetate buffer (TAE) by electrophoresis in 2% agarose gel. Reverse transcription was carried out in

a reaction mixture with a volume of 20 μL , which contained 0.5 $\mu\text{g}/\mu\text{L}$ of universal primer and 200 units of reverse transcriptase RevertAid. At the first stage, a mixture containing total RNA (at least 200 ng) and a universal primer was incubated at 72°C for 10 min. Next (second step), to a 15 μL reaction mixture 4 μL of 5x Buffer RT, 200 μM dNTP, and RevertAid reverse transcriptase were supplemented. cDNA synthesis at 45°C for 60 min was carried out. The reaction mixture for PCR contained 2 μL of cDNA, 1x Dream Taq Buffer, 200 μM dNTP, 0.2 μM reverse and forward specific primer for each virus and 1.5 units Dream Taq polymerase (Thermo Fisher Scientific Inc., Vilnius, Lithuania).

Next, MasterMixt was prepared using the following components: 8.80 μL of H_2O , 1.80 μL of 10X reaction mixture, 0.45 μL of 100 mM MgCl_2 , 1.20 μL 5 mM dNTPs, 1.80 μL primer F, 1.80 μL primer R, 0.15 μL Taq polymerase. The reaction program consisted of the following stages: denaturation at 95°C for 5 min; 30 cycles: denaturation for 30 sec at 95°C, aniling for 20 sec at 52°C, elongation for 40 sec at 72°C; last elongation at 72°C for 5 min. Amplification products in a 2% agarose gel in Tris-borate buffer (TBE) were investigated by gel electrophoresis. Confirmation of the RNA purity was obtained by the separation of the 28S and 18S ribosomal RNA on the electropherogram (Thermo Fisher Scientific Inc., Vilnius, Lithuania) [43].

Obtaining of Virus-Free Blackberry Planting Stocks. To obtain planting stocks, rooted *in vitro* plants were transferred to (250 ml) polyethylene containers with soil substrate: black soil (“Ahty” <https://almaty.flagma.kz/342682/>), peat (Kekkila DSM 1 W EXTRA, Finland), and perlite (Union Perlite, Almaty, RK <https://perlite.kz/>) in a percentage correlation of 50:40:10. The containers with the plants were covered with transparent plastic caps and kept to a three-layer polyethylene film greenhouse (240 m^2) with a temperature range from 18°C to 25°C and humidity from 40% to 80%. The temperature regime in the greenhouse was controlled using a floor-standing column-type air conditioner, Almacom ACP-60A (Almacom, China). The influence of temperature and humidity in the greenhouse on the survival and adaptation of the plants was monitored. After one week, the plastic caps were taken out for a period – 10-15 min, and later on, the ventilation duration was increased to 8 h. The adaptation period was for 3-6 weeks. For continued adaptation, the plastic caps were taken out.

Table 1 – Sequences of oligonucleotides used for virus detection.

Virus	Primer name	Sequence (5'→3')	Amplicon size (bp)	Annealing temperature (°C)	Reference
<i>ApMV</i>	<i>ApMV-F</i>	AGGGTCCTGAGCAGTCGAGA	264	64	[16]
	<i>ApMV-R</i>	GTTTGGAGGGGCTTCCCACT			
<i>BRNV</i>	<i>BRNV-F</i>	ATGCTGAGCCACTTGTGA	417	54	[24]
	<i>BRNV-R</i>	ATCTGGTGTGTTCCGCAT			
<i>BYVaV</i>	<i>BYVaV-F</i>	CGTAAGAAGTTCAACATCCA	180	58	[25]
	<i>BYVaV-R</i>	CTTCCAGAATAGAGCACTCG			
<i>RBDV</i>	<i>RBDV-F</i>	TTCATCCTCCAAATCTCAGCAAC	245	73	[26]
	<i>RBDV-R</i>	CGTCGACGGCACC GCCCACCACA			
<i>SNSV</i>	<i>SNSV-F</i>	CAGTGTTCACGGCTGCGAAG	823	69	[42]
	<i>SNSV-R</i>	GGGATCGATTGGTTAGGACCGTCAT			

Statistical Analysis. Fifteen explants of each variety for each treatment in triplicate (n=45) were used to initiate *in vitro* culture. For testing on the 523 medium, *in vitro* shoots were used in triplicate (n = 15). Results were statistically processed as the mean values ± standard error (SE). Means were compared using SYSTAT 13.0, Statistics Software; SYSTAT Software, Inc.: San Jose, CA, USA, 2009 [44]

Results and discussion

In Vitro Culture Initiation. After placing the surface-disinfected apexes into tubes containing culture medium (Figure 1), a visual inspection was conducted after one week to assess the number of viable explants, as well as the occurrence of necrosis and contamination. The results of visual inspection of the *in vitro* apexes of the three varieties Chester, Natchez and Chacanska Bestrna are presented in Figure 2.

Fungal contamination was not detected in any variety and any disinfection duration. Epiphytic bacterial contamination was noted in a small number of explants: with 5 minutes of disinfection – from 2.2 to 6.7%, on average 5.2%; with 7 minutes of disinfection – from 0 to 4.4%, on average 2.2%. The percentage of necrosis significantly increased in the apices of the Chester and Chacanska Bestrna varieties when the treatment duration increased to 7 minutes and averaged 47.4% for the three varieties compared to 24.4% when treated for 5 minutes. The percentage of viable apices without visual signs of contamination

was significantly higher with a 5-minute treatment in the Chester and Chachanska Bestrna varieties and on average for the three varieties was 70.4% compared to 50.4% with a 7-minute treatment.

In general, disinfection with mercuric chloride for 5 minutes was a gentler treatment, but sufficient to eliminate epiphytic contamination and obtain 60.0% viable shoots for ‘Chacanska Bestrna’, 71.1% for ‘Chester’ and 80.0% for ‘Natchez’ (Figure 2).

In contrast, all shoots of Chacanska Bestrna were affected by endophytic contamination, as shown in Figure 4 c highlighting the importance for further study the reasons it's susceptibility to endophytes. The results of testing on medium 523 can serve as the basis for optimizing protocols for different varieties, which in turn will increase the overall productivity and stability of the crop.

Virus detection. *In vitro* shoots of all three blackberry varieties were tested for the presence of five viruses: *Raspberry bushy dwarf virus* (RBDV), *Strawberry necrotic shock virus* (SNSV), *Apple mosaic virus* (ApMV), *Black raspberry necrosis virus* (BRNV), and *Blackberry yellow vein associated virus* (BYVaV). This test is necessary to assess virus infection and ensure the quality of cultures. Identifying viruses in the early stages allows to take measures to eliminate them and minimize risks during further plant propagation. Virus load research researches allow to select the most resistant varieties for successful micropropagation and improved agronomic characteristics. As a result, viruses were absent in all samples as shown on Figure 4.

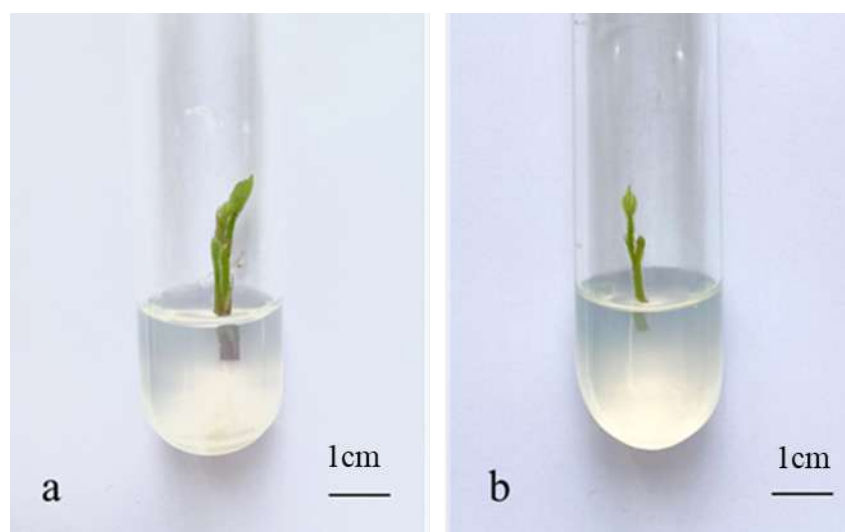


Figure 1 – Shoot apices of blackberry cultivars Natchez (a) and Chacanska Bestrna (b) newly cultured on Murashige and Skoog medium with doubled dose of iron chelate, 0.5 mg·L⁻¹ 6-benzylaminopurine, 0.01 mg·L⁻¹ indolyl-3-butyric acid, 30 g·L⁻¹ sucrose, 4 g·L⁻¹ agar, 1.25 g·L⁻¹ Gelrite™, pH 5.7. Scale bars = 1 cm

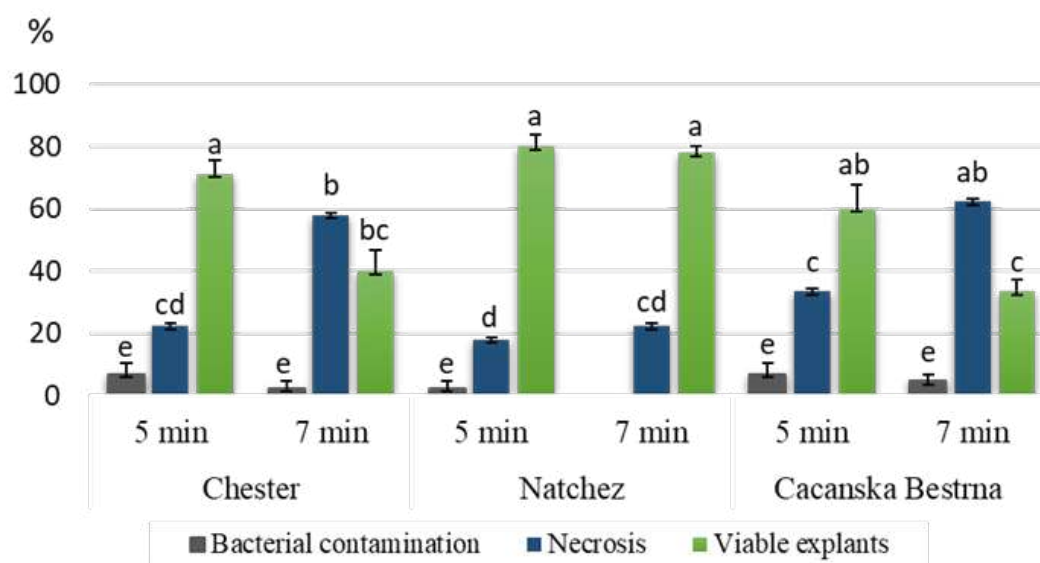


Figure 2 – Effect of duration disinfection with HgCl₂ (5 or 7 min) during *in vitro* initiation three blackberry varieties Chester, Natchez, and Chacanska Bestrna. The results are average values ± standard error (SE). Means denoted by different letters are significantly different at $p \leq 0.05$ using Tukey's mean separation test

Detection of Endophytic Contamination. Contamination of plant tissue culture by pathogens is indeed a serious problem in micropropagation, because even apparently aseptic shoots can contain endophytes contamination [44-45]. Careful inspection of explant purity is important to minimize the risk of endophytic contamination. The use of a specialized

523 medium allows to detect of these contaminants, improves the quality of the culture and increases the success of micropropagation and further cryopreservation of shoot tips [28, 36, 45]. The study revealed that all shoots of the Natchez and Chester varieties were aseptic, which may indicate their high resistance to infections, as shown in Figure 3.

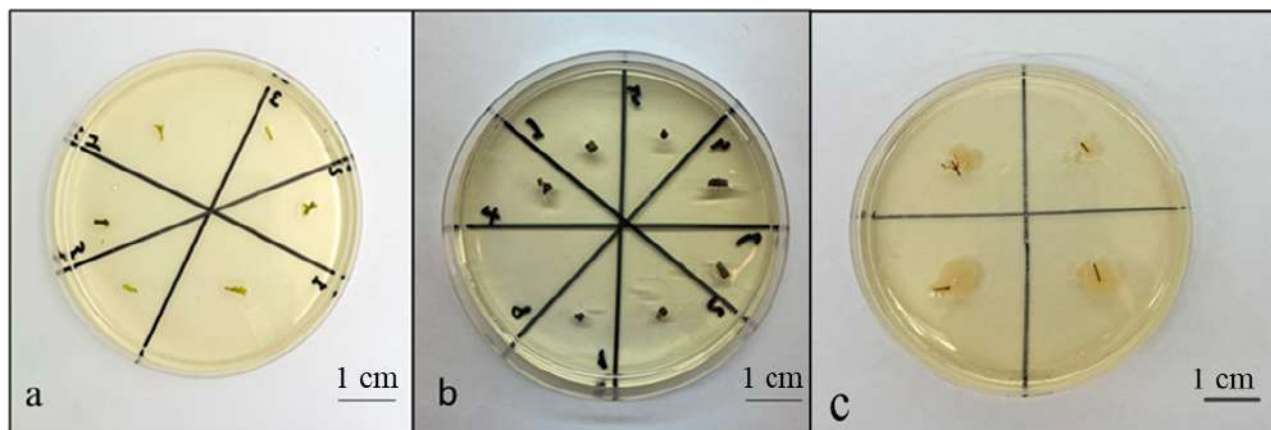


Figure 3 – Testing *in vitro* blackberry shoots for contamination on specialized bacteriological growth medium 523.

Clean cultures of Chester variety (a) and Natchez variety (b). Bacterial growth on and around shoot initials of the Chacanska Bestrna variety shoots on specialized bacteriological growth medium 523 (c). Scale bars = 1 cm

The absence of virus contamination may be attributed to the fact that the source material was obtained from certified planting stocks grown in container culture. Since these planting stocks were not propagated in open ground, they were less exposed to potential virus contamination, ensuring a virus-free plant material. This finding indicates that the *in vitro* cultures of all tested blackberry varieties are free from virus contamination, this is essential for future micropropagation, cryopreservation and planting stocks obtaining.

Obtaining contamination-free in vitro shoots using chemotherapy with PPM™. In light of the pervasive endophytic contamination affecting all specimens of the Chacanska Bestrna variety, subsequent experiments called for the transplantation of *in vitro*

shoots from this accession into a basic MS medium, enhanced with the bactericide PPM™. Following a meticulous examination for the absence of endophytic microflora on the specialized bacteriological medium 523, it was established that the formation of colonies on the MS medium with PPM™ had ceased entirely. The medium itself transformed, devoid of any signs of contamination. Thus, the addition of PPM™ to the culture medium gave good results, demonstrating the cessation of microbial growth as shown on figure 4. As a result, a method was developed for obtaining blackberry *in vitro* shoots that are free from endophytic contamination. The results of the set free of *in vitro* shoots from contaminant infection are given in the Table 2.

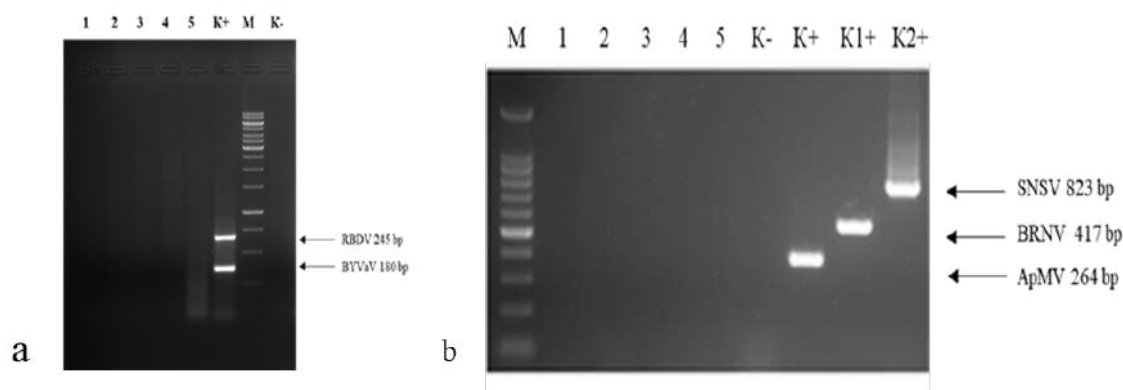


Figure 4 – Representative electrophoretic analysis of RT-PCR products from micropropagated blackberry accessions to test for the presence of five viruses: *Raspberry bushy dwarf virus* (RBDV), *Strawberry necrotic shock virus* (SNSV), *Apple mosaic virus* (ApMV), *Black raspberry necrosis virus* (BRNV), and *Blackberry yellow vein associated virus* (BYVaV). (a) K+ RBDV and BYVaV. (b) K+ SNSV, BRNV and ApMV. M – DNA marker for electrophoresis 100bp Plus (ThermoFisher), K – negative control; 1-2 – Chester, 3-4 – Natchez, 5 – Chacanska Bestrna

Specialized medium 523 contains amino acids from hydrolyzed casein, vitamins from yeast extract and sucrose as an energy source, therefore it is an ideal medium for bacteria and fungi to grow. In current experiments, contamination was observed in 100% of the control shoots (without PPM™ treatment) after 4 weeks of cultivation on specialized medium 523, contamination was already evident at the first week, indicating the effectiveness of this specialized bacteriological medium in detecting contamination. Therefore, our results show that PPM™ controlled *in vitro* shoots contamination on medium with PPM™

(0.2% v/v) for three cycles with 4 weeks duration (E1), the aseptic rates of shoots ranged from 46.7% to 100% (Table 2, E1) (Figure 5).

Results represent mean \pm standard error (SE). Control comprised of shoot basal segment were isolated from four-week-old cultures with contamination and cultured on basal medium without PPM™ for three passages of four weeks each (total of 12 weeks of cultivation). Average values denoted by different letters within each section were significantly different at $p \leq 0.05$ using Tukey's mean separation test.

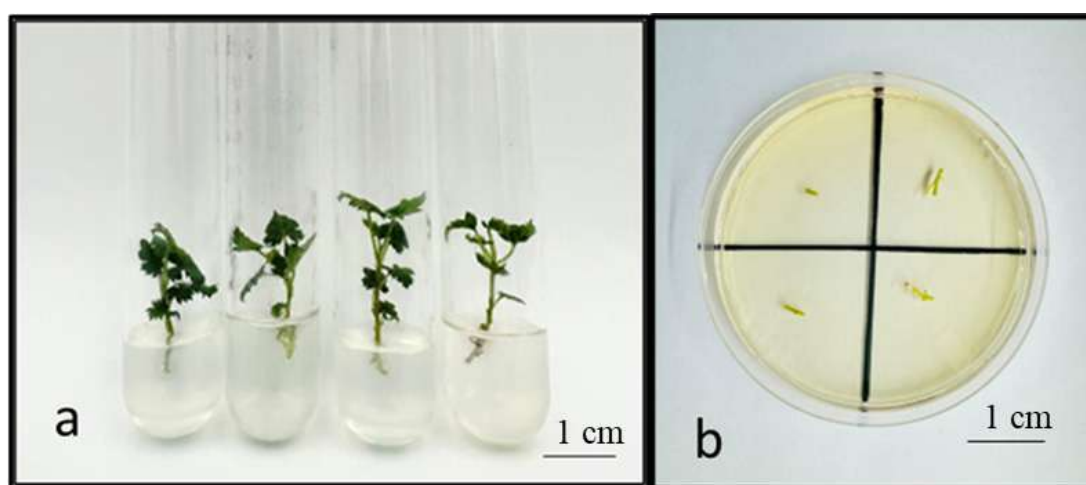


Figure 5 – Chacanska Bestrna variety four weeks after subcultivation on MS with doubled dose of iron chelate, 0.5 mg·L⁻¹ BAP, 0.01 mg·L⁻¹ IBA, 30 g·L⁻¹ sucrose, 4 g·L⁻¹ agar, 1.25 g·L⁻¹ Gelrite™, 0.2% (v/v) PPM™, pH 5.7. (a) Testing Chacanska Bestrna *in vitro* shoots for the contamination on specialized bacteriological growth medium 523. Shoot were grown 12 weeks (three subcultures of 4 weeks each) on MS medium with PPM™ (0.2% v/v) and then were transferred to MS medium without PPM™ and cultured for three additional subcultures (total of 24 weeks of cultivation). No bacterial growth detected (b). Scale bars = 1 cm

Table 2 – Percentage of aseptic blackberry Chacanska Bestrna *in vitro* shoots cultures grown for 12 weeks (three passages by 4 weeks duration each) in a medium with 0.2% v/v Plant Preservative Mixture™ (PPM™) (Experiment 1, E1), later pre-treated shoots from E1 grown in a medium without PPM™ for 12 weeks (three passages by 4 weeks duration each) (Experiment 2, E2) and then the 8 cultivation by 4 weeks duration each (32 weeks) from E2 (Experiment 3 (E3)

Experiment name	Number of subcultures	^z Aseptic shoots (%)
Control	the first subculture	0 ^a
	the second subculture	0 ^a
	the third subculture	0 ^a
Experiment 1 (E1)	the first subculture	46.7 \pm 6.7 ^b
	the second subculture	100 ^d
	the third subculture	100 ^d

Continuation of the table

Experiment name	Number of subcultures	^z Aseptic shoots (%)
Experiment 2 (E2)	the first subculture	86.3±17.4 ^c
	the second subculture	96.6±3.9 ^d
	the third subculture	100 ^d
Experiment 3 (E3)	the eighth subculture	100 ^d

Shoots obtained from E1 were transferred to medium without PPM™ and cultured for more than three subculture cycles by 4 weeks duration each (12 weeks in total) before testing microbial growth (E2). After 12 weeks of cultivation, bacterial contamination was completely removed. Further testing on 523 medium of *in vitro* shoots, cultured on MS medium without PPM™ after 28 weeks (Experiment 3 (E3)) also showed the absence of contaminated plants.

Studies by many authors show positive dynamics of using PPM™ for rejection contamination *in vitro* shoot culture. As the results show, the effect of PPM™ varies for different genotypes from 0 to 100% of aseptic shoots, which may indicate that the efficiency of that procedure for elimination of endophytic contamination condition on the type of tested plants and, mainly, on the type of contamination that has multiplied in the plant tissue [48-53.]. In the study obtaining, 100% of aseptic shoots were obtained *in vitro* for the blackberry variety Chacanska Bestrna without any negative effect on the growth of cultures *in vitro*. Perhaps this is due to the blackberry culture itself, since two of the three studied varieties were not at all susceptible to the action of contamination; perhaps the contamination was superficial and the selected concentration of the bactericide was successful.

Obtaining of Virus-Free Blackberry Planting Stocks. Already now in many countries it has significantly displaced raspberries, as it significantly surpasses them in terms of yield, transportability and medicinal properties. Commercially valuable varieties, such as those mentioned in this study, are unique thornless breeding specimens adapted to cultivation conditions. With proper agricultural techniques, their yield can reach 16-28 tons per hectare. If we consider that the original planting stocks are virus-free and free from endophytic contamination, the yield can be increased to 35 tons per hectare [1].

To obtain the planting stocks, shoots with roots were taken from a virus-free *in vitro* collection, free from endophytic contamination. It should be noted that blackberry root *in vitro* formation occurs independently on MS medium for micropropagation.

Rooted blackberry plants were transplanted into a soil substrate consisting of a mixture of black soil, peat, and perlite. For a week, the plants were adapted to reduced humidity by removing the plastic caps from the cultivation containers.

To ventilate the plants, the plastic cap was removed for 10-15 min, and in the next few days, the ventilation duration was increased to 8 h. The duration of planting stocks adaptation amounts from 3 to 6 weeks. In the greenhouse, where the plants were adapted, temperature and humidity were monitored daily. The survival rate of blackberry plants in the greenhouse at 20-23° reached 99.0%, while a decrease or increase in temperature led to a slight decrease in the survival rate of planting stocks to 94.3% and 93.0% respectively. When comparing statistical differences, no difference was noted between the options. However, when averaging the data, it was found that the optimal temperature for transferring aseptic plants to the soil is 20-23°C. Visually, the plants were also indistinguishable. Planting stocks adapted to greenhouse conditions are shown in Figure 6.

The planting stocks obtained from *in vitro* culture, of a high purity category and adapted to field conditions, will be used for the establishment of an elite nursery, as well as for mass production for subsequent commercialization within the framework of the project. Besides, the *in vitro* accessions will serve for conducting a wide range of biological research, including the long preservation and genetic resources international exchange for the creation of duplicate collections.



Figure 6 – Planting stocks of blackberry cultivar Chacanska Bestrna transplanted into a soil substrate: black soil, peat, and perlite (50:40:10) at 20–23°C and humidity from 40% to 80%. Scale bars = 1 cm

Conclusion

Bacteria, fungi and viruses are the constant threat to growth *in vitro* plants, however methods for controlling and, in some cases, eliminating contamination are already developed. In this research, the using of PPM™ (0.2% v/v) for 12 weeks of cultivation was found to be effective in controlling endophyte growth *in vitro* tissue cultures of the Chacanska Bestrna blackberry variety. Given that only one variety was affected by contamination in this case, there is a need for further testing of PPM™ on other blackberry varieties with bacterial outbreaks to confirm the study's results or for further investigation. From virus-free *in vitro* shoots of three blackberry varieties free from endophytic contamination, planting stocks

adapted to greenhouse conditions (20–23°C) and soil substrate were obtained, that suitable for planting in field conditions.

Acknowledgments

This research was funded by the Ministry of Science and Higher Education of Kazakhstan Republic, Program numbers BR21882024, BR18574099.

We sincerely thank Alina Zemtsova for her invaluable assistance in preparing this paper.

Conflict of interest

All authors are aware of the article's content and declare no conflict of interest.

References

- Food and Agriculture Organization of the United Nations., (from February 27, 2025 accessed on March 31.2025). Crops and Livestock Products. Production in 2022. Available online: <https://www.fao.org/faostat/en/#data/QCL>
- Jennings D.L. (1988) Raspberries and Blackberries, Their Breeding, Diseases and Growth; San Diego: Acad. Press Ltd, London UK, 230 p. ISBN 978-0123842404
- Dai J., Gupte A., Gates L., Mumper R.J., A comprehensive study of anthocyanin containing extracts from selected blackberry cultivars: extraction methods, stability, anticancer properties and mechanisms. *Food Chem. Toxicol.* 2009, vol 47, pp 837–847. <https://doi.org/10.1016/j.fct.2009.01.016>
- Legrand T., (2018) Overviews of food systems and agroindustry, value chains, and food loss and waste in the countries of eastern Europe and central ASIA. Food and Agriculture Organization of the United Nations Budapest, 75 p. ISBN 978-92-5-130620-8
- Mudasir I., Singh K.K. Propagation of Temperate Fruit Crops. *In book 2020, Innovative Agriculture and Botany Publisher* pp.119–135
- Reed B., Poonthong S.H., Hall K.H. Propagation of blackberries and related *Rubus* species. Blackberries and their hybrids *in book* 2017, pp 101–112 <https://doi.org/10.1079/9781780646688.0101>
- Roberto S.R., Colombo R.C. Innovation in Propagation of Fruit, Vegetable and Ornamental Plants. *Horticulturae* 2020, vol 6, p 23–31. <https://doi.org/10.3390/horticulturae6020023>
- Romadanova N.V., Kushnarenko S.V. Conservation of plant biodiversity by biotechnology methods Proceedings in Applied Botany, *Genetics and Breeding.* – 2023, vol 184(1), pp 239–248. <https://doi.org/10.30901/2227-8834-2023-1-239-248>
- Reed B.M., Poonthong S., Hall H.K. Propagation of blackberries and related species. *In Blackberries. CABI: Wallingford, UK,* 2017; pp 101–112. <https://doi.org/10.1016/j.fct.2009.01.016>

10. Tashmatova L.V., Matsneva O.V., Khromova T. M., Shakhov V.V. (2021) Optimization of individual elements of clonal micropropagation of fruit and berry crops in the production system of healthy planting material. International scientific and practical conference fundamental and applied research in biology and agriculture: current issues, achievements and innovation. Farba, P 8.
11. Dobrenkov E.A., Semenova L.G., Dunaeva S.E., Ukhatova Yu.V. Adaptation of test tube blackberry plants to field environmental conditions. *Proc. Appl. Bot. Genet. Breed.* 2017, vol 178, pp 24-30. <https://doi.org/10.30901/2227-8834-2017-1-24-30> (in Russian)
12. Strik B.C., Finn C.E. Blackberry production systems a worldwide perspective. *ActaHortic.* – 2012, vol 946, pp 341-347. <https://doi.org/10.17660/ActaHortic.2012.946.56>
13. Ružić D., Lazić T. Micropropagation as means of rapid multiplication of newly developed blackberry and black currant cultivars. *Agric. Conspec. Sci.* 2006, vol 71, pp 149-153.
14. Romadanova N.V., Mishustina S.A., Gritsenko D.A., Omasheva M.Y., Galiakparov N.N., Reed B.M., Kushnarenko S.V. Cryotherapy as a method for reducing the virus infection of apples (*Malus sp.*) // *Cryo Letters. London*, 2016. vol. 37(1). – P 1-9. <https://www.ncbi.nlm.nih.gov/pubmed/26964019>
15. Kushnarenko S.V., Romadanova N.V., Aralbayeva M.M., Zholanmanova S.Z., Alexandrova A.M., Karpova O. Combined ribavirin treatment and cryotherapy for efficient *Potato virus M* and *Potato virus S* eradication in potato (*Solanum tuberosum* L.) *in vitro* shoots // *In Vitro Cell. Dev. Biol. – Plant.* 2017. vol 53(4). – P. 425-432. <https://doi.org/10.1007/s11627-017-9839-0>
16. Martin R.R., Macfarlane S., Sabanadzovic S., Quito D., Poudel B., Tzanetakis I.E. Viruses and virus diseases of *Rubus*. *Plant Dis.* 2013, vol 97, pp 168-182. <http://dx.doi.org/10.1094/PDIS-04-12-0362>
17. Strik B., Martin R.R. Impact of *Raspberry bushy dwarf virus* on 'Marion' blackberry. *Plant Dis.* 2003, vol 87, pp 294-296. <https://doi.org/10.1094/PDIS.2003.87.3.294>
18. Medina C., Matus J.T., Zuniga M., San-Martin C., Arce-Johnson P. Occurrence and distribution of viruses in commercial plantings of *Rubus*, *Ribes* and *Vaccinium* species in Chile. *Cienc. Investig. Agrar.* 2006, vol 33, pp 23-28. <https://doi.org/10.7764/rcia.v33i1.324>
19. Barbara D.J., Morton. A., Knight. V.H. Occurrence and distribution of *Raspberry bushy dwarf virus* in commercial raspberries plantations in England and Wales. *Acta Hortic.* 2001. vol 551, pp 23-26. <https://doi.org/10.17660/ActaHortic.2001.551.2>
20. Spak J., Kubelkova D. Epidemiology of *Raspberry bushy dwarf virus* in the Czech Republic. *J. Phytopathol.* 2000, vol 148, pp 371-377. <https://doi.org/10.1046/j.1439-0434.2000.00513.x>
21. Valasevich N., Kukharchyk N., Kvarnheden A. Molecular characterization of *Raspberry bushy dwarf virus* isolates from Sweden and Belarus. *Arch. Virol.* 2011, vol 156, pp 369-374. <https://doi.org/10.1007/s00705-010-0912-9>
22. Chamberlain C.J., Kraus J., Kohnen P.D., Finn C.E., Martin R.R. First report of *Raspberry bushy dwarf virus* in *Rubus* multi bracteates from China. *Plant Dis.* 2003, vol 87, pp 603. <https://doi.org/10.1094/PDIS.2003.87.5.603A>
23. Wood G.A., Hall H.K. Source of *Raspberry bushy dwarf virus* in *Rubus* in New Zealand, and the indefectibility of some newer cultivars to this virus. *New Zeal. J. Crop Hort. Sci.* 2001, vol 29, pp 177-186. <https://doi.org/10.1080/01140671.2001.9514176>
24. Kolchenko M., Kapytina A., Kerimbek N., Pozharskiy A., Nizamdinova G., Khusnidinova M., Taskuzhina A., Gritsenko D. Genetic characterization of *Raspberry bushy dwarf virus* isolated from red raspberry in Kazakhstan. *Viruses* 2023, vol 15, pp 975. <https://doi.org/10.3390/v15040975>
25. Martin R.R., Tzanetakis I.E., Gergerich R., Fernández, G., Pesic, Z. *Blackberry yellow vein associated virus*: a new crinivirus found in blackberry. *Acta Hortic.* 2001, vol 656, pp 137-142. <https://doi.org/10.17660/ActaHortic.2004.656.21>
26. Halgren A., Tzanetakis I.E., Martin R.R. 2007. Identification, characterization, and detection of *Black raspberry necrosis virus*. *Phytopathology*. 2007, vol 97, pp 44–50. <https://doi.org/10.1094/PHYTO-97-0044>
27. Reed B.M., Tanprasert P. Detection and control of bacterial contaminants of plant tissue cultures. A review of recent literature. *Plant Tissue Cult. Biotechnol.* 1995, vol 1, pp 137–142.
28. Orlikowska T., Nowak K., Reed B. Bacteria in the plant tissue culture environment. *Plant Cell Tiss. Org. Cult.* 2017, vol 128, pp 487–508. <https://doi.org/10.1007/s11240-016-1144-9>
29. Romadanova N.V., Aralbayeva M.M., Zemtsova A.S., Alexandrova A.M., Kazybayeva S. Zh., Mikhailenko N.V., Kushnarenko S.V., Bettoni J.C. *In Vitro* collection for the safe storage of grapevine hybrids and identification of the presence of *Plasmopora viticola* Resistance Genes // *Plants*. 2024, 13, 1089. <https://doi.org/10.3390/plants13081089>
30. Kaluzna M., Mikiciński A., Sobiczewski P., Zawadzka M., Zenkteler E., Orlikowska T. Detection, isolation, and preliminary characterization of bacteria contaminating plant tissue cultures. *Acta Agrobot.* 2013, vol 66, pp 81-92. <https://doi.org/10.5586/aa.2013.054>
31. Tanprasert P., Reed B.M. Determination of minimal bactericidal and effective antibiotic treatment concentrations for bacterial contaminants from micropropagated strawberries. *In Vitro Cell. Dev. Biol. – Plant.* 1997, vol 33, pp 227-230. <http://dx.doi.org/10.1007/s11627-997-0027-5>
32. Reed B.M., Mentzer J., Tanprasert P., Yu X. Internal bacterial contamination of micropropagated hazelnut: identification and antibiotic treatment. *Plant Cell. Tiss. Org. Cult.* 1998, vol 52, pp 67-70. <https://doi.org/10.1023/A:1005989000408>
33. George M.W., Tripepi R.R. Plant Preservative Mixture™ can affect shoot regeneration from leaf explants of *chrysanthemum*, European birch, and rhododendron. *HortScience* 2001, vol 36, pp 768-769. <https://doi.org/10.21273/HORTSCI.36.4.768>
34. Ho W.J., Huang Y.K., Huang W.W., Huang Y.C., Chung J.P. Effective *in vitro* culture using dormant buds of nodal sections from a mature *Acacia* tree. *In Vitro Cell. Dev. Biol. – Plant.* 2021, vol 58, pp 437-446. <https://doi.org/10.1007/s11627-021-10235-8>
35. Romadanova N.V., Tolegen A.B., Koken T.E., Nurmanov M.M., Kushnarenko S.V. Chemotherapy of *in vitro* apple shoots as a method of virus's eradication // *International Journal of Biology and Chemistry* 2021, vol 14, p 5. <https://doi.org/10.26577/ijbch.2021.v14.i1.04>

36. Kushnarenko S., Aralbayeva M., Rymkhanova N., Reed B.M. Initiation pretreatment with Plant Preservative Mixture™ increases the percentage of aseptic walnut shoots. *In Vitro Cell. Dev. Biol. – Plant.* 2022, vol 58, pp 964-971. <https://doi.org/10.1007/s11627-022-10279-4>
37. Murashige T., Skoog F., A revised medium for rapid growth and bioassays with tobacco tissue cultures. *Physiol. Plant* 1962, vol 15, pp 473-497. <https://doi.org/10.1111/j.1399-3054.1962.tb08052.x>
38. Viss P.R., Brooks E.M., Driver J.A. A simplified method for the control of bacterial contamination in woody plant tissue culture. *In Vitro Cell. Dev. Biol.* 1991, vol 27, pp 42. <https://doi.org/10.1007/BF02632060>
39. Choudhary S.B., Kumar M., Chowdhury I., Singh R.K., Pandey S.P., Sharma H.K., Karmakar P.G. An efficient and cost effective method of RNA extraction from mucilage, phenol and secondary metabolite rich bark tissue of tossa jute (*C. olitorius L.*) actively developing phloem fiber. *Biotech.* 2016 vol 3, 6(1), p 100. <https://doi.org/10.1007/s13205-016-0415-9>
40. Constable F.E., Bottcher C., Kelly G., Nancarrow N., Milinkovic M., Persely D.M., Rodoni B.C. (2010) The seasonal detection of strawberry viruses in Victoria, Australia. 21st International Conference on Virus and other Graft Transmissible Diseases of Fruit Crops, Julius Kuhn Archiv. pp 27-34.
41. Gambino G. Perrone I., Gribaudo I. A rapid and effective method for RNA extraction from different tissues of grapevine and other woody plants. *Phytochem. Anal.* 2008, vol 19, pp 520-525. <https://doi.org/10.1002/pca.1078>
42. Jennings D.L. Raspberries and Blackberries: Their Breeding, Diseases and Growth. San Diego: Acad. Press Ltd, London UK, 1988. – pp 230.
43. Kokko H.I., Kivineva M., Kärenlampi S.O. Single-step immunocapture-PCR in the detection of Raspberry bushy dwarf virus. *Biotechniques.* 1996, vol 20, pp 842-846. <https://www.tandfonline.com/doi/abs/10.2144/96205st03>
44. SYSTAT. SYSTAT 13.0, Statistics Software; SYSTAT Software, Inc.: San Jose, CA, USA, 2009; Available online: <https://systatsoftware.com/> (accessed on 17 September 2024).
45. Romadanova N.V., Mishustina S.A., Matakova G.N., Kuhsnarenko S.V., Rakhimbaev I.R., Reed B.M. *In vitro* collection of Malus shoots cultures for cryogenic bank development in Kazakhstan // *Acta Horticulturae*, March 2016, vol 1113, pp 271-277. <http://dx.doi.org/10.17660/ActaHortic.2016.1113.40>
46. Lumsden P.J., Nicholas J.R., Davies W.J. Latent bacterial infections: epiphytes and endophytes as contaminants of micro-propagated plants; *Springer Nature: Cham, Switzerland*, 1994, pp 379-396. https://doi.org/10.1007/978-94-011-0790-7_43
47. Volk G.M., Bonnart R., Araújo de Oliveira A.C., Henk A.D. Minimizing the deleterious effects of endophytes in plant shoot tip cryopreservation. *Appl. Plant Sci.* 2022, vol 10, e11489. <https://doi.org/10.1002/aps3.11489>
48. Grimaldi F., Bastos F.E.A. Control of *in vitro* contamination during the establishment of *Pyrus communis* explants using Plant Preservative Mixture™ *Plant Cell Culture & Micropropagation* 2023, vol 19 pp 185-191. <https://doi.org/10.46526/pccm.2023.v19.185>
49. Kushnarenko S., Aralbayeva M., Rymkhanova N., Reed B.M. Initiation pretreatment with Plant Preservative Mixture™ increases the percentage of aseptic walnut shoots. *In Vitro Cell. Dev. Biol. – Plant.* 2022, vol 58, pp 964-971. <https://doi.org/10.1007/s11627-022-10279-4>
50. Orlikowska T., Zawadzka M., Zenkteler E., Sobiczewski P. Influence of the biocides PPM™ and *in vitro* fural on bacteria isolated from contaminated plant tissue cultures and on plant microshoots grown on various media. *J. Hortic. Sci. Biotechnol.* 2015, vol 87, pp 223-230. <https://doi.org/10.1080/14620316.2012.11512856>
51. Paul A.L., Semer C., Kucharek T., Ferl R.J. The fungicidal and phytotoxic properties of benomyl and PPM in supplemented agar media supporting transgenic arabidopsis plants for a space shuttle flight experiment. *Appl. Microbiol. Biotechnol.* 2001, vol 55, pp 480-485. <https://doi.org/10.1007/s002530000521>
52. Romadanova N.V., Tolegen A.B., Kushnarenko S.V., Zholdybayeva E.V., Bettoni J.C. Effect of Plant Preservative Mixture™ on endophytic bacteria eradication from *in vitro* grown apple shoots. *Plants* 2022, 11, 2624. <https://doi.org/10.3390/plants11192624>
53. Thomas P., Agrawal M., Bharathkumar C.B. Use of Plant Preservative Mixture™ for establishing *in vitro* cultures from field plants: Experience with papaya reveals several PPM™ tolerant endophytic bacteria. *Plant Cell Reports* 2017, vol 36 pp 1717-1730. <https://doi.org/10.1007/s00299-017-2185-1>

Information about authors

Arman Tolegen – PhD-student, M.Sc., Institute of Plant Biology and Biotechnology (Almaty, Kazakhstan, e-mail: tolegenarman7@gmail.com)

Natalya Romadanova – Candidate of Biological Sciences, Associate Professor, Institute of Plant Biology and Biotechnology (Almaty, Kazakhstan, e-mail: nataromadanova@gmail.com)

Moldir Aralbayeva – M.Sc., Institute of Plant Biology and Biotechnology (Almaty, Kazakhstan, e-mail: berim.moldir@mail.ru)









Nazgul Rymkhanova – PhD-student, M.Sc., Institute of Plant Biology and Biotechnology (Almaty, Kazakhstan, e-mail: nazka_0993@mail.ru)

Yulia Ukhatoeva – Candidate of Biological Sciences, Federal Research Center N.I. Vavilov All-Russian Institute of Plant Genetic Resources (Saint Petersburg, Russia, e-mail: y.ukhatova@vir.nw.ru)

Magamedgusein Agahanov – Candidate of Biological Sciences, Federal Research Center N.I. Vavilov All-Russian Institute of Plant Genetic Resources (Saint Petersburg, Russia, e-mail: m.agahanov@vir.nw.ru)

Natalya Mikhailenko – B.Sc., Master-student, Institute of Plant Biology and Biotechnology (Almaty, Kazakhstan, e-mail: georgi-nata@mail.ru)

Svetlana Kushnarenko – Candidate of Biological Sciences, Professor, Institute of Plant Biology and Biotechnology (Almaty, Kazakhstan, e-mail: sv.kushnarenko.bio@gmail.com)

S.M.R. Nazifi , N. Esfandiarpour , A. Motamedi ,
E. Jahanmard , N. Rahimi , F. Ansari ,
F. Masoudi , S. Sepahi* 

Laboratories of Food and Drug Control, Vice Chancellery for Food and Drug,
Isfahan University of Medical Sciences, Isfahan, Iran

*e-mail: Sepahi66@gmail.com

(Received 17 February 2025; received in revised form 8 May 2025; accepted 19 May 2025)

Evaluation of Different Sweetener Concentrations in Beverage Samples in Isfahan Market Using High Performance Liquid Chromatography

Abstract: Sweeteners were added in beverage formulations to provide sweetness with pleasant taste. In this paper, potent approach for quantification of acesulfame ok (ACE-ok), sodium saccharin (Na-SAC) and aspartame (ASP) contents in beverages had been applied with liquid chromatography (RP – HPLC) joint with diode array detection (DAD). Ninety-seven samples have been selected from Isfahan marketplace. Liquid chromatograph Agilent 1260 Infinity series was applied for analysis. Mobile phase was decided on as acetonitrile and phosphate buffer (pH= 3.5) with 15:85 extent ratio (V/V), and the float rate of the chromatographic device was Optimized at 1 ml min⁻¹ using an isocratic elution system. All the beverages were saccharin-free and the mean concentrations of acesulfame and aspartame were lower than the general standards of the Iran National Standards Organization (600 mg L⁻¹). All the products were showed the acceptable levels of sweeteners, but, periodical and exact evaluation of these sweeteners in the beverages are still suggested to provide consumer health.

Key words: Saccharine, aspartame, acesulfame, beverages, HPLC.

Introduction

As the world's population increases, the request for beverages is increasing, so the investigation of the type and amount of these additives has become a global health challenge. Beverage companies use different additives such as preservatives and sweeteners to food products to maintain quality, taste, pH, increase shelf life, appearance, and consistency to make the product economical [1].

Artificial sweeteners are often included in drinks to improve taste and look [2]. These food additives are permitted for use according to the law, and in most countries, there are regulations that establish the highest allowable levels of these additives[3] or prohibit those that may lead to issues like asthma [4], allergies [5], cancer risk [6], hyperactivity [7] and Parkinson's disease [8]. It's crucial for people to understand the dangers linked to consuming these fake components and to carefully decide on their drink intake.

Among the artificial samples, acesulfame potassium, aspartame, saccharin and sucralose have the

benefits such as cheaper rather than sweeteners and are more stable during food processing. Also, these sweeteners are not metabolized in the body and useful in patients with diabetes and overweight/obesity. However, in many countries, detecting the amount of sweeteners to avoid excessive addition or overuse has become important [9]. However, in most countries, detecting the content of artificial sweeteners to avoid extreme count or overuse has end up vital.

Evaluation and quantification of synthetic sweeteners is an important feature of quality control administration of meals stuff. To date, various analytical strategies had been detecting of sweeteners in beverage. Chromatographic technique such as high-performance liquid chromatography, (HPLC) [10, 11], gas chromatography (GC) [12], ion chromatography [13, 14] and spectroscopic techniques such as Infrared Spectroscopy (FTIR) [13-15] and UV/Vis Spectroscopy are in general used in quantification of sweeteners [16, 17].

Recently Cheng and co-workers developed a novel method by using column-switching UHPLC

single bond CAD for detecting 12 artificial and natural sweeteners [18]. In another work, Jankulovska developed a potent method for the determination of acesulfame (ACE-K), sodium saccharin (Na-SAC) and aspartame (ASP) in various drinks using reverse phase chromatographic system coupled with photodiode array detection technique [19].

Acesulfame (ACE-K), sodium saccharin (Na-SAC) and aspartame (ASP) are routine utilized in drinks as synthetic sweeteners. According to the Iran National Standards Organization, the acceptable range in carbonated soft drink is 600 mg kg⁻¹ for ASP and ACE-K and all beverages should be saccharin-free [20]. Also, the suitable range in beverages are 80 mg L⁻¹ for SAC, 350 mg L⁻¹ for ACE-K and 600 mg L⁻¹ for ASP based on European rules for food matrices additive [3].

In our study, HPLC-DAD method was utilized for the quantitation of ACE-K, SAC and ASP in different beverages available on the Isfahan markets. These sweeteners were chosen because they are mainly used in beverages, and HPLC method was used as an efficient technique because it is a fast, easy and obtainable method for many food quality centers.

Materials and methods

Instrumentation

HPLC analysis was performed with an Agilent 1260 Infinity II series contain a diode array detector (DAD) and quaternary pump, an autosampler part contain degasser, a thermostat and Adamas C18-Extreme (250*4.6 mm, 5 µm) column. The data was analyzed using Chem Station software. The pH of aqueous solutions was measured using a pH meter Metrohm (827, Switzerland). The solutions were sonicated with ultrasonic bath Elma. Both phosphate buffer and acetonitrile have been filtered through a 0.45 µm pore size filter (Whatman and MICROLAB).

Analytical standards and reagents

All the chemical substances have been used high purity grade or HPLC grade. Phosphoric acid (85.5%), methanol (>99.8%), acetonitrile (≥99.9 %), KH₂PO₄ (99%), and ultra-pure water have been purchased from Merck Chemical company, Germany. Analytical standards of Na-SAC (99.6%), ACE-K (99.4%), and ASP (99%) were obtained from Sigma-Aldrich chemical company.

Apparatus and chromatographic conditions

Analyst have been separated and quantified using a RP-HPLC system (Agilent Affinity 1260 II series) coupled with a degassing unit, pumps, autosampler,

column oven, UV-Vis diode array detector (UV-DAD) with a reverse phase C18 column (Adamas C18-Extreme, 250*4.6 mm, 5 µm) at constant column temperature (25 °C). The drinks have been tested with DAD detector at 220 nm under isocratic system by utilizing acetonitrile/buffer phosphate (15:85) as mobile phase under optimal flow rate (1 ml/min).

Preparation of standard solutions

A stock standard solution was prepared by dissolving 100 mg of each sweetener in a 100 ml volumetric flask with deionized water and brought up to volume. This solution contains 1000 ml/L of each sweetener and stored in brown glass for vessels. The working standard solutions were gained by diluting the sweeteners stock solutions in water to obtain aliquots of the following concentrations: 10, 20, 40, 60 and 80 mg L⁻¹ for Na-SAC and ASP and 4, 8, 16, 24 and 32 mg L⁻¹ for K-ACE. Working standard solutions were prepared daily.

Collection and preparation of samples

Commercially obtainable beverages (n = 97) were collected from the Isfahan market in Iran using a stratified random sampling method. All samples were collected in two different class, non-carbonated and carbonated drinks. In this work, samples were prepared easily. Carbonated drinks were placed in an ultrasound bath about 15 min at room temperature to eliminate the gasses. Then 10 ml of each sample transported into a 100 ml volumetric flask and up to a total volume with water. The non-carbonated semi solid samples were placed into a blender for 5 min until homogenized. The homogenized samples were vacuum filtered. After that, 10 ml of filtered was transported into a 100 ml volumetric flask and up to a total volume with water. The diluted solutions were then filtered with 0.45 µm syringe filter and were poured into a 2 mL sample vial for HPLC analysis. The filtered samples were injected replicate into the HPLC apparatus and the average values were calculated.

Preparation of buffer phosphate

0.1 g of potassium dihydrogen phosphate (KH₂PO₄) was poured into a 100 ml volumetric flask and up to a total volume with water. The buffer pH was set to 3.5 with diluted phosphoric acid (H₃PO₄). Filter under reduced pressure to remove insoluble substance before use with 0.45 µm membrane filter.

Statistical analysis

Statistical evaluation became finished by way of in Excel software program model 2019 in line with the descriptive exams. The attention of sweeteners becomes carried out in triplicate and final concentration were said as mean.

Results and discussion

Chromatographic settings were settled according to the European Standard EN-12856 [21]. In this manner, reverse phase C18 column was selected for the separation of ACE-K, Na-SAC and ASP because it could be used in different pH (2-9) of beverages [22]. UV-DAD detector was used for detection of artificial sweeteners because it shows suitable sensitivity in ppm levels for the quantities of artificial sweeteners. UV-DAD absorption was monitored at around 220. According to the literatures, the optimum separation for artificial sweeteners is in organic solvents by applying a phos-

phate buffer (pH 5-3.5) as a mobile phase [23]. Acetonitrile was selected as an organic solvent for quantification of sweeteners because of low back-pressure and shorter cutoff wavelength (190 nm) [24]. Mobile phase has been consisting of acetonitrile and phosphate buffer (V/V; 15:85, pH=3.5) at optimal flow rate of 1 ml min⁻¹ under isocratic program. A typical chromatogram of a standard mixture of ACE-K (80 mg L⁻¹), Na-SAC (80 mg L⁻¹) and ASP (32 mg L⁻¹), at 220 nm was showed in Figure 1. As illustrated in Figure 1, the samples had been detected in the following retention times: 13.93, 4.45 and 13.5 minutes for ACE-K, Na-SAC and ASP respectively.

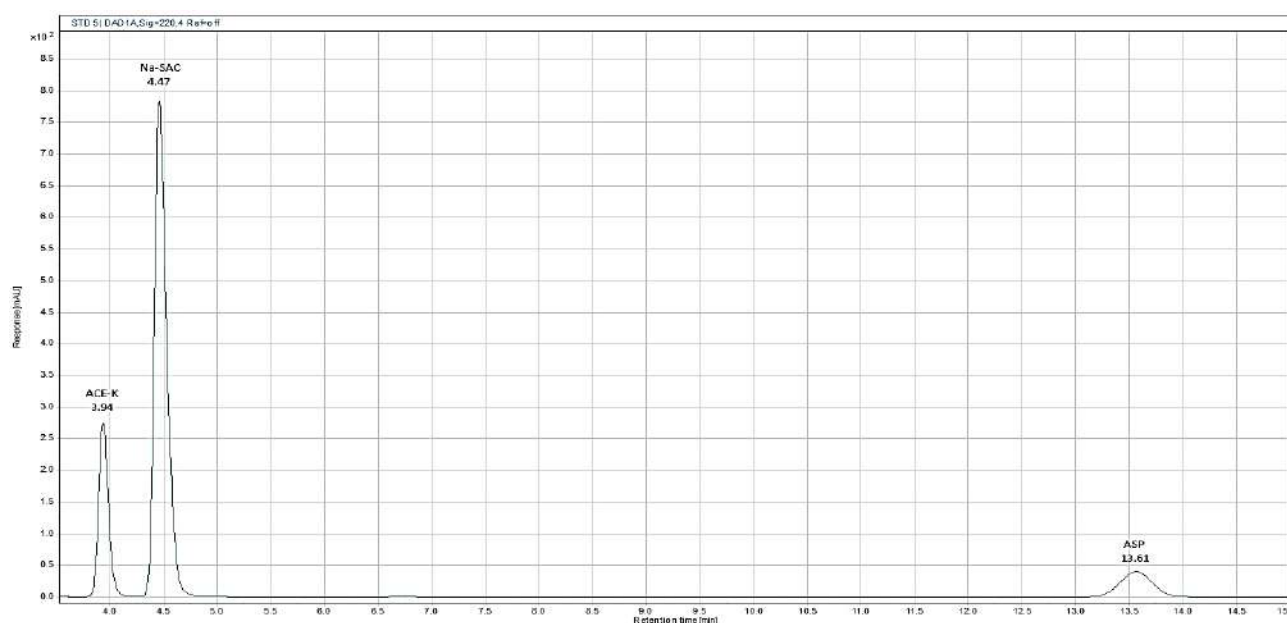


Figure 1 – Chromatograms of HPLC-DAD of a standard mixture of the examined sweeteners

For the linearity study, five concentration levels of synthetic sweeteners (10, 20, 40, 60 and 80 mg L⁻¹ for Na-SAC and ASP and 4, 8, 16, 24 and 32 mg L⁻¹ for ACE-K) were selected and calibration curves were constructed (Figure 2). The calibration curve was made of three replications and fitted to a straight line using log₁₀ scale values for both the x- and y-axes. Calibration equations and correlation coefficients (R²) data of the standard solutions of sweeteners are illustrated in Table 1. According to the coefficient's values, the method exhibited good linearity of the analytical response in the examined concentration level. As can be seen in Table 1, the correlation coef-

ficients for the standard curves of all sweeteners were more than 0.99, indicating that the method has suitable linearity.

The LOD is the lowest concentration of the sample that is detectable by of the analyte with certain level of certainty. The LOQ is the lowest concentration of the analyte that could be measured with appropriate precision and accuracy. The LOD and LOQ values are shown in Table 1. As shown in Table 1, the LOD values of sweeteners were 0.3, 0.2 and 4.2 ppm and the LOQ values were obtained 8, 8 and 13.8 ppm for ACE-K, Na-SAC and ASP respectively.

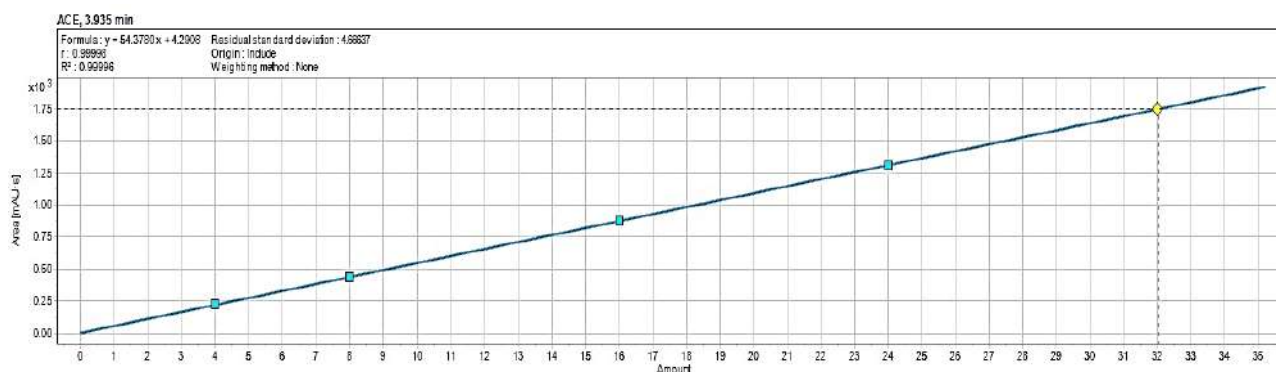


Figure 2 – The obtained calibration curve of ACE-K produce by HPLC–DAD method

Table 1 – Linearity and sensitivity obtained from the standard solutions of sweeteners (n=3)

Analyst	Calibration equations	R ²	LOD (mg L ⁻¹)	LOQ (mg L ⁻¹)
ACE-K	Y=54.241x+7.457	1	0.3	0.8
Na-SAC	Y=78.732x+14.405	1	0.2	0.8
Asp	Y=11.101x+15.657	0.9983	4.2	13.8

Repeatability is the precision under the same operational conditions over a short period of time [25]. In this study, the standard deviations (SD) of the pooled sample concentration were used to express the precision. The standard deviations were calculated for 12 and 8 samples of ACE-K and ASP respectively. The calculated standard deviations have been acquired 0.07 and 0.53 % for ACE-K and ASP respectively, since the results illustrated a proper intra-day precision.

Detected sweeteners (ACE-K, Na-SAC and ASP) by the optimized method were demonstrated in Table 2. According to the Table 2, between all the tested drinks, 12 samples contained acesulfame from 0.12 to 9.83 mg L⁻¹ and showed in allowed concentrations according to the guideline. Also, none of the samples

contained saccharin and aspartame were found in 8 samples ranging from 18.19 mg L⁻¹ to 40.42 mg L⁻¹ that were lower than the standard range. Based on our results, 12.37%, 8.24%, 0% of all samples contained acesulfame, aspartame and saccharine respectively and were in acceptable ranges. The used method showed good linearity in the examined concentration levels and the correlation coefficients were more than 0.99 for all sweeteners and demonstrated that the method is linear. The method sensitivity of the method was acceptable because of the LOQs were less than the lowermost standard concentration except for ASP. Nevertheless, the LOQs for ASP was obtained near to the lowest minimum standard concentration. The data showed that the method is adequate for the detection and quantification of analyzed sweeteners.

Table 2 – The finding Concentrations (mg L⁻¹) of sweeteners (ACE-K, Na-SAC and ASP) in the collected beverages

Samples	Sample details	ACE-K, mg L ⁻¹ *	Na-SAC, mg L ⁻¹	ASP, mg L ⁻¹
S1	Carbonated with orange flavour	4.95	N.D ¹	40.42
S2	Black carbonated drink	9.83	N.D	18.19
S3	carbonated with mango flavour	5.07	N.D	26.60
S4	Carbonated with mojito flavour	3.76	N.D	27.57
S5	Carbonated with tropical flavour	4.52	N.D	23.45
S6	Landa, carbonated with peach flavour	3.69	N.D	26.50

Continuation of the table

Samples	Sample details	ACE-K, mg L ⁻¹ *	Na-SAC, mg L ⁻¹	ASP, mg L ⁻¹
S7	Sugar-free carbonated drink	7.73	N.D	39.05
S8	Non-carbonated with strawberry flavour	1.77	N.D	N.D
S9	Non-carbonated with mojito flavour	0.13	N.D	19.43
S10	Non-carbonated with malt flavour	0.27	N.D	N.D
S11	Non-carbonated with cherry flavour	0.12	N.D	N.D
S12	Non-carbonated with lemon flavour	6.61	N.D	N.D
Note: * indicates No detection				

Conclusion

In spite of the risk associated with the excessive use of sweeteners, the safe use of these additives in beverages can improve pleasant taste. For this reason, checking the usage of sweeteners in the meals enterprise and monitoring their quantity in excessive intake foods consisting of beverages is crucial for consumer fitness and economics. In this study, the amount of the three most common sweeteners namely saccharine, potassium acesulfame and aspartame were determined in different beverage samples in Isfahan, Iran. RP-HPLC method was used for determination of sweeteners. Chromatographic settings were applied according to the European Standard EN-12856. For this purpose, reverse phase C18 column and UV-DAD detector were used for detection of artificial sweeteners. According to the previous published, the best separation for artificial sweeteners is in organic solvents by applying a phosphate buffer (pH 5-3.5) as a mobile phase. Acetonitrile is a good selection as an organic solvent for quantification of sweeteners because of low backpressure and shorter cutoff wavelength (190 nm). In the optimal conditions, the mobile phase

has been consisting of acetonitrile and phosphate buffer (V/V; 15:85, pH=3.5) at 1 ml min⁻¹ flow rate under isocratic system. resulting retention times for samples were 13.93 min for ACE-K, 4.45 min for Na-SAC and 13.5 min for ASP under adjusted conditions. According to the results, all the beverages were saccharin-free and the mean concentrations of acesulfame and aspartame were lower than the general standards of the Iran National Standards Organization (600 mg L⁻¹). All the products were showed the acceptable levels of sweeteners, but, periodical and exact evaluation of these sweeteners in the beverages are still suggested to provide consumer health.

Acknowledgments

The authors are thankful to Isfahan University of Medical Science for financial support of this work under grant agreement number 140310.

Conflict of interest

The authors declare that they have no conflicts of interest.

References

1. Silva M., Pereira K., Coelho M. (2019) Food additives used in non-alcoholic water-based beverages — A review. *J. Nutr. Health Food Eng.*, 9, pp. 109-121. <https://doi.org/10.15406/jnhfe.2019.09.00335>.
2. Wilk K., Korytec W., Pelczynska M., et al. (2022) The effect of artificial sweeteners use on sweet taste perception and weight loss efficacy: a review. *Nutrients*, 14, pp. 1261. <https://doi.org/10.3390/nu14061261>.
3. Mortensen A. (2006) Sweeteners permitted in the European Union: safety aspects. *Scandinavian Journal of Nutrition*, 50, pp. 104-116. <https://doi.org/10.1080/17482970600982719>.
4. Maslova E., Strom M., Olsen S.F., et al. (2013) Consumption of Artificially-Sweetened Soft Drinks in Pregnancy and Risk of Child Asthma and allergic rhinitis. *Plos. One*, 8, pp. 87261. <https://doi.org/10.1371/journal.pone.0057261>.
5. Cheng X., Wu T., Han L., et al. (2024) Association between added sugars intake and Parkinson's disease status in US adults: a cross-sectional study from NHANES 1990–2020. *Arch. Pub. Health*, 82, pp. 225. <https://doi.org/10.1186/s13690-024-01445-8>.
6. Pan H., Feng C., Zho Z., Huang J., et al. (2024) The causal association between artificial sweeteners and the risk of cancer: a Mendelian randomization study. *Food Funct.*, 15, pp. 4527-4537. <https://doi.org/10.1039/d3fo05756a>.

7. Gültekin F., Koc S., et al. (2023) Is There any Connection Between ADHD and the Additives in Sweetened Beverages? *Med. J. Nutrition Metab.*, 16, pp. 223-232. <https://doi.org/10.3233/MNM-230034>.
8. Sadighara, P., Safta M., Limam I., et al. (2023) Association between food additives and prevalence of allergic reactions in children: a systematic review. *Rev. Environ. Health*, 38, pp. 181-186. <https://doi.org/10.1515/reveh-2021-0158>.
9. Angelin, M., Kumar J., Vajravelu L. K., et al. (2024) Artificial sweeteners and their implications in diabetes: a review. *Front. Nutr.*, 11, pp. 1411560. <https://doi.org/10.3389/fnut.2024.1411560>.
10. De Sousa, R.C.S., Gomides D. F. M., Costa K., et al. (2024) Optimization and Validation of an Analytical Method for the Determination of Sweeteners in Beverages by HPLC-ELSD. *Food Anal. Method*, 17, pp. 207-225. <https://doi.org/10.1007/s12161-023-02562-w>.
11. Islam K., Meghla Y.T., Akhtaruzzaman M., Shamsur A.S., et. al. (2024) Quantitative determination of artificial sweeteners and sucrose in energy drinks and mango juice available in Dhaka city by UV-Spectrophotometric method. *Ital. J. Food Saf.*, 13, pp. 10914-21. <https://doi.org/10.4081/ijfs.2024.10914>.
12. Hashemi M., Habibi A., Jahanshahi N. (2011) Determination of cyclamate in artificial sweeteners and beverages using head-space single-drop microextraction and gas chromatography flame-ionisation detection. *Food chem.*, 124, pp. 1258-1263. <https://doi.org/10.1016/j.foodchem.2010.07.057>.
13. Jian-Ye G., Sun W., Zhang C.L., et al. (2016) An innovative approach to sensitive artificial sweeteners analysis by ion chromatography-triple quadrupole mass spectrometry. *Chin. J. Anal. Chem.*, 44, pp. 361-366. [https://doi.org/10.1016/S1872-2040\(16\)60914-3](https://doi.org/10.1016/S1872-2040(16)60914-3).
14. Zhu Y., et al. (2005) Separation and simultaneous determination of four artificial sweeteners in food and beverages by ion chromatography. *J. Chromatogr. A.*, 1085, pp. 143-146. <http://doi.org/10.1016/j.chroma.2004.12.042>.
15. Teklemariam T.A., Chou F., et al. (2024) ATR-FTIR spectroscopy and machine/deep learning models for detecting adulteration in coconut water with sugars, sugar alcohols, and artificial sweeteners. *Spectrochimica. Acta A. Mol. Biomol. Spectrosc.*, 322, pp. 124771. <http://doi.org/10.1016/j.saa.2024.124771>.
16. He Y.C., Fang S., Xu X. J. (2012) Simultaneous determination of acesulfame-K, aspartame and stevioside in sweetener blends by ultraviolet spectroscopy with variable selection by sipls algorithm. *Maced. J. Chem. Chem. Eng.*, 31, pp. 17-28. <http://doi.org/10.20450/mjce.2012.53>.
17. Bhavya Sri K., Saileela S., et.al. (2024) A novel method and validation for the quantification of sdacharin and aspartam in the local marketed products. *Int. J. Pharm. Res.*, 15, pp. 1745-1754. [http://doi.org/1754.10.13040/IJPSR.0975-8232.15\(6\)](http://doi.org/1754.10.13040/IJPSR.0975-8232.15(6)).
18. Cheng, S., Wang S., Zheng M., et al. (2024) Simultaneous analysis of natural and artificial sweeteners in sugar-free drinks and urine samples by column-switching UHPLC-charged aerosol detection method. *J. Chromatogr. A.*, 1713, pp. 464533. <http://doi.org/10.1016/j.chroma.2023.464533>.
19. Jankulovska M.S., Josimovska T., Velkoska-Markovska L. (2024) Development and validation of RP-HPLC method with UV-DAD detection for simultaneous determination of acesulfame K, sodium saccharin and aspartame in beverages. *Acta Chromatogr.* <https://doi.org/10.1556/1326.2024.01239>
20. Carbonated soft drink- Specifications 2016, 5th edition.
21. DIN12856 (1999) Foodstuffs –Determination of acesulfame-k, aspartame and saccharine – high performance liquid chromatographic method.
22. The Agilent Poroshell 120 EC-C18 Threaded Column. 2009, Agilent Technologies, Inc.
23. Amer, R.T., Goma A.M., et al. (2017) Determination of Synthetic Sweeteners in Some Food Commodities using Reversed Phase HPLC. *New York Sci. J.*, 10, pp. 121-128. <https://doi.org/10.7537/marsnys100617.17>.
24. Sun X. D., Wu H. L., Liu Z., et al. (2019) Rapid and sensitive detection of multi-class food additives in beverages for quality control by using HPLC-DAD and chemometrics methods. *Food Anal. Method.*, 12, pp. 381-393. <https://doi.org/10.1007/s12161-018-1370-3>.
25. Nogueira, R., Wollinger W., da Silva T. E., et al. (2011) Validation of a liquid chromatographic method for determination of related substances in a candidate certified reference material of captopril. *Braz. J. Pharma. Sci.*, 47, pp. 351-362. <https://doi.org/10.1590/S1984-82502011000200016>.

Information about authors

Seyed Mohamad Reza Nazifi – PhD, Assistant professor, Laboratories of Food and Drug Control, Vice Chancellery for Food and Drug, Isfahan University of Medical Sciences (Isfahan, Iran, e-mail: mohamad_nazifi@yahoo.com)

Narges Esfandiarpour – Master of science, Laboratories of Food and Drug Control, Vice Chancellery for Food and Drug, Isfahan University of Medical Science (Isfahan, Iran, e-mail: darya3088@gmail.com)

Azadeh Motamedi – Candidate of science, Laboratories of Food and Drug Control, Vice Chancellery for Food and Drug, Isfahan University of Medical Sciences (Isfahan, Iran, e-mail: azadeh.motamedi@yahoo.com)





Elham Jahanmard – PhD, Assistant professor, Laboratories of Food and Drug Control, Vice Chancellery for Food and Drug, Isfahan University of Medical Sciences (Isfahan, Iran, e-mail: elhamjahanmard@yahoo.com)

Narjes Rahimi – PhD, Assistant professor, Laboratories of Food and Drug Control, Vice Chancellery for Food and Drug, Isfahan University of Medical Sciences (Isfahan, Iran, e-mail: darya3088@gmail.com)

Fatemeh Ansari – Master of science, Laboratories of Food and Drug Control, Vice Chancellery for Food and Drug, Isfahan University of Medical Sciences (Isfahan, Iran, e-mail: f.ansari.r@gmail.com)

Fatemeh Masoudi – Master of science, Laboratories of Food and Drug Control, Vice Chancellery for Food and Drug, Isfahan University of Medical Sciences (Isfahan, Iran, e-mail: f.ansari.r@gmail.com)

Soheila Sepahi – Master of science, Laboratories of Food and Drug Control, Vice Chancellery for Food and Drug, Isfahan University of Medical Sciences (Isfahan, Iran, e-mail: sepahi66@gmail.com)

Zh.N. Uvaniskanova¹ , G.A. Seitimova^{1*} ,
G.Sh. Burasheva¹ , M.I. Choudhary² 

¹Al-Farabi Kazakh National University, Almaty, Kazakhstan

²H.E.J. Research Institute of Chemistry, International Centre for Chemical and Biological Sciences, University of Karachi, Karachi, Pakistan

*e-mail: sitigulnaz@mail.ru

(Received 14 March 2025; received in revised form 14 May 2025; accepted 19 May 2025)

Evaluation of *Canavalia ensiformis* L. beans: Comparative Fatty Acid Profile in Extracts and Analysis of Minerals and Proximate Composition

Abstract. This study investigates the proximate composition, mineral content, and fatty acid profile of *Canavalia ensiformis* L. beans extracted with various solvents. Proximate analysis revealed a high protein content (23.16%), moderate fiber levels (7.13%), and a total fat content of 2.35%. Elemental analysis identified potassium (18,696.87 mg/kg) as the most abundant macroelement, followed by calcium (1,886.81 mg/kg) and magnesium (1,500.98 mg/kg), whereas iron (50.43 mg/kg) and zinc (33.28 mg/kg) were the predominant microelements. Gas chromatography analysis of fatty acids showed that monounsaturated fatty acids (MUFA) dominated the lipid profile, particularly in the hexane (58.67%), ethanol (59.57%), and raw bean (61.11%) extracts. Oleic acid (C_{18:1n9c}) was the most abundant MUFA, reaching 51.39% in the hexane extract. Saturated fatty acids (SFA) were highest in the hexane extract (21.35%), primarily due to palmitic acid (C_{16:0}, 18.77%). Polyunsaturated fatty acids (PUFA) were most prevalent in the hexane extract (16.23%) and bean sample (16.08%), with linoleic acid (C_{18:2n6c}) being the major component. The aqueous extract contained notable amounts of γ -linolenic acid (C_{18:3n6}, 1.68%). These findings highlight the nutritional potential of *C. ensiformis* beans and suggest that solvent selection significantly influences lipid composition. The high MUFA and PUFA content, particularly in hexane and ethanol extracts, underscores their possible applications in food and pharmaceutical formulations.

Key words: *Canavalia ensiformis* L., GC analysis, proximate analysis, micro- and macroelements, fatty acids.

Introduction

Jack bean (*Canavalia ensiformis* L.) is a tropical leguminous plant from the *Fabaceae* family, known for its high protein content exceeding 20–40%. The rising protein consumption in developing countries, coupled with the high cost of protein imports, has driven the search for more affordable and widely available alternative protein sources [1]. In recent studies, Jack bean milk has the potential to emerge as a new type of plant-based milk. If developed, it could serve as an alternative for individuals with lactose intolerance, milk allergies, or those following a vegetarian diet [2]. Soaking and fermentation are the most commonly used methods for studying *C. ensiformis*, with good results, alongside germination, boiling, autoclaving, genetic manipulation, and other processing methods [3].

In the studies by Kanetro B. [4], the effect of germination of jack bean seeds on the functional properties of its flour was investigated. It was found that 72-hour germination significantly enhanced protein content, protein solubility, and foaming capacity due to an increased amount of hydrophobic amino acids, indicating its potential use in food products with improved nutritional and functional properties. Sutedja M. and her team [5] investigated flavonol glycosides from jack bean (*C. ensiformis*) for their α -glucosidase inhibitory activity, a key target in carbohydrate metabolism. The findings revealed potent inhibitory effects of certain compounds, indicating their potential as antidiabetic agents. Saldarriaga F. and his colleagues [6] conducted a study investigating the effects of pH and different light conditions (red, blue, and their combinations) on callus growth and the production of bioactive compounds in *C.*

ensiformis. Optimal growth and enhanced production of phenols, carotenoids, and antioxidant activity were achieved at pH 5.5 and under 1/3 red-blue (R-B LED) light conditions. In this context, there is increasing interest in studying *C. ensiformis* L. due to its rich composition of bioactive compounds such as phenols, carotenoids, and proteins such as urease and lectin, may be useful for developing supportive therapies or health-promoting applications.

This study investigated proximate, elements analysis of plant and the effect of different solvents on the extraction of fatty acids from *C. ensiformis* seeds.

Materials and methods

The mature *Canavalia ensiformis* L. beans were collected from Karachi, Pakistan. *C. ensiformis* (10 kg) were crushed and powdered using an electronic mill. The powdered beans of *C. ensiformis* were macerated in 80% EtOH three times, and the ethanol extract was evaporated under reduced pressure to yield a brown residue (427 g). Furthermore, the ethanol extract was suspended in distilled water and partitioned sequentially with *n*-hexane (85 g), dichloromethane (DCM) (3.67 g), ethyl acetate (2.66 g), and *n*-butanol (49 g), resulting in five portions.

Proximate analysis. The beans of *C. ensiformis* L. were analysed in triplicate for proximate composition: (total ash, dry matter, crude fiber, and fat contents) was conducted using standard methods of the Pharmacopoeia of the Republic of Kazakhstan and total crude protein by the Kjeldahl method [6].

Micro and macro element analysis was conducted using a Shimadzu AA 6200 (Japan) dual-beam atomic absorption spectrophotometer with flame and electrothermal atomization. Standard procedures were followed to ensure accuracy and reproducibility.

The fatty acid composition of the plant extracts was performed using a «Chromos-1000» (Russia) gas chromatograph equipped with a flame ionization detector (FID). A CP-Sil 88 for FAME 100x0.25x0.36 mm column was used for separation. Chromatographic Conditions: Oven Temperature Program: Initial temperature: 70 °C, hold for 3 min, Ramp: 8 °C/min to 120 °C, hold for 2 min, Ramp: 5 °C/min to 200 °C, hold for 4 min, Ramp: 7 °C/min to 220 °C, hold for 61.5 min, Total run time: 99.61 min. Instrument Temperatures: Column oven: 70 °C; Injector: 250 °C; FID detector: 280 °C. Carrier gas (nitrogen): 1.7 kgf/cm². Auxiliary nitrogen flows: 25 cm³/min and 40 cm³/min. Hydrogen: 20 cm³/min. Air: 200

cm³/min. The sample was dissolved in hexane as a solvent and injection volume of 0.1 µL.

Results and discussion

The proximate compositions were determined in triplicate, with all data presented on a dry weight basis and expressed as percentages (%). The moisture and ash content exhibited moderate levels, aligning with the standards outlined in the Pharmacopoeia of the Republic of Kazakhstan and the result is in agreement with the research investigation of Vadivel V. who reported values of 3.8% to 9.2% moisture and for ash values from 3.0% to 5.8% [7-8]. In the present study, the range of protein (23.16%) found lower than some other research [7, 9] (Table 1)

Table 1 – Proximate analysis of *Canavalia ensiformis* L. beans

Parameter	Percentage Values (Dry Weight Basis) ± SD
Ash	3.87 ± 0.19
Dry matter	96.13 ± 4.81
NDF	7.13 ± 1.06
Crude Protein	23.16 ± 1.39
Fat	2.35 ± 0.19
Moisture	6.51 ± 0.33
Carbohydrate	64.11 ± 3.21
Energy content, kcal/kJ	370/1579
Note: *NDF – Neutral Detergent Fiber	

The results of elemental analysis are given in Table 2. Among the macroelements, potassium (K) was the most abundant (18,696.87 mg/kg), playing a key role in cellular function, osmotic balance, and enzyme activation [10]. Calcium (Ca) (1,886.807 mg/kg) and magnesium (Mg) (1,500.978 mg/kg) contribute to bone health, muscle function, and metabolic processes, while sodium (Na) (395.864 mg/kg) regulates fluid balance and nerve transmission [11-12].

Regarding microelements, iron (Fe) (50.428 mg/kg) is crucial for oxygen transport and energy metabolism [13]. Zinc (Zn) (33.278 mg/kg) plays a vital role in immune function, wound healing, and enzymatic activity [14]. Copper (Cu) (11.273 mg/kg) is essential for redox reactions, connective tissue formation, and nervous system maintenance [15]. Manganese (Mn) (8.602 mg/kg) supports bone develop-

ment and antioxidant defense, whereas nickel (Ni) (8.929 mg/kg) is involved in enzyme function and microbial metabolism [15].

Table 2 – Mineral composition of *Canavalia ensiformis* L. beans

Minerals	Concentration, mg/kg
Zn	33.278
Cu	11.273
Pb	7.765
Cd	0.978
Fe	50.428
Ni	8.929
Mn	8.602
Ca	1886.807
Mg	1500.978
K	18696.87
Na	395.864

The fatty acid profile of *C. ensiformis* beans (Table 3) and its various solvent extracts revealed a diverse range of saturated, monounsaturated, and polyunsaturated fatty acids, highlighting their potential nutritional and functional significance. Saturated fatty acids were present in varying concentrations across different extracts. The total SFA content was highest in the hexane extract (21.346%) and the bean sample (18.629%), primarily due to the presence of palmitic acid ($C_{16:0}$) (18.768% and 13.180%, respectively) and stearic acid ($C_{18:0}$). These fatty acids are known to contribute to membrane stability and are

common in plant-based lipid sources [15]. The aqueous extract also showed a relatively high SFA content (10.916%), with notable amounts of stearic acid ($C_{18:0}$) (4.842%) and palmitic acid ($C_{16:0}$) (4.302%). However, shorter-chain saturated fatty acids such as butyric acid ($C_{4:0}$) and capric acid ($C_{10:0}$) were either absent or found in trace amounts.

Monounsaturated fatty acids (MUFA) constituted the dominant fraction in most extracts, particularly in the hexane (58.667%), 70% ethanol (59.565%), and raw bean (61.106%) samples. Oleic acid ($C_{18:1n9c}$) was the most abundant MUFA, accounting for 50.102% in the bean sample and 51.389% in the hexane extract, reinforcing the potential health benefits of these extracts in terms of cardiovascular health and anti-inflammatory properties [16-20]. The ethanol extract exhibited a significant proportion of myristoleic acid ($C_{14:1}$) (16.349%). Additionally, eicosenoic acid ($C_{20:1}$) was notable in the bean sample (9.296%) and hexane extract (6.121%), which could contribute to lipid metabolism regulation [21].

Polyunsaturated fatty acids (PUFA), particularly linoleic acid ($C_{18:2n6c}$) and linolenic acid ($C_{18:3n3}$), were found in notable amounts. The highest PUFA content was recorded in the hexane extract (16.229%) and bean sample (16.078%), with linoleic acid contributing significantly to these values. Linoleic acid is an essential fatty acid involved in cell membrane function and inflammatory response regulation. The aqueous extract contained γ -linolenic acid ($C_{18:3n6}$) (1.675%), which has been associated with anti-inflammatory and neuroprotective effects [22-25]. However, the DCM extract exhibited the lowest PUFA content (0.410%), suggesting its limited ability to extract these essential fatty acids.

Table 3 – Fatty acid profile of *C. ensiformis* beans extracted with various solvent

RT	Fatty acid	Concentration, %					
		<i>Canavalia ensiformis</i> L. beans	70 % EtOH extract	Hexane Extract	DCM extract	Butanol extract	Aqueous extract
16.47	$C_{4:0}$ Butyric acid	NF	NF	NF	NF	0.267	NF
29.48	$C_{10:0}$ Capric acid	0.020	NF	NF	NF	NF	0.825
34.38	$C_{12:0}$ Lauric acid	0.045	NF	NF	NF	NF	0.135
39.1	$C_{14:0}$ Myristic acid	0.346	NF	0.316	0.008	0.209	0.584
41.18	$C_{14:1}$ Myristoleic acid	0.200	16.349	0.276	0.007	0.408	0.108
43.6	$C_{15:1}$ Pentadecanoic acid	NF	NF	NF	NF	0.005	NF
43.85	$C_{16:0}$ Palmitic acid	13.180	9.242	18.768	0.498	3.739	4.302
45.87	$C_{16:1}$ Palmitoleic acid	0.870	1.638	0.664	0.019	2.023	0.298
46.28	$C_{17:0}$ Margaric acid	0.151	NF	0.170	NF	NF	NF
48.31	$C_{17:1}$ Margaroleic acid	0.331	3.870	0.218	NF	NF	NF

Continuation of the table

RT	Fatty acid	Concentration, %					
		<i>Canavalia ensiformis</i> L. beans	70 % EtOH extract	Hexane Extract	DCM extract	Butanol extract	Aqueous extract
48.87	C _{18:0} Stearic acid	1.436	NF	1.285	0.078	3.045	4.842
50.19	C _{18:1} (<i>trans</i> -9) Elaidic acid	0.247	1.169	NF	NF	12.786	4.479
50.81	C _{18:1n9c} Oleic acid	50.102	24.930	51.389	1.286	17.684	4.152
52.34	C _{18:2n6t} <i>trans</i> -Linoleic acid	NF	NF	NF	NF	0.353	0.156
53.85	C _{18:2n6c} Linoleic acid	14.696	9.518	15.378	0.399	3.544	NF
54.64	C _{18:3n3} Linolenic acid	0.547	NF	0.598	0.010	0.286	0.758
56.38	C _{18:3n6} γ -Linolenic acid	0.133	1.988	0.029	NF	1.675	NF
57.01	C _{20:0} Arachidic acid	1.628	NF	0.451	0.006	0.352	0.228
57.6	C _{20:1} Eicosenoic acid	9.296	2.367	6.121	0.142	0.418	NF
56.38	C _{20:3n6} Homo- γ -Linolenic acid	0.509	NF	0.091	NF	NF	0.102
65.09	C _{20:3n3} Eicosatrienoic acid	0.192	0.344	0.133	NF	0.337	0.254
60.9	C _{21:0} Heneicosic acid	0.070	NF	0.027	NF	NF	NF
66.09	C _{22:0} Behenic acid	0.185	NF	0.059	NF	NF	NF
72	C _{23:0} Tricosanoic acid	1.568	NF	0.270	0.005	NF	NF
76.28	C _{24:1} Nervonic acid	0.061	NF	NF	NF	NF	NF
Saturated acids		18.629	9.242	21.346	0.595	7.611	10.916
Monounsaturated acids		61.106	59.565	58.667	1.458	33.267	8.946
Polyunsaturated acids		16.078	11.849	16.229	0.410	6.196	2.587
Note: *NF – not found							

Conclusion

The results of this study provide valuable insights into the nutritional composition and fatty acid profile of *Canavalia ensiformis* L. beans. The beans were found to have a high protein content (23.16%) and moderate levels of fiber (7.13%) and fat (2.35%), making them a potential source of plant-based protein. Mineral analysis showed that potassium (18,696.87 mg/kg) was the most abundant macroelement, followed by calcium (1,886.81 mg/kg) and magnesium (1,500.98 mg/kg), indicating their potential contribution to essential dietary minerals.

Fatty acid analysis revealed that monounsaturated fatty acids (MUFA) were the predominant lipid fraction, with oleic acid (C_{18:1n9c}) reaching 51.39% in the hexane extract. Saturated fatty acids were highest in the hexane extract (21.35%), while polyunsaturated fatty acids, particularly linoleic acid (C_{18:2n6c}), were most abundant in the hexane (16.23%) and raw bean (16.08%) samples. The choice of extraction solvent significantly influenced the fatty acid composition, with hexane and ethanol yielding extracts rich in nutritionally beneficial lipids.

These findings highlight the nutritional potential of *C. ensiformis* beans and their possible applications in food and pharmaceutical industries. Further research is needed to explore the bioavailability of their nutrients, the effects of processing on lipid composition, and potential functional applications of the extracted compounds.

Acknowledgements

Z.N.U. would like to thank the Ministry of Higher Education and Science of the Republic of Kazakhstan for her supporting with a Ph.D. scholarship to work at the H.E.J. Research Institute of Chemistry at the International Centre for Chemical and Biological Sciences (ICCBS) in the University of Karachi, Pakistan. The Dr. Panjwani Centre for Molecular Medicine and Drug Research (PCMD) is also acknowledged for providing the facilities to carry out this work.

Conflict of interest

All authors are aware of the article's content and declare no conflict of interest.

References

1. Ramli N.A.M, Chen Y.H., Mohd Zin Z., Abdullah M.A.A., Rusli N.D., Zainol M.K. (2021) Effect of soaking time and fermentation on the nutrient and antinutrients composition of *Canavalia ensiformis* (Kacang Koro). *IOP Conf. Series: Earth and Env. Sci.*, 756, 012033. <https://doi.org/10.1088/1755-1315/756/1/012033>.
2. Sutedja A.M., Ito A., Yanasey E., Batubara I., Fardiaz D., Lioe H.N. (2022) Influence of jack bean (*Canavalia ensiformis* (L) DC) milk processing on bioactive compounds and its antioxidant activity. *Food Sci. Tech.*, 42, e11521. <https://doi.org/10.1590/fst.11521>.
3. Soetan K.O. (2008) Pharmacological and other beneficial effects of antinutritional factors in plants-A review. *African J. Biotech.*, 7, pp. 4713-21. <https://doi.org/10.4314/ajb.v7i25.59660>.
4. Kanetro B., Riyanto M., Pujmulyani D., Huda N. (2021) Improvement of Functional Properties of Jack Bean (*Canavalia ensiformis*) Flour by Germination and Its Relation to Amino Acids Profile. *Current Res. in Nutr. and Food Sci.*, V. 9(3), P. 812-822. <https://dx.doi.org/10.12944/CRNFSJ.9.3.09>.
5. Sutedja A.M., Yanase E., Batubara I., Fardiaz D., Lioe N.H. (2020) Identification and Characterization of α -Glucosidase Inhibition Flavonol Glycosides from Jack Bean (*Canavalia ensiformis* (L.) DC. *Molecules*, 25, P. 2481. <https://doi.org/10.3390/molecules25112481>.
6. Saldarriaga J.F., Cruz Y., López J.E. (2020) Preliminary study of the production of metabolites from *in vitro* cultures of *C. ensiformis*. *BMC Biotech.*, 20, P. 49 <https://doi.org/10.1186/s12896-020-00642-x>
7. Vadivel V., Janardhanan K. (2001) Diversity in nutritional composition of wild jack bean (*Canavalia ensiformis* L. DC) seeds collected from south India. *Food Chem.*, 74(4), P. 507-511. [https://doi.org/10.1016/S0308-8146\(01\)00175-3](https://doi.org/10.1016/S0308-8146(01)00175-3).
8. Solomon S.G., Okomoda V.T., Oguiche O. (2017) Nutritional value of raw *Canavalia ensiformis* and its utilization as partial replacement for soybean meal in the diet of *Clarias gariepinus* (Burchell, 1822) fingerlings. *Food Sci. Nutr.*, 6, P. 207-213. <https://doi.org/10.1002/fsn3.548>.
9. Ministry of Health of the Republic of Kazakhstan (2008) State Pharmacopoeia of the Republic of Kazakhstan, 1, 592. <https://labborg.kz/downloads/Methods/Gosudarstvennaya-farmakopeya-Respubliki-Kazakhstan-tom-I.pdf>.
10. Wang M., Qingsong Zheng Q., Qirong Sh., Shiwei G. (2013) The Critical Role of Potassium in Plant Stress Response. *Int. J. Mol. Sci.*, 14, pp. 7370-7390; <https://doi.org/10.3390/ijms14047370>.
11. Ciosek, Z., Kot, K., Kosik- Bogacka, D., Łanocha-Arendarczyk, N., Rotter, I. (2021) The Effects of Calcium, Magnesium, Phosphorus, Fluoride, and Lead on Bone Tissue. *Biomolecules*, 11, 506. <https://doi.org/10.3390/biom11040506>.
12. Strange K. (1992) Regulation of solute and water balance and cell volume in the central nervous system. *JASN*, 3(1), pp. 12-27. <https://doi.org/10.1681/ASN.V3112>.
13. Nikolaus B., Peter M. E. (2015) Oxidative Stress and the Homeodynamics of Iron Metabolism. *Biomolecules*, 5, pp. 808-847. <https://doi.org/10.3390/biom5020808>.
14. Chasapis C.T., Panagoula-Stamatina A. Ntouna, Spiliopoulou Ch.A., Stefanidou M.E. (2020) Recent aspects of the effects of zinc on human health. *Archives of Toxicology*, 94, pp. 1443-1460. <https://doi.org/10.1007/s00204-020-02702-9>.
15. An Y., Li S., Huang X., Chen X., Shan H., Zhang M. (2022) The Role of Copper Homeostasis in Brain Disease. *Int. J. Mol. Sci.*, 23, 13850. <https://doi.org/10.3390/ijms232213850>.
16. Jomova K., Makova M., Alomar S.Y., Alwasel S.H., Nepovimova E., Kuca K., Rhodes C.J., Valko M. (2022) Essential metals in health and disease. *Chem.-Bio. Interactions*, 367, 110173. <https://doi.org/10.1016/j.cbi.2022.110173>.
17. Saini R.K., Prasad P., Sreedhar R.V., Akhilender Naidu K., Shang X., Keum Y.S. (2021) Omega-3 Polyunsaturated Fatty Acids (PUFAs): Emerging Plant and Microbial Sources, Oxidative Stability, Bioavailability, and Health Benefits — A Review. *Antioxidants*, 10, 1627. <https://doi.org/10.3390/antiox10101627>.
18. Rimm E.B., Appel L.J., Chiuve S.E., Djoussé L., Engler M.B., Kris-Etherton P.M. Mozaffarian D., Siscovick D.S., Lichtenstein A.H. (2018) Seafood long-chain n-3 polyunsaturated fatty acids and cardiovascular disease: A science advisory from the American Heart Association. *Circulation*, 138, pp. 35-47. <https://doi.org/10.1161/CIR.0000000000000574>.
19. Wu H., Xu L., Ballantyne C.M. (2020) Dietary and pharmacological fatty acids and cardiovascular health. *J. Clin. Endocrinol. Metab.*, 105, pp. 1030-1045. <https://doi.org/10.1210/clinem/dgz174>.
20. Marangoni F., Agostoni C., Borghi C., Catapano A.L., Cena H., Ghiselli A., La Vecchia C., Lercker G., Manzato E., Pirillo A. (2020) Dietary linoleic acid and human health: Focus on cardiovascular and cardiometabolic effects. *Atherosclerosis*, 292, pp. 90-98. <https://doi.org/10.1016/j.atherosclerosis.2019.11.018>.
21. Naeini Z., Toupchian O., Vatannejad A., Sotoudeh G., Teimouri M., Ghorbani M., Nasli-Esfahani E., Koohdan F. (2020) Effects of DHA-enriched fish oil on gene expression levels of p53 and NF- κ B and PPAR- γ activity in PBMCs of patients with T2DM: A randomized, double-blind, clinical trial. *Nutr. Metab. Cardiovasc.*, 30, pp. 441-447. <https://doi.org/10.1016/j.numecd.2019.10.012>.
22. Bird J.K., Calder P.C., Eggersdorfer M. (2018) The role of n-3 long chain polyunsaturated fatty acids in cardiovascular disease prevention, and interactions with statins. *Nutrients*, 10, 775. <https://doi.org/10.3390/nu10060775>.
23. Dong S., He J., Luo Y., Han X. (2024) Transcriptome analysis of the molecular basis of 11-eicosenoic acid-mediated salt stress tolerance in rice. *Crop Science*, 64, pp. 2840-2853. <https://doi.org/10.1002/csc2.21311>.
24. Tomata Y., Larsson S.C., Hägg S. (2020) Polyunsaturated fatty acids and risk of Alzheimer's disease: A Mendelian randomization study. *Eur. J. Nutr.*, 59, pp. 1763-1766. <https://doi.org/10.1007/s00394-019-02126-x>.
25. Langley M.R., Triplet E.M., Scarisbrick I.A. (2020) Dietary influence on central nervous system myelin production, injury, and regeneration. *BBA-Mol. Basis Dis.*, 1866, 165779. <https://doi.org/10.1016/j.bbadis.2020.165779>

26. Zhou Y., Tao X., Wang Z., Feng L., Wang L., Liu X., Pan R., Liao Y., Chang Q. (2019) Hippocampus metabolic disturbance and autophagy deficiency in olfactory bulbectomized rats and the modulatory effect of fluoxetine. *Int. J. Mol. Sci.*, 20, 4282. <https://doi.org/10.3390/ijms20174282>.
27. Chang J.P., Chang S., Yang H., Chen H., Chien Y., Yang B., Su H., Su K. (2020) Omega-3 polyunsaturated fatty acids in cardiovascular diseases comorbid major depressive disorder-results from a randomized controlled trial. *Brain Behav. Immun.*, 85, pp. 14-20. <https://doi.org/10.1016/j.bbi.2019.03.012>.


Information about authors

Zhuldyz N. Uvaniskanova – PhD student, Al-Farabi Kazakh National University (Almaty, Kazakhstan, e-mail: zhuldyz.uvaniskanova@gmail.com)

Gulnaz A. Seitimova (corresponding author) – PhD, Associate Professor, Al-Farabi Kazakh National University (Almaty, Kazakhstan, e-mail: sitigulnaz@mail.ru)

Gaukhar Sh. Burasheva – Doctor of Chemical Sciences, Professor, Al-Farabi Kazakh National University (Almaty, Kazakhstan, e-mail: gauharbur@mail.ru)

Iqbal M. Choudhary – D.Sc., PhD, Professor, H.E.J. Research Institute of Chemistry, International Centre for Chemical and Biological Sciences (University of Karachi, Pakistan, e-mail: iqbal.choudhary@iccs.edu)

A.A. Auyeshov¹ , Ch.Z. Eskibayeva¹ , A.M. Ibrayeva¹ ,
K.T. Arynov^{2*} , A.K. Dikanbayeva^{1*} 

¹Mukhtar Auezov South Kazakhstan University, Shymkent, Kazakhstan

²Institute of Innovative Research and Technology, Almaty, Kazakhstan

*e-mail: i_technology@mail.ru; dikanbaeva86@mail.ru

(Received 14 May 2025; received in revised form 28 May 2025; accepted 7 June 2025)

Resource-efficient technology for the utilization of serpentine technogenic waste with the production of magnesium oxide

Abstract. The article discusses the possibility of using serpentine and serpentine waste from Zhitikara deposit for the production of inorganic magnesium compounds: MgSO_4 , $\text{Mg}(\text{OH})_2$ and MgO . The aim is to produce magnesium sulfate, whose quality characteristics would further enable the production of high-purity magnesium hydroxide and magnesium oxide. A step-by-step process for obtaining magnesium compounds is proposed, initially starting with the purified magnesium sulfate solution, from which magnesium hydroxide and magnesium oxide can be produced. The proposed process differs from other known methods in the choice of reagent for neutralizing and purifying the initial sulfate solution to obtain high-purity magnesium hydroxide and magnesium oxide.

A technical and economic analysis was conducted on the efficiency of producing industrially important inorganic magnesium compounds from serpentine waste derived from the processing of chrysotile ore at Zhitikara deposit. The technology's resource intensity, energy efficiency, and economic feasibility of the new approach to processing serpentine waste for the production of magnesium compounds are shown. The advantages of using an acid method in combination with thermally activated serpentine for neutralizing and purifying the initial sulfate leaching solution are discussed. Based on experimental data obtained from studying magnesium extraction processes from serpentine, as well as the production of magnesium hydroxide and magnesium oxide from the purified magnesium sulfate solution, and the technical and economic analysis of each stage, it is concluded that the proposed process becomes more efficient when the final product is magnesium oxide. The potential for utilizing technogenic waste containing serpentine for sustainable magnesium compound production is considered.

Key words: serpentine, magnesium sulfate, magnesium hydroxide, magnesium oxide, resource efficiency.

Introduction

In many regions of the world, including Kazakhstan, serpentinite is contained in mining dumps. Serpentinite waste processing allows to reduce the cost of production due to the zero cost of raw materials, reduce the volume of technogenic accumulations, implement the principles of "green" technologies, and provide a comprehensive extraction of valuable elements (Mg, Si, Fe, etc.) in the form of usable compounds. These advantages contribute to the formation of waste-free technological processes, which is important from the point of view of environmental sustainability and rational environmental management.

Serpentinite anthropogenic wastes generated during mining and processing of chrysotile raw materials and non-ferrous metal ores (chromium, nickel, cobalt, etc.) have accumulated in the world in the volume of hundreds of millions of tons and represent an environmental hazard. These wastes contain significant amounts of magnesium and silicon, and have good reactivity after thermal and acid activation. The advantages of their use also include their location near mining enterprises, which facilitates recycling, environmental impact reduction and reclamation of anthropogenic landscapes.

Serpentinite is widely distributed in ultramafic rocks of the Earth's crust. Large deposits are located in Russia (Urals), China, Canada, Brazil and other

countries. In Kazakhstan, large deposits of serpentinite (chrysotile) raw materials are located in the Kostanay region (Zhitikara deposit). These deposits are often associated with nickel and chromite ores, which in the future allows for the integrated development of deposits [1]. Currently, Zhitikara deposit is developed by Kostanay Minerals JSC. As a result of 65 years of operation some 300-350 million tons of chrysotile raw material processing waste were accumulated here.

It is known that serpentinites belong to complex silicates [2]. Their structure can be represented

as a two-dimensional compound of two types of geometric shapes – tetrahedrons and octahedrons (Figure 1). The silica tetrahedrons have silicon atoms in the center, while the octahedral inter-layer contains magnesium ions [3]. Typical chemical composition of serpentinite: MgO – 30-45%, SiO_2 – 35-45%, H_2O – 10-13%; FeO, Al_2O_3 , CaO and other components are also present in small amounts. The high MgO content makes serpentinite a promising source of magnesium for production of industrially important compounds and magnesium-bearing products.

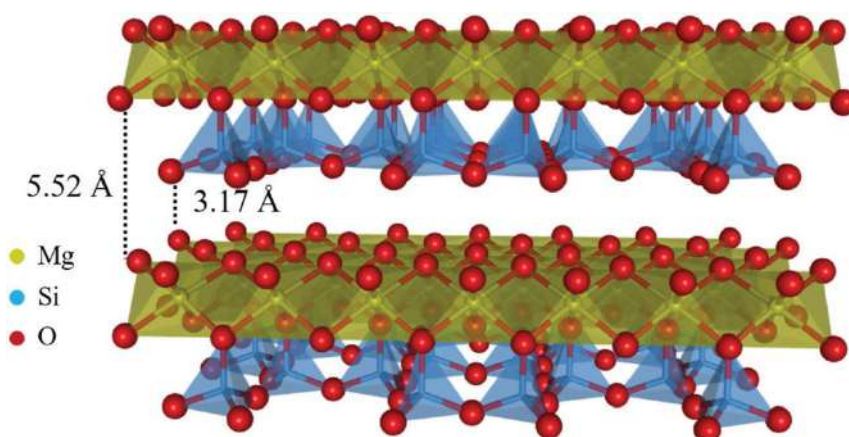


Figure 1 – Basic structure of serpentine [3]

The study of the possibility of using Zhitikara serpentinite or chrysotile raw material processing wastes is relevant, since there are no high-quality deposits of dolomite – traditional industrial raw material for obtaining inorganic magnesium compounds – on the territory of Kazakhstan. In this respect, the development of innovative scientific approaches to the use of accumulated serpentinite wastes of Zhitikara deposit can open new perspectives:

- creation of a processing cluster, development of new industries (production of magnesium compounds, magnesium fertilizers, etc.), transition to a sustainable “green” economy;
- integrated recycling allows to realize the “zero-waste” principle – waste becomes a raw material, and the accompanying by-products can be used in other industries.

Analysis of scientific literature in this area shows that so far there is no information on the forecast technical and economic indicators of potential products derived from serpentinite or serpentinite-containing industrial wastes of Zhitikara deposit using acid

processing methods. Such data could be of interest from a practical point of view. Obviously, unsolved technological problems still prevent the transition to the economic evaluation of serpentinite application as a source of magnesium for the production of its compounds. This aspect is particularly relevant in the context of the development of new technological solutions aimed at processing industrial wastes and potential attraction of investments for their industrial implementation.

Various studies of physical and chemical properties and thermo-acid behavior of serpentinite ores, as well as serpentinite wastes of extraction and concentration of chrysotile of Zhitikara deposit [4-7] showed that serpentinites of this deposit can be considered as a promising source of magnesium for the production of inorganic compounds – magnesium sulfate, hydroxide and oxide, which are in demand in various industries of Kazakhstan.

As a first step, the goal was set to obtain magnesium sulfate, the qualitative characteristics of which will further provide the possibility of synthesizing

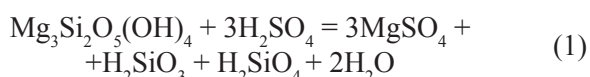
magnesium hydroxide and oxide of high purity. In the study special attention is paid to the processes of leaching of serpentinite with sulfuric acid solution, as well as the selection of reagents for neutralization and purification of the productive solution of magnesium sulfate.

On the basis of experimental data obtained during the study of the processes of MgSO_4 extraction and step-by-step synthesis of magnesium compounds – $\text{Mg}(\text{OH})_2$ and MgO , a technical and economic analysis was carried out to determine the resource and economic efficiency of their production from waste processing of serpentinite chrysotile raw materials of Zhitikara deposit.

Materials and methods

Dust-like material generated during extraction and concentration of chrysotile raw material of Zhitikara field (Kostanay region), with a particle size of 1-1.25 mm, was used as an anthropogenic waste in the research. Sulfuric acid (H_2SO_4 , chemical purity) was used as a leaching reagent, and initial technogenic waste with the same particle size (1-1.25 mm) thermoactivated at 750°C for 1 hour was used as a reagent for neutralization and purification of leaching solution (magnesium sulfate).

The stoichiometric amounts of acid and man-made waste used for the interaction were calculated on the basis of the assumed reaction corresponding to the following equation:



All analytical studies were performed using a JSM-6490LV scanning electron microscope (JEOL, Japan) complete with an INCA Energy 350 energy dispersive microanalyzer system.

Methodology. Preparation of magnesium sulfate included two stages:

1) leaching of technogenic waste with sulfuric acid;

2) neutralization and precipitation of impurity metal ions by increasing the pH of the suspension to 7.8-8.0 using thermally activated serpentinite.

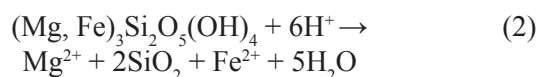
The processes of leaching, neutralization and solution purification were carried out in one reactor – a pyrex flask equipped with a thermometer, dosing device, filter and stirrer (Figure 2).



Figure 2 – Laboratory installation for obtaining magnesium sulfate solution: 1 – reactor, 2 – filter, 3 – thermometer, 4 – doser

Results and discussions

Analysis of modern researches and developments of technologies for obtaining magnesium compounds from serpentinite [8-13] shows that the main method of magnesium extraction in the form of its salts – sulfate, chloride, nitrate, as well as magnesium hydroxide and oxide – is acid leaching. In the process of acid treatment, serpentinite dissolves in solutions of inorganic acids (H_2SO_4 , HCl and HNO_3), as a result of which magnesium passes into solution. The generalized reaction scheme is represented as follows:



Heat treatment at $600-800^\circ\text{C}$ has also been found to activate the serpentinite structure by breaking the Mg-Si bonds [14-16]:



The above reactions are presented in a simplified form, because in practice both dissolution of serpentinite in acids and its disintegration during calcination are complex processes depending on the type of the source rock and its chemical and mineral composition [17, 18].

The increase of alkaline properties of serpentinite after heat treatment in the range of 725-750°C is an established fact [19], which justifies its use as a reagent for neutralization of acidic solutions.

Taking into account the above-mentioned, within the framework of experimental studies, the sulfuric acid method of serpentinite leaching was used, as well as heat-treated serpentinite for neutralization and purification of the initial sulfate solution. The latter, in turn, was used to obtain magnesium hydroxide and oxide according to the scheme presented in Figure 3.

In accordance with the scheme, laboratory studies of the processes of step-by-step production of purified magnesium sulfate, magnesium hydroxide and magnesium oxide solution were carried out. For each stage, the optimum conditions of the processes were determined. A technical and economic analysis was performed on the basis of scaling of quantitative data (expenditures of raw materials, reagents and thermal energy) obtained during laboratory experiments to assess the resource and economic efficiency of obtaining magnesium compounds from pulverized serpentinite waste generated during the processing of chrysotile raw materials. Tables 1-3 present specific costs, as well as resource and economic efficiency indicators of each stage of obtaining magnesium sulfate, magnesium hydroxide and magnesium oxide, calculated on the basis of fixed costs and material and energy balances.

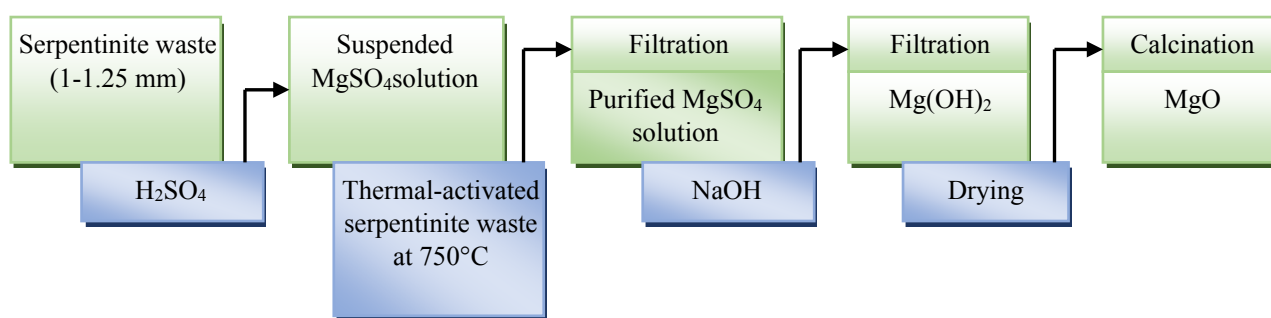


Figure 3 – Scheme of magnesium oxide production from serpentinite waste

Table 1 – Specific consumption of raw materials and energy resources for production of 1 ton of $\text{MgSO}_4 \cdot 7\text{H}_2\text{O}$ and resource and energy

Type of resource	UoM	Specificconsumption	Designation	
Specific consumption of raw materials and energy resources for production of 1 t of MgSO ₄ ·7H ₂ O				
ITW (industrial and technical waste)	tons	0.400	C_raw	
ITW-TA (industrial and technical waste thermoactivated at 750°C, for neutralization of acid slurry)	-	0.400	C_raw	
Sulfuric acid (H ₂ SO ₄ , density = 1.824 g/cm ³)	tons	0.444	C_reagent 1	
Water (technical)	tons	2.800	C_reagent 2	
Specific consumption of raw materials and energy resources to produce 0.400 tons of ITW-TA				
ITW	tons	0.462	C_raw	
Electricity (calcination)	kWh	92.4	C_energy	
Resource and energy efficiency of MgSO ₄ ·7H ₂ O (seven-water magnesium sulfate)				
Description	UoM	Q-ty	Unit price, USD	Cost, USD
Revenues	-	-	-	\$175.0
MgSO ₄ ·7H ₂ O	tons	1	\$175	\$175.0
Expenditures				\$60.0

Continuation of the table

TVET	tons	0.462	\$3	\$1.4
FTP-TA	tons	0.400	\$3	\$1.2
Sulfuric acid (H ₂ SO ₄ , density=1.824 g/cm ³)	tons	0.444	\$100	\$44.4
Water (H ₂ O, technical)	tons	2.800	\$1	\$2.8
Electro Energy (firing)	kWh	92.4	\$0.07	\$6.0
Others	-	-	-	\$4.2
Resource and energy efficiency				
Gross profit (margin)	-	-	-	\$115.0

Table 2 – Specific consumption of raw materials and energy resources for production of 1 ton of Mg(OH)₂ and resource and energy efficiency

Specific consumption of raw materials and energy resources for production of 1 t of Mg(OH) ₂				
Type of resource	UoM	Specific consumption	Designation	
MgSO ₄ ·7H ₂ O	tons	4.245	C_raw	
	tons	10.6		
NaOH (25% NaOH solution)	tons	1.380	C_reactive	
	tons	5.560		
H ₂ O	tons	4.2	C_reagent	
Resource and energy efficiency of Mg(OH) ₂ (magnesium hydroxide)				
Description	UoM	Q-ty	Unit price, USD	Cost
Revenues	-	-	-	\$1445
Mg(OH) ₂ (magnesium hydroxide)	tons	1	\$1200	\$1200
Na ₂ SO ₄ (sodium sulphate)	tons	2.450	\$100	\$245
Expenditures	-	-	-	\$950
MgSO ₄ ·7H ₂ O (seven-water magnesium sulfate)	tons	4.245	\$60	\$255.8
NaOH (sodium hydroxide)	tons	1.380	\$500	\$690.0
Water (H ₂ O, technical)	tons	4.2	\$1	\$4.20
Resource and energy efficiency				
Gross profit (margin)	-	-	-	+\$495.0

Table 3 – Specific consumption of raw materials and energy resources for production of 1 ton of MgO (magnesium oxide) and resource and energy efficiency

Specific consumption of raw materials and energy resources for production of 1 ton of MgO				
Type of resource	UoM	Specificconsumption	Designation	
Mg(OH) ₂ (magnesium hydroxide)	tons	1.470	C_raw	
Electricity	kWh	731.3	C_energy	
Resource and energy efficiency of MgO				
Description	UoM	Q-ty	Unit price, USD	Cost
Revenues	-	-	-	\$5000
MgO (magnesium oxide)	tons	1	\$5000	\$5000

Continuation of the table

Expenditures	-	-	-	1444.3
Mg(OH) ₂ (magnesium hydroxide)	tons	1.470	\$950	1397
Electricity	kWh	731.3	\$32.64	47.8
Resource and energy efficiency				
Gross profit (margin)	-	-	-	+\$3555.7

Comparative analysis of the revenues of each stage of the process of obtaining magnesium compounds in the series: magnesium sulfate solution (MgSO_4) \rightarrow $\text{Mg(OH)}_2 \rightarrow \text{MgO}$ shows that the use of serpentinite (including technogenic) resources becomes more resource- and energy-efficient in the deep processing of technogenic waste, when the end product is magnesium oxide (MgO). This is an important factor motivating further scientific and technological research in this direction.

Conclusion

The use of serpentinite as a source of magnesium to obtain industrially important compounds – magnesium sulfate, hydroxide and oxide – is a promising direction that combines technological, economic and environmental sustainability. The most effective methods are acid leaching and application of thermoactivated serpentinite at the

stages of neutralization and purification of sulfate solution, which provides obtaining of magnesium hydroxide and oxide with high quality characteristics. The development of these technologies allows to obtain in-demand inorganic magnesium compounds in various industries of Kazakhstan, because the volume of serpentinite technogenic raw materials allows to organize their production in any necessary quantity.

Acknowledgments

This study was funded by the Committee of Science and the Ministry of Education and Science of the Republic of Kazakhstan (Grant No. BR21882242).

Conflict of interest

All authors are aware of the article's content and declare no conflict of interest.

References

1. Punenkov S.E., Kozlov Yu.S. (2022) Hrizotil-asbest i resursosberezhenie v hrizotil-asbestovoj otrasli [Chrysotile asbestos and resource conservation in the chrysotile asbestos industry]. *Gornyy zhurnal Kazakhstana [Mining Journal of Kazakhstan]*, 1, pp. 5-10. <https://10.0.189.114/minmag.2022.204.4.001>
2. Pellant C. (1992) Smithsonian Handbooks: Rocks & Minerals. London: Dorling Kindersley, 256 p.
3. Carmignano O., Vieira S., Brandão P., Bertolli A., Lago R. (2020) Serpentinites: Mineral Structure, Properties and Technological Applications. *J. Braz. Chem. Soc.*, 31(1), pp. 2-14. <https://doi.org/10.21577/0103-5053.20190215>.
4. Auyeshov A., Arynov K., Yeskibayeva Ch., Dikanbayeva A., Auyeshov D., Raiymbekov Y. (2024) Transformation of Silicate Ions into Silica under the Influence of Acid on the Structure of Serpentine. *Molecules*, 29(11), pp. 2502. <https://doi.org/10.3390/molecules29112502>.
5. Auyeshov A., Arynov K., Yeskibayeva Ch., Satimbekova A., Alzhanov K. (2024) The Thermal Activation of Serpentine from the Zhitikarinsky Deposit (Kazakhstan). *Molecules*, 29(18), pp. 4455. <https://doi.org/10.3390/molecules29184455>.
6. Yeskibayeva Ch., Auyeshov A., Arynov K., Dikanbayeva A., Satimbekova A. (2024) Nature of serpentinite interactions with low-concentration sulfuric acid solutions. *Green Processing and Synthesis*, 13, pp. 20240034. <https://doi.org/10.1515/gps-2024-0034>.
7. Auyeshov A., Yeskibayeva Ch., Arynov K., Kolesnikov A. (2024) Aspects of waste recycling problems in chrysotile asbestos industry. *Mining Inf. Anal. Bull.*, 9, pp. 88-98. https://doi.org/10.25018/0236_1493_2024_9_0_88.
8. Velinskij V.V., Gusev G.M. Pat. 2097322 RF, S 01 V33/142. Sposob kompleksnoj pererabotki serpentinita [Method of complex processing of serpentine], publ. 27.11.1997.
9. Kuznecova T.V., Ioffe E.M., Kolbasov V.M. Pat. 2011638 RF, MPK C 01 F5/06. Sposob polucheniya oksida magniya iz serpentinita [Method for obtaining magnesium oxide from serpentinite], publ. 30.04.1994. Bul. № 28, 3 p.
10. Zulumyan N.O., Isaakyan A.R., Ovsepyan T.A. Pat. 2407704 RF, MPK C 01 B33/12. Sposob kompleksnoj obrabotki serpentinita [Method of complex processing of serpentinite], publ. 27.12.2010, 6 p.
11. Kalichenko I.I., Gabdullin A.N. Pat. 2292300 RF, MPK C01F5/02. Sposob pererabotki serpentinita [Method of processing serpentinite], publ. 27.01.2007.

12. Nazharova L.N. (1999) Solyanokislaya pererabotka serpentinita [Hydrochloric acid processing of serpentinite]: diss. for cand. chem.sci. Kazan', 152 p.
13. Sagarunyan S.A., Arustamyan A.G., Agamyan E.S., Arakelyan A.M., Sagarunyan A.S. Pat. № 2953 A Respublika Armeniya, S 01 V33/00, S 09 S1/00. Sposob kompleksnoj pererabotki serpentinitov [Method of complex processing of serpentinites], publ. 2014.
14. Mackenzie K.J.D., Meinhold R.H. (1994) Thermal reactions of chrysotile revisited: A ^{29}Si and ^{25}Mg MAS NMR study. *Am. Miner.*, 79(1), pp. 43-50.
15. Fedoročková A., Hreus M., Raschman P., Sučík G. (2012) Dissolution of magnesium from calcined serpentinite in hydrochloric acid. *Min. Eng.*, 32, pp. 1-4. <http://dx.doi.org/10.1016/j.mineng.2012.03.006>.
16. Zulumyan N.O., Isaakyan A.R., Oganessian Z.G. (2007) Novyj mnogoobeshchayushchij metod pererabotki serpentinitov [A promising new method for processing serpentinites]. *Russian J. Appl. Chem.*, 80, pp. 1020-1022.
17. Papahchyan L.R., Terzyan A.M., Isaakyan A.R., Zulumyan N.O. (2014) Izuchenie termoliza lizardita iz mestorozhdeniya Monti-Livornesi (Italiya) [Study of thermolysis of lizardite from the Monti Livornesi deposit (Italy)]. *Bull. State Univ. Agricul., ser. Chem. Nat. Protection Techn.*, 17(1), pp. 26-34.
18. Raschman P., Fedoročková A., Sučík G. (2013) Thermal activation of serpentine prior to acid leaching. *Hydrometallurgy*, 139, pp. 149-153. <https://doi.org/10.1016/j.hydromet.2013.08.010>.
19. Auyeshov A., Arynov K., Yeskibayeva Ch., Alzhanov K., Raiymbekov Y. (2024) Thermoacid Behavior of Serpentine of the Zhitikarinsky Deposit (Kazakhstan). *Molecules*, 29(16), pp. 3965. <https://doi.org/10.3390/molecules29163965>.

Information about authors:



Abdrazakh Auyeshov – Doctor of Technical Sciences, Professor, Mukhtar Auezov South Kazakhstan University (Shymkent, Kazakhstan, e-mail: centersapa@mail.ru)

Chaizada Yeskibayeva – Candidate of Technical Sciences, Associate professor, Mukhtar Auezov South Kazakhstan University (Shymkent, Kazakhstan, e-mail: yeskibayeva@internet.ru)

Aitkyl Ibrayeva – Chief specialist of the SRL "Applied Chemistry", Mukhtar Auezov South Kazakhstan University (Shymkent, Kazakhstan, e-mail: aytkul.ibraeva@mail.ru)

Kazhymuhan Arynov – Doctor of Technical Sciences, Professor, Institute of Innovative Research and Technology (Almaty, Kazakhstan, e-mail: i_technology@mail.ru)

Aizhan Dikanbayeva – Doctor PhD, Mukhtar Auezov South Kazakhstan University (Shymkent, Kazakhstan, e-mail: dikanbaeva86@mail.ru)

T.D. Sallal , A.M. Abbas* 

Collage of education for pure sciences (Ibn Al-haitham), University of Baghdad, Baghdad, Iraq

*e-mail: ahmed.m.a@ihcoedu.uobaghdad.edu.iq

(Received 15 April 2025; received in revised form 14 May 2025; accepted 22 May 2025)

Preparation and Characterization of Nano-Iron Oxide by using Iraqi Orange Plant Extract and Testing for Adsorption Efficiency

Abstract: Nanomaterials, including nanoparticles such as iron oxide nanoparticles, have received great attention from researchers due to their unique properties and applications. There are several diverse methods, including chemical, physical, and green biological methods, to prepare iron oxide nanoparticles. The green method was chosen because it is safer, purer, and less toxic compared to other methods. Therefore, the green method is a promising and environmentally friendly method in the near future. The aqueous extract of Iraqi orange leaves was used to prepare nano iron oxide, it was examined structurally and spectrally by several techniques (X-ray diffraction- XRD, Fourier transform infrared – FT-IR, field emission scanning electron microscopy – FESEM, energy disperse X-ray spectroscopy – EDX, and UV-vis spectroscopy). Through the diagnosis, it was proven that the nano iron oxide was successfully prepared in a spherical form with an average size equal to 68.5 nm. The nano iron oxide particles were tested to remove the crystal dye from its aqueous solution, where the removal percentage reached 61% at 298K, dose adsorbent = 0.01 g, contact time = 90 min, and initial concentration = 11 mg/L. This indicates the possibility of using nano iron oxide which preparing by green method in the field of water treatment.

Key words: Fe₃O₄ NPs, green method, orange leaf aqueous extract, adsorption, crystal violet dye.

Introduction

Nanotechnology and nanoscience are among the most important modern discoveries because they are the foundation of various areas of modern life. Therefore, they can be described as those materials that are manufactured at a scale of 1-100 nanometers. This size results in dramatic changes in a number of physical and chemical properties of the material. There are several methods for preparing nanomaterials, including chemical reduction, electro-optical deposition, co-deposition, spray thermal decomposition, hydrothermal, and sol-gel [1, 2].

Recently, researchers have focused on conducting an extensive study on the use of magnetic nanoparticles (α -Fe₂O₃, γ -Fe₂O₃, Fe₃O₄, and FeO) in various general and biomedical applications [3-5]. Hematite (α -Fe₂O₃) is one of the most stable forms of iron oxide. It also has outstanding properties in corrosion treatment, chemical stability, optics, magnetism, and biodegradability at a low cost, which provides ease and possibility of application in various modern applications. Applications of hematite nanoparticles include gas sensors, storage media, dyes, catalysis,

corrosion treatment, solar energy conversion, and water purification [6-8].

There are various methods for manufacturing iron nanoparticles. Some are chemical by using chemical solvents, which can produce toxic chemicals, making it a dangerous and unsafe method. Other methods are physical, but they are expensive because they require high energy. These reasons make us look for other safe and environmentally friendly methods. This is represented by green methods by using living materials and parts in the preparation process [9]. Several previous studies have addressed the preparation of metal nanoparticles and their oxides using the green method through plant extracts and their parts (leaves and roots) as reducing agents [10-13]. Green synthesis of nanoparticles is highly cost-effective, environmentally friendly, and non-toxic. In this green synthesis route, biomolecules in the plant system can act as capping and reducing agents and increase the reduction rate and stability of nanoparticles [14, 15].

In this research, we have performed a green synthesis process for α -Fe₂O₃ nanoparticles using aqueous extract of Iraqi orange tree leaves. The prepared iron oxide nanoparticles were characterized by sev-

eral methods (FT-IR, XRD, FESEM, EDX, and UV-VIS), and the prepared samples were tested to determine their efficiency in removing the violet crystal dye from their aqueous solution.

Materials and methods

Materials and Reagents. Solutions and reagents were prepared according to analytical standards and without further purification. Iron nitrate $\text{Fe}(\text{NO}_3)_3 \cdot 6\text{H}_2\text{O}$ (Sigma-Aldrich), ammonia hydroxide (NH_4OH) (Sigma-Aldrich), and distilled water. All solutions were prepared with distilled water. Leaves of the orange plant were collected from the local area of Baghdad city in Iraq. Crystal violet dye (CV) $\text{C}_{25}\text{H}_{30}\text{N}_3\text{Cl}$ for adsorption tests.

Preparation of leaves of orange plant extract. Orange leaves were collected from one of the orchards of the Suleiman Pak area located on the Tigris River in Baghdad Governorate. They were then washed with distilled water several times to get rid of dust and other pollutants. After washing, the leaves were dried at room temperature for seven days without exposing them to sunlight. Bitter orange extract was prepared in water by adding 200 ml of distilled water to 20 grams of dried bitter orange leaf powder in a 500 ml beaker with continuous stirring and heating at a temperature of 60°C for an hour. Then the mixture was left after heating for 24 hours. The next day, the filtration process was carried out to obtain a clear brown bitter orange extract, which is then stored in special, tightly sealed bottles. and refrigerated for further use.

Synthesis and characterization of iron oxide nanoparticles. 10 mL of a 0.01 M solution of iron nitrate with distilled water was placed in a beaker with stirring using a magnetic stirrer (Hot Plate and Magnetic Stirrer, LMS-100, Korea) for 30 min. Then it was continuously stirred in a reducing agent and a covering agent of the prepared orange leaf extract until the mixture turned dark brown and a precipitate formed. To ensure a homogeneous reaction, this process was carried out with continuous stirring. The collected precipitate solution was centrifuged (Hermie Laborti Chink Type Z 200 A, 6000 rpm, Germany) at 5000 rpm for 20 min with DI water repeatedly. The dried precipitate powder was heated at 700°C for 8 h (Furnaces oven Vindon LTD, Oldham, England) to obtain dark red Fe_3O_4 nanoparticles.

The NPs were characterized by using a field emission scanning electron microscope (FESEM, ZEISS model: Sigma VP-UK). X-ray diffraction (XRD) patterns were obtained using Siemens model

D500, Germany. Surface functional groups of the NPs were determined by using Fourier-transform infrared spectroscopy (FTIR, IRPrestige-21 Shimadzu, Japan). The optical transmission/absorption spectra of the particles in deionized water were recorded using a UV-VIS spectrometer (Shimadzu 1800, Japan) and energy disperse x-ray spectroscopy (EDX, Oxford Instruments, UK).

Adsorption experiments. The adsorption experiment was conducted by applying a continuous system by taking a weight (0.01 g) of the Fe_3O_4 NPs and bringing it into contact with the volume (10 ml) of (CV) dye solution at a concentration of 11 mg/L by using a water bath shaker (Labtech, South Korea) at laboratory temperature, 150 rpm agitation speed, and over time periods 0–120 min, and each sample is separated by a centrifuge in order to be measured. Each solution was analyzed by the spectrometer (Shimadzu 1800, Japan), and the amount of adsorbed dye and the percentage of adsorption (A%) are calculated through the following equations (1, 2), respectively [16, 17]:

$$q_e = \left(\frac{C_o - C_t}{m} \right) V \quad (1)$$

$$\%A = \left(\frac{C_o - C_t}{C_o} \right) \times 100 \quad (2)$$

where C_o and C_t are the CV dye concentrations at time ($t = \text{zero}, t$) respectively. The $V(\text{L})$ represents the volume of the CV dye solution, whereas $m(\text{g})$ symbolizes the adsorbent weight [18, 19].

Results and discussion

Characterization of Fe_3O_4 NPs

XRD analysis. Figure 1 shows the XRD pattern of the intermediate iron oxide nanoparticles in orange leaf water extract within the range ($2\theta = 5-80^\circ$) showed weak and few peaks, reflecting the low level of crystallinity in the resulting material. In addition, the diffraction peaks were identified at $31.18, 33.34, 35.79, 40.95, 49.56, 54.27$, and 64.14 , respectively, indexed to 10-2, 104, 110, 20-4, and 116, which belong to magnetite nanoparticles Fe_3O_4 (JCPDS 00-019-062). There were no additional peaks in the XRD pattern, indicating the high purity of the $\alpha\text{-Fe}_2\text{O}_3$ nanoparticles. The average crystallite size calculated using the Debye-Scherrer equation for the synthesized green hematite nanoparticles was about 68.5 nm [20, 21].

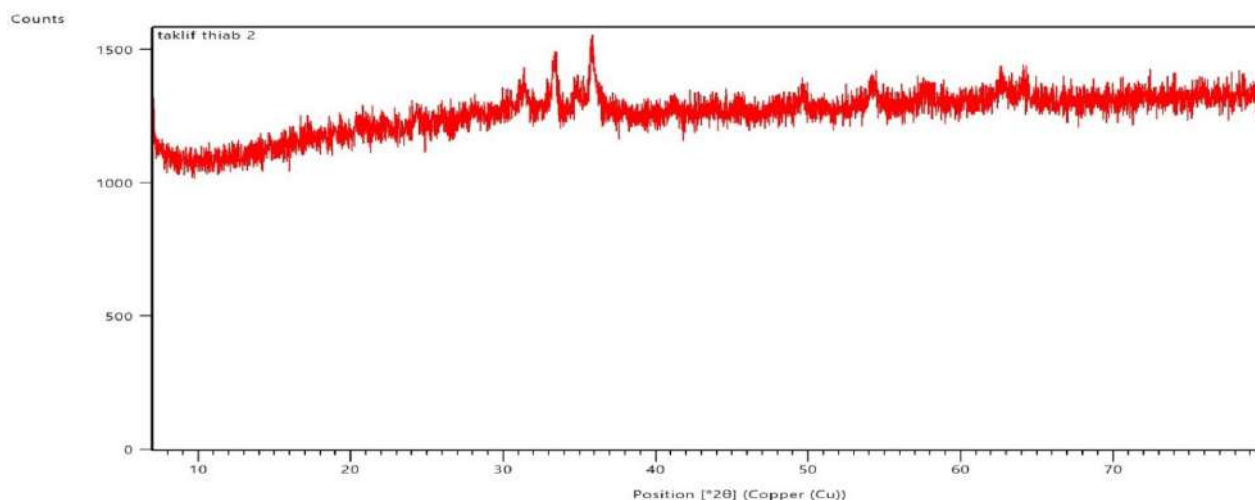


Figure 1 – XRD pattern of iron oxide (α -Fe₂O₃)

FT-IR analysis. Figure 2 FTIR analysis shows the functional groups of phytochemicals and Fe₃O₄ nanoparticles within the range 400-4000 cm⁻¹. Weak peaks were found at 3087 and 2885 cm⁻¹ due to the stretching of the aromatic and aliphatic C-H groups, respectively. There is also a peak at 1510 cm⁻¹ attributed to the stretching of the N=O group, while the peak 1112 cm⁻¹ is attributed to the stretching

of C-O. Therefore, all peaks can be attributed to the phytochemicals in the aqueous extract, which are supposed to be responsible for the reduction of metal ions and their forms to the nanomaterials. The presence of magnetite nanoparticles can also be confirmed by the strong peaks around 455 and 534 cm⁻¹ corresponding to the Fe-O stretches of Fe₃O₄ [22, 23].

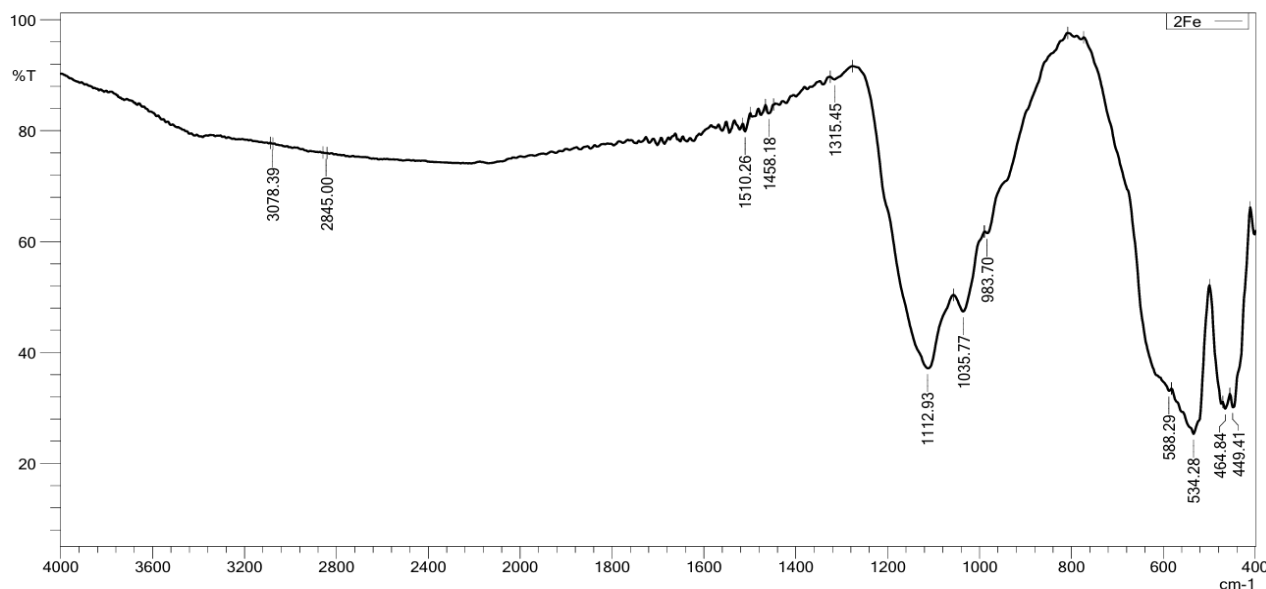


Figure 2 – Spectrum FT-IR pattern of iron oxide NPs

FE-SEM analysis. Figure 3 shows a field-emitted scanning electron microscope image of the surface morphology of the synthesized iron oxide nanoparticles in the orange leaf aquatic extract at a magnification level of 100 nm. The image showed the aggregation

of particles in the form of extended, heterogeneous, semi-spherical nano-clusters of Fe_3O_4 . The size of these particles reaches 30 nm in that specific part of the image, and it agrees with the average size calculated according to XRD data in being less than 100 nm [24].

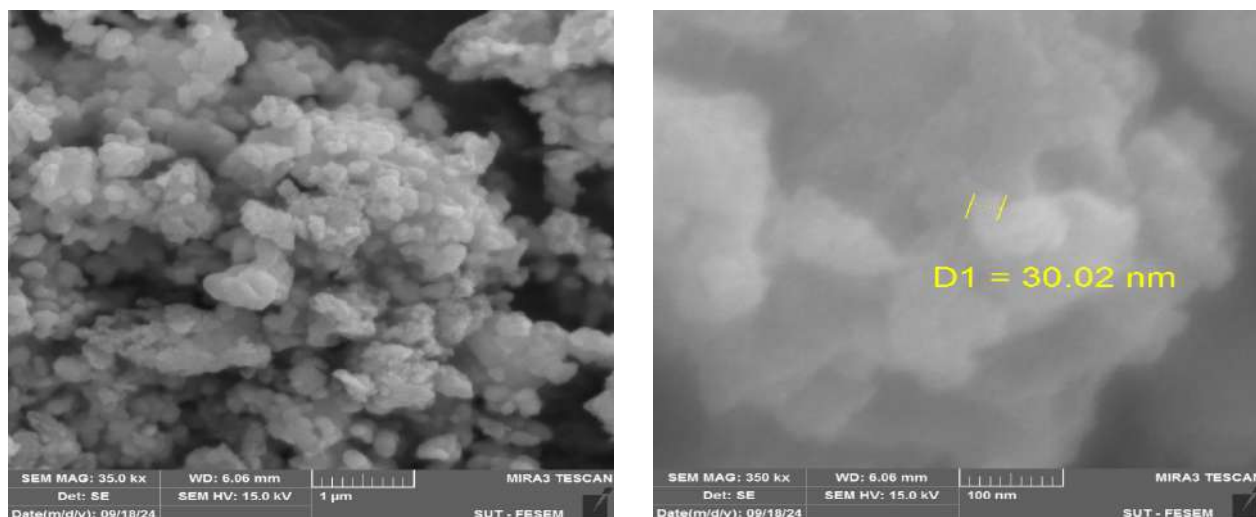


Figure 3 – SEM observation of iron oxide NPs at 100nm, 1 μm

EDX Analysis. Figure 4 shows the energy dispersion X-ray (EDX) results of Fe_3O_4 nanoparticles that were manufactured in a green and environmentally friendly way (orange leaf aquatic extract). The per-

centages of the elements that make up the resulting nano-iron oxide were as follows: 80.04% of O and 19.96% of Fe, indicating the success of preparing nano-iron oxide with high purity [25, 26].

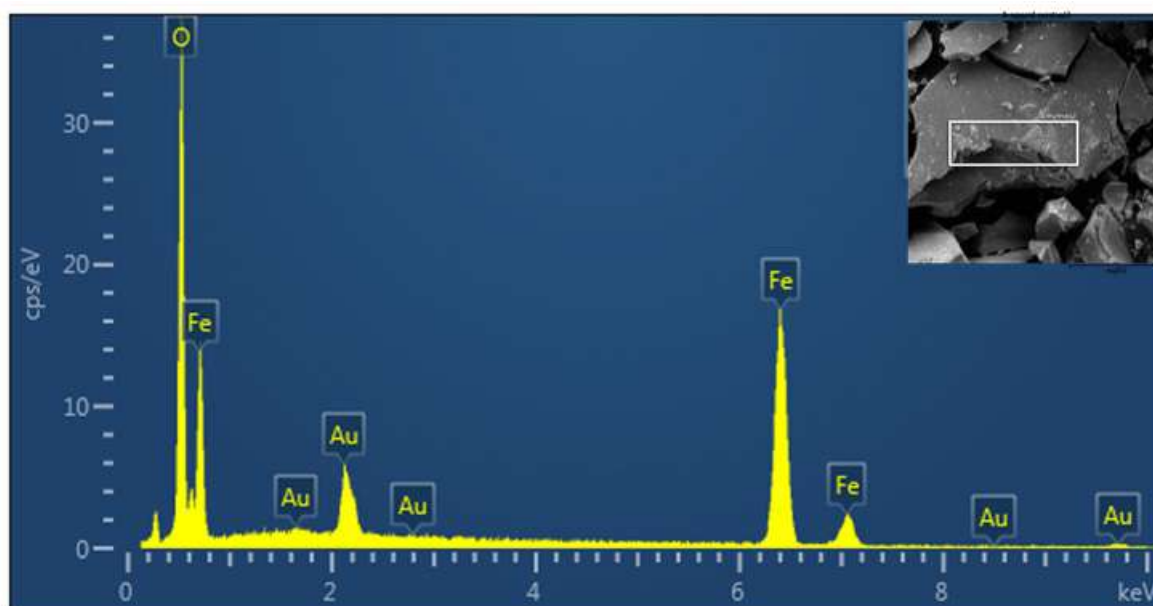


Figure 4 – EDX Analysis of iron oxide NPs

UV-vis analysis. Figure 5 shows the UV-vis spectrum in the range 300-600 nm and here reflects the characteristic formation of nanoparticles during

color change based on absorption spectra. The characteristic peak at 318 nm confirmed the formation of Fe_3O_4 nanoparticles [23].

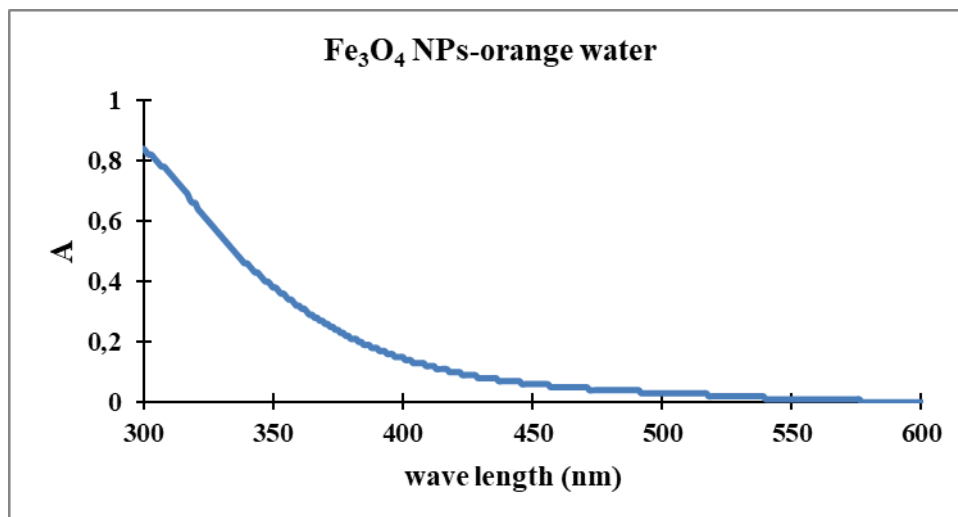


Figure 5 – UV-Vis spectrum of iron oxide NPs

Study of CV dye adsorption. The adsorption efficiency of iron nanoparticles CV dye was studied over a time period of 15-180 min and at constant conditions including pH 7, initial CV concentration of 11 mg/L, Fe_3O_4 nanoparticle weight of 0.01 g, and vibration speed of 150 rpm at 298 K. The amount of adsorbed CV dye increases with time and reaches

equilibrium at about 90 min, after which the removal rate remains constant. This may indicate that CV particles with a large surface area can adhere to the Fe_3O_4 nanoparticle adsorbent for at least 90 min after saturation of the unoccupied surface sites, with adsorption efficiency up to 61% ($q_e = 6.7$ mg/g) as shown in Figures 6 and 7 [27, 28].

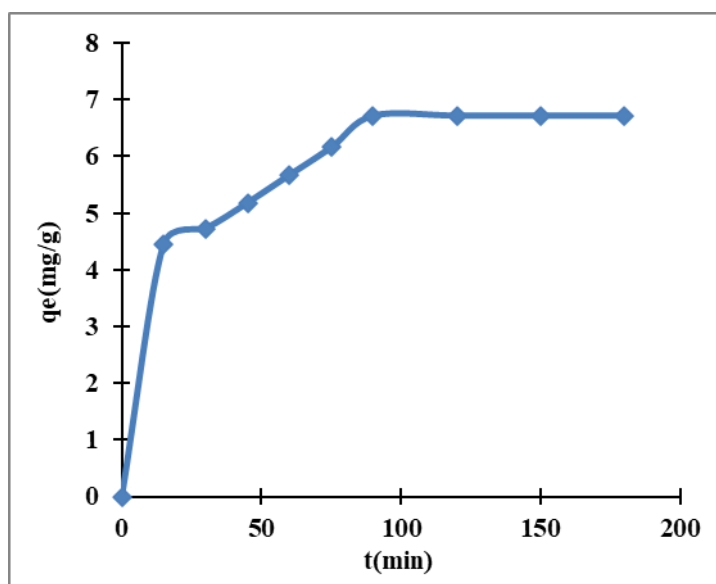


Figure 6 – Effect of contacting time on the quantity adsorption of CV dye on Fe_3O_4 NPs

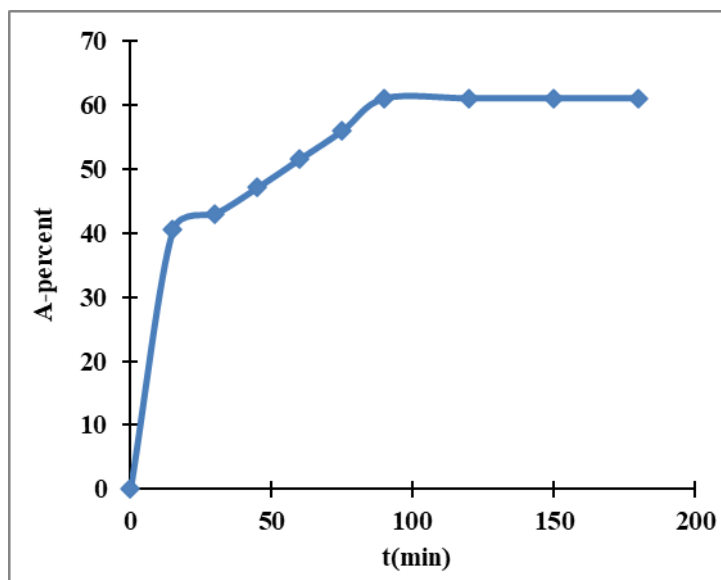


Figure 7 – Effect of contacting time on the percent adsorption of CV dye on Fe_3O_4 NPs

Conclusion

This study concludes the success of applying the green method by using the aqueous extract of orange leaves with reduction and coating in the preparation of nano-ferric oxide particles. This was confirmed by using several techniques. Through the X-ray diffraction technique (XRD) and the Debye-Scherrer equation and matching it with standard data, we conclude that they are low-crystalline nanomaterials with an average size of 68.5 nm. From the Fourier transform infrared technique (FT-IR), the presence of the active group Fe-O which is due to the nano-iron oxide, while we concluded the semi-spherical shape from the images of the scanning electron microscope with the emission field (FESEM). By measuring the disperse energy of the X-ray spectroscopy (EDX) and the ratio of iron to oxygen, we found that the prepared materials are iron oxide with high purity. From measuring the UV-vis spectroscopy, there is a broad

peak starting from wave length 400 nm and extending to 300 nm, which indicates that the prepared material is nano-iron oxide. The nano-iron oxide was tested in the field of treating water pollution with organic dyes, which is the crystal violet dye (CV), and showed good efficiency in removing the CV dye. The purple crystalline color gives a good impression of the efficiency of green materials in water treatment.

Acknowledgments

The authors thank the Department of Chemistry, College of Education for Pure Sciences, Ibn Al-Haytham, University of Baghdad for their assistance with tools, equipment, and laboratories.

Conflict of interest

The authors declare the absence a conflict of interest warranting disclosure in this article.

References

1. Veeranna S., Burhanuddin A., Khanum S., Narayan S. L., Pratima K. (2013) Biosynthesis and antibacterial activity of silver nanoparticles. *Res. J. Biotechnol.*, 8, pp. 11-17. https://www.researchgate.net/publication/287478569_Biosynthesis_and_antibacterial_activity_of_silver_nanoparticles
2. Lassoued A., Dkhil B., Gadri A., Ammar S. (2017) Control of the shape and size of iron oxide ($\alpha\text{-Fe}_2\text{O}_3$) nanoparticles synthesized through the chemical precipitation method. *Results Phys.*, 7, pp. 3007-3015. <https://doi.org/10.1016/j.rinp.2017.07.066>.
3. Ali A., Zafar H., Zia M., ul Haq I., Phull A.R., Ali J.S., Hussain A. (2016) Synthesis, characterization, applications, and challenges of iron oxide nanoparticles. *Nanotechnol Sci Appl.*, 9, pp. 49-67. <https://doi.org/10.2147/NSA.S99986>.



4. Wu W., He Q., Jiang C. (2008) Magnetic iron oxide nanoparticles: synthesis and surface functionalization strategies. *Nanoscale Res. Lett.*, 3, pp. 397-415. <https://doi.org/10.1007/s11671-008-9174-9>.
5. Teja A.S., Koh P.Y. (2009) Synthesis, properties, and applications of magnetic iron oxide nanoparticles. *Prog. Cryst. Growth Charact. Mater.*, 55, pp. 22-45. <https://doi.org/10.1016/j.pcrysgrow.2008.08.003>.
6. Kefeni K.K., Msagati T. A., Nkambule T.T., Mamba B.B. (2018) Synthesis and application of hematite nanoparticles for acid mine drainage treatment. *J. Environ. Chem. Eng.*, 6, pp. 1865-1874. <https://doi.org/10.1016/j.jece.2018.02.037>.
7. Wu C., Yin P., Zhu X., OuYang C., Xie Y. (2006) Synthesis of hematite (α -Fe₂O₃) nanorods: diameter-size and shape effects on their applications in magnetism, lithium ion battery, and gas sensors. *J. Phys. Chem. B*, 110, pp. 17806-17812. <https://doi.org/10.1021/jp0633906>.
8. Alshehri A., Malik M. A., Khan Z., Al-Thabaiti S.A., Hasan N. (2017) Biofabrication of Fe nanoparticles in aqueous extract of Hibiscus sabdariffa with enhanced photocatalytic activities. *RSC Adv.*, 7, pp. 25149-25159. <https://doi.org/10.1039/C7RA01251A>.
9. Ruddaraju L.K., Pammi S.V.N., sankar Guntuku G., Padavala V.S., Kolapalli V.R.M. (2020) A review on anti-bacterials to combat resistance: From ancient era of plants and metals to present and future perspectives of green nano technological combinations. *Asian J. Pharm. Sci.*, 15, pp. 42-59. <https://doi.org/10.1016/j.ajps.2019.03.002>.
10. Pallela P.N.V.K., Ummey S., Ruddaraju L.K., Pammi S.V.N., Yoon S.G. (2018) Ultra Small, mono dispersed green synthesized silver nanoparticles using aqueous extract of *Sida cordifolia* plant and investigation of antibacterial activity. *Microb. Pathog.*, 124, pp. 63-69. <https://doi.org/10.1016/j.micpath.2018.08.026>.
11. Acharyulu N.P.S., Madhu Kiran P., Pratap K., Kalyani R.L., Pammi S.V.N. (2014) Room temperature synthesis and evaluation of antibacterial activity of silver nanoparticles using *Phyllanthus amarus* leaf extract. *J. Bionanoscience*, 8, pp. 190-194. <https://doi.org/10.1166/jbns.2014.1220>.
12. Radhi I.M., Abd S.S., Faraj R.A.S., Abbas A.M., Himdan T.A. (2024) Using activated and modified adsorbent surfaces from banana peels to remove the green Janus dye: A Kinetic, Isothermal, and Thermodynamic Study. *Mong. J. Chem.*, 25, pp. 1-15. <https://doi.org/10.5564/mjc.v25i52.3450>.
13. Pallela P.N.V.K., Ummey S., Ruddaraju L.K., Kollu P., Khan S., Pammi S.V.N. (2019) Antibacterial activity assessment and characterization of green synthesized CuO nano rods using *Asparagus racemosus* roots extract. *SN Appl. Sci.*, 1, pp. 1-7. <https://doi.org/10.1007/s42452-019-0449-9>.
14. Pallela P.N.V.K., Ummey S., Ruddaraju L.K., Gadi S., Cherukuri C.S.L., Barla S., Pammi S.V.N. (2019) Antibacterial efficacy of green synthesized α -Fe₂O₃ nanoparticles using *Sida cordifolia* plant extract. *Heliyon*, 5, pp. e02765. <https://doi.org/10.1016/j.heliyon.2019.e02765>.
15. Hemalatha S., Venkatesan R.S. (2021) Fabrication of Iron Oxide Nano Particle Using Cassia Auriculata leaf Extract and its Characterization. *Ann Rom Soc Cell Biol*, 25, pp. 1683-1689. <http://annalsofscb.ro/index.php/journal/article/view/1614>.
16. Jasim M.A., Abbas A.M., Radhi I.M. (2021) Preparation and characterization of biomass-alumina composite as adsorbent for safranin-o dye from aqueous solution at different temperatures. *AIP Conf. Proc.*, 2372, pp. 120001-120012. <https://doi.org/10.1063/5.0068746>.
17. Abbas A.M., Abd S.S., Abdulhadi H.T. (2018) Kinetic Study of Methyl Green Dye Adsorption from Aqueous Solution by Bauxite Clay at Different Temperatures. *Ibn al-Haitham J. Pure Appl. Sci.*, 31, pp. 58-66. <https://doi.org/10.30526/31.1.1853>.
18. Mizhir A.A., Al-Lami H.S., Abdulwahid A.A. (2022) Kinetic, isotherm, and thermodynamic study of bismarck brown dye adsorption onto graphene oxide and graphene oxide-grafted-poly (n-butyl methacrylate-co-methacrylic acid). *Baghdad Sci. J.*, 19, pp. 0132-0132. <https://doi.org/10.21123/bsj.2022.19.1.0132>.
19. Saed S.A., AL-Mammar D.E. (2021) Influence of Acid Activation of a Mixture of Illite, Koalinite, and Chlorite Clays on the Adsorption of Methyl Violet 6B Dye. *Iraqi J. Sci.*, 62(6), pp. 1761-1778. <https://doi.org/10.24996/ijss.2021.62.6.2>.
20. Rasha T.S., Dunya E.A. (2023) Adsorption of Azo Dye Onto TiO₂ Nanoparticles Prepared by a Novel Green Method: Isotherm and Thermodynamic Study. *Iraqi J. Sci.*, 64(8), pp. 3779-3792. <https://doi.org/10.24996/ijss.2023.64.8.5>.
21. Abbas A.M., Mohammed Y.I., Himdan T.A. (2017) Adsorption kinetic and thermodynamic study of congo red dye on synthetic zeolite and modified synthetic zeolite. *Ibn al-Haitham J. Pure Appl. Sci.*, 28, pp. 54-72. <https://jih.uobaghdad.edu.iq/index.php/j/article/view/190>.
22. Abbas A.M., Abdulrazzak F.H., Radhi I.M., Himdan T.A., Hussein F.H. (2020) Purification Techniques for Cheap Multi-Walled Carbon Nanotubes. *J. Phys. Conf. Ser.*, 1660, pp. 012022. <https://doi.org/10.1088/1742-6596/1660/1/012022>.
23. Rufus A., Sreeju N., Philip D. (2016) Synthesis of biogenic hematite (α -Fe₂O₃) nanoparticles for antibacterial and nanofluid applications. *RSC Adv.*, 6, 94206-94217. <https://doi.org/10.1039/C6RA02040C>.
24. Jawad H., Abbas A.M. (2021) Study of Efficacy Adsorption of Methyl Green by Attapulgit and Modified Attapulgit Clay from Aqueous Solution. *Ibn al-Haitham J. Pure Appl. Sci.*, 34, pp. 19-29. <https://doi.org/10.30526/34.1.2550>.
25. Kazem M.S., Abbas A.M. (2022) Study of inorganic doping of kaolin clay, a kinetic study of adsorption of methyl green dye from its aqueous solutions. *Eurasian Chem. Commun.*, 4(12), pp. 1218-1227. <https://doi.org/10.22034/ecc.2022.342243.1467>.
26. Abbas A.M., Merza S.H. (2020) Preparation and Characterization of Graphene Oxide-Attapulgit composite and its use in kinetic study of Alizarin Dye Adsorption from Aqueous Media. *Egypt. J. Chem.*, 63, pp. 561-572. <https://doi.org/10.21608/ejchem.2019.15600.1946>.

27. Yass D.A., Abbas A.M. (2024) Study the efficiency of titanium dioxide nanoparticles for water treatment from Congo red dye. *Her. Bauman Mosc. State Tech. Univ. Ser. Nat. Sci.*, 115, pp. 121–131. <https://vestniken.bmstu.ru/eng/catalog/chem/orch/1163.html>.
28. Faraj R.A.S., Abbas A.M. (2021) Loading and Activating a Carbon Surface and Applied for Congo Red Adsorption, Kinetic Study. *J. Phys. Conf. Ser.*, 1879, pp. 022076. <https://doi.org/10.1088/1742-6596/1879/2/022076>.

Information about authors

Takleef Dheyab Sallal – Assistant Lecturer, College of education for pure sciences (Ibn Al-haitham), University of Baghdad (Baghdad, Iraq, e-mail: sallaltakleef535@gmail.com)

Ahmed Mohammed Abbas – PhD, Assistant Professor, College of education for pure sciences (Ibn Al-haitham), University of Baghdad (Baghdad, Iraq, e-mail: ahmed.m.a@ihcoedu.uobaghdad.edu.iq)

A.A. Minkayeva¹ , L. Azilbek¹ , U. Amzeyeva^{1,2} ,
T. Karunakaran³ , X. Liu⁴ , X. Shang⁵ , N. Muzaffarova⁶ , J. Jenis^{1*} 

¹The Research Center for Medicinal Plants, Al-Farabi Kazakh National University, Almaty, Kazakhstan

²Research Institute for Natural Products & Technology, Almaty, Kazakhstan

³Centre for Drug Research, University Sains Malaysia, Pulau Pinang, Malaysia

⁴Beijing Technology and Business University, Beijing, China

⁵Lanzhou Institute of Husbandry and Pharmaceutical Sciences, CAAS, Lanzhou, China

⁶Department of Medical and Biological Chemistry, Termez branch of Tashkent Medical Academy, Termez, Uzbekistan

*e-mail: janarjenis@kaznu.kz

(Received 29 April 2025; received in revised form 8 June 2025; accepted 18 June 2025)

Comparative investigation of *Rheum tataricum* and *Rheum palmatum*

Abstract: Medicinal plants have played a crucial role in both traditional and modern medicine for centuries. Among these, *Rheum tataricum* and *Rheum palmatum* have attracted significant attention due to their diverse pharmacological properties and rich chemical compositions. Despite their widespread use, detailed comparative studies of these species remain limited. This study aims to provide a comprehensive evaluation of their morphological characteristics, chemical profiles, and pharmacological effects to enhance their application in medicine and drug development. The study involved the identification of liposoluble constituents in *R. tataricum* and *R. palmatum* using Gas Chromatography-Mass Spectrometry (GC-MS). The chemical compositions of both species were investigated, and their bioactive compounds were quantified. The pharmacological significance of key compounds such as oleic acid, hexadecanoic acid, octadecadienoic acid, chrysophanol, and apocynin was evaluated based on existing literature.

GC-MS analysis revealed distinct differences in the chemical compositions of *R. tataricum* and *R. palmatum*. The Chinese species, *R. palmatum*, contained twenty-four compounds, with oleic acid (53.9±0.09%) as a predominant constituent. In contrast, *R. tataricum* from Kazakhstan contained eighteen compounds, with a notably higher content of chrysophanol (35.1±0.05%). Hexadecanoic acid (18.9%) was found to be a major component in both species, demonstrating moderate antibacterial activity. Other bioactive compounds such as octadecadienoic acid, 9,10-anthracenedione, apocynin, and orcinol were detected, indicating their potential therapeutic applications.

This comparative study provides valuable insight into the chemical compositions and pharmacological relevance of *R. tataricum* and *R. palmatum*. The significant variation in bioactive compound concentrations suggests distinct therapeutic potentials. These findings support the rational use of these medicinal plants in pharmaceutical applications and highlight their relevance in both drug discovery and traditional medicine practices.

Key words: Medicinal plants, *Rheum tataricum*, *Rheum palmatum*, phytochemical content, GC-MS.

Introduction

Medicinal plants have long held a pivotal position in both traditional and modern medicine. For centuries, they have been the cornerstone of treating a wide array of diseases and health conditions, and their significance in the medical field is indisputable [1]. Among the vast number of medicinal plants, *Rheum tataricum* and *Rheum palmatum* have emerged as two highly valuable species that have attracted global research interest.

Rheum tataricum, commonly referred to as Tatarian rhubarb, belongs to the genus *Rheum* in the family Polygonaceae. It is mainly distributed in certain regions of Central Asia and Eastern Europe, thriving in mountainous areas with specific climate and soil conditions [2]. Its root, which is thick and fleshy with a brownish-black outer layer, has been used in traditional medicine for its laxative and anti-inflammatory properties [3]. Traditional healers have prepared it in various forms such as decoctions, powders, and tinctures to treat digestive disorders such as constipa-

tion and indigestion, as well as to relieve joint pain, inflammation, and treat various skin diseases [4]. In terms of its chemical composition, *Rheum tataricum* is rich in anthraquinones, such as emodin, chrysophanol, and aloe-emodin, which are thought to contribute to its laxative and anti-inflammatory effects. It also contains flavonoids, tannins, and polysaccharides, which may play roles in its antioxidant and immunomodulatory activities [5].

Rheum palmatum, also known as Chinese rhubarb, is another member of the genus *Rheum*. It is native to China and widely distributed in the mountainous regions of western and central China [6]. Growing in high-altitude areas with a cool climate and well-drained soil, it has a large and robust root with a dark brown or blackish outer bark. In traditional Chinese medicine, it has a long and rich history of use. Considered one of the most important medicinal plants, it is used for a broad range of therapeutic purposes. The root and rhizome are commonly used, and it is renowned for its strong purgative effect, often used to treat constipation and to clear internal heat [7]. Additionally, it exhibits antibacterial, anti-inflammatory, and antioxidant properties and has been applied in the treatment of liver diseases, infectious diseases, and certain types of cancers [8]. *Rheum palmatum* is also abundant in anthraquinones, but the content and proportion of different anthraquinone derivatives may vary compared to *Rheum tataricum*. Besides anthraquinones, it contains other bioactive components such as stilbenes, phenolic acids, and volatile oils. These compounds contribute to its diverse pharmacological activities, including antibacterial, anti-inflammatory, and antioxidant effects [9].

With the increasing interest in natural products for medicinal purposes, a comprehensive understanding of these two plants becomes crucial for further exploration and utilization. Their rich chemical compositions and diverse biological activities make them promising sources for developing of new drugs and therapies [10].

Research Objectives. The primary aim of this study is to conduct a detailed comparison between *Rheum tataricum* and *Rheum palmatum*. This comparison will cover their morphological characteristics, chemical compositions, pharmacological effects, and clinical applications. By systematically analyzing the differences and similarities between these two species, we intend to provide a scientific basis for their rational utilization and development. Such a comparison will not only facilitate better identification and classification of these plants but also contribute to a

more in-depth understanding of their potential in the pharmaceutical and medical fields.

Research Significance. From a theoretical perspective, this comparative study will greatly enrich the knowledge base of medicinal plant science. It will deepen our understanding of the relationships between different species within the *Rheum* genus and contribute to the development of plant taxonomy and pharmacognosy [11]. By identifying the unique features and properties of *Rheum tataricum* and *Rheum palmatum*, we can gain valuable insights into the evolutionary adaptations and biological functions of these plants.

In practical terms, the results of this study will have significant implications for drug development and clinical application. Understanding the differences in chemical compositions and pharmacological effects between the two plants can assist researchers in selecting the most suitable plant material for specific drug targets. This can lead to the development of more effective and targeted drugs, shortening the cost and time of drug discovery. Moreover, for traditional medicine practitioners, this research can provide scientific evidence to support the rational use of these plants in clinical practice, thereby improving the safety and efficacy of traditional therapies [12].

Materials and methods

Plant raw material. *Rheum tataricum* was collected during the plant expedition around the Almaty region in May 2024. Specifying, 12 kilometers away from Kokbek village with the geographical location coordinates 43.400270 and 78.806415 referring to latitude and longitude, accordingly. *Rheum palmatum* were acquired from China, as it is endemic to Chinese lands. Both species were slightly washed with pure water, dried in sunless place, crushed into small pieces by After being thoroughly dried in the shade, raw materials were crushed into small pieces using a herb grinder machine 2500Y (Yongkang Boou Hardware Products Co., Ltd., China) and stored at room temperature.

Quantitative and qualitative analysis

The moisture content and ash of raw herbal plant materials were determined in accordance with the standards of the state Pharmacopeia [13, 14].

Analytical balances, a SNOL 67/350 dryer (AB UMEGA, Lithuania), a muffle furnace, and a desiccator can be used to quantitatively assess raw materials, including moisture content and ash percentage. Extractive compounds must be identified using a reflux condenser, drier, and balances. Flavonoids,

free organic acids, alkaloids, saponins, tannins, and coumarins are common bioactive classes that can be qualitatively analyzed using equipment such as a flask, reflux condenser, and analytical balances. A UV-5500 UV-VIS spectrophotometer (Shanghai Metash Instruments Co., Ltd, China) was used at various wavelengths to determine the content of flavonoids, saponins, and coumarins. The burette is used to titrate and measure the concentration of free organic acids and alkaloids. Polysaccharides are identified after drying the extract to a uniform volume.

Determination of organic compounds by gas chromatography-mass spectrometry

The analysis of the samples was performed using gas chromatography coupled with mass spectrometric detection (GC-MS) utilizing an Agilent 7890A gas chromatograph and 5975C mass spectrometric detector. The exact conditions including split ratio, velocity and temperature change are shown in the Table 1.

Detection and Data Processing: Detection was conducted in SCAN mode, covering the m/z range of 34–850. Agilent MSD ChemStation software (version 1701EA) was used for system control, data recording, and result processing. Data analysis included determination of retention times, peak areas, and spectral data interpretation using the mass spectrometric detector.

Spectral Libraries: The identification of mass spectra was performed using the Wiley 7th Edition and NIST'02 libraries, containing over 550,000 spectra.

Table 1 – Condition of analysis for organic compounds identification by GC-MS

<i>Analysis conditions</i>	
Sample Volume	0.5 μ L
Sample Insertion Temperature	280 °C
Split Ratio	10:1
Solvent Delay	10 minutes
Chromatographic Column	DB-WAXetr capillary column
Carrier Gas	Helium
Constant velocity	1 mL/min
<i>Temperature Program</i>	
Initial temperature	40°C
Heating rate	5°C/min
Final temperature	260°C (held for 5 minutes)
Total analysis time	49 minutes

Results and discussion

Quantitative and qualitative analysis of bioactive constituent classes

As a fundamental step, the cleaned and dried plant material was checked for authenticity that implies the content of moisture, ash and substances extracted by different concentration of water-ethanol concentrations. The classes of biologically active compounds identified include flavonoids, polysaccharides, free organic acids, coumarins, tannins. The results of identification are shown in Table 2.

Table 2 – The quantitative-qualitative analysis of *R. tataricum* and *R. palmatum*

Authenticity	<i>R. tataricum</i> , %	<i>R. palmatum</i> , %
Moisture	4.30	3.30
Ash content	8.50	8.32
Extractive substances (50% EtOH)	20.9	21.3
Extractive substances (70% EtOH)	38.5	40.1
Extractive substances (96% EtOH)	36.0	32.2
Content of BAC, %		
Free organic acids	0.88	0.47
Flavonoids	0.06	0.04
Polysaccharides	6.36	2.07
Tannins	7.40	3.67
Coumarins	3.64	2.40

The analysis of *R. tataricum* and *R. palmatum* revealed differences in moisture content, ash content, and extractive substances obtained using various ethanol concentrations. These findings provide insights into the composition of these species and their potential applications in different industries. Moisture content plays a critical role in the stability and storage of plant materials. *R. tataricum* exhibited a higher moisture content (4.30%) compared to *R. palmatum* (3.30%). This difference may indicate varying degrees of hygroscopicity and suggests that *R. tataricum* might require more stringent drying conditions to prevent microbial growth and degradation. The ash content, which represents the total mineral composition of the plant material, was similar between the two species, with *R. tataricum* containing 8.50% and *R. palmatum* containing 8.32%. These values suggest that both species have comparable inorganic constituents, which may influence their potential use in pharmaceutical or food applications.

The yield of extractive substances varied depending on the ethanol concentration used. When extracted with 50% ethanol, *R. palmatum* yielded a slightly higher extractive content (21.3%) compared to *R. tataricum* (20.9%). This trend continued with 70% eth-

anol, where *R. palmatum* (40.1%) exhibited a greater extractive yield than *R. tataricum* (38.5%). However, at 96% ethanol, *R. tataricum* (36.0%) had a higher yield than *R. palmatum* (32.2%). These variations indicate differences in the solubility of phytochemicals present in the plants, suggesting that *R. palmatum* may contain more polar compounds while *R. tataricum* retains higher levels of less polar compounds. In general, 70% ethanol-water solvent is more effective and appropriate than 50% and 96% ethanol.

The observed differences in extractive yields imply that different solvent concentrations may be required to optimize the extraction of bioactive compounds from these species. The higher yield in 70% ethanol extraction suggests the presence of a significant amount of both polar and non-polar compounds in both plants. Additionally, the higher extractive yield in 96% ethanol for *R. tataricum* indicates potential for extracting lipophilic components, which could be relevant for pharmaceutical and cosmetic applications. Overall, these findings provide valuable insights into the chemical composition of *R. tataricum* and *R. palmatum*, contributing to the understanding of their potential applications in herbal medicine, nutraceuticals, and related fields.

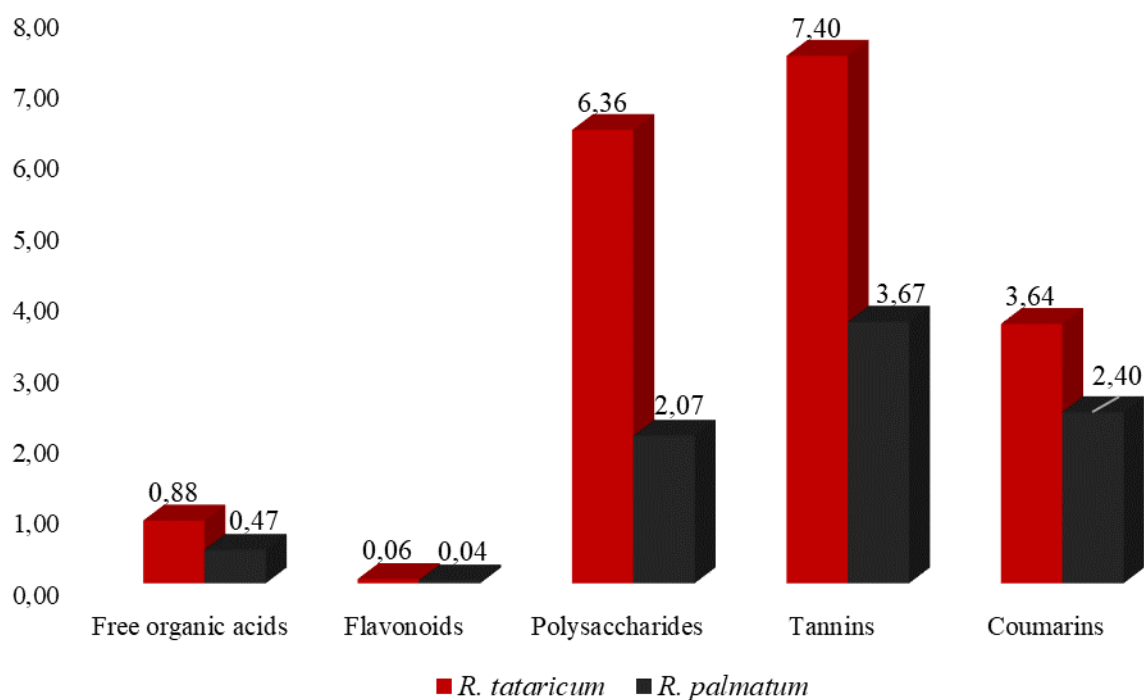


Figure 1 – Comparative content of bioactive compounds in *R. tataricum* and *R. palmatum*

The comparative analysis of biologically active compounds (BACs) in *Rheum tataricum* and *Rheum palmatum* revealed significant differences in their composition. The content of free organic acids in *R. tataricum* (0.88%) was almost twice as high as that in *R. palmatum* (0.47%). This suggests that *R. tataricum* may exhibit stronger acidity, potentially influencing its pharmacological properties, such as antimicrobial and digestive activities. The higher level of free organic acids in *R. tataricum* could contribute to its greater solubility and enhanced bioavailability of active components.

Flavonoid content was slightly higher in *R. tataricum* (0.06%) compared to *R. palmatum* (0.04%). Flavonoids are known for their antioxidant, anti-inflammatory, and cardioprotective effects. The minor difference in flavonoid content indicates that both species may have similar antioxidant potential, though *R. tataricum* may have a slight advantage in this regard.

A notable difference was observed in the polysaccharide content, with *R. tataricum* containing a significantly higher amount (6.36%) compared to *R. palmatum* (2.07%). Polysaccharides are essential bioactive compounds known for their immunomodulatory, prebiotic, and anti-inflammatory properties. The substantial difference suggests that *R. tataricum* may offer superior immune-boosting benefits and better support for gut health compared to *R. palmatum*. Tannin levels in *R. tataricum* (7.40%) were considerably higher than in *R. palmatum* (3.67%). Tannins are known for their astringent properties and their ability to enhance wound healing, provide antimicrobial effects, and regulate digestion. The higher tannin content in *Kazakhstani Rheum* suggests it may have stronger therapeutic potential in gastrointestinal

health and antimicrobial applications. The coumarin content in *R. tataricum* (3.64%) was also higher than in *R. palmatum* (2.40%). Coumarins possess anticoagulant, anti-inflammatory, and antimicrobial properties. The increased presence of coumarins in *R. tataricum* may indicate greater potential for cardiovascular protection and anti-inflammatory applications compared to *R. palmatum*.

Overall, the results indicate that *R. tataricum* consistently contains higher levels of biologically active compounds compared to *R. palmatum*. This suggests that *R. tataricum* may have a broader pharmacological spectrum and potentially stronger therapeutic effects. The higher concentrations of polysaccharides, tannins, and coumarins in *R. tataricum* make it a promising candidate for applications in immune support, gastrointestinal health, and cardiovascular protection. However, further studies on bioavailability, pharmacokinetics, and clinical efficacy are necessary to validate these findings and determine their practical applications.

Gas chromatography combined with mass spectrometry assay

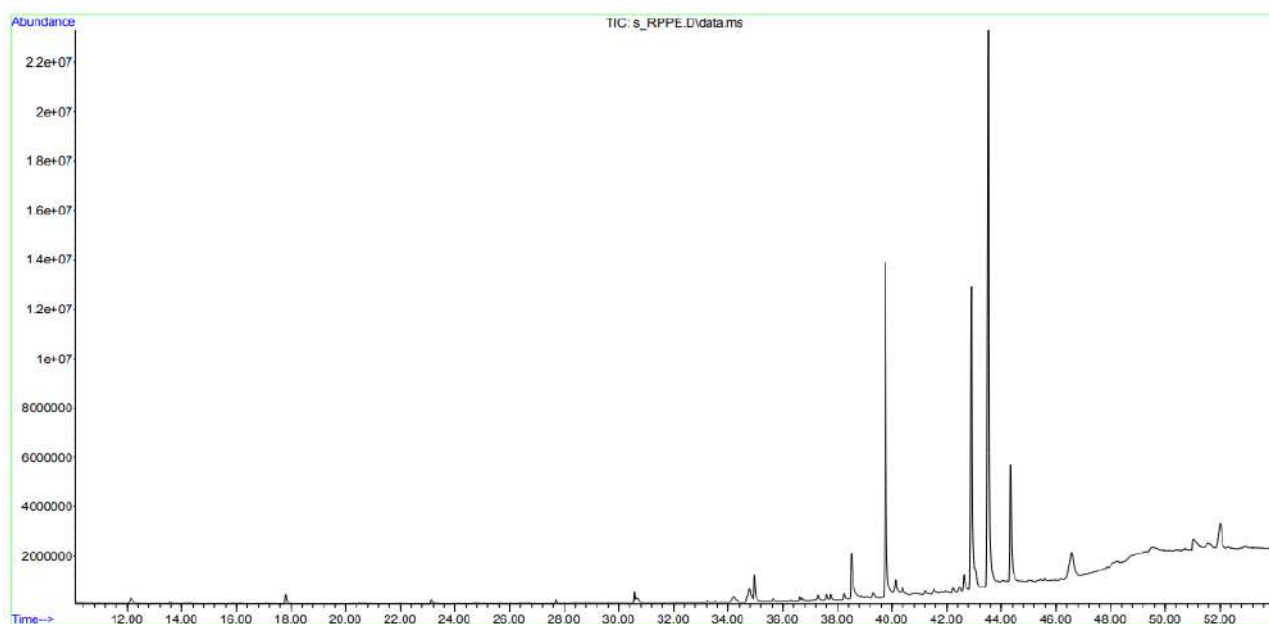
Liposoluble constituents presenting in *R. tataricum* and *R. palmatum* species were identified through the analysis of petroleum ether extracts applying GC-MS. Chinese species, *R. palmatum* consist of twenty-four compounds in general, results are presented in Table 3 together with chromatogram represented in Figure 2. The results of *Rheum tataricum* from Kazakhstan shown in Table 4 and Figure 4, where 18 compounds were identified in general. The content of two species differentiates slightly. All data are expressed as the mean \pm standard deviation of three replicates.

Table 3 – Results of chromatographic analysis of the petroleum ether extract of *R. palmatum*

№	Retention time, min	Constituents	Probability of identification, %	Content, %
1	12.15	1-Butoxy-1-isobutoxy-butane	89	0.9 \pm 0.01
2	17.80	Cyclohexanol, 5-methyl-2-(1-methylethyl)-	92	0.8 \pm 0.01
3	20.50	Benzenepropanoic acid, α -methyl-	68	0.1 \pm 0.01
4	23.13	Benzyl nitrile	90	0.4 \pm 0.01
5	27.70	Eugenol	89	0.3 \pm 0.01
6	30.58	Phenol, 2,4-bis(1,1-dimethylethyl)-	89	0.2 \pm 0.01
7	34.21	Ethyl Oleate	84	1.0 \pm 0.01
8	34.78	9,12-Octadecadienoic acid, ethyl ester	85	1.7 \pm 0.01
9	34.95	Hydrocinnamic acid	90	1.8 \pm 0.01

Continuation of the table

№	Retention time, min	Constituents	Probability of identification, %	Content, %
10	35.64	Ethyl 9,12,15-octadecatrienoate	76	0.3±0.01
11	36.61	Dibutyl phthalate	85	0.2±0.01
12	36.69	Tetradecanoic acid	71	0.2±0.01
13	37.61	2-Butanone, 4-(4-hydroxy-3-methoxyphenyl)-	83	0.3±0.01
14	37.75	Benzenebutanoic acid, 2,5-dimethyl-	76	0.3±0.01
15	38.25	Pentadecanoic acid	77	0.3±0.01
16	38.51	2-Propenoic acid, 3-phenyl-	92	4.2±0.03
17	39.32	Hexadecanoic acid, 1-(hydroxymethyl)-1,2-ethanediyl ester	66	0.5±0.02
18	39.77	Hexadecanoic acid	94	18.9±0.2
19	40.13	9-Hexadecenoic acid	80	1.7±0.02
20	40.40	2-Butanone, 4-(4-hydroxyphenyl)-	81	0.7±0.01
21	42.63	Octadecanoic acid	80	1.4±0.01
22	43.53	Oleic Acid	94	53.9±0.09
23	44.33	9,12,15-Octadecatrienoic acid, (Z,Z,Z)-	92	8.0±0.01
24	51.04	9,10-Anthracenedione, 1,8-dihydroxy-3-methyl-	70	1.8±0.02

Figure 2 – Chromatogram of *Rheum palmatum* L. petroleum ether extract

According to GC-MS analysis of Chinese species of *Rheum*, the higher content of oleic acid (53.9±0.09 %) at 43.53 minutes can be observed. Oleic acid, as shown in Figure 3A, is the predominant monounsaturated fatty acid in the human bloodstream [15]. Within the brain, it serves as a crucial component of membrane phospholipids and is abundantly pres-

ent in myelin [16]. A notable reduction in oleic acid levels has been reported in the brains of individuals suffering from major depressive disorder and Alzheimer's disease [17]. Like all free fatty acids, oleic acid primarily functions as an energy source and a structural element of cell membranes. Consequently, oleic acid is now acknowledged as a multifunctional

nutraceutical and a potent biomolecule. One of its most distinctive properties is its antioxidant capability, as it can directly influence both the synthesis and activity of antioxidant enzymes [18].

Furthermore, Hexadecanoic acid, also known as palmitic acid, with concentration of 18.9 ± 0.2 % identified at 39.77 minutes can be assumed as one of the major components in *Rheum* species. Hexadecanoic

acid (Figure 3B) exhibited moderate antibacterial activity against *S. aureus*, *B. subtilis*, *E. coli*, and *K. pneumoniae* at a maximum concentration of 50 $\mu\text{g/ml}$. For example, Ganesan et al. reported the biological activity of hexadecanoic acid derived from *Ipomoea eriocarpa* and suggests its potential application as a natural antioxidant and antibacterial agent in the pharmaceutical industry [19].

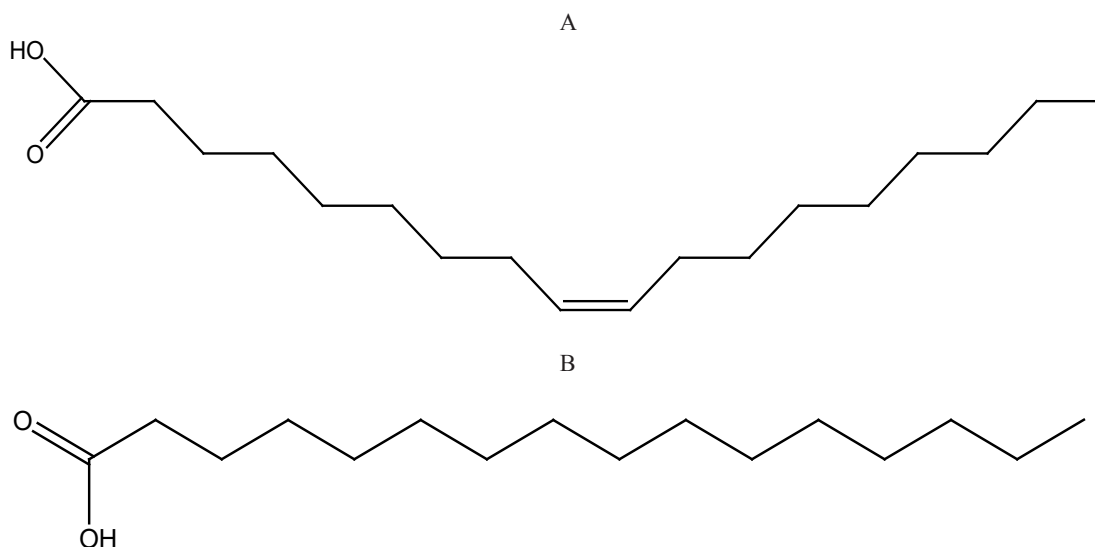


Figure 3 – Structures of oleic acid (A) and Hexadecanoic acid (B)

Other constituents as 9,12,15-Octadecatrienoic acid, (Z,Z,Z)- (8.0 %) and 2-Propenoic acid, 3-phenyl- (4.2 %) are also essential biochemical components in this medicinal plant. Octadecadienoic acid (ODA) is an essential fatty acid, meaning that the human body is unable to synthesize it and must obtain it through dietary intake [20]. ODA serves as a precursor to two

crucial long-chain omega-3 fatty acids, eicosapentaenoic acid and docosahexaenoic acid, both of which play a significant role in inhibiting prostate tumor growth, supporting brain development, promoting cardiovascular health, regulating metabolic-inflammatory responses, and influencing conditions such as obesity, diabetes, and mental disorders [21].

Table 4 – Results of chromatographic analysis of the petroleum ether extract of *R. tataricum*

№	Retention time, min	Constituents	Probability of identification, %	Content, %
1	11.05	Heneicosane	71	1.9 ± 0.02
2	11.43	Cyclohexanol, 5-methyl-2-(1-methylethyl)-, acetate, (1 α ,2 α ,5 β)-	81	1.4 ± 0.01
3	12.95	Cyclohexanol, 1-methyl-4-(1-methylethyl)-	95	7.9 ± 0.02
4	15.62	Hentriacontane	70	3.0 ± 0.01
5	18.23	Benzyl nitrile	72	1.4 ± 0.01
6	25.57	Phenol, 2,4-bis(1,1-dimethylethyl)-	92	6.2 ± 0.01

Continuation of the table

№	Retention time, min	Constituents	Probability of identification, %	Content, %
7	28.13	1H-2-Benzopyran-1-one, 3,4-dihydro-8-hydroxy-3-methyl-	91	17.9±0.04
8	29.17	Octadecanoic acid, ethyl ester	72	2.6±0.02
9	29.30	Phthalic acid, isobutyl 4-octyl ester	68	0.9±0.02
10	29.68	Phthalic acid, isobutyl 4-octyl ester	65	7.2±0.03
11	30.48	Apocynin	63	3.1±0.01
12	31.61	Dibutyl phthalate	90	1.3±0.02
13	32.21	7,9-Di-tert-butyl-1-oxaspiro(4,5)deca-6,9-diene-2,8-dione	66	0.5±0.01
14	34.76	Hexadecanoic acid	75	1.9±0.02
15	35.22	Benzoic acid, 4-hydroxy-3,5-dimethoxy-, hydrazide	68	0.6±0.01
16	37.69	Orcinol	75	2.1±0.01
17	41.17	2',4'-Dihydroxy-3'-methylacetophenone	88	5.0±0.02
18	46.00	9,10-Anthracenedione, 1,8-dihydroxy-3-methyl-	86	35.1±0.05

Compared to *R. palmatum*, the content of 9,10-Anthracenedione, 1,8-dihydroxy-3-methyl- (chrysophanol) in *R. tataricum* (35.1±0.05%) is several times higher. It is the major anthraquinone found in *Rheum* species. Chrysophanol (Figure 5A), a naturally derived anthraquinone compound, has shown great promise in cancer therapy due to its wide range of biological activities [22].

Moreover, there is quantitatively 17.9±0.04% of 1H-2-Benzopyran-1-one, 3,4-dihydro-8-hydroxy-3-methyl- (Figure 5B), which exhibits cytotoxic activity and accelerates the growth of SIV branch [23]. Additionally, two other significant compounds were identified: cyclohexanol, 1-methyl-4-(1-methylethyl)-, which is a tertiary alcohol (7.9±0.02 %) and phthalic acid, isobutyl 4-octyl ester (7.2±0.03 %).

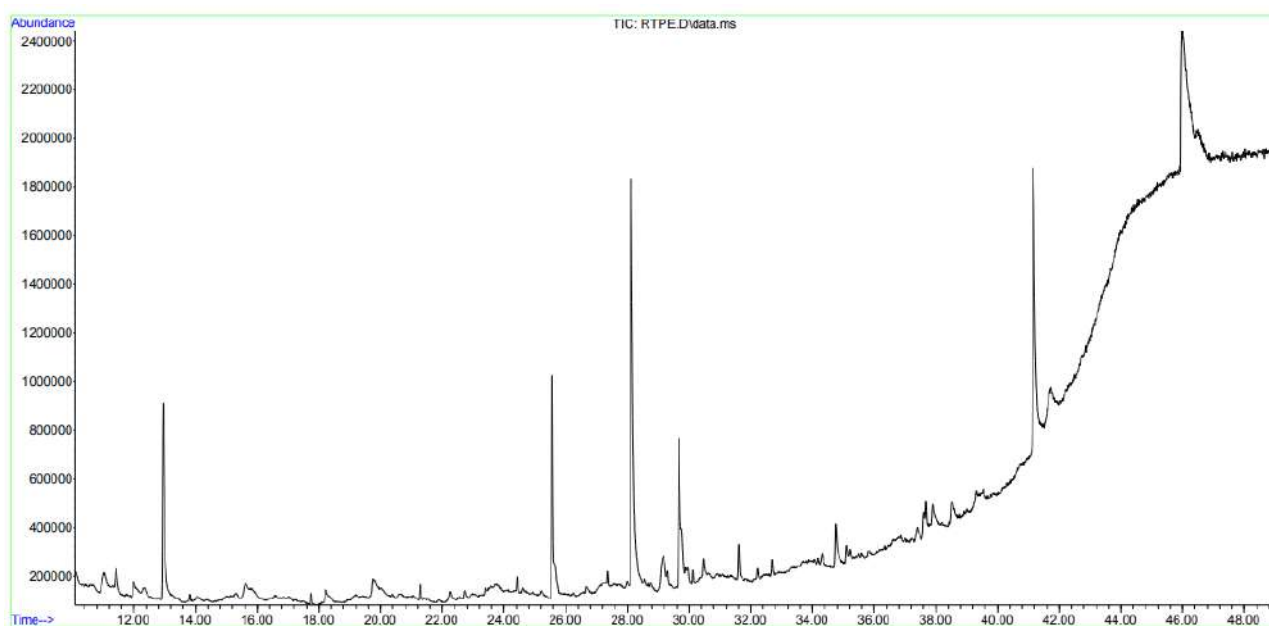


Figure 4 – Chromatogram of *Rheum tataricum* L. petroleum ether extract

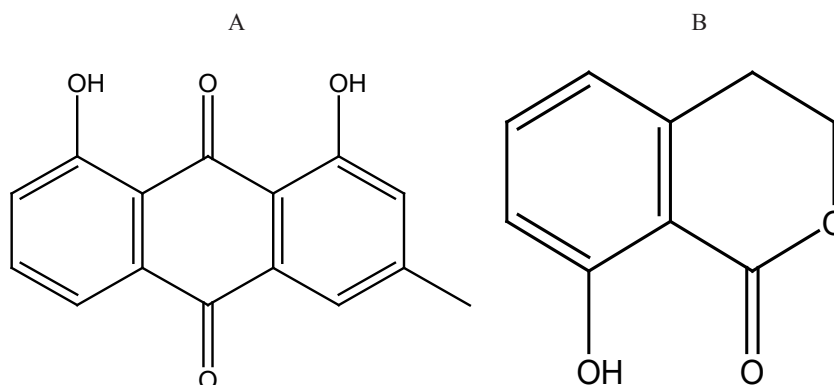


Figure 5 – Structures of Chrysophanol (A) and 1H-2-Benzopyran-1-one, 3,4-dihydro-8-hydroxy-3-methyl- (B)

Apocynin (3.1 ± 0.01 %) is a naturally occurring acetophenone that has demonstrated potential in alleviating a range of disorders, such as diabetic complications, neurodegenerative diseases, cardiovascular conditions, lung cancer, hepatocellular carcinoma, pancreatic cancer, and pheochromocytoma [24].

Orcinol (2.1 ± 0.01 %) is a naturally occurring phenolic compound found in lichens and plants and is widely used for detecting pentoses in Bial's test. It has been assessed for its antioxidant properties against 1,1-diphenyl-2-picrylhydrazyl (DPPH), as well as its antiradical activity [25, 26].

Conclusion

This study provides a comprehensive comparative analysis of *Rheum tataricum* and *Rheum palmatum*, focusing on their morphological characteristics, chemical compositions, pharmacological effects, and potential applications in the pharmaceutical industry. These comparative findings, reported for the first time, demonstrate that *Rheum tataricum* contains significantly higher levels of several biologically active compounds compared to *Rheum palmatum*. Notably, the polysaccharide content in *R. tataricum* reached 6.36%, more than three times higher than in *R. palmatum* (2.07%), while tannins were present at 7.40% versus 3.67%. Additionally, coumarin levels in *R. tataricum* were 3.64% compared to 2.40% in *R. palmatum*. These elevated values suggest that *R. tataricum* may have greater therapeutic potential, particularly in supporting immune function, gastrointestinal health, and cardiovascular protection, emphasizing the need for further pharmacological and clinical studies.

Through GC-MS analysis, the key differences in the chemical composition of two *Rheum* species were identified. Notably, *Rheum tataricum*, collected from Kazakhstan, exhibited a high content of biologically active compounds such as chrysophanol, 1H-2-Benzopyran-1-one, 3,4-dihydro-8-hydroxy-3-methyl-, and Cyclohexanol, 1-methyl-4-(1-methylethyl)-, which demonstrates significant antioxidant, antibacterial, and anticancer properties. The increased presence of these compounds suggests that *R. tataricum* is rich in phytochemicals and possesses strong pharmacological potential comparable to or even exceeding that of *Rheum palmatum*.

Given the similar therapeutic effects and the abundance of *Rheum tataricum* in Kazakhstan, this species presents itself as a viable alternative to *R. palmatum* in the domestic pharmaceutical market. Its cultivation and utilization could reduce dependence on imported Chinese rhubarb, thereby promoting local production and enhancing the sustainability of Kazakhstan's medicinal plant industry. Furthermore, the economic and ecological benefits of utilizing a native species align with the growing global trend toward the use of regionally sourced natural products in pharmaceutical applications.

In conclusion, our study highlights the potential of *Rheum tataricum* as a valuable medicinal resource with applications in drug development and traditional medicine. Future research should focus on further pharmacological testing, optimization of extraction methods, and clinical studies to fully unlock its therapeutic potential and establish it as a cornerstone of Kazakhstan's pharmaceutical industry.

Acknowledgments

This study was supported by the International Project in collaboration with the Central Asia Center of Drug Discovery and Development of the Chinese Academy of Sciences (Grant No. CAM202404).

Conflict of interest

All authors are aware of the article's content and declare no conflict of interest.

References

1. Wagner H., Bladt S. (1996) Plant Drug Analysis: A Thin – Layer Chromatography Atlas, Springer, 369 p. e-ISBN 978-3-642-00574-9. <https://z-lib.fm/book/2052871/000488/plant-drug-analysis-a-thin-layer-chromatography-atlas.html>.
2. Editorial Committee (2003) Flora of China. Science Press & Missouri Botanical Garden Press.
3. Li X., et al. (2018) Chemical constituents and pharmacological activities of *Rheum* plants: A review. *J. of Ethnopharm.*, 210, pp. 118-132.
4. Wang Y., et al. (2015) Traditional uses, phytochemistry, and pharmacology of *Rheum*: A review. *Evid. – Based Complem. and Alt. Med.*, 2015, pp. 1-18.
5. Zhang Y., et al. (2020) Chemical constituents and pharmacological activities of *Rheum tataricum* L.: A review. *J. of Pharm. Anal.*, 10(3), pp. 195-203.
6. Wu Z.Y., Raven P.H. (1994-2013) Flora of China. Beijing: Science Press; St. Louis: Missouri Botanical Garden Press.
7. Chang H.M., But P.P. (1987) Pharmacology and Applications of Chinese Materia Medica. World Scientific.
8. Zhang Y., et al. (2019) Chemical constituents and pharmacological activities of *Rheum palmatum* L.: A review. *Chin. J. Nat. Med.*, 17(11), pp. 801-813.
9. Chen X., et al. (2021) Chemical constituents and pharmacological activities of *Rheum palmatum* and its clinical application: A review. *Chin. J. Exp. Trad. Med. Formulae*, 27(5), pp. 234-242.
10. Cragg G.M., Newman D.J. (2013) Natural products: A continuing source of novel drug leads. *Biochimica et Biophysica Acta (BBA) – General Subjects*, 1830(6), pp. 3670-3695. <https://doi.org/10.1016/j.bbagen.2013.02.008>.
11. Heywood V.H. (Ed.). (1993). Flowering plants of the world, Ed. 2, pp. 336. ISBN 978-0-7134-7422-0.
12. Newall C.A., Anderson L.A., Phillipson J.D. (1996) Herbal Medicines: A Guide for Health – Care Professionals. Pharmaceutical Press. ISBN 978-0-85369-289-8.
13. Kazakhstan state Pharmacopeia (2008). Almaty: Zhibek zholy, 592-609.
14. Muzychkina R.A., Korulkin D.Yu., Abilov Zh.A. (2004) Kachestvennyy i kolichestvennyy analiz osnovnykh grupp BAV v lekarstvennom rastitel'nom syr'ye i fitopreparatakh [Qualitative and quantitative analysis of the main groups of BAses in medicinal raw materials and phytopreparations]. Almaty: Kazakh University.
15. Teres S., et al. (2008) Oleic acid content is responsible for the reduction in blood pressure induced by olive oil. *Proceedings of the National Acad. Sci.*, 105(37), pp. 13811-13816. <https://doi.org/10.1073/pnas.0807500105>.
16. Mazzocchi A., Leone L., Agostoni C., Pali-Schöll I. (2021) The secrets of the Mediterranean diet. Does [only] olive oil matter? *Adv. in Med. Biochem., Genom., Physiol., Pathol.*, pp. 545-563. eBook ISBN 9781003180449.
17. Escrich R., Costa I., Moreno M., et al. (2019) A high-corn-oil diet strongly stimulates mammary carcinogenesis, while a high-extra-virgin-olive-oil diet has a weak effect, through changes in metabolism, immune system function and proliferation/apoptosis pathways *J. Nutr. Biochem.*, 64, pp. 218-227. <https://doi.org/10.1016/j.jnutbio.2018.11.001>.
18. Bilal R.M., Liu C., Zhao H., et al. (2021) Olive oil: nutritional applications, beneficial health aspects and its prospective application in poultry production. *Front. Pharmacol.*, 12, pp. 723040. <https://doi.org/10.3389/fphar.2021.723040>.
19. Ganesan T., Subban M., Christopher Leslee D.B., et al. (2024) Structural characterization of *n*-hexadecanoic acid from the leaves of *Ipomoea eriocarpa* and its antioxidant and antibacterial activities. *Biomass Conv. Bioref.*, 14, pp. 14547-14558. <https://doi.org/10.1007/s13399-022-03576-w>.
20. Burdge G.C. (2006) Metabolism of α -linolenic acid in humans. *Prostaglandins, leukotrienes and essential fatty acids*, 75(3), pp. 161-168. <https://doi.org/10.1016/j.plefa.2006.05.013>.
21. Parvathi K., Kandeepan C., Sabitha M., Senthilkumar N., Ramya S., Boopathi N.M., Ramanathan L., Jayakumararaj R. (2022) In-silico Absorption, Distribution, Metabolism, Elimination and Toxicity profile of 9,12,15-Octadecatrienoic acid (ODA) from *Moringa oleifera*. *J. Drug Deliv. Ther.*, 12(2), pp. 142-150. <http://dx.doi.org/10.22270/jddt.v12i2-s.5289>.
22. Liu D., Zhu K., Guo T., et al. (2024) Chrysophanol: A Promising Natural Compound in Cancer Therapy–Mechanistic Insights and Future Perspectives. *Pharm. Res.*, 210, pp. 107502. <https://doi.org/10.1016/j.phrs.2024.107502>.
23. Yang J.X., Qiu S., She Z., Lin Y. (2014) A new isochroman derivative from the marine fungus *Phomopsis* sp. (No. Gx-4). *Chem. Nat. Compd.*, 50, pp. 424-426. <https://doi.org/10.1007/s10600-014-0976-y>.
24. Savla S.R., Laddha A.P., Kulkarni Y.A. (2021) Pharmacology of apocynin: a natural acetophenone. *Drug metabolism rev.*, 53(4), pp. 542-562. <https://doi.org/10.1080/03602532.2021.1895203>.
25. Bonesi M., Xiao J., Tundis R., Aiello F., Sicari V., Loizzo M.R. (2019) Advances in the tyrosinase inhibitors from plant source. *Current med. chem.*, 26(18), pp. 3279-3299. <https://doi.org/10.2174/0929867325666180522091311>.

26. Oliveira M.S.C., de Morais S.M., Magalhães D.V., et al. (2011) Antioxidant, larvicidal and antiacetylcholinesterase activities of cashew nut shell liquid constituents. *Acta Tropica*, 117(3), pp. 165-170. <https://doi.org/10.1016/j.actatropica.2010.08.003>.

Information about authors

Ayaulym Minkayeva – 2-year Master student, The Research Center for Medicinal Plants, Al-Farabi Kazakh National University (Almaty, Kazakhstan, e-mail: minkaeva.a@gmail.com)

Laila Azilbek – 1-year PhD student, the Research Center for Medicinal Plants, Al-Farabi Kazakh National University (Almaty, Kazakhstan, e-mail: azilbek94@inbox.ru)

Ulpan Amzeyeva – PhD student, The Research Center for Medicinal Plants, Al-Farabi Kazakh National University; Research Institute for Natural Products & Technology (Almaty, Kazakhstan, e-mail: ulpan-92.kz@mail.ru)

Thiruventhan Karunakaran – PhD, Centre for Drug Research, University Sains Malaysia (Pulau Pinang, Malaysia, e-mail: thiruventhan@usm.my)

Xinqi Liu – PhD, Professor, Beijing Technology and Business University (Beijing, China, e-mail: liuxinqi111@qq.com)

Xiaofei Shang – PhD, Professor, Lanzhou Institute of Husbandry and Pharmaceutical Sciences, CAAS (Lanzhou, China, e-mail: shangxiaofei@caas.cn)

Nazokat Muzaffarova – PhD, Faculty of Chemistry, Termez State University (Termez, Republic of Uzbekistan, e-mail address: hilolanazokat2010@gmail.com)

Janar Jenis – PhD, Professor, The Research Center for Medicinal Plants, Al-Farabi Kazakh National University (Almaty, Kazakhstan, e-mail: janarjenis@kaznu.kz)

F. Mas'ud* , V.D. Paramita ,
Z. Zulmanwardi , H.R. Yuliani 

Politeknik Negeri Ujung Pandang, Makassar, Indonesia

*e-mail: fajri888@poliupg.ac.id

(Received 4 May 2025; received in revised form 16 May 2025; accepted 27 May 2025)

Optimization of dietary fiber extraction from corn stalks and product characterization

Abstract: This research optimizes dietary fiber extraction from corn stalks and addresses its potential use in processed meat and fish products. The research aims to optimize dietary fiber extraction from corn stalk and characterize its potential as a food ingredient. Corn stalks were extracted using NaOH for dietary fiber, the procedure involved cleaning, drying, extraction, bleaching, and drying. RSM optimization using Design-Expert software determined optimal NaOH concentration and extraction time for dietary fiber yield. Products were characterized by FTIR, SEM, and BET, as well as determining WHC and OHC. This study optimized the extraction of dietary fiber from corn stalk using NaOH. RSM identified optimal conditions, i.e., NaOH concentration (A) = 25.96% and extraction time (B) = 65.39 min, yielding 34.47% dietary fiber. Validation trials resulted in a $34.38 \pm 0.04\%$ yield. Product characterization (FT-IR, SEM, BET), as well as assessments of WHC and OHC demonstrate the potential of corn stalk as a dietary fiber source and its use as a filler for processed meat and fish products. Optimization of dietary fiber extraction from corn stalks, achieved a yield of 34.47%. The findings highlight the feasibility of corn stalks as a source of dietary fiber in processed foods and the use of NaOH in extraction for large-scale production.

Key words: chemical extraction, corn stalks, dietary fiber, Response Surface Methodology, sodium hydroxide.

Introduction

Food crops, such as corn, are cultivated year-round, but only the fruit is consumed, leaving a significant amount of waste. The yearly yield of corn stalks is projected to be close to 1 billion tons [1]. In the stem part, there are about 30-50% of the total weight of the plant, depending on the variety, growth conditions, and cultivation methods. Corn stalks contain cellulose fiber, which has potential as a source of dietary fiber and fillers in the processing of fishery products, such as meatballs and nuggets. This potential is particularly feasible, as the current filler-wheat flour is an imported product, which adds to production costs. Moreover, the availability of corn stalks is abundant, renewable, and sustainable, making them an ideal alternative.

In the processing of fishery products, fillers are essential to the role in product quality, improving emulsion properties, enhancing characteristics and sensory attributes, reducing cooking shrinkage, increasing water and oil-holding capacities, and lower-

ing production costs. Additionally, processed fishery products often fall short of meeting dietary fiber requirements. The recommended daily intake is 25 g per 2,000 calories or 30 g per 2,500 calories, while meatballs on the market typically contain only 0.5% fiber per serving. Long-term consumption of synthetic fibers can have detrimental effects on both health and environmental sustainability [2].

Dietary fiber plays a crucial role in the diet by supporting the digestive system, aiding the movement of food through the intestines, and facilitating the removal of waste from the body. Adults need 25-30 g of fiber per day, which should be obtained from food rather than supplements. A meta-analysis conducted by the World Health Organization (WHO) found that consuming at least 25 to 29 g of fiber per day can help protect against various diseases [3].

The addition of dietary fiber to food products is one way to increase human fiber intake [4, 5]. Interest in adding dietary fiber to animal products is increasing because of its possible health benefits [6]. In the meat processing industry, meeting the nutri-

tional claim standards of “source of dietary fiber” and “high fiber food” requires a minimum of 3 g or 6 g of dietary fiber per 100 g of product. These claims can enhance the market potential of dietary fiber-rich meat and fish products and provide consumers with healthier food choices. The concentration of dietary fiber in meatballs is of industrial significance because it meets the nutritional criteria for these claims. Adding up to 6 g of dietary fiber per 100 g can also affect the sensory quality of meatball products [7].

The flour is a versatile food ingredient extensively used in the production of emulsified meat products, such as meatballs [8]. The flour acts as an active filler in the meat protein matrix, improving gel properties and increasing the firmness and cutting ability of emulsified meat products [9]. Flour, when combined with dietary fiber, can further enhance the quality of these products to meet dietary fiber needs.

Cellulose in nature is not found in its pure form but rather as part of lignocellulose, a complex of cellulose, hemicellulose, and lignin. Since cellulose and lignin are bound together, a method is needed to separate cellulose from lignin; this process is known as “delignification”. Delignification breaks down the lignocellulose structure, making cellulose more accessible and dissolving the lignin content, which facilitates the separation of lignin from the fiber.

The use of NaOH in the delignification process can break the ether bonds connecting lignin to cellulose, remove lignin, and increase biomass porosity [9]. In addition, the bleaching process can use several chemicals, such as sodium hypochlorite, alkali compounds, and acids, these chemicals can hydrolyze and bleach the product. The application of this process in industry is very feasible to apply, because the methods and equipment needed are relatively simple. However, process control is important to be carried out carefully because cellulose can be degraded under certain process conditions. Therefore, the optimum extraction process conditions are important to know to produce high-quality products and achieve high efficiency in order to save production costs.

Some research has focused on modeling and optimizing cellulose extraction. For example, from orange peels, palm trees, wheat straw, and corn cobs [8, 9, 11]. However, modeling and optimization of cellulose extraction from corn stalks, which has the potential to be used as dietary fiber, have not been discussed. This study aims to determine the opti-

mal conditions for dietary fiber extraction from corn stalks, characterize the product, and explore the potential of dietary fiber from corn stalks as a food ingredient.

Materials and methods

NASA 29 variety hybrid corn stalks as samples were obtained from Maros Regency, South Sulawesi, Indonesia. Sodium hydroxide (NaOH) (Merck, Germany) and sodium metabisulfite ($\text{Na}_2\text{S}_2\text{O}_5$) (Aditya Birla) were purchased from a local chemical shop.

Cellulose fiber extraction: Corn stalk samples were cleaned, washed, and chopped using a disk mill and dried to a water content of 6%. The extraction process used a stainless steel vessel equipped with a stirrer and a gas stove as a heater. Dietary fibers were extracted using chemical methods. Each experimental unit used 100 g of sample and 1000 mL of NaOH solution, the extraction process takes place at 90°C. After the extraction, the samples were washed with clean running water until the pH of the water reached 7. Then, bleaching was performed by soaking the samples in a 5% $\text{Na}_2\text{S}_2\text{O}_5$ solution for 60 min, followed by filtration using a nylon filter cloth. The samples were dried to a water content of about 4 to 5%, then packed in plastic bags and weighed to calculate the dietary fiber yield (Equation 1). The samples were then placed in a cooling room for further analysis and characterization.

$$\text{Yield (\%)} = \frac{\text{dietary fiber (g)}}{\text{corn stalk (g)}} \times 100 \quad (1)$$

Optimization and modeling using Response Surface Methodology (RSM). The parameters monitored were the NaOH concentration (%), which was labeled A, and the processing time (min), which was labeled B. To determine the impact of A and B as process parameters on dietary fiber yield (Y), optimization and modeling were carried out using RSM, the experimental data was acquired via Design Expert Version 13 (Stat-Ease, Inc., USA), and used to optimize and model the process. Two central composite design (CCD) factors were used to monitor the optimal A (%) and B (min) to achieve a high dietary fiber yield (Y) as responses. The midpoint of the process was set at 25% for variable A and 60 min for variable B (Table 1).

Table 1 – Parameters considered, range and levels of independent variables

Independent variables	Range and levels of independent variables				
	-α	-1	0	1	+α
A (%)	10.86	15	25	35	45.86
B (min)	39.14	50	60	70	74.14

Product characterization: The obtained dietary fiber products were then characterized using Fourier transform infrared spectroscopy (FT-IR), scanning electron microscopy (SEM), and Brunauer-Emmett-Teller (BET). Determining the water-holding capacity (WHC) and oil-holding capacity (OHC) has also been carried out. SEM analysis used instrument SEM, Hitachi SU1000, and FlexSEM 1000 II. Double-sided adhesive carbon tape was used to secure the dried sample to a specimen stub, and a spray of air was used to remove any extra fiber. Using a SCD500 vacuum turbo evaporator system, a platinum coating with a thickness of 10-20 nm was deposited on the sample surface. A Quanta 250 FEG scanning electron microscope (Hitachi SU1000, Flex SEM 1000 II) was used to take micrographs of the sample surfaces at 500× magnification and a voltage of 5.00 kV. FT-IR spectroscopy analysis (the ALPHA FTIR spectrometer Bruker Optics GmbH & Co. KG, Germany), was used to obtain FT-IR spectra of samples. The dried samples were analyzed from 4000 to 500 cm⁻¹, slit number 4 cm⁻¹, and 24 scans were conducted for each sample.

For analysis of BET, the sample was analyzed on the Anton Paar Nova Touch instrument. Samples with appropriate particle size are selected, and it was ensured that the sample was dried and free from contamination. The sample cell was filled with the correct amount according to the analysis requirements. The degassing profile was set according to the sample type. This process removes adsorbates present on the sample surface prior to BET analysis. The sample cell was placed on the degassing station, and the process was started according to the specified profile. The dewar was filled with liquid nitrogen to the specified level indicator, and the degassed sample cell was installed on the appropriate analysis station. The analysis profile was selected according to the sample type, the analysis process was started, and the instrument was allowed to run until completion.

WHC was determined using a modified procedure from Jia et al. [12]. A sample weighing 1.0 g was mixed with 70 mL of aquadest and stirred for 4 h. The resulting turbid liquid was then centrifuged at 3000 rpm for 15 min, the surplus water was then meticulously eliminated. The weight of the wet sample was recorded and then placed in an oven at 105°C until it reached a constant weight. The sample was weighed to calculate the WHC of the obtained dietary fiber (Equation 2).

$$\text{WHC (g/g)} = \frac{(\text{wet weight} - \text{dry weight})}{\text{dry weight}} \quad (2)$$

The method adapted from Abdul-Hamid and Luan [13] was used to evaluate OHC using a 1.0 g sample. The sample was placed in a centrifuge tube and mixed with excess corn oil. The centrifuge tube was stirred for 30 seconds every 5 min, and after 30 min, the tube was centrifuged at 1600 rpm for 20 min. The oil and water attached to the inside of the tube were cleaned after the excess oil was carefully separated, and the tube was weighed to calculate the OHC of the obtained dietary fibers (Equation 3).

$$\text{OHC (g/g)} = \frac{\text{Oil retained}}{\text{Original dried fiber sample}} \quad (3)$$

Results and discussion

The 2² factorial design including the appropriate responses as the yield of dietary fibers extracted from corn stalks through a chemical process using NaOH, is shown in Table 2. The effects of variables A and B on the response Y of dietary fiber were studied during experimentation. The data showed that the response Y ranged from 31.12 to 34.53%. The main purpose of this chemical extraction process is to produce as much dietary fiber as possible from the corn stalks. For the selected models, the sum of squares sequential model was run for the Y as shown in Table 3.

Table 2 – 2² Factorial design of CCD, A (%), B (min), and Y (%) as responses

A (%)	B (min)	Y (%)
15	50	31.65
35	50	31.27
15	70	32.44
35	70	33.44
10.86	60	31.25
39.14	60	32.56
25	45.86	31.12
25	74.14	33.86
25	60	34.53
25	60	34.12
25	60	34.23
25	60	34.15
25	60	34.05

Table 3 – Sequential model sum of squares

Source	Sum of squares	DF	Mean square	F-value	p-value
Total vs. Mean	14135.23	1	14135.23	-	-
Mean vs. Linear	6.6	2	3.3	2.4	0.1411
Linear vs. 2FI	0.4761	1	0.4761	0.3222	0.5842
2FI vs. Quadratic	12.86	2	6.43	103.62	< 0.0001 ^a
Quadratic vs. Cubic	0.2946	2	0.1473	5.26	0.0589 ^b
Residual	0.1399	5	0.028	-	-
Total	14155.61	13	1088.89		

Note: ^aSuggested; ^bAliased

The effects of variables A and B on the response Y were studied during experimentation. The quadratic response surface model can be seen in the analysis of variance at Table 4. According to CCD of RSM utilizing Design-Expert version 13 software, the maximum Y was achieved under the experimental conditions of A = 25.96% for B = 63.47 min. Under

these process conditions, the maximum response (Y) was 34.47%.

Numerical optimization and modeling of the extraction process: A model that is defined in terms of real variables can accurately depict the percentage of dietary fiber that is extracted from corn stalks, as in Equation 4.

Table 4 – Response surface quadratic model of analysis of variance

Response: Dietary fiber yield					
Source	Sum of Squares	DF	Mean square	F- value	p-value
Model	19.94	5	3.99	64.26	< 0.0001*
A	0.7642	1	0.7642	12.31	0.0099
B	5.84	1	5.84	94.08	< 0.0001

Continuation of the table

Response: Dietary fiber yield					
Source	Sum of Squares	DF	Mean square	<i>F</i> - value	<i>p</i> -value
A²	0.4761	1	0.4761	7.67	0.0277
B²	9.28	1	9.28	149.48	< 0.0001
AB	5.17	1	5.17	83.35	< 0.0001
Residual	0.4345	7	0.0621	-	-
Lack of Fit	0.2946	3	0.0982	2.81	0.1721 ^{ns}
Mean	32.97		R²	0.9787	
Std. Dev.	0.2491		Expected R²	0.8865	
C.V. %	0.7555		Adjusted R²	0.9634	
Note: * Significant; ^{ns} Not significant					

$$Y (\%) = -4.77137 + 0.401345A + 1.03404B + 0.003450AB - 0.011549A^2 - 0.008624B^2 \quad (4)$$

where A = NaOH concentration (%) and B = extraction time (min).

The models are significant for Y according to the analysis of variance (Anova). The correlation coefficient value was used to assess the quality of the models that were created. The coefficient of determination (R²) value of 0.97 shows that the models adequately represent the true connection between the selected variables (A and B). The *F*-value and *p*-value were used to assess the importance of the various terms in each coefficient. A small *p*-value and a large *F*-value would suggest a more significant effect on the related response variable [14].

The model terms are considered significant if the *p*-value is less than 0.05. A, B, AB, A², and B² are important model terms in this instance. The lack of fit is not significant in relation to the pure error, according to the lack of fit *F*-value of 2.81. A *F*-value of this magnitude has a 17.21% probability of being the result of noise. A good fit is indicated by a lack of fit that is not statistically significant.

Figure 1 is a 2D and 3D graphical representation of the variable A and variable B model on the Y. A higher yield of dietary fiber will result from raising the NaOH concentration and lengthening

the extraction period. The 2D and 3D contour plots play an important role in visualizing and gaining a better understanding of the relationships between variables A and B and the measured response Y. 2D and 3D contour plots are essential in this study because they offer a visual approach to analyzing and optimizing processes by directly observing the relationships between variables A and B and response Y.

A 2D contour plot shows the independent variables A and B affecting Y in two dimensions. The contour plot depicts the areas where the response value remains constant. This helps identify patterns or trends in the experimental data, while a 3D contour plot provides a three-dimensional representation of the relationship between the two independent variables, in this case A and B, with respect to Y as the response. A 3D contour plot is helpful in visualizing more complex interactions between the variables and the response. The 2D contour plot shows the independent variables A and B which affect Y in two dimensions. The contour plot describes the area where the response value remains constant. This helps identify patterns or trends in experimental data, while 3D contour plots give three dimensional representations of the relationship between two independent variables, in this case A and B, in connection with Y in response. 3D contour plot helps in visualizing more complex interactions between variables and responses.

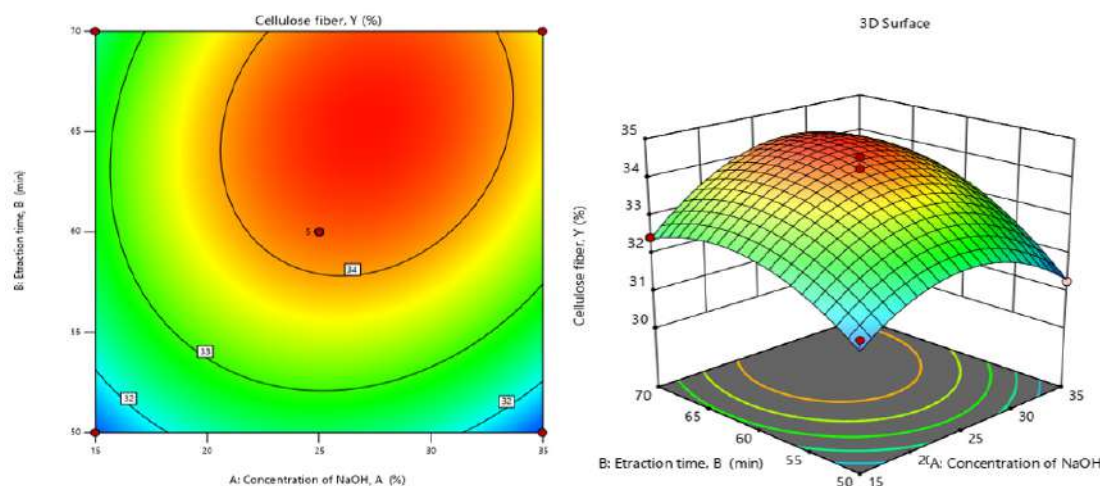


Figure 1 – Contour 2D and 3D surface curves of A and B

The 2D and 3D contour plots visualize the location of the optimum response point area, so that the process conditions can be determined that produces the best performance. In the 2D contour plot, researchers can comprehensively understand how changes in one variable can affect the response when other variables are kept constant, so that the direct effect of a single variable to the response can be well understood. In the 3D contour plot, we can understand the effect of two variable interactions on the response when the other variables are kept constant. Based on the comprehensive understanding of the contour plot visualization, researchers can design advanced optimization research by focusing on a significant variable affecting the process to produce high -quality products and achieve the effectiveness and efficiency of a chemical process. The next step is verification and validation of the RSM results on a laboratory scale to ensure feasibly methods and models are applied in the industry.

Related to Figure 1, it can be explained that the maximum Y is achieved when using $A = 25.96\%$ and $B = 65.39$ min. If variables A and B are smaller or larger than these values, then the Y is not maximum. Based on the coefficient value of the regression model (Equation 2), where the coefficient $B > A$, it can be explained that the influence of variable B is greater in obtaining the maximum Y compared to the influence of variable A. This can also be proven from the estimated coefficient value, where the value of $B > A$, or the value of $B = 0.8544$, and the value of $A = 0.3091$.

More about dietary fiber extraction, the alkaline hydrolysis breaks the bonds between the lignin and hemicellulose's ester groups, aryl-ether, carbon-

carbon, and aryl-aryl groups, reducing the amount of lignin and hemicellulose [14]. Increasing the concentration of NaOH, on the other hand, will result in the uncontrolled hydrolysis of cellulose's functional groups, lowering the product's cellulose content. The recovery of cellulose fibers is positively impacted by longer extraction times as well; however, prolonged extraction leads to cellulose degradation and a reduction in cellulose yield.

Alkali treatment with NaOH is very effective in achieving complete biomass hydrolysis. This method effectively dissolves lignin and hemicellulose fractions while causing minimal cellulose dissolution. It works by breaking down the biomass cell walls, dissolving matrix hemicellulose and lignin, as well as breaking the α -ether bonds between these components, as well as the ester bonds associated with them [11]. The impact on hemicellulose can vary depending on the processing conditions [15]. The efficiency of this treatment is influenced by several factors, including temperature, concentration, duration, type of raw material used, and lignin content in the material [16].

In RSM, desirability and predicted response Y are also visualized as in Figure 2. The desirability value helps guide decisions and provides a clear figure of how well an experimental condition meets the desired objectives. The NaOH concentration and extraction duration were tuned to "within range" in order to maximize the dietary fiber extraction process. The "maximize" dietary fiber content was selected. The results indicate that the extraction of dietary fiber can be finished in a comparatively short amount of time. In addition, the analysis confirmed that corn

stalks contain a significant amount of cellulose, supporting their potential as a source of dietary fiber and as a food ingredient. The composition variation is in-

fluenced by factors such as species, geographic location, age, and climate, as noted in previous studies [17].

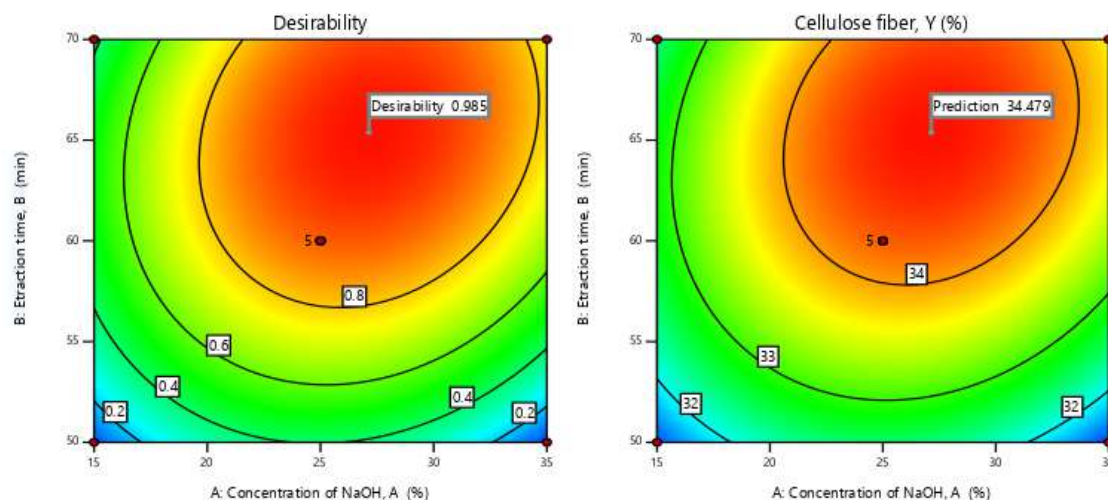


Figure 2 – Desirability and response Y prediction, show the ideal set of process variables that will yield the maximum dietary fiber content response

In chemical process optimization, “desirability” refers to a systematic approach used to evaluate and improve the performance of a process based on multiple criteria or objectives. The concept is often implemented through a “desirability function,” which helps combine multiple responses into a single metric for optimization. The desirability function measures how desirable a particular outcome is, typically ranging from 0 (not desirable) to 1 (very desirable). Different responses, in this case dietary fiber yield, can be converted into a desirability score, allowing for a comprehensive evaluation.

The application of RSM in chemical process research can help researchers to explore the influence of several variables on the intended response and achieve optimum process conditions. Overall desirability can be known from the desirability value of each intended response so that researchers can make decisions regarding the optimum chemical process conditions appropriately. Desirability considers several factors, identifying optimum process conditions by balancing all factors involved in a chemical process. Thus, decision-making on a chemical process can be more effective, efficient, and feasible.

Verification model: Verification of optimal dietary fiber extraction conditions was carried out using optimized parameters. For model verification, triplicate experiments were used. This was to show that the

optimal extraction condition solution recommended by the RSM produced dietary fibers according to the predicted values. The average yield, according to the data, was 34.47%, which was close to the verification value of $34.38 \pm 0.04\%$. The average yield value of dietary fibers produced during the verification procedure was slightly less than the prediction but not significantly different, so the model created can be used to maximize the extraction of dietary fibers from corn stalks and is reliable and adequate in its predictions. These results indicate that the dietary fiber extraction model from corn stalks obtained from the verification process can be applied to actual applications.

Characteristics of the product. Cellulose fiber is needed in food processing as a dietary fiber and as a filler in processed meat and fishery products such as meatballs or fish balls. The filler and source of dietary fiber currently used is wheat flour, but additional dietary fiber from other sources is still needed. The ability of flour to absorb high water is needed in this case because it has an impact on the texture, taste, and consistency of the final product. Flour with good water absorption capacity can produce a softer and chewier product texture, the quantity of water that the flour absorbs determines the elasticity and density of the dough. Flour that absorbs water well can help bind other ingredients so that the final product is more stable and does not easily crumble. In products

that require fermentation, such as bread, the ability of flour to absorb water affects the gas formation process needed for dough development, flour with good water absorption capacity tends to be more durable because it can control the water content in the dough.

Highly porous cellulose fibers usually have good WHC because their porous structure allows for greater water retention. This makes it suitable for applications in products that require moisture, such as in wet food products or as a binder. The WHC value of corn stalks dietary fiber was found to be 5.1 ± 0.04 (g/g), this value can explain the great potential of corn stalks dietary fiber as a food ingredient. In this case, corn stalks dietary fiber can be combined with wheat flour or rice flour as a source of fiber and filler in the processing of meat and other fishery products that require flour for dough. Corn stalks dietary fiber has the potential to be combined with wheat flour because wheat flour has a low WHC of 1.85 g/g [18].

In line with WHC, OHC is also important in food processing and has several significant impacts, namely that flour that is able to absorb oil well can provide a crispier and softer texture to products, such as cakes and pastries. Good oil absorbers can help bind flavors and aromas and provide a more specific taste to food products. Related to product stability, the ability of flour to absorb oil can increase product stability, help prevent fat separation from dough or mixtures, and provide moisture. Flour that absorbs oil can also help maintain moisture in food products,

which is important for maintaining freshness. In the baking process, flour that absorbs oil can contribute to the formation of the desired crust and color. The OHC value of good flour ranges from 1.0 to 2.0 g oil/g flour [19]. Wheat flour has an OHC value of 1.05 (g/g) [20]. Related to OHC, dietary fiber tends to have a lower value, often ranging from 1 to 2 g oil/g fiber. This is because dietary fiber absorbs more water than oil. The OHC value of corn stalks dietary fiber in this study was found to be 1.2 ± 0.03 (g/g).

Dietary fiber products were further characterized by FTIR, SEM, and BET instruments. Spectral analysis of the functional group of dietary fibers before and after treatment with NaOH has been carried out using FT-IR infrared spectroscopy. Figure 3 shows that there are two main regions of absorption, namely the region with a wavenumber range from 500 to 1600 cm^{-1} . The absorption bands near 3303 and 2907 shifted slightly to 2864 cm^{-1} for the $-\text{CH}_2$ group of dietary fibers, the treated stalks are linked to asymmetric stretching of C-H bonds and hydrogen-bonded OH groups [21]. The characteristic signals at 1358 cm^{-1} correspond to the deformation vibrations of CH_2 and CH groups [22, 23]. The peak located at 1145 cm^{-1} is linked to asymmetric C-O-C stretching. After hemicellulose, lignin, and pectin were removed, the broad peak at about 1013 cm^{-1} represents the C-O stretching vibrations in cellulose that varied little. The C-O group connected to the β -glycosidic link was also identified as the source of the peak at 883 and 891 cm^{-1} [24, 25].

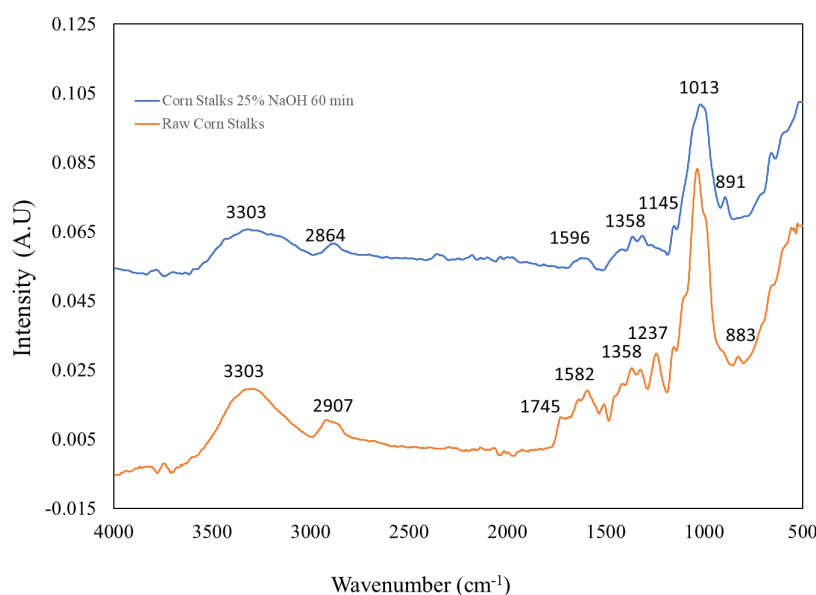


Figure 3 – FT-IR spectra of corn stalks as the sample and dietary fiber extracted from corn stalks as the product

Furthermore, the carbonyl group of aromatic acids present in lignin and hemicellulose in raw maize stalks was identified as the cause of the shoulder peak at 1582 and 1596 cm^{-1} . The FTIR bands at 1745 and 1237 cm^{-1} in corn stalks are associated with the carbonyl ($\text{C}=\text{O}$) stretching and C-O stretching vibration, respectively, primarily from ester groups present in hemicellulose. These peaks often indicate the presence of acetyl or ester linkages within hemicellulose, which are responsible for its structural role in the plant cell wall. The intensity of this band can decrease after chemical treatments, such as alkaline process-

ing, as hemicellulose and associated esters are removed [25].

SEM was used to analyze the raw material's microstructure (Figure 4). The surface of the raw corn stalks displays a rough, uneven, filamentous structure. This filamentous nature results from the presence of wax layers, pectin, and other impurities, such as lignin and hemicellulose, which bind the cell walls of the corn stalks together. However, after treatment with 25% NaOH for 60 min, the rough, filamentous surface breaks down, revealing a fibrous structure. The NaOH dissolves the wax, pectin, hemicellulose, and lignin, leaving behind only cellulose fibers.

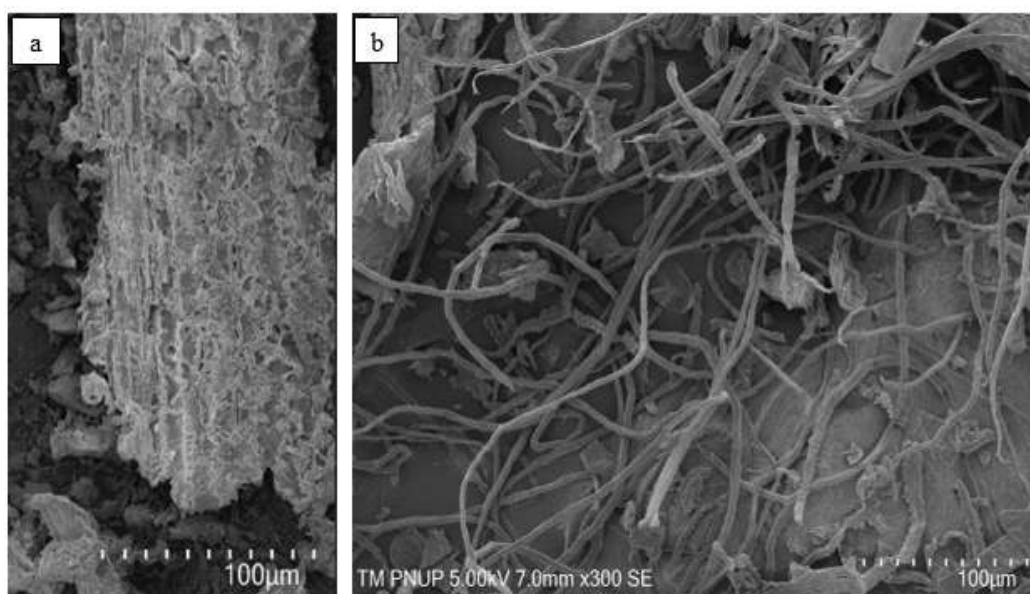


Figure 4 – SEM analysis of corn stalks (a) and dietary fiber extracted from corn stalks after 60 min treatment with 25% NaOH (b)

Analysis of corn stalks dietary fiber products using the BET can be seen in Figure 5. The graph shows that most of the pores are >2 nm in size, this value indicates that the existing pores are mesopores. This fairly large pore size correlates with the large absorption capacity of dietary fiber products for water and oil. Figure 5 shows the adsorption and desorption capabilities of dietary fiber products, which are almost comparable. This means that the product has almost the same absorption capacity in absorbing (adsorption) and releasing (desorption) water and oil. In this result, adsorption refers to the ability of

water molecules to adhere to the surface of dietary fiber products, while desorption is the ability of water and oil molecules to be released back into the environment. These two abilities are almost the same, so that corn stalks dietary fiber products have a good balance between water absorption and release, which can impact the quality, texture, and shelf life of the product in its application in the food sector or other industries. This balance is especially important in the context of the storage and use of dietary fiber products because it can impact the physical and chemical properties of the processed products.

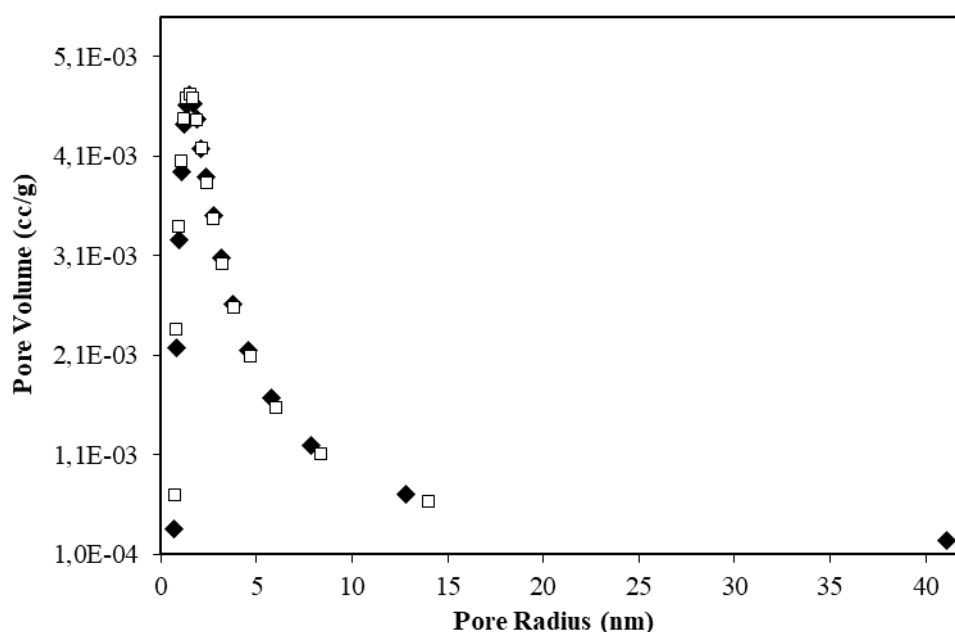


Figure 5 – Analysis of dietary fiber products from corn stalks using the BET instrument (♦ Adsorption and □ Desorption)

The pore surface area obtained was $3.07 \text{ m}^2/\text{g}$, pore size = $0.7\text{--}41 \text{ nm}$, adsorption pore volume = $3.58\text{E-}03 \text{ cc/g}$, desorption pore volume = $3.60\text{E-}03 \text{ cc/g}$. The adsorption and desorption abilities of dietary fiber products that are almost the same are considered good in several ways, including: 1) Moisture balance: Products with balanced adsorption and desorption abilities can maintain optimal humidity so that these conditions can prevent the product from becoming too dry or too humid, which can affect its quality; 2) Product stability: This balance can help maintain the stability of dietary fiber products during storage, reducing the risk of lump formation or mold growth due to excessive moisture; and 3) Performance in the processing: In the food processing, dietary fibers that can absorb and release water well can provide better texture and consistency in the final product.

This study provides a model of the optimum conditions for the process of extracting dietary fiber from corn stalks. The effect of the interaction NaOH concentration and extraction time was achieved at 25.96% NaOH for 65.39 min and produced a yield of dietary fiber of 34.47% , and at the laboratory scale verification stage, a yield of 34.38% was produced. These results promise the feasibility of this method for industrial-scale applications. An important result of this study is that the optimum conditions for the process of extracting dietary fiber from corn stalks

were achieved at a NaOH concentration of 25.96% and an extraction time of 65.39 min , producing dietary fiber of 34.38% .

Based on the results of product characterization, namely WHC and OHC analysis, as well as analysis using FT-IR, SEM, and BET instruments, it provides scientific evidence of the product's feasibility as a source of dietary fiber that supports the potential use of the product as a food ingredient. The implication of this study is the availability of an effective and efficient method for extracting dietary fiber from corn stalks. In addition, the results of this study offer an alternative source of dietary fiber that is abundant, renewable, and sustainable as a filler, especially in meat and fish processing. Recommendations for further research include exploring the application of corn stalk fiber in various food matrices and investigating the long-term stability and sensory properties of products containing this dietary fiber.

Conclusion

This study provides a model of optimal conditions for the process of extracting dietary fiber from corn stalks. The optimum conditions in relation to NaOH concentration and extraction time were achieved at 25.96% NaOH for 65.39 min . Under these conditions, the yield of dietary fiber obtained was 34.47% , and at the laboratory scale verification stage, it was

produced as much as 34.38%. These results confirm the feasibility of this method to be applied on a larger scale. Product characterization based on FT-IR, SEM, BET, WHC, and OHC analyses illustrates the feasibility of the product as a source of dietary fiber and filler in food processing. The implication of this study is the availability of an effective, efficient, and feasible method for extracting dietary fiber from corn stalks that can be applied in industry. In addition, the results of this study inform the existence of an alternative source of dietary fiber that is abundant, renewable, and sustainable to be applied as a filler, especially in meat and fish processing. Recommendations for further research include an exploratory study of the application of corn stalk fiber in various food preparations such as bread, cakes, and noodles/pasta. In addition, research related to the long-term

stability and sensory properties of products containing this dietary fiber.

Acknowledgments

Grant funds from the Directorate of Academic Higher Vocational Education, Kementerian Pendidikan, Kebudayaan, Riset dan Teknologi Republik Indonesia, No:382/SPK/D.D4/PPK.01.APTV/VIII/2024, August 26, 2024.

Conflict of Interest

The authors declare no conflicts of interest or personal relationships with other people or organizations that can inappropriately influence this work.

References

1. Deng W., Feng Y., Fu J., Guo H., et al. (2023). Catalytic conversion of lignocellulosic biomass into chemicals and fuels. *Green. Energy Environ.*, 8, pp. 10-114. <https://doi.org/10.1016/j.gee.2022.07.003>.
2. Yu Z.D., Zhang B.L., Yu F.Q., Xu G.Z., et al. (2012). A real explosion: The requirement of steam explosion pretreatment. *Bioresour Technol.*, 121, pp. 335-341. <https://doi.org/10.1016/j.biortech.2012.06.055>.
3. Zhang C.Y., Su X.J., Xiong X.Y., Hu Q.L., et al. (2016). ^{60}Co - γ radiation-induced changes in the physical and chemical properties of rapeseed straw. *Biomass Bioenergy.*, 85, pp. 207-214. <https://doi.org/10.1016/j.biombioe.2015.11.022>.
4. Liu Y., Chen J.P., Wu X.F., Wang K.Q., et al. (2015). Insights into the effects of γ -irradiation on the microstructure, thermal stability and irradiation-derived degradation components of microcrystalline cellulose (MCC). *RSC Adv.*, 5, pp. 34353-34363. <https://doi.org/10.1039/C5RA03300D>.
5. Fu B.A., Chen M.Q., Li Q.H., Song J.J. (2018) Non-equilibrium thermodynamics approach for the coupled heat and mass transfer in microwave drying of compressed lignite sphere. *Appl. Therm. Eng.*, 133, pp. 237-247. <https://doi.org/10.1016/j.appltherm.2018.01.036>.
6. Kartika S.D., Mohsen G., Yuthana P. (2025). Dietary fiber supplementation in animal products: recent developments, commercial applications and sustainability impact. *Food Bioscience*, 106668. <https://doi.org/10.1016/j.fbio.2025.106668>.
7. SriBala G., Chennuru R., Mahapatra S., Vinu R. (2016). Effect of alkaline ultrasonic pretreatment on crystalline morphology and enzymatic hydrolysis of cellulose. *Cellulose.*, 23, pp. 1725-1740. <https://doi.org/10.1007/s10570-016-0893-2>.
8. Owusu-Ansah P., Besiwhah E.K., Bonah E., Amagloh F.K. (2022). Rheology and microstructure of myofibrillar protein-starch composite gels: Comparison of native and modified starches. *Appl Food Res.*, 2(1), pp. 100044. <https://doi.org/10.1016/j.afres.2022.100044>.
9. Wu M., Wang J., Ge Q., Yu H., Xiong Y.L. (2018). Rheology and microstructure of myofibrillar protein-starch composite gels: Comparison of native and modified starches. *Int. J. Biol. Macromol.*, 118, Part A, pp. 988-996. <https://doi.org/10.1016/j.ijbiomac.2018.06.173>.
10. Wang M., Zhou D., Wang Y., et al. (2016). Bioethanol production from cotton stalks: A comparative study of various pretreatments. *Fuel.*, 184, pp. 527-532. <https://doi.org/10.1016/j.fuel.2016.07.061>.
11. Kim J.S., Lee Y.Y., Kim T.H. (2016). A review on alkaline pretreatment technology for bioconversion of lignocellulosic biomass. *Bioresour Technol.*, 199, pp. 42-48. <https://doi.org/10.1016/j.biortech.2015.08.085>.
12. Jia M., Chen J., Liu X., Xie M., et al. (2019). Structural characteristics and functional properties of soluble dietary fiber from defatted rice bran obtained through *Trichoderma viride* fermentation. *Food Hydrocolloids.*, 94, pp. 468-474. <https://doi.org/10.1016/j.foodhyd.2019.03.047>.
13. Abdul-Hamid A., Yu S.L. (2000). Functional properties of dietary fibre prepared from defatted rice bran. *Food Chem.*, 68(1), pp. 15-19. [https://doi.org/10.1016/S0308-8146\(99\)00145-4](https://doi.org/10.1016/S0308-8146(99)00145-4).
14. Yolmeh M., Habibi N.M., Farhoosh R. (2014). Optimization of ultrasound-assisted extraction of natural pigment from annatto seeds by response surface methodology (RSM). *Food Chem.*, 155, pp. 319-324. <https://doi.org/10.1016/j.foodchem.2014.01.059>.
15. Hubbell C.A., Ragauskas A.J. (2010). Effect of acid-chlorite delignification on cellulose degree of polymerization. *Bioresour Technol.*, 101, pp. 7410-7415. <https://doi.org/10.1016/j.biortech.2010.04.029>.
16. Ciftci D., Flores R.A., Saldaña M.D. (2018). Cellulose fiber isolation and characterization from sweet blue lupin hull and canola straw. *J. Polym. Environ.*, 26, pp. 2773-2781. <https://doi.org/10.1007/s10924-017-1164-5>.

17. Ramdhonee A., Jeetah P. (2017). Production of wrapping paper from banana fibres. *J. Environ. Chem. Eng.*, 5, pp. 4298-4306. <https://doi.org/10.1016/j.jece.2017.08.011>.
18. Joshi A.U., Liu C., Sathe S.K. (2015). Functional properties of select seed flours. *LWT Food Sci. Technol.*, 60, pp. 325-331. <https://doi.org/10.1016/j.lwt.2014.08.038>.
19. Phillips G.O., Williams P.A. (2000). Food Hydrocolloids. (2 Eds.). Cambridge: Woodhead Publishing, pp.710-723.
20. Salim M.R., Asik J., Sarjadi M.S. (2021). Chemical functional groups of extractives, cellulose and lignin extracted from native *Leucaena leucocephala* bark. *Wood Sci. Technol.*, 55, pp. 295-313. <https://doi.org/10.1007/s00226-020-01258-2>.
21. Ciolacu D.E., Ciolacu F., Popa V.I. (2011). Amorphous cellulose-structure and characterization. *Cellul Chem Technol.*, 45(1), pp. 13-21. <https://www.researchgate.net/publication/279897864>.
22. Sun X.F., Xu F., Sun R.C., Fowler P., et al. (2005). Characteristics of degraded cellulose obtained from steam-exploded wheat straw. *Carbohydr. Res.*, 340, pp. 97-106. <https://doi.org/10.1016/j.carres.2004.10.022>.
23. Reddy K.O., Ashok B., Reddy K.R.N., Feng Y.E., et al. (2014). Extraction and characterization of novel lignocellulosic fibers from *Thespesia lampas* plant. *Int. J. Polym. Anal. Charac.*, 19, pp. 48-61. <https://doi.org/10.1080/1023666X.2014.854520>.
24. Seki Y., Sarikanat M., Sever K., Durmuşkahya C. (2013). Extraction and properties of *Ferula communis* (chakshir) fibers as novel reinforcement for composites materials. *Composites, Part B.*, 44, pp. 517-523. <https://doi.org/10.1016/j.compositesb.2012.03.013>.
25. Vârban R., Crişan I., Vârban D., Ona A., et al. (2021). Comparative FT-IR prospecting for cellulose in stems of some fiber plants: Flax, velvet leaf, hemp and jute. *Appl. Sci.*, 11(18), pp. 8570. <https://doi.org/10.3390/app11188570>.

Information about authors

Fajriyati Mas'ud – PhD, Associate Professor, Politeknik Negeri Ujung Pandang (Makassar, Indonesia, e-mail: fajri888@poliupg.ac.id)

Vilia Darma Paramita – PhD, Associate Professor, Politeknik Negeri Ujung Pandang (Makassar, Indonesia, e-mail: viliadarma@poliupg.ac.id)

Zulman Wardi – Master of Science, Associate Professor, Politeknik Negeri Ujung Pandang (Makassar, Indonesia, e-mail: zulward62@poliupg.ac.id)

Yuliani HR – Master of Science, Assistant Professor, Politeknik Negeri Ujung Pandang (Makassar, Indonesia, e-mail: yulianihr@poliupg.ac.id)

K. Akatan^{1*}, N. Kaiyrbekov¹, A. Demeukhan¹,
 A. Battalova¹, E. Shaimardan², M. Beisebekov²,
 F. Kholiya³, Zh. Ibraeva⁴, S. Kabdrakhmanova^{3*}

¹S. Amanzholov East Kazakhstan University, Ust-Kamenogorsk, Kazakhstan

²Scientific Center of Composite Materials, Almaty, Kazakhstan

³Satbayev University, Almaty, Kazakhstan

⁴Abai Kazakh National Pedagogical University, Almaty, Kazakhstan

*e-mail: ahnur.hj@mail.ru, sanaly33@mail.ru

(Received 4 June 2025; received in revised form 9 June 2025; accepted 14 June 2025)

Synthesis of Cellulose based Hydrogel with High Absorption Capacity

Abstract. In this work, the possibility of obtaining biohydrogels from carboxymethyl cellulose (CMC) and hydroxyethyl cellulose (HEC) using citric acid (CA) as a cross-linking agent was investigated. CMC and HEC used in the work were synthesized from microcrystalline cellulose obtained from sunflower seed husks (SFH). More specifically, local agricultural waste was used as a raw material source for the monomers used to produce the hydrogel. The chemical and crystal structures of the synthesized hydrogel were analyzed using FTIR and XRD techniques, with comparisons made to the initial monomers. The thermal stability of the synthesized hydrogel was 580°C, and the mechanical strength was 134 kPa. According to the kinetics of swelling in water, it was found that the degree of swelling in the first two hours was 500%. The hydrogel synthesized on the basis of cellulose showed high potential for use as a biodegradable composite sorbent for purification of water from heavy metals, drug delivery and protect plants from drought.

Key words: biohydrogel; carboxymethylcellulose; hydroxyethylcellulose; citric acid; swelling kinetics.

Introduction

Hydrogels are three-dimensional polymer matrices that have the ability to swell significantly in aqueous media due to the retention of a large volume of liquid in their structure without dissolution [1]. This feature determines their application in various fields – from biomedicine to agriculture, from sensor devices to substance delivery systems [2]. In recent years, growing attention has been directed toward the development of biodegradable hydrogels derived from natural, renewable resources — primarily polysaccharides such as cellulose, alginates, chitosan, and their derivatives [3].

The use of natural polymers to produce biohydrogels is associated not only with their environmental safety, but also with a high degree of biocompatibility, low cytotoxicity and availability of raw materials.

Cellulose, as the most common natural polysaccharide on Earth, is of particular interest in the context of hydrogel synthesis due to the possibility of chemical modification and cross-linking under mild conditions [4]. Such derivatives easily form gel-like

structures through both physical and chemical cross-linking [5].

The physicochemical characteristics of biohydrogels directly depend on the nature of the polymer used, the method of cross-linking, the degree of substitution of functional groups and the synthesis conditions [6]. The main parameters that determine the functionality of the gel system are the degree of swelling, porosity, mechanical strength, thermal stability and degradation kinetics [7-9].

In the study, hydrogels were synthesized for drug delivery and heavy metal ion sorption in water using hydroxyethyl cellulose (HEC) and carboxymethylcellulose (CMC) as monomers, methylene bisacrylamide (MBA) and epichlorohydrin (ECH) as cross-linking agents. According to the study results, the hydrogel using MBA as a cross-linking agent was pH sensitive, releasing 85.2% of the drug at pH 7.4. On the other hand, the hydrogel using ECH as a cross-linking agent was able to sorb up to 90% of Cu²⁺ in water within one hour. However, the use of synthetic cross-linking agents in these studies does not allow the obtained hydrogels to be fully assessed as

biohydrogels. In this regard, the possibility of using organic acids as cross-linking agents, such as citric, succinic, fumaric and malic acids, has been widely studied in recent scientific works [10-11]. The studies have established that the use of natural organic acids as cross-linking agents increases the biocompatibility of the hydrogel, its chemical and physical structural stability, as well as its sorption capacity [12-13].

Based on the results of the literature review, the development of fully biocompatible cellulose-based materials is consistent with the goals of “Sustainable Development”, the study investigated the possibility of synthesizing CMC and HEC from microcrystalline cellulose (MCC) obtained from local agricultural waste and then cross-linking CMC and HEC with citric acid to obtain a hydrogel. The physicochemical properties of the obtained hydrogel were determined.

Materials and methods

Materials. The following reagents were used in this work: epichlorohydrin (99%); sodium hydroxide (NaOH, $\geq 98\%$); urea (carbamide, $\text{CH}_4\text{N}_2\text{O}$, $\geq 99\%$); citric acid ($\geq 99.5\%$); acetic acid (CH_3COOH , $\geq 99\%$); ethanol ($\text{C}_2\text{H}_5\text{OH}$, 95%). All chemical reagents were purchased from Sigma Aldrich and used without further purification.

Obtaining of MCC. To obtain microcrystalline cellulose, plant raw material – sunflower seed husks (SFH) – was used. MCC was obtained based on the method of Battalova, A., et al., 2024 [14]. A sample of 10 g of SFHs was measured, and a SFH to polyacrylic acid (PAA) ratio of 1:14 g/mL was used. The mixture was subjected to continuous vigorous stirring and boiled at $90 \pm 5^\circ\text{C}$ in a rotary flask. After heating, the mixture was cooled using a condenser to achieve delignification. The resulting MCC was then brought to $25 \pm 2^\circ\text{C}$, filtered, and washed with distilled water until neutral. Finally, it was dried at $80 \pm 2^\circ\text{C}$ for 6 hours until a stable weight was attained (Figure 1).

Synthesis of carboxymethylcellulose (CMC)
To prepare CMC, 5 g of microcrystalline cellulose (MCC) were combined with 100 ml of 95% ethanol and 10 ml of 45% NaOH solution in a flask. The mixture was stirred at 750 rpm using a magnetic stirrer for 60 minutes at room temperature. Subsequently, 5 ml of trichloroacetic acid were added, and the reaction mixture was heated in a water bath at 60°C for another 60 minutes while stirring. After cooling to room temperature, the mixture was neutralized to a pH of 6–7 using glacial acetic acid. The resulting product was filtered through paper and washed with

500 ml of 80% ethanol using a Soxhlet extractor for 3 hours. Finally, the synthesized CMC was air-dried at room temperature. (Figure 2).



Figure 1 – Obtained MCC sample



Figure 2 – Synthesized CMC

Obtaining of hydroxyethyl cellulose (HEC). To prepare the alkaline system, a NaOH/urea/water mixture in a volume ratio of 5:7.3:50 (ml) was added to 50 ml of distilled water and stirred for 10 minutes. The resulting solution was then placed in a freezer at -12°C for 6 hours. After cooling, it was allowed to thaw at room temperature, and a 5% suspension of microcrystalline cellulose was prepared. While continuously stirring, 45 ml of epichlorohydrin were

gradually added to the suspension. The reaction was maintained at 25 °C for 1 hour using a magnetic stirrer, followed by further incubation at 50 °C for 5 additional hours. The final product was neutralized with acetic acid and washed with distilled water until a neutral pH of 7 was reached. The suspension was subsequently frozen for 24 hours and lyophilized at -40 °C (Figure 3).



Figure 3 – Synthesized HEC

Obtaining biohydrogel. The biohydrogel was synthesized based on a mixture of CMC and HEC polymers, using citric acid (CA) as a crosslinking agent. For this purpose, a polymer solution with a total concentration of 2% by weight (relative to water) was prepared in distilled water at room temperature, with a mass ratio of CMC:HEC of 2:1, respectively. Considering the faster solubility of HEC, it was first dissolved in water, obtaining a moderately viscous transparent solution within 5 minutes. After that, CMC was added to the solution and stirring was continued for 24 hours, which resulted in the formation of a viscous homogeneous gel-like solution. Then citric acid was added to the mixture in an amount equal to 15% of the polymer composition weight. To preliminarily remove moisture, the samples were dried at a temperature of $40 \pm 2^\circ\text{C}$ for 24 hours. After this, heat-induced crosslinking was carried out at a temperature of $80 \pm 5^\circ\text{C}$ for the next 24 hours, with periodic monitoring of the state of the samples (Figure 4). The hydrogel synthesized during the study was conventionally designated as CMC/HEC hydrogel.

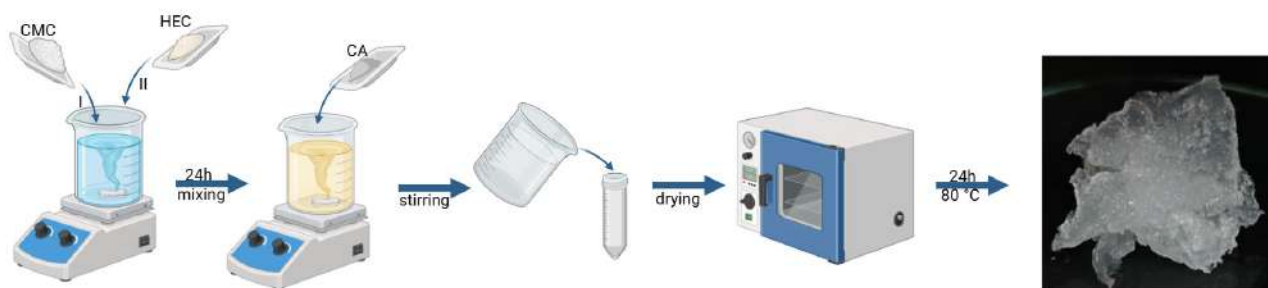


Figure 4 – Synthesis scheme of CMC/HEC hydrogel

IR-Fourier analysis. FTIR spectra were recorded using an FT-801 spectrometer (Simex, Russia) with a resolution of 1 cm^{-1} over the wavelength range of $500\text{--}4000\text{ cm}^{-1}$. The standard KBr pellet method was used, with the sample and potassium bromide mixed in a 1:10 ratio. Measurements were conducted at 25°C with 100 scans per sample. Prior to use, the potassium bromide was ground and preheated at 200°C for 3 hours to remove moisture.

XRD analysis. The crystalline structures of the samples were examined using an XPertPRO dif-

fractometer (Malvern Panalytical Empyrean, Netherlands) equipped with monochromatic $\text{CuK}\alpha$ radiation. Scanning was performed in the 2θ range of $10^\circ\text{--}45^\circ$ with a step size of 0.02° . The X-ray tube operated at a voltage of 45 kV and a current of 30 mA, with a measurement time of 0.5 seconds per step.

TGA analysis. The thermal properties of the hydrogel were investigated using a BXT-TGA 103 differential thermogravimetric analyzer (China) under an argon atmosphere. The analysis was conducted

over a temperature range of 30–700 °C, with a heating rate of 10 ± 1 °C per minute. The initial sample mass was approximately 20 ± 2 mg.

Mechanical properties. The mechanical properties of the obtained CMC/HEC hydrogel were determined by compression using a TA.XT-3000 texture analyzer (China) under standard conditions at a temperature of 25 ± 2 °C. Cylindrical hydrogel samples with a diameter of about 10 mm and a height of 10 mm were formed for testing, the surfaces of which were leveled to distribute the load uniformly. A metal cylindrical probe with a diameter of 25 mm was used as a loading element. The tests were carried out in compression mode with the following parameters: approach speed – 1.0 mm/s, compression speed – 0.5 mm/s, probe penetration depth – 5 mm or until sample failure, maximum load – up to 500N. The sample was placed in the center of the device platform, after which the probe performed a vertical movement at a given speed.

Study of the swelling kinetics of biohydrogel. Hydrogel samples weighing 0.1 g were placed in a container with distilled water at a temperature of 25 ± 1 °C, periodically removed, excess water was removed with filter paper and weighed until a constant mass was achieved. The swelling degree (Q , g/g) was calculated as the ratio of the mass of the swollen hydrogel to the initial mass of the dry sample. The experiments were carried out in triplicate with subsequent averaging of the results. The swelling degree α was calculated using the formula:

$$\alpha (\%) = (m - m_0) / m_0 * 100\% \quad (1)$$

where m is the mass after swelling of CMC/HEC hydrogel, m_0 is the initial mass of CMC/HEC hydrogel.

Results and discussion

FTIR analysis. Comparative IR spectra of the initial monomers and the synthesized hydrogel are shown in Figure 5. FTIR of CMC (Fig. 5a) is characterized by the presence of a broad band at about 3420 cm^{-1} , attributed to the stretching vibrations of hydroxyl groups (O–H), and a band at 2920 cm^{-1} , corresponding to vibrations of methylene groups (C–H) [15–17]. CMC is also typically characterized by the presence of pronounced carboxylate bands at 1640 and 1630 cm^{-1} , caused by asymmetric and symmetric stretching vibrations of COO^- groups, and a band at about 1060 cm^{-1} (C–O–C), associated with glycosidic bridges [18–19].

Figure 5b FTIR HEC revealed a broad absorption at 3358 cm^{-1} due to the O–H stretching vibration [16]. Another medium absorption band is present at 2875.57 cm^{-1} characterizing the C–H stretching vibration. The peaks at 1690 cm^{-1} and 1407 cm^{-1} were assigned to the O–H plane strain and C–H symmetric bending vibrations respectively in CH_2O [19]. Moreover, the beta-(1,4) glycoside bond was indicated by the absorption band present at 930 cm^{-1} . The absorption peak at 1120 cm^{-1} is due to the C–O antisymmetric vibration [20]. Similarly, the absorption peak at 1030 cm^{-1} is attributed to the C–O–C valence vibration in the glucopyranose structure [21].

The IR spectra of CMC/HEC hydrogel showed the characteristic absorption peaks of CMC and HEC, indicating the successful preparation of the hydrogel (Fig. 5c). A slight shift of OH groups from 3350 cm^{-1} to 3450 cm^{-1} was observed in the comparative study with CMC and HEC. This indicates the successful crosslinking of CMC and HEC by citric acid to form the biohydrogel. In addition, it was noted that the signals of carboxyl and OH groups in the range of $1630\text{--}1690 \text{ cm}^{-1}$ in the spectra of the original CMC and HEC monomers overlap with each other in the spectrum of the CMC/HEC hydrogel and shift to 1740 cm^{-1} . This is explained by a decrease in the mobility of the carboxyl and hydroxyl groups linked to each other. [22–23]. This also corresponds to the characteristic stretching band of the carbonyl group associated with the formation of ester bonds in the hydrogel network, which confirms successful crosslinking and formation of the hydrogel.

XRD analysis. Comparative diffraction patterns of the initial CMC and HEC monomers and the synthesized CMC/HEC hydrogel are shown in Figure 6. In the CMC and HEC samples, diffraction peaks were recorded at 2θ 20.5° and 22.4° . This is typical for the crystal structure of cellulose II, which corresponds to hkl 110 [24]. A peak at 2θ 22.4° was found in the diffraction pattern of the CMC/HEC hydrogel. It is evident that the intensity of the diffraction peak decreased by 2 times compared to CMC and HEC. This is due to the destruction of the crystalline structures of CMC and HEC during chemical crosslinking and an increase in amorphous structures. [25]. Similar results were obtained in X-ray diffraction analysis of hydrogels synthesized from commercial CMC/HEC in [9, 26] studies. It can be concluded that the increased amorphous structure of cellulose monomers can affect the free movement of polymer units in the hydrogel matrix and the free penetration of liquids into the hydrogel.

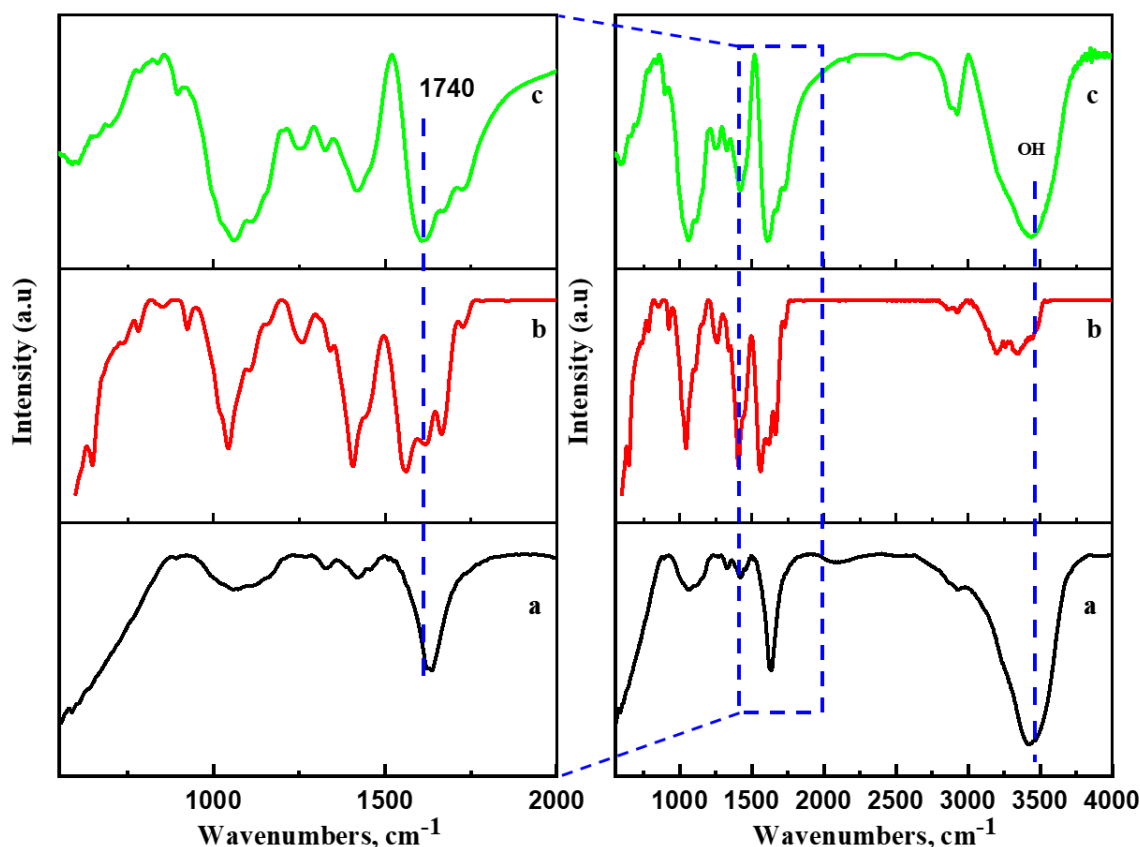


Figure 5 – IR spectra: a) CMC; b) HEC c) CMC/HEC hydrogel

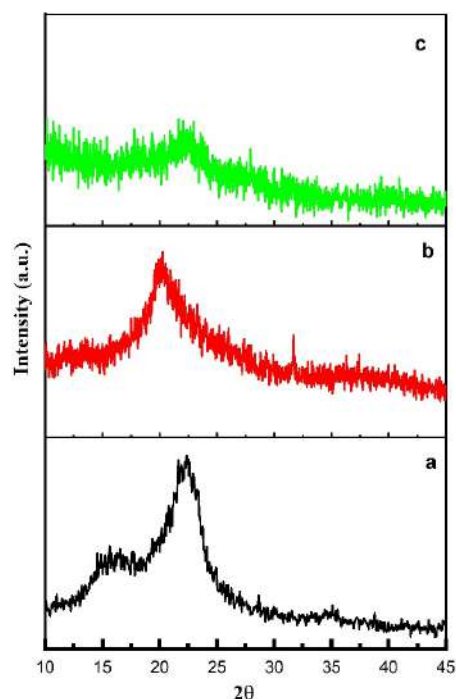


Figure 6 – XRD spectra: a) CMC; b) HEC
c) CMC/HEC hydrogel

TGA analysis. TGA curves of the presented samples show differences in thermal stability and mechanisms of their thermal decomposition (Fig. 7).

TGA of CMC shows three main stages of mass loss (Fig. 7a). The first stage (up to about 200°C) is associated with the evaporation of adsorbed moisture and accounts for about 15% of the total mass. The second and most pronounced stage (200–540°C) corresponds to thermal destruction of the main chain of the cellulose polymer and decarboxylation of carboxyl groups [27, 28], the mass loss is in the range of 40–45%. The last stage of decomposition (above 400°C) is associated with further carbonization and pyrolysis of the polymer, with the formation of a small ash residue after 600°C [29].

The HEC also exhibits a three-stage thermal degradation process (Fig. 7b). The first stage (up to 200°C) is similar to CMC and involves the loss of sorbed water (~17%). The main stage (200–430°C) is accompanied by significant mass loss (~65%) due to the destruction of hydroxyethyl side groups and the main polymer skeleton [27, 30]. In the temperature range of 450°C and above, slow carbonization and

decomposition of residual organic compounds occurs with almost complete combustion in the region of temperatures of 800°C.

The hydrogel shows improved thermal stability compared to individual monomers, which is reflected in a smoother curve and a shift in the decomposition stages towards higher temperatures (Fig. 7c). At the initial stage (up to 200°C), the hydrogel does not lose mass. At temperatures of 200–580°C, 50% of the hydrogel mass undergoes degradation. This occurs due to the rupture of the main glucosidic bonds in the molecules of the original monomers and the ester bonds formed by citric acid [28]. The final stage of thermal degradation occurs at temperatures of 580–800°C. During this period, the hydrogel loses 60% of its initial mass and undergoes depolymerization. As a result, decomposition into CO₂ and other volatile organic compounds occurs. Ikrame Ayouch et. al. 2021 [22] found that the thermal stability of CMC/HEC hydrogel is 365°C. In this study, it was found that the thermal stability of the synthesized hydrogel reaches 580°C. This is 1.5 times higher than the previous study.

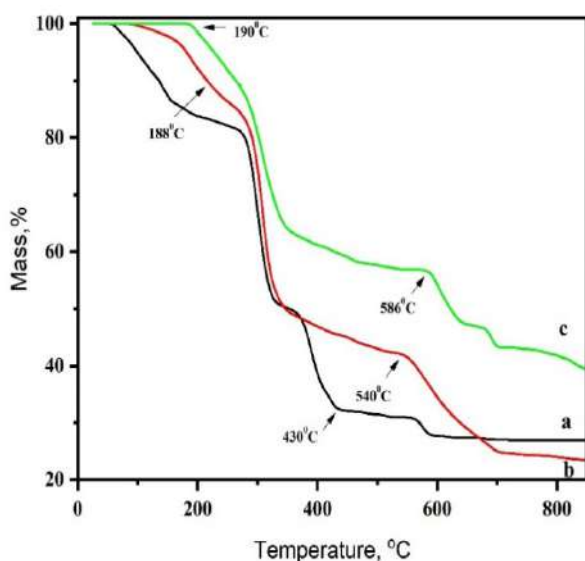


Figure 7 – TGA curves: a) CMC; b) HEC; c) CMC/HEC hydrogel

Mechanical properties of hydrogel. Figure 8 shows the mechanical strength of CMC/HEC hydrogel. The curve shows a gradual increase in stress until reaching a maximum value of about 134 kPa at 22 seconds, followed by a sharp drop, characteristic of the destruction of the material structure. This

type of curve indicates the elastic-plastic behavior of the hydrogel: first, elastic deformation occurs (linear increase in pressure with a small slope), then comes the region of plastic deformation and stress accumulation (a steeper section of the curve to the maximum), after which brittle destruction of the structure occurs.

The achieved high strength index (134±4 kPa) indicates good mechanical properties of the hydrogel and points to the formation of an effective spatial network formed due to chemical crosslinking of the initial polymers. Such mechanical stability is associated with strong ether bonds that arise from the interaction of carboxyl groups of citric acid and hydroxyl groups of cellulose polymers [31]. In studies [32, 33] it was found that the mechanical strength of cellulose-based hydrogels was similar to the results obtained in this study.

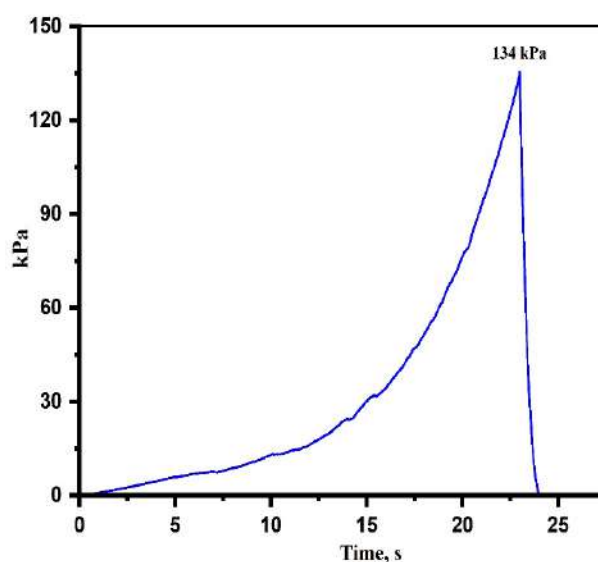


Figure 8 – Mechanical strength curve of CMC/HEC hydrogel

Study of hydrogel swelling kinetics. Figure 9 shows the kinetics of hydrogel swelling in water. The process of hydrogel swelling in water was carried out for two days until the mass stabilized. The swelling process can be divided into two stages. the hydrogel exhibited a swelling degree of up to 500±25% within the first two hours, indicating a rapid and intensive swelling process. This accelerated water absorption is attributed to the abundance of hydrophilic groups – such as hydroxyl and carboxyl – in the monomer units of the hydrogel, which pro-

mote the quick diffusion of water molecules into the polymer network [34]. In the second stage, between 2 and 30 hours, the degree of hydrogel swelling decreased by half, and the degree of swelling was $225 \pm 15\%$. This indicates that the hydrogel structure is compacted due to the saturation of hydrophilic groups in the monomer molecules with water molecules, and the process of water repulsion along it occurs, and equilibrium is established [35, 36]. Thus, the swelling kinetics confirms the efficiency of the hydrogel in retaining a significant volume of water, which is due to its hydrophilic nature and stable three-dimensional structure. Zhou J. et al. (2007) and Jitka Sotolařová et al. (2021) [37, 38] studied the swelling kinetics of cellulose-based hydrogels in water and obtained results similar to those of the present study.

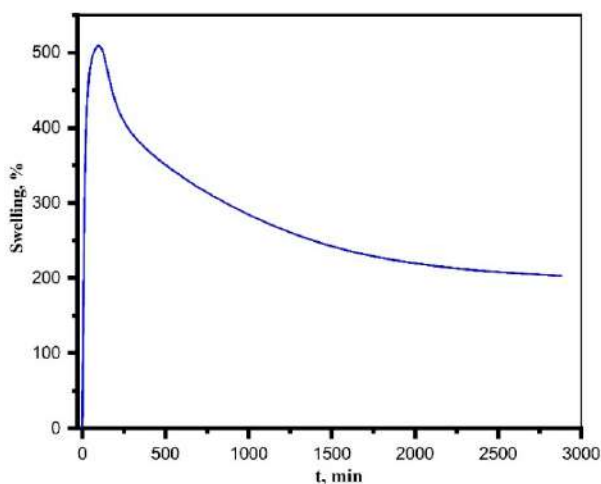


Figure 9 – Swelling kinetics curve of CMC/HEC hydrogel

Conclusion

In the course of the study, a biohydrogel based on CMC and HEC was synthesized using citric acid as a cross-linking agent. Based on the results obtained, the IR Fourier method determined that the hydrogel is cross-linked by hydroxyl and carboxyl groups of citric acid and the original monomers, CMC and HEC molecules. According to X-ray structural analysis, the crystalline structure of the CMC/HEC hydrogel has increased amorphism compared to the original monomers. The degree of swelling of the hydrogel in water reached 500% in the first two hours, and after 30 hours it decreased by 2 times, and the saturation process occurred. Resistance to external mechanical loads was 134 kPa. According to the TGA analysis, it was found that 50% of the initial mass of the hydrogel is subject to thermal degradation in the temperature range of 200-580°C, and 60% of the initial mass is lost in the temperature range of 580-800°C. Based on the results obtained, it can be seen that the CMC/HEC hydrogel has high potential for use in agricultural production as a soil conditioner to protect plants from drought, as well as for the sorption of heavy metal ions in water by immobilizing complexones in the matrix and as a carrier for the sorption of drugs in pharmaceuticals.

Acknowledgements

This research has been funded by the Science Committee of the Ministry of Science and Higher Education of the Republic of Kazakhstan (Grant No. AP23490029).

Conflict of interest

All authors are aware of the article's content and declare no conflict of interest.

References

1. Aswathy S.H., Narendra Kumar U., Manjubala I. (2022) Physicochemical Properties of Cellulose-Based Hydrogel for Bio-medical Applications. *Polym.*, 14(21), pp. 4669. <https://doi.org/10.3390/polym14214669>.
2. Koshenaj K., Ferrari G. (2024) A Comprehensive Review on Starch-Based Hydrogels: From Tradition to Innovation, Opportunities, and Drawbacks. *Polym.*, 16(14), pp. 1991. <https://doi.org/10.3390/polym16141991>.
3. Manuel M., Jennifer A. (2023) A Review on Starch and Cellulose-Enhanced Superabsorbent Hydrogel. *J. Chem. Rev.*, 5(2), pp. 183-203. <https://doi.org/10.22034/jcr.2023.382452.1209>.
4. Sringam J., et al. (2022) Improving Mechanical Properties of Starch-Based Hydrogels Using Double Network Strategy. *Polym.*, 14(17), pp. 3552. <https://doi.org/10.3390/polym14173552>.
5. Ahmed E.M. (2015) Hydrogel: Preparation, characterization, and applications: A review. *J. Adv. Res.*, 6(2), pp. 105-121. <https://doi.org/10.1016/j.jare.2013.07.006>.
6. Thakur V.K., Thakur M.K. (2014) Processing and characterization of natural cellulose fibers/thermoset polymer composites. *Carbohydr. Polym.*, 109, pp. 102-117. <https://doi.org/10.1016/j.carbpol.2014.03.039>.

7. Zhao W., Jin X., Cong Y., Liu Y., Fu J. (2018) Degradable Natural Polymer Hydrogels for Articular Cartilage Tissue Engineering. *J. Chem. Techn. Biotechn.*, 93(2), pp. 403-421. <https://doi.org/10.1002/jctb.3970>.
8. Kadry G., Aboelmagd E.I., Ibrahim M.M. (2019) Cellulosic-based hydrogel from biomass material for removal of metals from waste water. *J. Macromol. Sci., Part A*, 61(6), pp. 419-428. <http://dx.doi.org/10.1080/10601325.2019.1640063>.
9. Wen X., Bao D., Chen M., Zhang A., Liu C., Sun R. (2015) Preparation of CMC/HEC Crosslinked Hydrogels for Drug Delivery. *BioRes.*, 10(4), pp. 8339-8351. <http://dx.doi.org/10.15376/biores.10.4.8339-8351>.
10. Oladosu Y., Rafii M.Y., Arolo F., Chukwu S.C., Salisu M.A., Fagbohun I.K., Muftaudeen T.K., Swaray S., Haliru B.S. (2022) Superabsorbent Polymer Hydrogels for Sustainable Agriculture: A Review. *Horticulturae*, 8, pp. 605. <https://doi.org/10.3390/horticulturae8070605>.
11. Seki, Y., Altinisik, A., Demircioğlu, B. et al. (2014) Carboxymethylcellulose (CMC)–hydroxyethylcellulose (HEC) based hydrogels: synthesis and characterization. *Cellulose*, 21, pp. 1689-1698. <https://doi.org/10.1007/s10570-014-0204-8>.
12. Zhang W., Liu Y., Xuan Y., Zhang S. (2022) Synthesis and Applications of Carboxymethyl Cellulose Hydrogels. *Gels*, 8, pp. 529. <https://doi.org/10.3390/gels8090529>.
13. Nasution H., Harahap H., Dalimunthe N.F., Ginting M.H.S., Jaafar M., Tan O.O.H., Aruan H.K., Herfananda A.L. (2022) Hydrogel and Effects of Crosslinking Agent on Cellulose-Based Hydrogels: A Review. *Gels*, 8(9), pp. 568. <https://doi.org/10.3390/gels8090568>.
14. Battalova A., Ibraeva Z., Kabdrakhmanova S., Akatan K., Shaimardan E., Demeukhan A., Tursyngazykyzy A., Beisebekov M., Maussumbayeva A. (2024) Comparative characteristics of microcrystalline cellulose obtained from the rice waste production of Kazakhstan. *Chem. Bull. Kaz. Nat. Univ.*, 113(4), pp. 14-23. <https://doi.org/https://doi.org/10.15328/cb1386>.
15. Tang Q., Zhang Y., Li Y., Yang H. (2022) Biodegradable Hydrogels for Biomedical Applications. *Gels*, 8(11), pp. 695. <https://doi.org/10.3390/gels8110695>.
16. Denagbe W., Mazet E., Desbrières J., Michaud P. (2025) Superabsorbent polymers: Eco-friendliness and the gap between basic research and industrial applications. *React. Funct. Polym.*, 214, pp. 106278. <https://doi.org/10.1016/j.reactfunctpolym.2025.106278>.
17. Fan M., Dai D., Huang B. (2019) Fourier Transform Infrared Spectroscopy for Natural Fibres. *Fourier Transf. -Mat. Anal.*, 3, pp. 45-68. <https://doi.org/10.5772/intechopen.80207>.
18. Kassab Z., Abdellaoui Y., Hamid M., Achaby M.El. (2020) Cellulosic materials from pea (*Pisum Sativum*) and broad beans (*Vicia Faba*) pods agro-industrial residues. *Mater. Lett.*, 280, pp. 128539. <https://doi.org/10.1016/j.matlet.2020.128539>.
19. Darbasizadeh B., Fatahi Y., Feyzi-barnaji B., Arabi M., Motasadzadeh H., Farhadnejad H., Moraffah F., Rabiee N. (2019) Crosslinked-polyvinyl alcohol-carboxymethyl cellulose/ZnO nanocomposite fibrous mats containing erythromycin (PVA-CMC/ZnO-EM): Fabrication, characterization and in-vitro release and anti-bacterial properties. *Int. J. Biol. Macromol.*, 141, pp. 1137-1146. <https://doi.org/10.1016/j.ijbiomac.2019.09.060>.
20. Gong T., Hou Y., Yang X., Guo Y. (2019) Gelation of hydroxyethyl cellulose aqueous solution induced by addition of colloidal silica nanoparticles. *Int. J. Biol. Macromol.*, 134, pp. 547-556. <https://doi.org/10.1016/j.ijbiomac.2019.05.069>.
21. Kassab Z., Boujemaoui A., Ben Youcef H., Hajlane A., Hannache H., Achaby M.El. (2019) Production of cellulose nanofibrils from alfa fibers and its nanoreinforcement potential in polymer nanocomposites. *Cellulose*, 26, pp. 9567-9581. <https://doi.org/10.1007/s10570-019-02767-5>.
22. Ayouch I., Kassem I., Kassab Z., Barrak I., Barhoun A., Jacquemin J., Draoui K., El Achaby M. (2021) Crosslinked carboxymethyl cellulose-hydroxyethyl cellulose hydrogel films for adsorption of cadmium and methylene blue from aqueous solutions. *Surf. Interf.*, 24, pp. 101124. <https://doi.org/10.1016/j.surfin.2021.101124>.
23. Seki Y., Altinisik A., Demircioglu B., Tetik C. (2014) Carboxymethylcellulose (CMC)-hydroxyethylcellulose (HEC) based hydrogels: Synthesis and characterization. *Cellulose*, 21, pp. 1689-1698. <https://doi.org/10.1007/s10570-014-0204-8>.
24. Battalova A., Kabdrakhmanova S., Akatan K., Shaimardan E., Beisebekov M., Karzhaubayeva A., Kantay N., Ibraeva Zh., Thomas S. (2025) Synthesis and Application of Biodegradable Cellulose Hydrogels From Sunflower Husks as a Water-Retaining Material in Agriculture. *J. Polym. Sci.*, pp. 1-12. <https://doi.org/10.1002/pol.20240486>.
25. Yang S., Fu S., Liu H., Zhou Y., Xueyun L. (2011) Hydrogel Beads Based on Carboxymethyl Cellulose for Removal Heavy Metal Ions. *J. Appl. Polym. Sci.*, 119(2), pp. 1204-1210. <https://doi.org/10.1002/app.32822>.
26. Akar E., Altınışık A., Seki Y. (2012) Preparation of pH- and ionic-strength responsive biodegradable fumaric acid cross-linked carboxymethyl cellulose. *Carbohydr. Polym.*, 90(4), pp. 1634-1641. <https://doi.org/10.1016/j.carbpol.2012.07.043>.
27. Luo X., Liu C., Wang Y., Huang Y., Yao J. (2020) Preparation and characterization of hydroxyethyl cellulose/poly(vinyl alcohol) composite films with improved mechanical and water resistance properties. *Cellulose*, 27(11), pp. 6535-6546. <https://doi.org/10.1007/s10570-020-03221-8>.
28. Demitri C., Scalera F., Madaghiele M., Sannino A., Maffezzoli A. (2018) Potential of cellulose-based superabsorbent hydrogels as water reservoir in agriculture. *Int. J. Polym. Sci.*, pp. 1-6. <https://doi.org/10.1155/2018/4350734>.
29. Wang M., Chen X., Zhang H., Zhang Y. (2019) Thermal decomposition and kinetic analysis of carboxymethyl cellulose based polymer electrolytes. *J. Therm. Anal. Calorim.*, 135(3), pp. 2305-2313. <https://doi.org/10.1007/s10973-018-7442-2>.
30. Barud H.S., de Araújo Júnior A.M., Santos D.B., de Assunção R.M.N., Meireles C.S., Cerqueira D.A., Ribeiro C.A. (2008) Thermal behavior of cellulose derivatives. *J. Therm. Anal. Calorim.*, 93(3), pp. 817-821. <https://doi.org/10.1007/s10973-007-8439-1>.
31. Chang C., Peng J., Zhang L., Pang J. (2021) Cellulose-based hydrogels: Preparation, properties, and applications. *Polym. Rev.*, 61(2), pp. 257-307. <https://doi.org/10.1080/15583724.2020.1861143>.
32. Aswathy S.H., NarendraKumar U., Manjubala I. (2022). Physicochemical Properties of Cellulose-Based Hydrogel for Bio-medical Applications. *Polym.*, 14(21), pp. 4669. <https://doi.org/10.3390/polym14214669>.

33. Ciolacu D.E., Suflet D.M. (2019) Cellulose-Based Hydrogels for Medical/Pharmaceutical Applications. Elsevier B.V.: Amsterdam, The Netherlands. ISBN 9780444637741.
34. Li J., Mooney D.J. (2016) Designing hydrogels for controlled drug delivery. *Nat. Rev. Mat.*, 1(12), pp. 16071. <https://doi.org/10.1038/natrevmats.2016.71>.
35. Kabiri K., Omidian H., Hashemi S.A., Zohuriaan-Mehr M.J. (2011) Synthesis and characterization of hydrogels. *Eur. Polym. J.*, 47(2), pp. 1133-1145. <https://doi.org/10.1016/j.eurpolymj.2011.02.022>.
36. Peppas N.A., Sahlin J.J. (1989) A simple equation for the description of solute release. III. Coupling of diffusion and relaxation. *Int. J. Pharm.*, 57(2), pp. 169-172. [https://doi.org/10.1016/0378-5173\(89\)90306-2](https://doi.org/10.1016/0378-5173(89)90306-2).
37. Zhou J., Chang C., Zhang R., Zhang L. (2007) Hydrogels prepared from unsubstituted cellulose in NaOH/urea aqueous solution. *Macromol. Biosci.*, 7(6), pp. 804-809. <https://doi.org/10.1002/mabi.200700007>.
38. Sotolářová J., Vinter Š., Filip J. (2021) Cellulose derivatives crosslinked by citric acid on electrode surface as a heavy metal absorption/sensing matrix. *Coll. Surf. A: Physicochem. Eng. Aspects*, 628, pp. 127242. <https://doi.org/10.1016/j.colsurfa.2021.127242>.

Information about authors

Kydyrmolla Akatan – PhD, S. Amanzholov East Kazakhstan University (Oskemen, Kazakhstan, e-mail: ahnur.hj@mail.ru)

Nariman Kaiyrbekov – Junior research assistant, S. Amanzholov East Kazakhstan University (Oskemen, Kazakhstan, e-mail: narimankayrbekov@gmail.com)

Ansagan Demeukhan – Junior researcher, S. Amanzholov East Kazakhstan University (Oskemen, Kazakhstan, e-mail: demeuhanansagan@gmail.com)

Ainur Battalova – Junior researcher, S. Amanzholov East Kazakhstan University (Oskemen, Kazakhstan, e-mail: 2012kausar@mail.ru)

Esbol Shaimardan – PhD, Scientific Center of Composite Materials (Almaty, Kazakhstan, e-mail: esbol_shay@mail.ru)

Madiar Beisebekov – PhD, Scientific Center of Composite Materials (Almaty, Kazakhstan, e-mail: make1987@mail.ru)

Faisal Kholiya – PhD, Satbayev University (Almaty, Kazakhstan, e-mail: faisalkholiya91@gmail.com)

Zhanar Ibraeva – Candidate of Chemical Sciences, Associate Professor, Abai Kazakh National Pedagogical University (Almaty, Kazakhstan, e-mail: Zhanar-ibraeva@mail.ru)

Sana Kabdrakhmanova – Candidate of Technical Sciences, Associate Professor, Satbayev University (Almaty, Kazakhstan, e-mail: sanal33@mail.ru)

U. Rahma , M. Zulfajri* , S. Ismulyati 

Universitas Serambi Mekkah, Banda Aceh, Indonesia

*e-mail: muhammad.zulfajri@serambimekkah.ac.id

(Received 3 May 2025; received in revised form 19 May 2025; accepted 29 May 2025)

Evaluation of anthocyanin extracted from Lempeni (*Ardisia Elliptica* L.) fruit as a new natural acid-base indicator

Abstract: The *Ardisia elliptica* species is usually known as Lempeni fruit has a purplish red color which contains the color pigment of anthocyanins. This work aimed to obtain anthocyanins from Lempeni fruit and applied them as new acid-based indicators. The extraction method was carried out using a combination solvent containing ethanol and HCl with appropriate ratio, followed by the addition of anthocyanin-containing extract with acid and base solutions. The results showed that anthocyanin from Lempeni fruit induced a significant color response depending on the pH values of acid-base solutions. The color was changed to red in acidic environments and brownish green in alkaline environments. Besides, the filter paper indicator and acid-base titrations were performed with good performances. The utilization of a natural acid-base indicators from anthocyanins offers potential applications in qualitative analysis and scientific education, by exploring new sources of anthocyanins. This research contributes to the understanding of the potential use of anthocyanins from Lempeni fruit in environmentally friendly and economical analytical chemistry applications.

Key words: Extraction, Anthocyanin; Lempeni fruit; Natural indicator; Acid base.

Introduction

Anthocyanins are a group of water-soluble pigments widely distributed in the plant kingdom, particularly in fruits, vegetables, and flowers [1]. These natural compounds are responsible for a wide range of colors such as red, purple, and blue, which vary depending on their molecular structure and the pH of their environment [2]. In acidic conditions, anthocyanins typically appear red, while in neutral conditions they may turn purple, and in alkaline environments they can shift to bluish-green [3]. This reversible color change makes anthocyanins not only visually striking but also functionally useful as natural pH indicators [4]. Their ability to respond sensitively and rapidly to pH variations has attracted significant attention for applications in analytical chemistry, environmental monitoring, food packaging, and even cosmetics.

Indicators are substances that exhibit a specific color at a particular pH level and undergo a noticeable color change when the pH shifts [5]. This transformation provides a visual signal to determine whether a solution is acidic or basic. While synthetic indicators such as phenolphthalein, methyl orange, bromothymol blue, and methyl red are commonly used in laboratories,

they often raise concerns due to toxicity, high production costs, and environmental persistence [6]. In light of these concerns, researchers have increasingly turned to plant-based alternatives that are biodegradable, less toxic, and often more accessible [7]. Natural indicators derived from plant pigments offer a safer and more sustainable option for educational, laboratory, and field-based pH testing [8].

Several studies have demonstrated the extracts of anthocyanins from various plant sources for use as natural indicators such as purple cabbage, magenta, amaranth, red beet, flamingo lily, passion flower, garden dahlia, mulberry, jungle flame flower, *Butea monosperma*, etc. [9, 10]. Besides, Ernawati and Rahayu investigated the extraction of anthocyanins from mangosteen peel using ethanol: HCl solvents [11]. Their results indicated that the ethanol-HCl solvent combination produced the most concentrated extract with the clearest and most intense color transitions across acidic and basic conditions when applied to filter paper. This study highlighted the importance of solvent selection of optimizing anthocyanin yield and indicator effectiveness, setting a precedent for further research into other anthocyanin-rich plant materials.

One such promising yet underutilized source is Lempeni (*Ardisia elliptica* L.) fruit, which is known

for its deep coloration and significant anthocyanin content [12]. Locally known in Indonesia as “lempeni,” this fruit refers to *Ardisia elliptica*, a tropical shrub or small tree native to Southeast Asia, including Indonesia, Malaysia, and India. Figure 1 shows the Lempeni fruit with black peel color. Despite its abundance in certain tropical regions, Lempeni fruit has not been extensively studied for its chemical properties or potential applications. Utilizing this fruit as a raw material for natural pH indicators not only adds value to a locally available botanical resource but also supports the development of green analytical techniques. The exploration of such lesser-known species contributes to biodiversity utilization and promotes innovation in sustainable chemistry practices.

In this work, anthocyanins were extracted from Lempeni fruit using the maceration methods, with a solvent mixture of 96% ethanol and 1% HCl (1:1), over a 24-h period. The resulted extract was evaluated across a full pH spectrum (pH 1-14), both through spot tests and application on filter paper, to observe the color changes at various pH levels. Furthermore, the usability of the extract in acid-base titrations will be tested to assess its functionality compared to conventional synthetic indicators. By examining both the qualitative and quantitative performance of Lempeni's anthocyanins, this study aimed to validate their effectiveness in real-world analytical scenarios. The broader goal of this work was to advance the development of natural, biodegradable, and cost-effective pH indicators derived from local plant sources.



Figure 1 – The Lempeni fruit appearance

Materials and methods

Materials and Equipment. Lempeni fruit samples were collected directly from the coastal area of Kuala Baru Laut, Aceh Singkil, Indonesia. The chemical reagents involved included distilled water (H_2O), 96% ethanol (C_2H_5OH), hydrochloric acid (HCl), sodium hydroxide (NaOH), acetic acid (CH_3COOH), and ammonium hydroxide (NH_4OH). The equipment employed in this study consisted of a stir bar, grinder, filter paper, burette, funnel, Erlenmeyer flask, beaker, volumetric flask, analytical balance, dropper pipette, measuring pipette, drop plate, test tubes, rotary evaporator, and a UV-Vis spectrophotometer.

Lempeni fruit extraction. 200 grams fruit were washed, drained, and dried until the fruit was completely dried. Then, the samples were ground into a fine powder using a grinder. 50 grams of the powder were placed into 500 mL beaker containing a solvent (96% ethanol + 1% HCl, 1:1). The mixture was stirred using a glass spatula to ensure the complete mixing of them. The mixture was subsequently subjected to maceration at room temperature and kept for 48 hours, with occasional stirring every 6 hours. After that, the mixture was filtered using a Whatman filter paper and concentrated using a rotary evaporator to obtain the fruit extract without solvent.

Determination of anthocyanins. To determine the maximum wavelength, Lempeni fruit extract was placed into a cuvette and analyzed using a UV-Vis spectrophotometer within the wavelength range of 400-800 nm. The maximum absorbance value was then recorded. Following this, a qualitative test for anthocyanin content was carried out using two methods. In the first method, 2 M HCl was added to the extract in a test tube, which was then heated at $100^\circ C$ for 2 minutes. The sample was observed for any color change, if the red color remained stable, it indicated the presence of anthocyanins. In the second method, 2 M NaOH was added dropwise to a separate sample. A color change from red to blue-green that gradually faded confirmed the presence of anthocyanins [13].

Testing Lempeni Fruit Extract as an Indicator. Five drops each of HCl, NaOH, CH_3COOH , and NH_4OH solutions were placed into separate wells of a drop plate. The pH of each solution was measured using a pH meter. Subsequently, 5-8 drops of Lempeni fruit extract were added to each well, and the resulting color changes were observed to assess the extract's response at known pH levels.

Preparation of Acid-Base Indicator Paper. Whatman filter paper was used as the base for the indicator. Lempeni fruit extract was poured into a basin, and the filter paper was fully immersed in the extract for approximately 2 hours. After soaking, the paper was removed and placed on a tray or baking sheet to air dry. Once completely dry, the paper was observed for any color development, then cut into strips measuring 1 x 4.5 cm. These strips, referred to as Lempeni fruit indicator paper, were then tested in various solutions including HCl, NaOH, CH₃COOH, and NH₄OH. The indicator paper was considered stable if it turns dark red or pink in acidic solutions and changes to green, yellow, or purple in alkaline solutions.

Titration Using Lempeni Fruit Extract as an Indicator. A total of 10 mL of a strong acid solution (0.1 N HCl) was pipetted into a 250 mL Erlenmeyer flask, followed by the addition of 3 drops of Lempeni fruit extract as an indicator. The solution was then titrated with a strong base (0.1 N NaOH) until a visible color change occurred. This procedure was repeated three times, and the volume of NaOH used in each titration was recorded. The same method was applied to a strong base (0.1 N NaOH), which was titrated with a strong acid (0.1 N HCl). Additionally, titrations were performed for a weak acid (0.1 N CH₃COOH) using a strong base (0.1 N NaOH), and for a weak base (0.1 N NH₄OH) using a strong acid (0.1 N HCl), with the volume of titrant used in each case being recorded. For comparison, each titration was also repeated using standard indicators (phenolphthalein and methyl orange) in place of the Lempeni fruit extract.

Results and discussion

Lempeni fruit extraction process. The extraction of Lempeni fruit was conducted using the maceration technique, a method that involves soaking plant material in a solvent to draw out the desired compounds [14]. Initially, the fruit is ground with a grinder, then immersed in an organic solvent for a specified duration. Maceration is widely favored for isolating natural substances due to its simplicity and low cost [15]. During soaking, pressure differences inside and outside the cell walls cause them to break down, allowing secondary metabolites in the cytoplasm to dissolve into the solvent, resulting in effective extraction. The soaking time can be adjusted as needed. In this process, maceration was performed over 48 hours (2x24 hours), with stirring every 6 hours. After maceration, the extract was filtered to separate the solid residue from the liquid extract. The ideal extraction time was found to be two days, as longer contact between the solvent and the plant material allows for

more thorough extraction. However, if this contact exceeds the optimal duration, compound degradation can occur [16]. A limitation of the maceration method is its relatively low efficiency, as only about 40% of the active compounds are extracted, and some may become less soluble. Therefore, temperature evaporation is used to concentrate the extract. This is done with a rotary evaporator, which effectively removes the solvent without damaging the compounds. However, excessive pressure during evaporation can degrade sensitive compounds like anthocyanins. In this process, the extract was concentrated at 40°C for 90 minutes, resulting in a thick red Lempeni fruit extract.

Determining the maximum wavelength of Lempeni fruit extract. To identify the maximum wavelength of Lempeni fruit extract, a UV-Vis spectrophotometer was used. This instrument measures absorbance within the visible light spectrum, which ranges from 400 to 800 nm. This range is suitable because the compounds responsible for anthocyanins which typically absorb light within this region. Based on Figure 2, the Lempeni fruit extract exhibited its peak absorbance within the 400-800 nm range and the broad absorption peak ranged from 450 to 550 nm, which is consistent with the absorption spectrum of the anthocyanin color groups [17]. This peak absorbance was essential in identifying the most effective wavelength for analyzing or utilizing the extract, such as in dye applications or compound quantification. The wavelength at which this maximum occurs represents the optimal point for future spectrophotometric measurements of the extract.

Anthocyanin verification test. To confirm the presence of anthocyanins in Lempeni fruit extract, a qualitative test was conducted using acidic and basic solutions. Anthocyanins are pH-sensitive pigments, so their color tends to change depending on the pH level of the solution [18]. In this test, 2 M HCl, a strong acid, was added to the Lempeni fruit extract to observe any visible color change. The mixture was then heated for 5 minutes to ensure proper reaction. After heating, it was observed that the color of the Lempeni fruit extract remained unchanged compared to its initial appearance. Figures 3a-b show the original extract as a control sample and the extract after the addition of 2 M HCl after heating, respectively. Under acidic condition, the color of solution was consistent, suggesting that the extract contains anthocyanins which tend to maintain their red to purple in acidic environments. This finding confirms that anthocyanins are present in Lempeni fruit extract, indicating the stability of this pigment under acidic conditions.

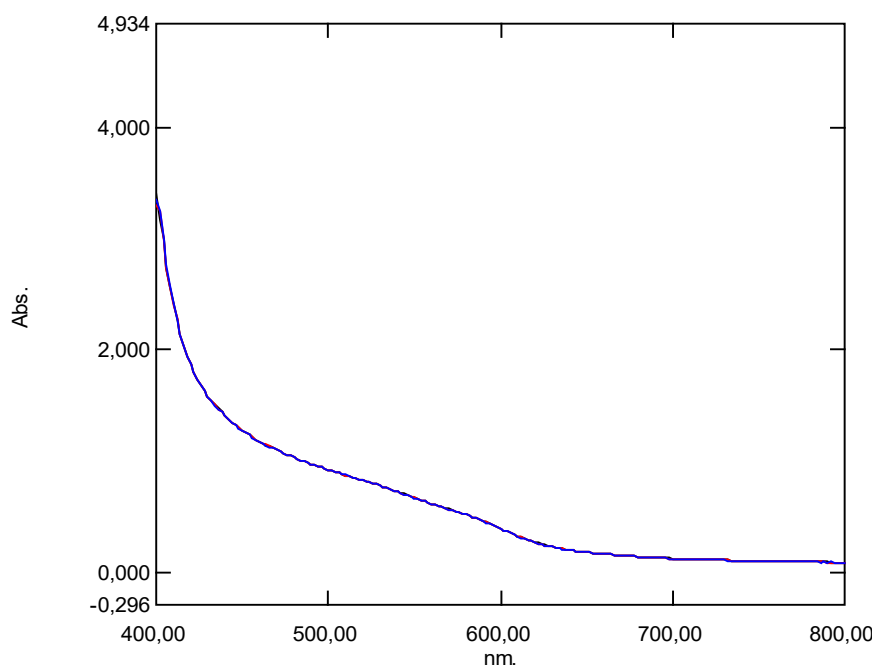


Figure 2 – The UV-Vis absorbance of anthocyanins from Lempeni fruit extract

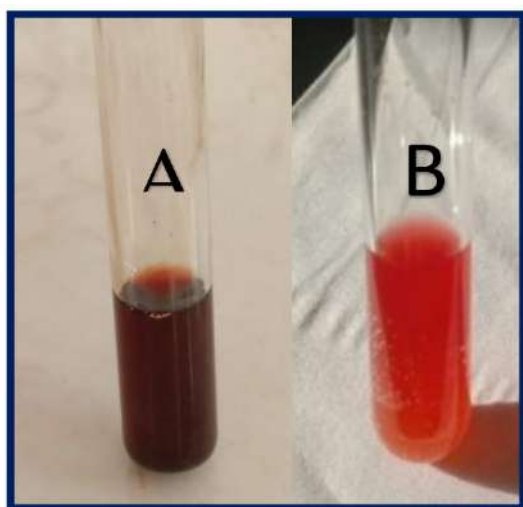


Figure 3 – Color change of extract with HCl solution

In the next phase of the anthocyanin verification test, the Lempeni fruit extract was treated with a strong base to observe its response to alkaline conditions. A few drops of 2 M NaOH solution were added to the extract. As a result, a visible color change occurred from the original hue to a brownish green, as shown in Figure 4. Figure 4 visually compares the untreated extract (A) with the extract after the addi-

tion of 2 M NaOH (B). The transition to a brownish green color upon exposure to an alkaline environment is a clear indicator of the presence of anthocyanins. The solution appeared in red to pink color in the acidic conditions and changed to green or yellow-brown color under alkaline conditions.

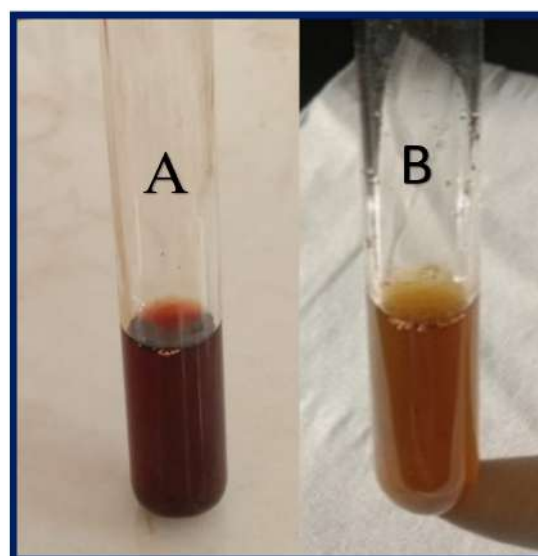


Figure 4 – The appearance of extract' color change after adding NaOH solution

This color change further illustrates a typical trait of anthocyanins, as their molecular structure changes with pH variations, influencing their light absorption and reflection properties. The observation showed that the color of the extract changed to brownish green after adding NaOH as a basic solution. But it remained pink color in acidic solutions even after heating (Figure 3), indicating the presence of anthocyanin compounds. In addition, the anthocyanin induces greater stability in acidic conditions, whereas they commonly produce color's change in basic conditions owing to their reactivity and cationic characters. This phenomenon not only demonstrates the anthocyanin existence but also has potential as a new natural indicator.

Performance of natural indicator from extract. Anthocyanins exhibit several colors based on the pH

values of environments. These typical characteristics offer them suitable as the pH indicators. Before the use of Lempeni fruit extract as a natural acid-base indicator in titration, it is important to identify its certain pH range for color changes. Subsequently, the extract was introduced into two acidic solutions (HCl and CH_3COOH) and two basic solutions (NaOH and NH_4OH) in order to test their color changes. Figure 5 and Table 1 exhibit a visual observation of the color changes when the extract interacted with the solutions of HCl (1), NaOH (2), CH_3COOH (3), and NH_4OH (4). The extract color appeared from purplish red to vivid red in acidic solutions. Meanwhile, the extract color changed from purplish red to brownish green in basic solutions. These naked eye color changes are specific character of anthocyanins, which react susceptibly to pH changes.

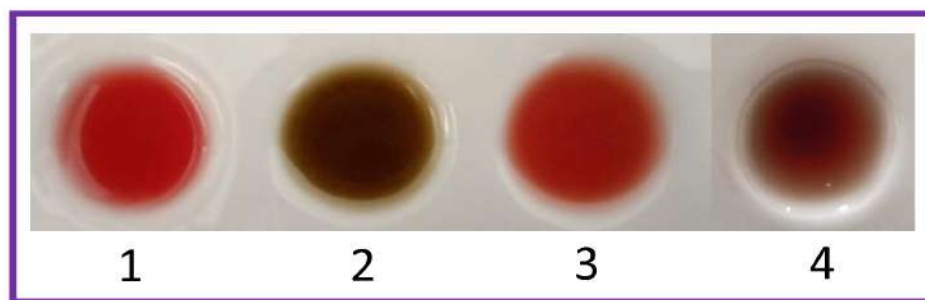


Figure 5 – The change in color of acid-base solutions after mixing with the extract

Table 1 depicts the results of the discoloration of the extract mixing with several solutions. The fruit extract was still in red in acid solutions (HCl and CH_3COOH), indicating the stability of anthocyanins. In NaOH, which is a strong base, the extract changed to dark green, while in NH_4OH , a milder base, it transformed into a brownish red. These unique changes further validate the existence of anthocyanins and illustrate their effectiveness as a natural pH indicator. Color variation happens as anthocyanins experience

structural modifications at various pH levels, resulting in different molecular forms [19]. At low pH, they primarily appear as flavylum cations, which are red in color. As the pH rises, the structure changes, resulting in greenish or brownish shades caused by the degradation or creation of quinonoidal and chalcone forms [20]. Understanding this behavior is crucial for employing Lempeni fruit extract successfully as a natural and eco-friendly indicator in acid-base titrations.

Table 1 – The color change of extract after adding into acidic and basic solutions

Extract	Solution	Type	Discoloration
Lempeni Fruit	HCl	Strong Acid	Red
	NaOH	Strong Base	Brownish green
	CH_3COOH	Weak Acid	Red
	NH_4OH	Weak Base	Brownish red

Acid-base indicator paper from Lempeni fruit extract. Lempeni fruit extract served as an acid-base indicator due to its ability to change color when exposed to various solutions such as HCl, NaOH, CH₃COOH, and NH₄OH. According to Ernawati and Rahayu [21], filter paper is commonly used for this purpose. Filter paper, made of pure cellulose, has excellent absorption properties. As shown in Figure 6, when dipped in HCl and CH₃COOH, the indicator paper made with Lempeni extract did not show

any color change. However, it turned dark green in NaOH and brownish in NH₄OH. The observed color changes are due to the purplish-red pigment found in anthocyanins, which can function as chemosensory compounds in acid-base indicators. Anthocyanins are sensitive to pH changes; in acidic environments (pH < 7), the paper remains red, while in basic environments (pH > 7), it shifts to dark green. Therefore, based on the above data, Lempeni fruit extract can be effectively used as a natural pH indicator.

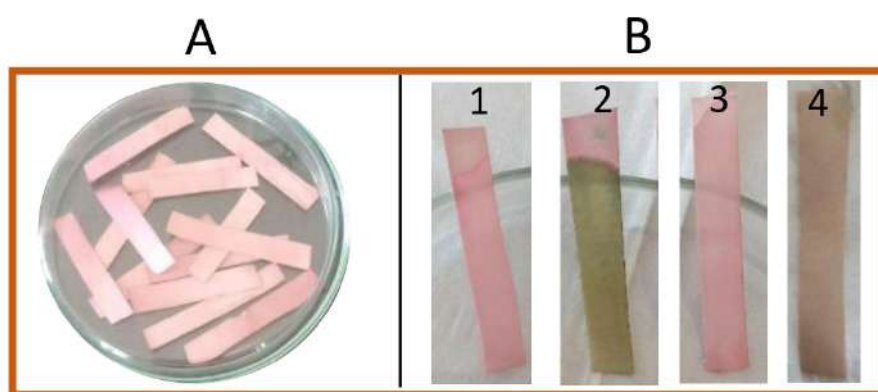


Figure 6 – (a) Filter paper and (b) the results of color changes after being dipped in acidic and basic solutions

Lempeni fruit extract indicator for acid-base titration. Acid-base indicators can exist in neutral, positively charged, or negatively charged forms [22]. Some indicators display a single color, with that appearance affected not only by pH but also by the indicator's concentration. For instance, phenolphthalein (PP) is a single-color indicator that works within a pH range of 8.0-9.6 where colorless in its acidic form and pink in its basic form [23]. Lempeni extract shows promise as a natural acid-base indicator. To evaluate its effectiveness, acid-base titration experiments were performed using this extract alongside standard indicators like PP and methyl orange (MO). Both acid and base concentrations were set at 0.1 N. The titrations conducted included four combinations: strong acid with strong base, strong base with strong acid, strong acid with weak base, and strong base with weak acid. Specifically, the titration pairs were NaOH vs HCl, HCl vs NaOH, NaOH vs CH₃COOH,

and HCl vs NH₄OH. In each experiment, three drops of the Lempeni extract, PP, and MO were added to the titrand, with 10 mL of titrant used. Initial colors were recorded immediately after adding the indicators. The findings exhibited that the fruit extract could identify titration endpoints accurately, nearly matching those observed with the standard and commercial indicators. The change of pink color to green color happened at almost same volume addition, indicating that the anthocyanin derived from the fruit extract responded similarly to the commercial indicators. The pink color in acidic solutions changed to brownish in basic ones, informing that the extract functions as a pH indicator for basic solutions. The changes in color dan pH values across different titration combinations are summarized in Table 2. Hence, the results suggest that the Lempeni fruit extract is an alternative indicator toward commercial acid-base indicators.

Table 2 – The changes in colors and pH values at the end point of the titration

Titrand	Titrant	Indicator	Color Changes	pH
HCl 10.00 mL	NaOH 9.05 mL	Phenolphthalein	Colorless to pink	8.52
	9.10 mL	Methyl Orange	Orange to yellow	6.23
	9.95 mL	Fruit Extract	Pink to brownish green	8.55
NaOH 10.00 mL	HCl 12.70 mL	Phenolphthalein	Pink to colorless	6.83
	12.25 mL	Methyl Orange	Yellow to orange	3.86
	12.90 mL	Fruit Extract	Brownish green to colorless	6.88
CH ₃ COOH 10.00 mL	NaOH 7.20 mL	Phenolphthalein	Colorless to pink	8.40
	7.50 mL	Methyl Orange	Yellow to orange	4.23
	7.35 mL	Fruit Extract	Pink to brownish green	8.38
NH ₄ OH 10.00 mL	HCl 8.10 mL	Phenolphthalein	Pink to colorless	5.02
	8.50 mL	Methyl Orange	Yellow to pink	3.65
	8.97 mL	Fruit Extract	Brownish red to colorless	5.30

Conclusions

In this study, the anthocyanin compound from Lempeni fruit was extracted and used as a natural acid-base indicator. Using the maceration method with a mixture of 96% ethanol and 1% HCl, the anthocyanin-rich extract was obtained and tested across a broad pH spectrum. Results showed consistent and distinct color changes, shifting from red in acidic environments to brownish green and brownish red under alkaline conditions. These observations, supported by UV-Vis spectrophotometric analysis, confirmed the presence and stability of anthocyanins in the extract, particularly within the 450-550 nm absorbance range. The extract's color sensitivity to pH made it a valuable candidate for various applications. When tested on indicator paper, Lempeni extract produced clear and predictable color changes in response to strong and weak acids and bases. More importantly, in titration experiments, the extract reliably indicated endpoint detection, performing comparably to standard synthetic indicators such as phenolphthalein and methyl orange. These results illustrate the accu-

racy and real-world utility of Lempeni fruit extract in analytical chemistry. As a plant-derived, biodegradable substitute for synthetic indicators, it provides both ecological and economic benefits. Its ease of use and efficiency also render it a useful educational resource for instructing on acid-base reactions in an eco-friendly manner. In general, Lempeni anthocyanins demonstrate essential attributes of a natural pH indicator, underscoring the fruit's viability a local resource for sustainable analytical practices in both educational and laboratory environments.

Acknowledgments

The authors thank to Lab of Chemical Analysis and Instrumentation at Universitas Serambi Mekkah dan Lab of Natural Science at Universitas Syiah Kuala for providing research facilities.

Conflict of interest

All authors are aware of the article's content and declare no conflict of interest.

References

1. Mattioli R., Francioso A., Mosca L., Silva P. (2020) Anthocyanins: A comprehensive review of their chemical properties and health effects on cardiovascular and neurodegenerative diseases. *Molecules*, 25(17), pp. 3809. <https://doi.org/10.3390/molecules25173809>.
2. He J., Giusti M.M. (2010) Anthocyanins: natural colorants with health-promoting properties. *Annu. Rev. Food Sci. Technol.*, 1, pp. 163-187. <https://doi.org/10.1146/annurev.food.080708.100754>.
3. Khoo H.E., Azlan A., Tang S.T., Lim S.M. (2017) Anthocyanidins and anthocyanins: colored pigments as food, pharmaceutical ingredients, and the potential health benefits. *Food Nutr. Res.*, 61, pp. 1361779. <https://doi.org/10.1080/16546628.2017.1361779>.

4. Tuslinah L., Yuliana A., Arisnawati D., Rizkuloh L.R. (2022) Comparison of color change to pH range and acid-base titration indicator precision test of multiple ethanol extracts. *Trends in Sci.*, 19(1), pp. 1446. <https://doi.org/10.48048/tis.2022.1446>.
5. Sajin K.A., Anoobkumar K.I., Rasa O.K. (2020) pH indicators: a valuable gift for analytical chemistry. *Saudi J. Med. Pharm. Sci.*, 6(5), pp. 393-400. <https://doi.org/10.36348/sjmps.2020.v06i05.001>.
6. Okoduwa S.I.R., Mbora L.O., Adu M.E., Adeyi A.A. (2015) Comparative analysis of the properties of acid-base indicator of Rose (*Rosa setigera*), allamanda (*Allamanda cathartica*), and Hibiscus (*Hibiscus rosa-sinensis*) flowers. *Biochem. Res. Int.*, 2015, pp. 381721. <http://dx.doi.org/10.1155/2015/381721>.
7. Maqsood W., Sheikh T.A., Al-Baqami S.M., et al. (2025) Efficacy of plant extracts as green indicators in acid-base titrimetric analysis: Perspective towards green chemistry. *Microchem. J.*, 213, pp. 113613. <https://doi.org/10.1016/j.microc.2025.113613>.
8. Hailu F.W., Fanta S.W., Tsige A.A., et al. (2025) Development of simple and biodegradable pH indicator films from cellulose and anthocyanin. *Discov. Sustain.*, 6, pp. 220. <https://doi.org/10.1007/s43621-025-00916-4>.
9. Hoa V.T., Thang N.Q., Tan L.V., Tran L.T.T. (2023) Exploring plant species in Vietnam for the production of pH indicator paper. *Trop. J. Nat. Prod.*, 7(10), pp. 4889-4893. <http://www.doi.org/10.26538/tjnpr/v7i10.25>.
10. Kalakonda S.N., Atla S.R., Puvvada R.N., Nalli P.K., Sheik I., Prasad R. (2023) Green indicators-an ecofriendly endpoint. *Int. J. Pharm. Invest.*, 13(2), pp. 206-214. <http://www.doi.org/10.5530/ijpi.13.2.028>.
11. Kurniawati A., Alauhdin M. (2020) Ekstraksi dan analisis zat warna ekstrak kulit buah manggis (*Garciana mangostana* L.) serta aplikasinya sebagai indikator asam-basa. *Indo. J. Chem. Sci.*, 9(1), pp. 56-62. <http://www.doi.org/10.15294/ijcs.v9i1.37377>.
12. Dhafina W.A., Salleh H., Daud M.Z., Ghazali M.S.M. (2018) Low cost dye-sensitized solar cells based on zinc oxide and natural anthocyanin dye from *Ardisia elliptica* fruits. *Optik*, 172, pp. 28-34. <https://doi.org/10.1016/j.ijleo.2018.06.041>.
13. Qi Q., Chu M., Yu X., Xie Y., Li Y., Du Y., Liu X., Zhang Z., Shi J., Yan N. (2023) Anthocyanins and proanthocyanidins: chemical structures, food sources, bioactivities, and product development. *Food Rev. Int.*, 39(7), pp. 4581-4609. <https://doi.org/10.1080/87559129.2022.2029479>.
14. Zhang M., Zhao J., Dai X., Li X. (2023) Extraction and analysis of chemical compositions of natural products and plants. *Separations*, 10(12), pp. 598. <https://doi.org/10.3390/separations10120598>.
15. Bitwell C., Indra S.S., Luke C., Kakoma M.K. (2023) A review of modern and conventional extraction techniques and their applications for extracting phytochemicals from plants. *Sci. African*, 19, pp. e01585. <https://doi.org/10.1016/j.sciaf.2023.e01585>.
16. Gan C.-Y., Latiff A.A. (2011) Optimisation of the solvent extraction of bioactive compounds from *Parkia speciosa* pod using response surface methodology. *Food Chem.*, 124(3), pp. 1277-1283. <https://doi.org/10.1016/j.foodchem.2010.07.074>.
17. Wahyuningsih S., Wulandari L., Wartono M.W., Munawaroh H., Ramelan A.H. (2017) The effect of pH and color stability of anthocyanin on food colorant. *IOP Conf. Ser.: Mater. Sci. Eng.*, 193, pp. 012047. <https://doi.org/10.1088/1757-899X/193/1/012047>.
18. Alizadeh-Sani, M., Tavassoli M., Mohammadian E., Elhasani A., Khaniki G.J., Priyadarshi R. Rhim J.-W. (2021) pH-responsive color indicator films based on methylcellulose/chitosan nanofiber and barberry anthocyanins for real-time monitoring of meat freshness. *Int. J. Biol. Macromol.*, 166, pp. 741-750. <https://doi.org/10.1016/j.ijbiomac.2020.10.231>.
19. Enaru B., Dretcanu G., Pop T.D., Stanila A., Diaconeasa Z. (2021) Anthocyanins: factors affecting their stability and degradation. *Antioxidants*, 10(12), pp. 1967. <https://doi.org/10.3390/antiox10121967>.
20. Pina F., Oliveira J., Freitas V.D. (2015) Anthocyanins and derivatives are more than flavylum cations. *Tetrahedron*, 71, pp. 3107-3114. <https://doi.org/10.1016/j.tet.2014.09.051>.
21. Ernawati D., Rahayu T. (2017) Pengaruh jenis pelarut dalam ekstraksi kulit buah manggis (*Garcinia mangostana*) sebagai kertas indikator asam basa. Seminar Nasional Pendidikan Biologi dan Saintek II, Surakarta, Indonesia, pp. 405-410.
22. Kahlert H., Meyer G., Albrecht A. (2016) Color maps of acid-base titrations with color indicators: how to choose the appropriate indicator and how to estimate the systematic titration errors. *ChemTexts*, 2, pp. 7. <https://doi.org/10.1007/s40828-016-0026-4>.
23. Rahmawati S., Aminah S., Nuryanti S., Vivi Dia Afrianti Sangkota V.D.A., Hapsarina. (2023) Flower extract tapak dara (*Catharanthus roseus* L.) as acid-base indicator. *Malaysian J. Chem.*, 25(5), pp. 207-215. <https://doi.org/10.55373/mjchem.v25i5.207>.

Information about authors

Ulfa Rahma – Bachelor Degree, Department of Chemistry Education, Universitas Serambi Mekkah (Banda Aceh, Indonesia, e-mail: ulfarahmasalawatisyafnur@gmail.com)

Muhammad Zulfajri – PhD, Assistant Professor, Department of Chemistry Education, Universitas Serambi Mekkah (Banda Aceh, Indonesia, e-mail: muhammad.zulfajri@serambimekkah.ac.id)

Sri Ismulyati – Master Degree, Lecturer, Department of Chemistry Education, Universitas Serambi Mekkah (Banda Aceh, Indonesia, e-mail: sriismul@gmail.com)

Content

Editorial.....	3
A. Amanzhan, E.E. Schultz, B.S. Adekenov, O.V. Maslova, M.K. Ibraev, S.M. Adekenov Synthesis of new acetylharmin derivatives and their neurotropic activity	4
O.G. Cherednichenko, A.L. Pilyugina, D.E. Azizbekova, A.S. Amirgaliyeva, K.B. Bepalova Genomic stability and adaptation in Kazakh Tobet dogs: a cytogenetic analysis	17
A.B. Hejran, V.K. Yadav, P. Niazi Prevalence and impact of Hepatitis B Virus (HBV) in Lashkar Gah City, Afghanistan: A Case Study	25
T. Ismagambetova, D. Arman, M. Zholdassova Source reconstruction of electrical brain activity during attention network task performance	47
D.E. Karabalayeva, M.S. Kurmanbayeva, S.K. Mukhtubayeva, M.Zh. Zhumagul, A.B. Kusmangazinov, R.K. Anatoliy Study of <i>Trollius dschungaricus</i> Regel (Ranunculaceae Juss.) in the flora of the Saty Gorge	57
O.Yu. Maslov, M.A. Komisarenko, S.V. Ponomarenko, S.V. Kolisnyk, T.P. Osolodchenko, M.Yu. Golik, S.I. Polishchuk Comparing phytochemical profile, antimicrobial and antioxidant activities of anthocyanin raspberry fruit thick and catechins green tea leaf extracts	70
M. Narmuratova, S. Orazova, A. Serikbayeva, Zh. Narmuratova, A. Zhardamalieva Mare's milk as a source of biologically active immunoglobulins: a review of scientific data	81
A.B. Tolegen, N.V. Romadanova, M.M. Aralbayeva, N.K. Rymkhanova, Y.V. Ukhatova, M.M. Agahanov, N.V. Mikhailenko, S.V. Kushnarenko Utilizing Plant Preservative Mixture™ to eliminate endophytic bacterial contamination and establish <i>in vitro</i> cultures of blackberry varieties.....	89
S.M.R. Nazifi, N. Esfandiarpour, A. Motamedi, E. Jahanmard, N. Rahimi, F. Ansari, F. Masoudi, S. Sepahi Evaluation of Different Sweetener Concentrations in Beverage Samples in Isfahan Market Using High Performance Liquid Chromatography	100
Zn.N. Uvaniskanova, G.A. Seitimova, G.Sh. Burasheva, M.I. Choudhary Evaluation of <i>Canavalia ensiformis</i> L. beans: Comparative Fatty Acid Profile in Extracts and Analysis of Minerals and Proximate Composition.....	106
A.A. Auyeshov, Ch.Z. Eskibayeva, A.M. Ibrayeva, K.T. Arynov, A.K. Dikanbayeva Resource-efficient technology for the utilization of serpentine technogenic waste with the production of magnesium oxide	112
T.D. Sallal, A.M. Abbas Preparation and Characterization of Nano-Iron Oxide by using Iraqi Orange Plant Extract and Testing for Adsorption Efficiency	119
A.A. Minkayeva, L. Azilbek, U. Amzeyeva, T. Karunakaran, X. Liu, X. Shang, N. Muzaffarova, J. Jenis Comparative investigation of <i>Rheum tataricum</i> and <i>Rheum palmatum</i>	127
F. Mas'ud, V.D. Paramita, Z. Zulmanwardi, H.R. Yuliani Optimization of dietary fiber extraction from corn stalks and product characterization	138
K. Akatan, N. Kaiyrbekov, A. Demeukhan, A. Battalova, E. Shaimardan, M. Beisebekov, F. Kholiya, Zh. Ibraeva, S. Kabdrakhmanova Synthesis of Cellulose based Hydrogel with High Absorption Capacity	150
U. Rahma, M. Zulfajri, S. Ismulyati Evaluation of anthocyanin extracted from Lempeni (<i>Ardisia Elliptica</i> l.) fruit as a new natural acid-base indicator	159